PHASE BEHAVIOUR MODELLING OF SYSTEMS CONTAINING GAS HYDRATES AND ASPHALTENES

by

AMIR HOSSEIN MOHAMMADI

BSc, MSc

Submitted for the Degree of Doctor of Philosophy in

PETROLEUM ENGINEERING

Institute of Petroleum Engineering

Heriot-Watt University

Edinburgh, Scotland/UK

March 2006

ABSTRACT

Gas hydrates are crystalline compounds formed from a combination of water molecules with suitably sized non-polar or slightly polar molecules under certain conditions of temperature and pressure. They are well known for their role in the blockage of subsea pipelines and oil and gas production / processing facilities, which is a major concern for the petroleum industry. On the other hand, asphaltenes are the toluene / benzene soluble fractions that precipitate from petroleum when an excess (25 to 40 times) of n-heptane / n-pentane is mixed with petroleum and waiting at least four hours before filtering. Asphaltene precipitation causes fouling in the reservoir, in the well, in the pipeline and in the oil production and processing facilities.

In this study, predictive methods and thermodynamic models to predict the hydrate and asphalt free zone of hydrocarbon fluids were developed for field applications. The topics studied included estimation of water content of natural gases in equilibrium with the liquid water, ice and gas hydrates, prediction of hydrate inhibition effects of mixed salt and organic inhibitor and finally modelling asphaltene precipitation conditions.

The results showed that the existing predictive methods show large deviations for predicting the water content of natural gases at low temperature conditions and therefore, new predictive tools were developed. Furthermore, the application of a thermodynamic model was extended to mixed salt and chemical inhibitor commonly used in petroleum production and transportation. This will provide a basis for the

design of production and transportation facilities, particularly for deepwater applications. A new correlation for predicting the hydrate inhibition effect of single and mixed thermodynamic inhibitors was also developed.

A theoretical study was conducted to investigate asphaltene precipitation from petroleum fluids during petroleum production and transportation. The results showed that it is possible to use a polymer model namely the Scott-Magat theory combined with an equation of state to predict asphaltene precipitation from reservoir fluids.

To my parents and all members of my family

For their patience and encouragement

ACKNOWLEDGEMENTS

This work was carried out between October 2001 - March 2006 (MPhil and PhD) in Institute of Petroleum Engineering, Heriot-Watt University. I would like to express my deep thanks to my parents and all members of my family, for their unlimited encouragement and excessive support, without which it would be impossible for me to achieve the goal of pursuing this degree.

I would truly appreciate the help given by my teachers, especially Mr Feizabadi at primary school and Mr Saachi and Mr Mirzaee at high school for their encouragement. Thanks are also extended to my MSc thesis supervisor at Tehran University, Prof. G. Abolhamd, for her support and encouragement.

I am indebted to Mrs Nader Amir Ehsani, Samad Shahri and Shahram Shodjaee of National Iranian Oil Company/ Tabriz Refinery who where a source of support during 1998-2001. In many more ways, these individuals assisted me.

I have been fortunate enough to develop friendships and colleagial relations with people from Centre for Gas Hydrate Research and Reservoir Fluid Studies Group at Heriot-Watt University. who have supported me. I am especially grateful to Prof. Bahman Tohidi and Prof. Ali Danesh for their guidance and suggestions. I also owe my thanks to Prof. Adrian C. Todd and Dr. Fatollah Gozalpour for their encouragement. To everyone, my thanks and gratitude goes out. I am lucky to enjoy the friendships and support of many people.

This work was part of a Joint Industrial Project funded by a consortium consisting of Shell UK Exploration and Production, TOTAL, Statoil, Petrobras, Marathon, Gaz de France, Schlumberger, ABB, and the U.K. Department of Trade and Industry, whose support is gratefully acknowledged. I also wish to thank the Centre for Gas Hydrate Research/Institute of Petroleum Engineering/Heriot-Watt University for full scholarship through Joint Industrial Projects.

ACADEMIC REGISTRY
Abstract of Thesis Form

HERIOT WATT UNIVERSITY

Candidate

Name *(in capitals):*	AMIR HOSSEIN MOHAMMADI	Matric Number:	00030761S
School/PGI:	INSTITUTE OF PETROLEUM ENGINEERING	Degree Sought:	PHD
Title of Thesis: (complete in upper and lower case)	PHASE BEHAVIOUR MODELLING OF SYSTEMS CONTAINING GAS HYDRATES AND ASPHALTENES		

Signature:	Amir Hossein Mohammadi	Date:	2-FEB-2006

Abstract

Gas hydrates are crystalline compounds formed from a combination of water molecules with suitably sized non-polar or slightly polar molecules under certain conditions of temperature and pressure. They are well known for their role in the blockage of subsea pipelines and oil and gas production / processing facilities, which is a major concern for the petroleum industry. On the other hand, asphaltenes are the toluene / benzene soluble fractions that precipitate from petroleum when an excess (25 to 40 times) of n-heptane / n-pentane is mixed with petroleum and waiting at least four hours before filtering. Asphaltene precipitation causes fouling in the reservoir, in the well, in the pipeline and in the oil production and processing facilities.

In this study, predictive methods and thermodynamic models to predict the hydrate and asphalt free zone of hydrocarbon fluids were developed for field applications. The topics studied included estimation of water content of natural gases in equilibrium with the liquid water, ice and gas hydrates, prediction of hydrate inhibition effects of mixed salt and organic inhibitor and finally modelling asphaltene precipitation conditions.

The results showed that the existing predictive methods show large deviations for predicting the water content of natural gases at low temperature conditions and therefore, new predictive tools were developed. Furthermore, the application of a thermodynamic model was extended to mixed salt and chemical inhibitor commonly used in petroleum production and transportation. This will provide a basis for the design of production and transportation facilities, particularly for deepwater applications. A new correlation for predicting the hydrate inhibition effect of single and mixed thermodynamic inhibitors was also developed.

A theoretical study was conducted to investigate asphaltene precipitation from petroleum fluids during petroleum production and transportation. The results showed that it is possible to use a polymer model namely the Scott-Magat theory combined with an equation of state to predict asphaltene precipitation from reservoir fluids.

See reverse side for notes

ACADEMIC REGISTRY
Research Thesis Submission

Name:	AMIR HOSSEIN MOHAMMADI		
School/PGI:	INSTITUTE OF PETROLEUM ENGINEERING		
Version: *(i.e. First, Resubmission, Final)*	FINAL	Degree Sought:	PHD

Declaration

In accordance with the appropriate regulations I hereby submit my thesis and I declare that:

1) the thesis embodies the results of my own work and has been composed by myself
2) where appropriate, I have made acknowledgement of the work of others and have made reference to work carried out in collaboration with other persons
3) the thesis is the correct version of the thesis for submission*.
4) my thesis for the award referred to, deposited in the Heriot-Watt University Library, should be made available for loan or photocopying, subject to such conditions as the Librarian may require
5) I understand that as a student of the University I am required to abide by the Regulations of the University and to conform to its discipline.

* *Please note that it is the responsibility of the candidate to ensure that the correct version of the thesis is submitted.*

Signature of Candidate:	Amir Hossein Mohammadi	Date:	2-FEB-2006

Submission

Submitted By *(name in capitals)*:	AMIR HOSSEIN MOHAMMADI
Signature of Individual Submitting:	Amir Hossein Mohammadi
Date Submitted:	3-MARCH-2006

For Completion in Academic Registry

Received in the Academic Registry by *(name in capitals)*:	VAL MURDOCH		
Method of Submission *(Handed in to Academic Registry; posted through internal/external mail)*:	Handed in to AR		
Signature:	Valerie A Murdoch	Date:	3/3/06

TABLE OF CONTENTS

LIST OF MAIN SYMBOLS

AAD	Average absolute deviation
AD	Absolute deviation
ART	Acoustic resonance technique
BIP	Binary interaction parameter
BOP	Blowout preventer
CMC	Critical micelle concentration
D-H	Debye-Hückel electrostatic term
EG	Ethylene glycol
EOR	Enhanced Oil Recovery
EoS	Equation of state
HC	Hydrocarbon
IFT	Interfacial tension
LLE	Liquid-liquid equilibrium
LST	Light-scattering technique
MEK	Methyl ethyl ketone
NDD	Non density dependent mixing rules
NG	Natural gas
PNA	Paraffin-naphthane-aromatic
PR	Peng – Robinson equation of state
SAFT	Statistical associated fluid theory
SARA	Saturates, aromatics, resins and asphaltenes
SCN	Single carbon number
SRK	Soave-Redlich-Kwang equation of state
STO	Stock tank oil

VLE	Vapour-liquid equilibrium
VLLE	Vapour – liquid – liquid equilibrium
VPT – EoS	Valderrama modification of Patel-Teja equation of state
WAT	Wax appearance temperature
A	Electrolyte model parameter/ Constant
A´	Parameter of *two-suffix Margules* activity coefficient model
A_1	Parameter
B	Electrolyte model parameter/ Constant
B_1	Parameter
C	Langmuir constant/ Constant/ *Whitson* characterisation factor
C_1	Parameter
C_2	Parameter
C_p	Average heat capacity of natural gas
C_r	Resin concentration in the liquid phase
D	Formation volume factor
F	Parameter of the equation of state/ Molar fraction of phase / Correction factor/ Function
G	Gas/ Gibbs free energy
H	Hydrate/ Molar enthalpy
I	Ice/ Ionic strength based on molality of salt in pure water
K	Equilibrium ratio
K_w	Watson characterisation factor
L	Liquid
L1	Oil-rich phase
L2	Asphalte phase

M	Metal of valence x/ Molecular weight/ Number of non-asphaltenic components
Mo	Corrected molecular weight
$\overline{M_N}$	Average molecular weight
N	Number of experimental points/ Number of components
$\overline{N}$	An integer equal to 4, 5, 10 or 11
P	Pressure
Q	Quadruple point
R	Universal gas constant
R'	Pipe radius
$\overline{R}$	Cavity radius
S	Molar entropy/ Specific gravity
T	Temperature
U	Overall-heat transfer coefficient
V	Vapour
$\overline{V}$	Volume
W	Weight percent of the inhibitor in the aqueous liquid
X	Inhibitor concentration in volume percent
Z	Compressibility factor
dw_i	Fraction of the asphaltene of molecular weight M_i
min	Minimum
max	Maximum
nc	Number of components
sI	Structure-I
sII	Structure-II

sH	Structure-H
a	Attractive parameter of the equation of state/ Constant in the binary interaction parameter of salt model/ Constant
$\bar{a}$	Parameter of the equation of state
b	Parameter of the equation of state/ Constant in the binary interaction parameter of salt model/ Margules coefficient
c	Parameter of the equation of state/ Constant in the binary interaction parameter of salt model/ a normalisation constant/ Constant
c_1	Constant in thermodynamic inhibitor correlation
c_2	Constant in thermodynamic inhibitor correlation
c_3	Constant in thermodynamic inhibitor correlation
d	Constant in the binary interaction parameter of salt model/ Density/ Constant
$\dot{d}$	Molar density ($kgmol/m^3$)
$\bar{d}$	Density (kg/m^3)
e	Constant in the binary interaction parameter
f	Fugacity/ Function
g	Gas
h	Binary interaction parameter between the dissolved salt and a non-electrolyte component
k	Binary interaction parameter for the classical mixing rules/ Correction factor
k'	Boltzmann's constant
$\bar{k}$	Interaction parameter in dielectric constant mixing rule of salt-free mixture

l	Binary interaction parameter for the asymmetric term/ An interaction parameter in Scott-Magat theory
$\dot{m}$	Mass flow-rate of natural gas
n	Number of moles/ Number of non-electrolyte components/ Number of ions that results from salt/ Refractive index
p	Pressure in psia
r	Distance
t	Temperature in ^{o}F
u	Parameter of the equation of state in general form
v	Molar volume
$\bar{v}$	Number of cavities of type m per water molecule in the unite cell
w	Parameter of the equation of state in general form/ Weight percent of salt/ Weight fraction of asphaltene in the reservoir fluid
$w(r)$	Spherically symmetric cell potential function
x	Liquid mole fraction/ Mole fraction in the liquid phase/ Salt-free mixture mole fraction/ Mole fraction of inhibitor
$\bar{x}$	Location of hydrate formation
y	Vapour mole fraction/ Mole fraction in the vapor state
z	Coordination number/ Specified molar composition of component i in the feed/ Mole fraction in natural gas/ Mole fraction in oil

Greek

Γ	Potential energy of interaction between two molecules / Gamma function
ΔC_{pw}	Heat capacity difference between the empty hydrate lattice and liquid water,

$\Delta C^{\bullet}_{pw}$	Reference heat capacity difference between the empty hydrate lattice and liquid water at 273.15 K
$\overline{\Delta G}$	Partial molar Gibbs free energy of mixing
ΔH_{fus}	Molar enthalpy of fusion
ΔH^{vap}	Enthalpy of vaporisation of hydrocarbons
Δh_w	Enthalpy difference between the empty hydrate lattice and ice / liquid water
Δh_w^0	Enthalpy difference between the empty hydrate lattice and ice at ice point and zero pressure
ΔT	Hydrate suppression/ Freezing point depression temperature
$\Delta u_m{}^V$	Energy change upon isothermal vaporisation of one mole of the maltene to the ideal gas state
ΔV	Volume change
Δv_w	Molar volume difference between the empty hydrate lattice and ice / liquid water
$\Delta \mu_w$	Chemical potential difference between the empty hydrate lattice and ice / liquid water
$\Delta \mu_w^{\circ}$	Chemical potential difference between the empty hydrate lattice and ice at ice point and zero pressure
$\Delta \mu_w^{\beta-H}$	Chemical potential difference of water between the empty hydrate lattice and the hydrate phase
$\Delta \mu_w^{\beta-I/L}$	Chemical potential difference of water between the empty hydrate lattice and the ice/liquid water phase

Φ	Volume fraction
Ψ	Power parameter in the EoS
Ω	Parameter in the EoS
α	Kihara hard-core radius/ Degree of salt ionization/ distribution function parameter
$\alpha(T_r)$	Temperature dependent function
β	Distribution function parameter
ε	Characteristic energy
ϕ	Fugacity coefficient
γ	Activity coefficient/ Gas gravity
δ	Solubility parameter
η	Salt-free mixture dielectric constant
θ	A physical property such as the critical properties, acentric factor, normal boiling point, density and specific gravity, refractive index parameter, and surface tension
θ_∞	Limiting value for that property as $M \rightarrow \infty$.
$\bar{\theta}$	Power coefficient
μ	Chemical potential
π	Number of phases
ρ	Density
σ	Collision diameter
σ^*	$\sigma^* = \sigma - 2\alpha$
χ	Interaction parameter between asphaltenes and maltene
ω	Acentric factor

ϖ	Parameter of distribution function

Superscript

DH	Debye-Hückel electrostatic term
HC	Hydrocarbon
EL	Electrostatic term
EoS	Equation of state term
Sat	Property at saturation
A	Asymmetric properties
C	Classical properties
D	Deposit (asphalt) phase
E	Excess
H	Hydrate
I	Ice
L	Liquid
T	Total
V	Vapour
sub	Sublimation properties
p	Asphalt phase
s	Oil phase
β	Empty hydrate lattice
∞	Infinite dilution
0	Reference property/ Standard state
1	Non-temperature dependent term in NDD mixing rules
2	Temperature dependent term in NDD mixing rules

Subscripts

CO_2	Carbon dioxide
HC	Hydrocarbon compound
EL	*Debye-Hückel* electrostatic contribution
E	Environment
I	Ice/ Symbol of temperature at $x = 0$
N_2	Nitrogen
T	Total
al	Alcohol, Hydrate organic inhibitor
asphalt	Asphalt
dilutor	Dilutor
exp	Experimental property
hydrate	Hydrate
ice	Ice
min	Minimum
max	Maximum
Non-Electrolyte	Non-electrolyte term
prd	Predicted property
pure,w	Pure water
salt	Salt
a	Index for properties/ asphaltene
b	Index for properties
c	Critical property
*c**	Index for properties
g	Gas

i, j	Molecular species
m	Type *m* of cavities/ Salt-free mixture/ Maltene/ minimum
p	Polar compound/ Asphalt phase
r	Reduced properties
s	Salt/ Oil phase
t	Temperature
w	Water
x	Valence
0	Reference property/ Symbol of freezing point of pure water (273.15 K)/ Oil
1	First quadruple point
2	Second quadruple point

CHAPTER 1

INTRODUCTION

Flow assurance is one of the key disciplines in petroleum exploration and production operations. The objective of flow assurance is to ensure uninterrupted flow of production from reservoirs to surface facilities at minimum capital and operation costs. Avoiding gas hydrates, asphaltene and wax are among the important aspects of flow assurance. Accurate knowledge of phase behaviour in systems containing gas hydrates and asphaltene is crucial to the design and operation of pipelines and production/ processing facilities.

Gas hydrates are solid crystalline compounds formed from mixtures of water and guest molecules of suitable sizes. Based on hydrogen bonding, water molecules form unstable lattice structures with several interstitial cavities. The gas molecules can occupy the cavities and, when a minimum number of cavities are occupied, the crystalline structure becomes stable and solid gas hydrates are formed, even at temperatures well above the ice point.

Since the 1930s the phenomenon of gas hydrate formation has been closely linked to the extraction of hydrocarbons from the earth's crust. Hammershmidt discovered that natural gas hydrates, and not ice as previously thought, were responsible for the blockage of gas transmission lines (1). Between the first discovery of gas hydrates in the early 1800s and the observation by Hammerschmidt (1) in the 1930s, gas hydrates were mainly regarded as a scientific curiosity without any practical implications. The fact that gas hydrates became associated with economical and safety matters in the petroleum industry kick-started an ever increasing research into the subject.

Today, from an engineering point of view, the all-important issue is hydrate control during petroleum exploration and production. Low seabed temperatures combined with high fluid pressures promote formation of clathrates in reservoir hydrocarbon-water fluid mixtures. Hydrates can block pipelines, subsea transfer lines, and, in the event of a gas kick during drilling, form in the well, in risers, *BOP*s (Blow-Out Preventers) and chokelines. Due to the above problems, considerable efforts are being put into the development of methods and tools, capable of predicting hydrate phase behaviour for related fluids. Furthermore, laboratory experiments are often carried out, generally to improve and to validate the predictive models.

The knowledge of gas hydrate phase behaviour is, on a whole, well documented. Especially the issue of hydrate phase boundary determination has received much attention over the years (2). Today, comprehensive thermodynamic models, mostly based on equations of state and statistical thermodynamics, are available for hydrate equilibrium predictions. However, competitive oil and gas prices together with increasing concerns for the environment requires ever more accurate modelling and necessitates novel hydrate control procedures. Probably the main areas of concern are the development of low dosage inhibitors, use of natural surfactants, and the introduction of environmental friendly chemical inhibitors. Lately, a significant shift in research efforts from thermodynamic to kinetic modelling of gas hydrates and a changing hydrate paradigm from apprehension to avoidance to risk management has been reported (2).

Not only competitive oil and gas prices and environmental issues justify continuing hydrate research with respect to petroleum exploration and production, new challenges also keep appearing such as the discovery of structure-H (3), record water depths in deepwater drilling with higher demands of hydrate control (2,4), and the use of hydrates

as a means of transporting stranded gas (5).

Naturally occurring gas hydrates are also of great significance in their potential for as strategic energy reserve and the possibilities for CO_2 disposal by sequestration. In the 1960s and 70s huge gas hydrate reserves were discovered in the permafrost regions and the deep-sea sediments, extending gas hydrate research into geosciences. Of particular interest are areas such as, quantifying the stability and amount of in-situ hydrates, and the possibility of commercial exploitation of the gas trapped in the hydrates. Gas hydrates in permafrost regions and deepwater sediments also received renewed interest in the 1990s when they were linked with global climate changes (6). Gas hydrates in subsea sediments can pose a potential geohazard to deepwater hydrocarbon drilling and production operations. Hydrates may act as a gas trap, with seafloor gas seeps and mud volcanoes, common to hydrate areas in hydrocarbon-rich provinces (e.g. Gulf of Mexico), as possible evidence for potentially hazardous excess gas at shallow depths. Drilling operations could cause pressure, temperature or chemical changes in sediments, which could cause dissociation of gas hydrates, resulting in seabed instability, gas release/blow-outs and potentially causing wellbore collapse.

Besides causing problems in the petroleum industry and being of great geoscientific interest the use of gas hydrates have also been suggested for many other purposes. Some of these are separation processes, such as desalination of seawater and waste water treatment (7, 8), storage of polluting gases (9), the application within the field of biotechnology (10) and etc.

This work focuses on the flow assurance issues associated with gas hydrates, which is detailed in the following chapters. As mentioned earlier, asphaltene is another important flow assurance concern. Asphaltenes are the toluene / benzene soluble

fractions that precipitate from petroleum when an excess (25 to 40 times) of n-heptane / n-pentane is mixed with petroleum and waiting at least four hours before filtering (11). Asphaltenes do not have a unique structural formula and their structure depends on the way they are formed, i.e. depending on the geo-chemistry of the crude oil (11). These studies show that asphaltenes are composed of condensed polynuclear aromatic hydrocarbons with aliphatic side chains and heteroatoms such as *N*, *O* and *S* found in both aromatic and non-aromatic portions. Polar molecules of asphaltenes also consist of metal (*Ni, V, Fe*) content of heavy oils, in addition to heteroatoms. The ratio of hydrogen/ carbon atoms is approximately around 0.8-1.4 and their molecular weights are typically in the 500-50,000 ranges (11).

Aphaltenes and resins (compounds soluble in n-pentane but insoluble in propane) may associate to form large aggregates of high molecular weight. As early as 1938, it was recognised that asphaltenes and resins form micelle particles (12). The asphaltene micelle particle has a core, which is formed by several aggregated asphaltene molecules with bipolar resin molecules adhered on the surface of the core. For the residue from heavy oil, a micelle is composed of 100 asphaltene molecules with a core diameter of 66 Å. If not for the resins, most of the asphaltene material would immediately precipitate from the crude oil due to a low solubility of asphaltene monomeric molecules in the bulk of the petroleum fluid (11).

Asphaltene precipitation causes fouling in the reservoir, in the well, in the pipeline and in the oil production and processing facilities. During production as the oil pressure drops, above the bubble point of some crudes, especially those containing high fractions of saturates, asphaltenes may precipitate. During enhanced oil recovery (*EOR*) when compressed gases, such as methane or carbon dioxide, are injected into the reservoir, asphaltenes may also precipitate. Once crude are brought to the surface, they are

commonly mixed in the field, in tankers and/or piplines. Blending crudes can also upset the delicate balance and precipitate asphaltenes. It is of great interest to be able to predict the conditions that lead to asphaltene precipitation.

Although several models have been proposed in recent years, none of them is capable of predicting precipitation of asphaltene satisfactorily. One of the fundamental difficulties encountered in modelling the phase behaviour of asphaltene-containing systems is the lack of suitable characterisation parameters. It is hard to model asphaltene precipitation because of the tendency of asphaltenes to aggregate, which makes their characterisation difficult. This aggregation tendency is caused by the polar nature of asphaltenes components, which has not been well understood yet. In fact, asphaltenes are not well-identified components/ mixtures. They consist of several polar components of aromatic nature with high molecular weights. In the majority of the cases, the complexity of the asphaltene fraction leads to the assumption that the asphaltenes can be regarded as one single pseudo-component (monodisperse). The main drawback of the monodisperse models is that they do not take into account the aggregation phenomenon of asphaltenes. In fact, the aggregation process produces a molecular weight distribution of aggregates, which also causes a polydispersity in asphaltene properties.

In this work, thermodynamic aspects of gas hydrate and asphaltene stability in petroleum production and transportation have been investigated. The study involves the modelling hydrate formation conditions in low water content systems (Chapters 3 and 4), inhibition effects of salt and/or organic inhibitor (Chapter 5), and modelling and issues of asphaltene precipitation in petroleum production (Chapters 6 and 7).

In order to assess the above outlined topics, thermodynamic formulations for gas hydrate formation and dissociation as well as asphaltene precipitation are needed. The

modelling of gas hydrates and asphaltenes is outlined in Chapter 2.

Production, transportation and processing of natural gases, especially in cold regions has renewed interest in determining the water content in the gases. The estimation of water content in gases, particularly at equilibrium with hydrates is difficult, because of the very low concentration of water in the gaseous phase. Literature survey reveals the availability of few sets of experimental data for water content of gases in equilibrium with hydrates and all other data represent metastable liquid water – gas equilibrium. Therefore, few predictive methods for the water content of gases at low temperatures, especially in equilibrium with hydrates have been reported in the literature as these methods are generally based on experimental data. Modelling water content of natural gases is treated in Chapters 3 and 4, which describes predicting water content of gases in equilibrium with liquid water (or ice) and gas hydrates, respectively. A thermodynamic model based on the Valderrama modification of the Patel-Teja equation of state and non-density mixing rules is extended to estimate the water content/ water dew point of gases. The results are then compared with independent data from the literature. A semi – empirical approach based on equality of fugacity concept is proposed for estimating the water content of natural gases. To take into account the presence of acid gases, a new analytical correction factor is then proposed. The results are then compared with some experimental data and other predictive methods.

Salts and chemical hydrate inhibitors can be used in avoiding gas hydrate problems in drilling, production and transportation. For ultra-deep waters, a combination of salts and organic inhibitors is generally required to prevent gas hydrate formation. In Chapter 5, a previously reported thermodynamic model for phase behaviour modelling of systems containing salt(s) is extended to systems containing salt and organic inhibitor. A number of experimental data have been used in the validation of the model.

A correlation for predicting the hydrate inhibition effects of single and mixed thermodynamic inhibitors is then constructed based on the results of the above model. The possibility of predicting hydrate inhibition effects of thermodynamic inhibitors from freezing point depression of the aqueous phase due to the presence of salt and/or organic inhibitor could have a real practical use, as measuring freezing point depression of aqueous phase is easier than hydrate suppression temperature. A simple equation, which relates hydrate inhibition effects of thermodynamic inhibitors to freezing point depression of aqueous phase, is developed.

The asphaltene precipitation is generally regarded as a source of problems in production, transportation and processing of reservoir fluids. Accurate information, including reliable thermodynamic model is necessary to avoid asphaltene precipitation problems. In Chapters 6 and 7, novel approaches for predicting asphaltene precipitation conditions are discussed. To estimate asphaltene flocculation/precipitation, a thermodynamic approach based on equation of state (*EoS*) is developed to predict the effect of temperature and pressure on asphaltene phase boundaries and to estimate the amount of the precipitated phase and the effect of changes in the system compositions. The polydispersity of asphaltenes is taken into account in molecular weight, mole fraction and critical properties. An appropriate mixing rule based on "*EoS + Gibbs free energy*" method is employed in order to obtain the attractive term. With the aim of calculating the Gibbs free energy term in the mixing rule of polydispers equation of state model, an activity coefficient approach is tested for modelling asphaltene flocculation/precipitation. The results of the model are compared with some literature data on asphaltene flocculation in light systems. However, the main limitation of activity coefficient models is that they cannot efficiently account for the effect of pressure on condensed phases. Therefore, activity coefficient approach is only used to

calculate the Gibbs free energy term in the polydispers equation of state approach. The results of developed polydispers equation of state approach are then compared with some selected data from the literature. The study investigates the impact of various parameters on asphaltene precipitation.

The conclusions of this thesis and recommendations for future work are presented in Chapter 8.

REFERENCES

1. Hammerschmidt, E.G. Formation of Gas Hydrates in Natural Gas Transmission Lines. *Industrial and Engineering Chemistry* 1934, *26(8)*, 851-855.
2. Sloan, E.D. Clathrate Hydrates of Natural Gases. 2nd ed., Marcel Dekker Inc., New York, 1998 (Also: Sloan, E. D. A changing hydrate paradigm from apprehension to avoidance to risk management. *Fluid Phase Equilibria* 2005, *228-229*, 67-74).
3. Ripmeester, J.A.; Tse, J.S.; Ratcliffe, C.I.; Powell, B.M. A New Clathrate Hydrate Structure. *Nature* 1987, *325*, 135-135.
4. Barker, J.W.; Gomez, R.K. Formation of Hydrates During Deepwater Drilling Operations. *Journal of Petroleum Technology* March 1989, 297-301.
5. Gudmundsson, J.S.; Anderson, V.; Levik, O.I.; Parlaktuna, M. Hydrate Concept for Capturing Associated Gas. SPE 50598, *proceedings of the 1998 SPE European Petroleum Conference*, 20-22 October, The Hague, The Netherlands, 247-258, 1998.
6. Henriet, J.-P.; Mienert, J. (eds) Gas Hydrates: Relevance to world margin stability and climatic change, Geological Society, London, Special Publications, 137, 1998.
7. Fabuss, B.M.; Korosi, A. Vapour Pressures of Binary Aqueous Solutions of NaCl, KCl, Na2SO4 and MgSO4 at Concentrations and Temperatures of Interest in Desalination Processes. *Desalination* 1966, 1, 140-148.
8. Gaarder, C.; Ngan, Y.T.; Englezos, P. Crystallization of Mechanical Pulp-Mill Effluents Through Hydrate Formation For the Recovery of Water. *ACS Symposium Series* 1994, *554*, 114-123.
9. Ohgaki, K.; Inoue, Y. A Proposal for Gas Storage on the Bottom of the Ocean, using Gas Hydrates. *International Chemical Engineering* 1994, *34(3)*, 417-419.
10. Nagahama, K.; Noritomi, H.; Koyama, A. Enzyme recovery from reversed micellar solution through formation of gas hydrates. *Fluid Phase Equilibria* 1996, *116*, 126-132.
11. Speight, J.G. The Chemistry and Technology of Petroleum, Marcel Dekker, New York. 1991.
12. Nellensteyn, F.I. The Colloidal Structure of Bitumens. The Science of Petroleum, Oxford University Press, London, 4, 2760, 1938.

CHAPTER 2

THERMODYNAMIC DESCRIPTIONS OF PHASES

2.1 INTRODUCTION

Sir Humphrey Davy's observation of chlorine hydrate in 1810 is generally regarded as the discovery of gas hydrates. Sir Davy formed a solid from an aqueous solution of chlorine cooled to below 9°C. In the following decades, hydrates of other, mainly inorganic, compounds were found. However, gas hydrates were not linked to matters outside the laboratory, and indeed the petroleum industry, until the 1930's when Hammerschmidt concluded that natural gas hydrates were responsible for blockage of gas transmission lines (1).

Gas hydrates are nonstoichiometric species, belonging to the group of clathrates. They should be distinguished from the stoichiometric hydrates common to inorganic chemistry, e.g., $CaSO_4 \cdot 2H_2O$ (gypsum). Clathrates are inclusion compounds, consisting of a host and a guest species. Clathrates can be aqueous, e.g., gas hydrates with water as the host, as well as nonaqueous, e.g., clathrasils with SiO_2 acting as the host.

Gas hydrates are, as other clathrates, crystalline compounds. By hydrogen bonding water molecules arrange into cavities, which become stable by entrapping guest molecules. When different sized cavities arrange themselves into crystals different hydrate structures appear. Not all cavities in the crystal structure need to be occupied by a guest molecule in order for the structure to be stable.

Three gas hydrate structures are commonly known to the petroleum industry. They are, hydrate structure-I (sI), structure-II (sII), and structure-H (sH). Some properties of the three hydrate structures are given in Table 2.1. Figure 2.1 presents the shape of the different gas hydrate cavities in the three structures.

Hydrate sI consists of a 12 Å body centred cubic unit cell with six small and two large cavities. The small cavities are dodecahedrons, i.e., polyhedra with 12 pentagonal faces (5^{12}). The large cavities have 12 pentagonal faces and 2 hexagonal faces ($5^{12}6^2$). Hydrate sI can accommodate guests with diameters up to 6 Å in size.

Hydrate sII also consists of two different polyhedra. The small cavities are, as for sI, dodecahedrons (5^{12}) whereas the large cavities have 12 pentagonal faces and 4 hexogonal faces ($5^{12}6^2$). Eight $5^{12}6^2$ and sixteen 5^{12} cavities link together to form a diamond cubic lattice with a cell parameter of 17.3 Å. Hydrate sII accommodates molecules up to around 7 Å in diameter. Jeffrey (2) has treated the properties of sI and sII in depth.

Hydrate sH was only discovered recently by Ripmeester and his group (3). In contrast to hydrate sI and sII, sH forms a hexagonal crystal lattice with the lattice parameters, a =12.26 Å and c = 10.17 Å. Hydrate sH consists of three different sized cavities, i.e., the dodecahedron (5^{12}), a medium sized cavity with 3 square faces, 6 pentagonal faces, and 3 hexagonal faces ($4^3 5^6 6^3$), and a large cavity with 12 pentagonal faces and 8 hexagonal faces ($5^{12}6^8$). Three 5^{12} cavities, two $4^3 5^6 6^3$ cavities and one $5^{12}6^8$ cavity form the unit cell of sH. Due to the large $5^{12}6^8$ cavity sH can accommodate molecules as large as almost 10 Å in diameter (1).

Unlike gas hydrates, asphaltenes do not have a unique structural formula and their structure depends on the way they are formed, i.e. depending on the geo-chemistry of the crude oil. By definition, asphaltenes are the toluene / benzene soluble fractions that precipitate from petroleum when an excess (25 to 40 times) of n-heptane / n-pentane is mixed with petroleum and waiting at least four hours before filtering. Asphaltenes are composed of condensed polynuclear aromatic hydrocarbons with aliphatic side chains and heteroatoms such as *N*, *O* and *S* found in both aromatic and non-aromatic portions. Polar molecules of asphaltenes also consist of metal (*Ni, V, Fe*) content of heavy oils, in addition to heteroatoms.

Asphaltenes and resins (compounds soluble in n-pentane but insoluble in propane) may associate to form large aggregates of high molecular weight. As early as 1938, it was recognised that asphaltenes and resins form micelle particles. Asphaltene micelle particle has a core, which is formed by several aggregated asphaltene molecules; bipolar resin molecules are adhered on the surface of the core. For the residue from heavy oil, a micelle is composed of 100 asphaltene molecules with a core diameter of 66 Å. If not for the resins, most of the asphaltene material would immediately precipitate from the crude due to a low solubility of asphaltene monomeric molecules in the bulk of the petroleum fluid. Figures 2.2 and 2.3 show the shape of the asphaltene micelle particles oil systems.

In the following paragraphs the modelling of natural gas hydrate and asphaltene is outlined with reference to hydrate formation and asphaltenes precipitation in the petroleum industry. A typical hydrate calculation problem may besides the three hydrate structures involve several other phases, e.g., vapour (V), liquid hydrocarbon (L_{HC}), water (L_W), ice (I). Furthermore, chemical inhibitors, e.g., methanol, and salts may also be present, leading to relatively complex calculations. Consequently,

asphaltenes precipitation problem could involve vapour, liquid hydrocarbon and asphalt phases.

2.2 THERMODYNAMIC DESCRIPTION

For a chemical system to be at thermodynamic equilibrium, the chemical potential of each component throughout the system must be uniform:

$$\mu_{i1} = \ldots = \mu_{ij} = \ldots = \mu_{i\pi} \quad , \qquad i = 1, 2, \ldots, N \tag{2.1}$$

where μ_{ij} is the chemical potential of component i in phase j, N is the number of components and π the number of phases. For an isothermal system Equation 2.1 reduces to equality of fugacity for each component in different phases:

$$f_{i1} = \ldots = f_{ij} = \ldots = f_{i\pi} \quad , \qquad i = 1, 2, \ldots, N \tag{2.2}$$

In the most general case, i.e., when all components are present in all phases, there will be $N(\pi\text{-}1)$ such equations. In addition, material balances impose another set of $N+\pi$ equations:

$$z_i = \sum_{j}^{\pi} F_j x_{ij} \tag{2.3}$$

$$\sum_{i}^{N} x_{ij} = 1 \tag{2.4}$$

where z_i is the specified composition of the feed, F_j the fraction in moles of phase j, and x_{ij} the mole fraction of component i in phase j. Totally, Equation 2.2 to 2.4 result in $\pi(N+1)$ equations with an equal number of unknowns.

Concerning equilibrium calculations two cases are of interest, phase boundary calculations where $F_j = 0$, and flash calculations where $F_j \neq 0$ for all included phases.

In this work the general multiphase flash routine by Cole and Goodwin (4) is adopted to solve the system, explicit expressing the fugacities of all components of all phases, including the hydrate phase, as functions of temperature, pressure and composition (5). This approach enables use of, e.g., the Michelsen flash algorithm and phase stability calculations by minimisation of the Gibbs free energy (6, 7).

In the following sections, the models and equations used for evaluating the fugacities in various phases common to hydrate / asphaltene calculations are described in more details.

2.2.1. Fluid phase equilibria

Danesh et al. (8) compared 10 equations of state with classical mixing rules for predicting the phase behaviour and volumetric properties of hydrocarbon fluids. They concluded that the Valderrama modification (9) of the Patel and Teja cubic equation of state (*VPT-EoS*) (10) was superior to the other tested equations of state, particularly when the *EoS* were compared without any use of binary interaction parameters (*BIP*s). In this work the *VPT-EoS* is used to model all the fluid phases, i.e., V, L_{HC}, and L_W for hydrate calculation problem, as it is believed that this *EoS* is a strong tool for modelling systems containing water and alcohols (11).

The *VPT EoS* is given by:

$$P = \frac{RT}{v-b} - \frac{\bar{a}\alpha(T_r)}{v(v+b)+c(v-b)} \tag{2.5}$$

with:

$$\bar{a} = \frac{\Omega_a R^2 T_c^2}{P_c} \tag{2.6}$$

$$b = \frac{\Omega_b R T_c}{P_c} \tag{2.7}$$

$$c = \frac{\Omega_c R T_c}{P_c} \tag{2.8}$$

$$\alpha(T_r) = \left[1 + F\left(1 - T_r^{\Psi}\right)\right]^2 \tag{2.9}$$

where P is the pressure, T is the temperature, v is the molar volume, R is the universal gas constant, and $\Psi = 1/2$. The subscripts c and r denote critical and reduced properties, respectively.

The coefficients Ω_a, Ω_b, Ω_c, and F are given by:

$$\Omega_a = 0.66121 - 0.76105 Z_c \tag{2.10}$$

$$\Omega_b = 0.02207 + 0.20868 Z_c \tag{2.11}$$

$$\Omega_c = 0.57765 - 1.87080 Z_c \tag{2.12}$$

$$F = 0.46286 + 3.58230(\omega Z_c) + 8.19417(\omega Z_c)^2 \tag{2.13}$$

where Z_c is the critical compressibility factor, and ω is the acentric factor. Avlonitis et al. (11) relaxed the constraints on F and Ψ for water and methanol in order to improve the predicted vapour pressure and saturated volume for these compounds:

Methanol: $F = 0.76757, \quad \Psi = 0.67933$

Water: $F = 0.72318, \quad \Psi = 0.52084$

Later, Tohidi-Kalorazi (12) relaxed the alpha function for water, $\alpha_w(T_r)$, using experimental water vapour pressure data in the range of 258.15 to 374.15 K, in order to improve the predicted water fugacity:

$$\alpha_w(T_r) = 2.4968 - 3.0661 T_r + 2.7048 T_r^2 - 1.2219 T_r^3 \tag{2.14}$$

The relation of Avlonitis et al. (11) for methanol and Tohidi-Kalorazi (12) for water are used in the present work.

Other polar components have also been modelled using the *VPT-EoS*. In order to obtain satisfactory results for these components, it was not found necessary to adopt approaches similar to that for water and methanol.

Nonpolar-nonpolar binary interactions in fluid mixtures are described by applying classical mixing rules as follows:

$$a = \sum_i \sum_j x_i x_j a_{ij} \tag{2.15}$$

$$b = \sum_i x_i b_i \tag{2.16}$$

$$c = \sum_i x_i c_i \tag{2.17}$$

$$a_{ij} = (1 - k_{ij})\sqrt{a_i a_j} \tag{2.18}$$

where k_{ij} is the standard binary interaction parameter.

For polar-nonpolar interaction, however, the classical mixing rules are not satisfactory and more complicated mixing rules are necessary. In this work the non-density dependent (*NDD*) mixing rules developed by Avlonitis et al. (11) are applied to describe mixing in the a-parameter:

$$a = a^C + a^A \tag{2.19}$$

where a^C is given by the classical quadratic mixing rules (Equation 2.15 and 2.18). The term a^A corrects for asymmetric interaction which cannot be efficiently accounted for by classical mixing:

$$a^{A} = \sum_{p} x_p^2 \sum_{i} x_i a_{pi} l_{pi} \tag{2.20}$$

$$a_{pi} = \sqrt{a_p a_i} \tag{2.21}$$

$$l_{pi} = l_{pi}^{0} - l_{pi}^{1}(T - T_0) \tag{2.22}$$

where p is the index of polar components. The *BIP*s used in the *NDD* mixing rules in this work for already modelled systems are given in Tables 2.2, 2.3.

Using the above *EoS* and the associated mixing rules the fugacity of each component in all fluid phases is calculated from:

$$f_i = x_i \phi_i P \tag{2.23}$$

where P is the pressure, and x_i and ϕ_i is the mole fraction and the fugacity coefficient of component i, respectively. The calculation of the fugacity coefficients using the *NDD* mixing rules, for a general *EoS* as well as the *VPT-EoS*, is given in Appendix A.1.

2.2.2. Electrolyte solutions

When electrolytes are present the fugacities in the water rich phase are calculated by combining the equation of state with the Debye-Hückel electrostatic contribution for taking into the account the effect of salt (14):

$$\ln \phi_i = \ln \phi_i^{EoS} + \ln \gamma_i^{EL} \qquad i = 1, 2, ..., N \tag{2.24}$$

where N is the number of non-electrolyte components, ϕ_i is the fugacity coefficient of component i, ϕ_i^{EoS} is the fugacity coefficient of component i calculated by an EoS, neglecting the electrostatic effect, and γ_i^{EL} is the contribution of the electrostatic term. Using the Debye-Hückel activity coefficient, the final form of the second term in Equation 2.24 becomes (14)

$$\ln \gamma_i^{DH} = \frac{2AM_m h_{is}}{B^3} f\left(BI^{1/2}\right) \tag{2.25}$$

where M_m is the salt-free mixture molecular weight determined as a molar average, and h_{is} is the interaction coefficient between the dissolved salt and a non-electrolytic compound. The function $f\left(BI^{1/2}\right)$ is obtained from (14):

$$f\left(BI^{1/2}\right) = 1 + BI^{1/2} - \frac{1}{\left(1 + BI^{1/2}\right)} - 2\ln\left(1 + BI^{1/2}\right) \tag{2.26}$$

where I is the ionic strength. The parameters A and B are given by (14):

$$A = \frac{1.327757 \cdot 10^5 d_m^{1/2}}{(\eta_m T)^{3/2}} \tag{2.27}$$

$$B = \frac{6.359696 d_m^{1/2}}{(\eta_m T)^{1/2}} \tag{2.28}$$

where d_m is the density of the salt-free mixture and η_m is the salt-free mixture dielectric constant which can be calculated from (14):

$$\eta_m = x_w \eta_w \tag{2.29}$$

x_w and η_w are the salt-free mole fraction and dielectric constant of water, respectively. The dielectric constants of dissolved non-electrolyte compounds have been neglected, relative to that of water (14).

Tohidi et al. (13) presented values for the binary interaction parameter, h_{ws}, between water and dissolved salt for 9 electrolytes. Later, Østergaard (15) extended the work for more salts. Two sets of experimental data were used to optimise h_{ws}, i.e., vapour pressure depression of water due to the presence of salt at 373.15 K and freezing point depression of water due to the presence of salt.

In this work, the above model is extended to modelling the phase behaviour of electrolyte solutions containing organic inhibitors by taking into account interaction of all species in the aqueous solution and by correcting the system properties, such as, dielectric constant, density and molecular weight.

2.2.3. Ice phase

The fugacity of a pure solid can, as for a supersaturated pure liquid, be calculated using the Poynting correction, i.e., assuming that the volume of the supersaturated phase is constant at the volume for the saturated phase (16, 17). For ice the expression becomes:

$$f_w^I = \phi_w^{sat} P_I^{sat} \exp\left(\frac{v_I\left(P - P_I^{sat}\right)}{RT}\right) \tag{2.30}$$

where f_w^I is the fugacity of water in the ice phase, ϕ_w^{sat} is the water fugacity coefficient in the vapour phase at pressure equal to the ice vapour pressure, P_I^{sat} is the ice vapour pressure, v_I is the ice molar volume, R is the universal gas constant, and P and T is the system pressure and temperature, respectively.

The ice molar volume (cm^3/mol) is calculated using following expression (12):

$$v_I = 19.655 + 0.0022364 \times (T - 273.15) \tag{2.31}$$

where v_I and T are in $cm^3/gmol$ and *Kelvin*, respectively and the ice vapour is calculated using (12):

$$\log(P_I^{sat}) = -1033/T + 51.06 \times \log(T) - 0.09771 \times T + 7.036 \times 10^{-5} \times T^2 - 98.51 \tag{2.32}$$

where T and P_I^{sat} are in *Kelvin* and *mmHG*, respectively. It should be noted that the above equation was developed in the range of 183.15 to 273.15 K (12).

2.2.4. Hydrate phase equilibria

The van der Waals and Platteeuw (18) statistical thermodynamic model, based on ideal solution theory, is used to model the gas hydrate phases. The model, similar to Langmuir gas adsorption theory, considers the guest molecule to move around in a spherical cavity constructed of water molecules. Each cavity contains at most one guest molecule, and there is no interaction between the encaged molecules (19). Furthermore, the presence of the guest molecule in the cavity does not distort the hydrate crystal lattice.

The fugacity of water in the hydrate phase is given by (17):

$$f_w^H = f_w^\beta \exp\left(-\frac{\Delta\mu_w^{\beta-H}}{RT}\right) \tag{2.33}$$

where f_w^β is the fugacity of water in the empty hydrate lattice, and R and T are the gas constant and absolute temperature, respectively. $\Delta\mu_w^{\beta-H}$ is the chemical potential difference of water between the empty hydrate lattice, μ_w^β, and the hydrate phase, μ_w^H, and is obtained from the van der Waals and Platteeuw expression (17, 19):

$$\Delta\mu_w^{\beta-H} = \mu_w^\beta - \mu_w^H = RT\sum_m \nu_m \ln\left(1+\sum_j C_{jm} f_j\right) \tag{2.34}$$

where ν_m is the number of cavities of type m per water molecule in the unit cell, f_j is the fugacity of the gas component j. C_{jm} is the Langmuir constant, which accounts for the gas-water interaction in the cavity. Numerical values for the Langmuir constant can be calculated by choosing a model for the guest-host interaction. van der Waals and Platteeuw (18) used the Lennard-Jones potential function and showed that the Langmuir constant is a function of temperature according to the relation (17-19):

$$C_{jm}(T)=\frac{4\pi}{kT}\int_0^{\infty}\exp\left(-\frac{w(r)}{kT}\right)r^2dr \tag{2.35}$$

where k is Boltzmann's constant. The function $w(r)$ is the spherically symmetric cell potential in the cavity, with r measured from centre, and depends on the intermolecular potential function chosen for describing the encaged gas-water interaction. In the present work the Kihara potential function is used as described in Section (2.2.5).

The fugacity of water in the empty hydrate lattice, f_w^{β} in Equation 2.33, is given by (17):

$$f_w^{\beta}=f_w^{I/L}\exp\left(\frac{\Delta\mu_w^{\beta-I/L}}{RT}\right) \tag{2.36}$$

where $f_w^{I/L}$ is the fugacity of pure ice or liquid water and the quantity inside the parentheses is given by the following equation (17, 20):

$$\begin{aligned}\frac{\Delta\mu_w^{\beta-I/L}}{RT}&=\frac{\mu_w^{\beta}(T,P)}{RT}-\frac{\mu_w^{I/L}(T,P)}{RT}\\&=\frac{\Delta\mu_w^{0}}{RT_0}-\int_{T_0}^{T}\frac{\Delta h_w^{\beta-I/L}}{RT^2}dT+\int_{P_0}^{P}\frac{\Delta v_w^{\beta-I/L}}{RT}dP\end{aligned} \tag{2.37}$$

where μ_w^{β} and $\mu_w^{I/L}$ are the chemical potential of the empty hydrate lattice and of pure water in the ice (I) or the liquid (L) state, respectively. P is the equilibrium pressure and T_0 is the absolute temperature at the ice point. $\Delta\mu_w^0$ is the reference chemical potential difference between water in the empty hydrate lattice and pure water in the ice phase at 273.15 K. $\Delta h_w^{\beta-I/L}$ and $\Delta v_w^{\beta-I/L}$ are molar enthalpy and volume differences between an empty hydrate lattice and ice or liquid water. $\Delta h_w^{\beta-I/L}$ is given by the following equation (17, 20):

$$\Delta h_w^{\beta-l/L} = \Delta h_w^0 + \int_{T_0}^{T} \Delta C_{pw} dT \tag{2.38}$$

where Δh_w^0 is the enthalpy difference between the empty hydrate lattice and ice, at the ice point and zero pressure. The heat capacity difference between the empty hydrate lattice and the pure liquid water phase is also temperature dependent and the equation recommended by Holder et al. (20) is used:

$$\Delta C_{pw} = -37.32 + 0.179(T - T_0) \qquad T > T_0 \tag{2.39}$$

Furthermore, the heat capacity difference between hydrate structures and ice is set equal to zero.

Using the approach by Parrish and Prausnitz (19), Metha and Sloan (21) later extended the van der Waals and Platteeuw (18) thermodynamic model to include structure-H hydrates. Table 2.4 presents the reference properties of the hydrate structures used in this work, as reported by Parrish and Prausnitz (19), Dharmawardhana et al. (22), and Mehta and Sloan (21).

2.2.5. Relating the Langmuir constant to cell potential parameters

In order to employ the statistical thermodynamic model, outlined in the previous section, a model is needed to evaluate the interaction energy between water and guest molecules in the hydrate. In the original work by van der Waals and Platteeuw (18) the Lennard-Jones 6-12 potential was used. However, McKoy and Sinanôglu (23) suggested that the Kihara potential for spherically symmetric molecules (24) was better for both larger and also non-spherical molecules. The latter potential function is used in this work.

According to the Kihara model each molecule has an impenetrable hard core surrounded by penetrable soft electron clouds. The Kihara potential function is identical to that of Lennard-Jones except that the intermolecular distance is taken not as that between the molecular centres but rather as the minimum distance between the surfaces of the molecule cores. The Kihara potential function with three adjustable parameters is given as (19):

$$\Gamma(r)=\infty \qquad r=2\alpha \tag{2.40}$$

$$\Gamma(r)=4\varepsilon\left[\left(\frac{\sigma^*}{r-2\alpha}\right)^{12}-\left(\frac{\sigma^*}{r-2\alpha}\right)^{6}\right] \qquad r>2\alpha \tag{2.41}$$

where $\Gamma(r)$ is the potential energy of interaction between two molecules when the distance between their centres is equal to r. ε is the depth of the energy well, α is the radius of the spherical molecular core, $\sigma^*=\sigma-2\alpha$, where σ is the collision diameter, i.e., the distance where $\Gamma=0$. The Kihara model has three adjustable parameters, namely, α, σ, and ε. Figure 2.4 shows the Kihara potential as function of the distance between two molecules.

Based on the chosen potential energy function the spherically symmetric cell potential in the cavities (Equation 2.35) needs to be derived. McKoy and Sinanôglu (23) summed up all these guest-water binary interactions inside the cell to yield an overall cell potential:

$$w(r)=2z\varepsilon\left[\frac{(\sigma^*)^{12}}{R^{11}r}\left(\delta^{10}+\frac{\alpha}{R}\delta^{11}\right)-\frac{(\sigma^*)^{6}}{R^{5}r}\left(\delta^{4}+\frac{\alpha}{R}\delta^{5}\right)\right] \tag{2.42}$$

$$\delta^N=\frac{1}{N}\left[\left(1-\frac{r}{R}-\frac{a}{R}\right)^{-N}-\left(1+\frac{r}{R}-\frac{a}{R}\right)^{-N}\right] \tag{2.43}$$

where z is the coordination number of the cavity, R is the free cavity radius, r is the distance of the guest molecule form the cavity centre, and N, is an integer equal to 4, 5, 10, or 11.

Tohidi-Kalorazi (12) and Østergaard (15) described the optimisation procedure employed for determining the Kihara potential parameters and reported these parameters for conventional gas hydrate forming components, which were used in this work (Table 2.5).

2.2.6. Asphaltene phase equilibria

The main assumption in this work is that asphaltene precipitation is considered as a reversible process, and thus, allowing the use of molecular thermodynamics. First, a vapour-liquid flash calculation is performed on reservoir fluid using a model based on an appropriate *EoS* with random mixing rules. Calculation of asphaltene phase equilibria is then made on the remaining liquid hydrocarbon phase, assuming asphaltenes precipitation does not have any effect on vapour-liquid equilibrium of reservoir fluid.

2.2.6.1. Activity coefficient based model

A new approach based on the Scott-Magat (25) polymer theory, in which it is assumed that asphaltenes have a distribution of molecular weight is used for estimating asphaltene precipitation/solubility. To determine the solubility/precipitation from the liquid hydrocarbon phase, one must utilise the equilibrium conditions between the two-phases:

$$\overline{\Delta G_m} = \overline{\Delta G_m'} \qquad (2.44).$$

$$\overline{\Delta G_i} = \overline{\Delta G_i'} \tag{2.45}$$

where $\overline{\Delta G_m}$ and $\overline{\Delta G_i}$ are partial molar Gibbs free energies of mixing of the maltene (asphaltene free oil) and of the *i*th fraction of the asphaltene and the *prime* represents the asphalt phase. There are, of course, *i* simultaneous equations of the type of equation (2.45), one for each distinct fraction of asphaltene:

$$ln\Phi_m+(1-\Phi_m)(1-\frac{1}{\overline{M}_N})+\chi(1-\Phi_m)^2=ln\Phi_m'+(1-\Phi_m')(1-\frac{1}{\overline{M}_N'})+\chi(1-\Phi_m')^2 \tag{2.46}$$

$$ln\Phi_i+1-\frac{M_i}{\overline{M}_N}(1-\Phi_m)-M_i\Phi_m+\chi M_i\Phi_m^2=ln\Phi_i'+1-\frac{M_i}{\overline{M}_N'}(1-\Phi_m')-M_i\Phi_m'+\chi M_i\Phi_m'^2 \tag{2.47}$$

where Φ_m and Φ_i are the volume fractions of maltene and the *i*th fraction of asphaltenes, respectively. M_i is the molecular weight of the *i*th fraction of asphaltenes and $\overline{M}_N$ is the average molecular weight. χ stands for interaction parameter between asphaltenes and maltene, which is defined as:

$$\chi=\frac{V_m[(\delta_m-\delta_a)^2+2l\delta_m\delta_a]}{RT} \tag{2.48}$$

where δ stands for the solubility parameter and subscripts m and a indicate maltene and asphaltene, respectively. R, T and l represent the universal gas constant, temperature and an interaction parameter, respectively.

The solubility can finally be expressed as:

$$\text{Asphaltene fraction dissolved}=\int_{M_\infty}^{\infty}\frac{f(M)dM}{1+(\frac{\rho_0}{\rho_a})(\frac{w_a}{1-w_a})\times\frac{1}{(\Phi_a')_{M=\infty}}\times\exp(A_\infty M)} \tag{2.49}$$

where,

$$A_\infty=2\chi(\Phi_a')_{M=\infty}+ln[1-(\Phi_a')_{M=\infty}] \tag{2.50}$$

and $(\Phi_a')_{M=\infty}$ is a function of χ alone:

$$ln[1-(\Phi_a')_{M=\infty}]+(\Phi_a')_{M=\infty}+\chi(\Phi_a')^2_{M=\infty}=0 \qquad (2.51)$$

In the above equations, $f(M)$ is a molecular weight distribution function, M_m stands for minimum molecular weight of asphaltenes. ρ_a, ρ_0 and w_a are the density of asphaltene, density of oil, weight fraction of asphaltene in the reservoir fluid, respectively.

2.2.6.2. Equation of state based model

In this model, it is assumed that asphaltenes form a liquid phase free of other components, in other word only asphaltenes precipitate into a new liquid phase. As mentioned in section 2.2.6.1, in reality, all the fractions could potentially partition. However, allowing all components to partition significantly increases the time for the equation of state based model to converge. Furthermore, the liquid state of asphaltene corresponds with the visual observations, where the precipitated phase is seen as a sticky phase, at reservoir temperatures.

In this model, a simple multiphase flash routine is adopted to solve the system, explicitly expressing the fugacities of all components of all phases, as functions of temperature, pressure and composition. An appropriate *EoS* with appropriate mixing rules is used to calculate fugacities.

The upper boundary of asphaltene precipitation is a thermodynamic transition of asphaltenes from a single-phase hydrocarbon above its saturation pressure to the precipitated phase. To calculate the upper boundary of asphaltene precipitation, a two-phase equilibrium calculation is made:

$$f_i^{HC}=f_i^{D} \qquad i=M+1, N \qquad (2.52)$$

The lower boundary of asphaltene precipitation is a thermodynamic transition of asphaltenes from the precipitated phase to a two-phase hydrocarbon system. For calculation of the lower boundary of asphaltene precipitation, a vapour-liquid-liquid equilibrium calculation is done.

$$f_i^V = f_i^L \qquad i=1,M \tag{2.53}$$

$$f_i^V = f_i^L = f_i^D \qquad i=M+1, N$$

In the above equations, f_i is the fugacity of component i, and superscripts HC, V, L and D represent the hydrocarbon, vapour, liquid and deposit (asphalt) phases, respectively and the subscripts M and N correspond to the number of non-asphaltenic components and the total number of components in the system, respectively.

The amount of the precipitated asphaltene is estimated by either a two-phase flash calculation (between the upper point and the saturation point) or a vapour-liquid-liquid flash calculation (between the lower point and the saturation point). To find the number of the existing phases in equilibrium, it is necessary to do a phase stability analysis by using the Gibbs free energy minimisation method. For this purpose, a reasonable maximum number of phases at equilibrium are assumed and then the model searches for the non-existing phases using material balance restrictions, as discussed in the negative flash approach.

Two cases have been investigated:

1) Asphaltene as a single pseudo component

2) Asphaltene as a continuous family

2.3 CONCLUSIONS

The thermodynamic formulations used in this work have been outlined. They include an *EoS* based fluid phase model, a statistical thermodynamic hydrate model, a Poynting correction based ice model, a combined *EoS* and activity coefficient based electrolyte model, a polymer based asphaltene model and an equation of state based asphaltene model. The Valderrama modification of the Patel and Teja cubic equation of state with non-density dependent mixing rules is used in thermodynamic modelling of all fluid phases in hydrate modelling section (Section 2.2.1). Ice is modelled as a subcooled liquid (Section 2.2.3) and electrolyte solutions are modelled by combining the equation of state model with a modified Debye-Hückel electrostatic term (Section 2.2.2). The hydrate phases are modelled by the solid solution theory of van der Waals and Platteeuw (Section 2.2.4). Asphaltenes are modelled by the Scott-Magat (25) polymer theory (Section 2.2.6) or an equation of state based asphaltene model (Section 2.2.7).

TABLES

Table 2.1. Hydrate unit cell characteristics of structure-I, II, and H (1).

Structure	I		II		H		
Crystal system	Cubic		Cubic		Hexagonal		
Lattice parameter/Å	12		17.3		$a = 12.26, c = 10.17$		
H_2O/unit cell	46		136		34		
Total No. of cavities/ unit cell	8		24		6		
Cavity type	5^{12}	$5^{12}6^2$	5^{12}	$5^{12}6^4$	5^{12}	$4^3 5^6 6^3$	$5^{12}6^8$
Radius of cavity/Å	3.95	4.3	3.91	4.73	3.91	4.06	5.71
Coordination No.	20	24	20	28	20	20	36
Cavities/unit cell	2	6	16	8	3	2	1

Table 2.2. *BIP*s (12) between natural gas main component (*hc*) and methanol (*al*) for the *VPT-EoS* (9) and *NDD* mixing rules (11).

System	k_{al-hc}	l_{al-hc}^{0}	$l_{al-hc}^{1} \times 10^4$
Methane- Methanol	0.2538	0.7319	6.88
Ethane- Methanol	0.0137	0.0519	21.7
Propane- Methanol	0.0278	0.0779	0.00
n-Butane- Methanol	0.1465	0.2917	0.00
Nitrogen- Methanol	0.2484	1.0440	7.22
Hydrogen Sulphide- Methanol	0.0694	0.1133	0.00
Carbon Dioxide- Methanol	0.0510	0.0700	11.56

(*BIP*s between natural gas main component and water are given in Chapter-3).

Table 2.3. *BIP*s (12) between natural gas main components for the *VPT-EoS* (9).

System	Carbon Dioxide	Nitrogen	Hydrogen Sulphide
Methane	0.092	0.035	0.080
Ethane	0.134	0.038	0.095
Propane	0.128	0.070	0.088
n-Butane	0.138	0.114	0.050
Nitrogen	-	-	0.176
Hydrogen Sulphide	-	-	-
Carbon Dioxide	-	-0.036	0.088

Table 2.4. Thermodynamic reference properties for hydrate structure-I, II, and H.

Structure	I	II	H
$\Delta\mu_w^0/(\text{Jmol}^{-1})$	1297[#]	937[#]	914.38[¤]
$\Delta h_w^0/(\text{Jmol}^{-1})^{\dagger}$	1389[#]	1025[#]	846.57[¤]
$\Delta v_w^0/(\text{cm}^3\text{mol}^{-1})^{\ddagger}$	3.0[§]	3.4[§]	3.85[¤]

† In the liquid water region subtract 6009.5 J/mol from Δh_w^0.

‡ In the liquid water region add 1.601 cm^3/mol to Δv_w.

Dharmawardhana et al. (22).

§ Parrish and Prausnitz (19).

¤ Mehta and Sloan (21).

Table 2.5. Kihara potential parameters for gas-water interactions (12).

Component	α /	σ^* /	(ε/k') / K
Methane	0.2950	3.2512	153.69
Ethane	0.4880	3.4315	183.32
Propane	0.7300	3.4900	189.27
n-Butane	1.0290	3.4000	210.58
Nitrogen	0.3350	3.2171	128.39
Carbon Dioxide	0.7530	2.9040	171.97
Hydrogen Sulphide	0.7178	2.8770	210.58

$\sigma^* = \sigma - 2\alpha$

FIGURES

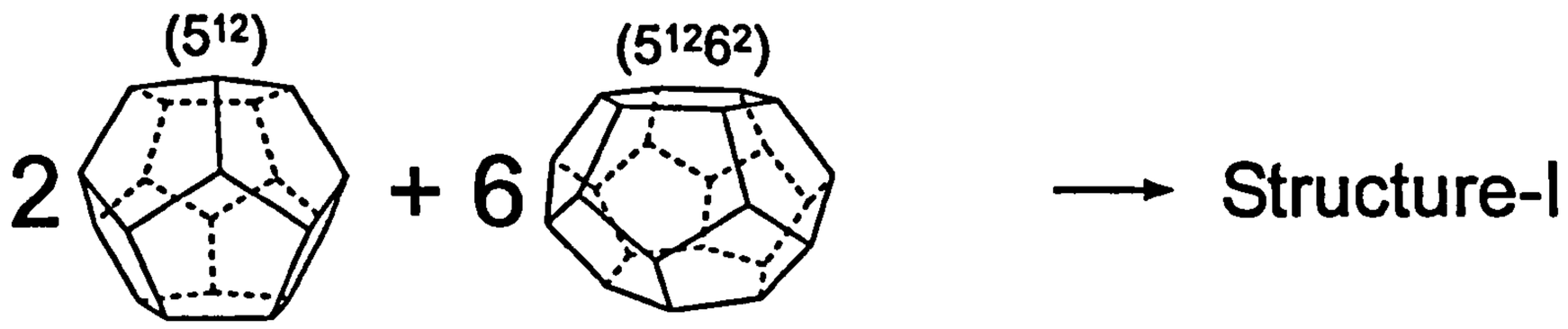

Figure 2.1. Cavities in gas hydrate structures.

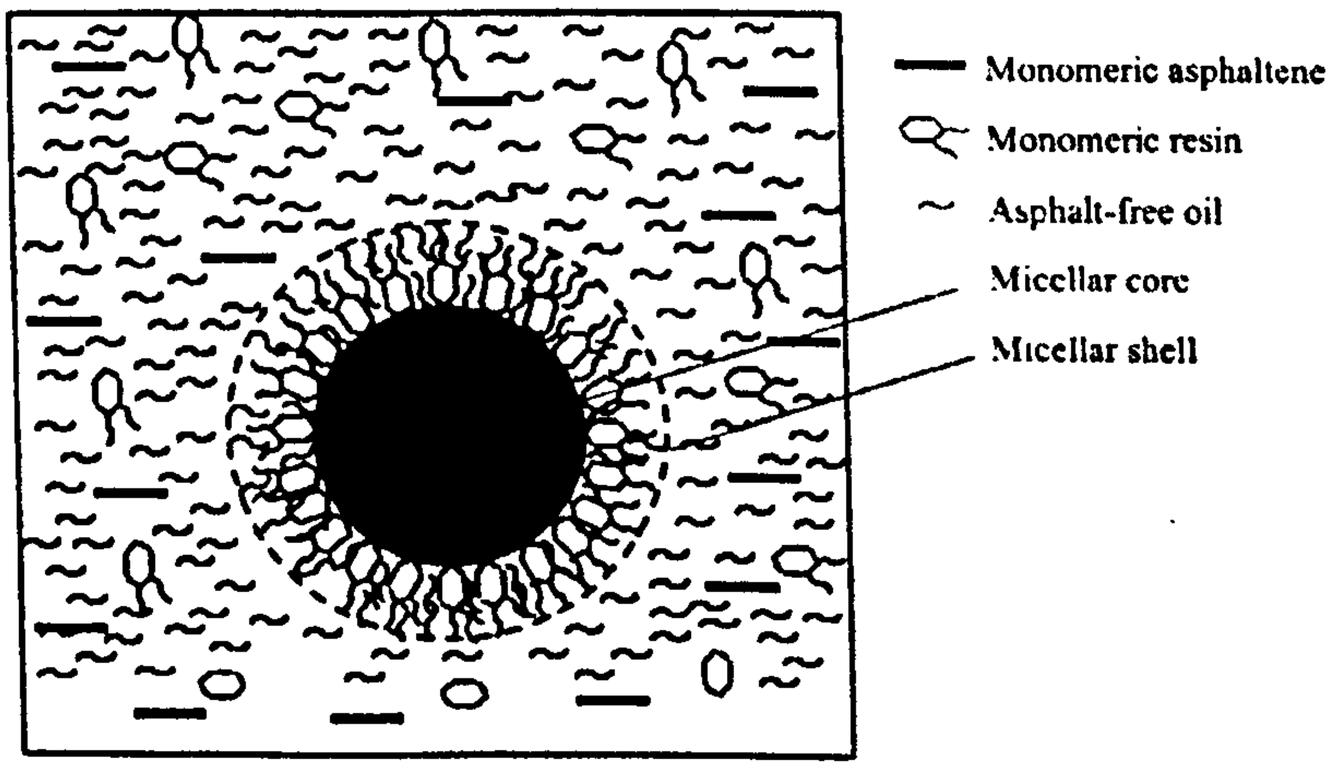

Figure 2.2. Schematic of a micelle in crude (26).

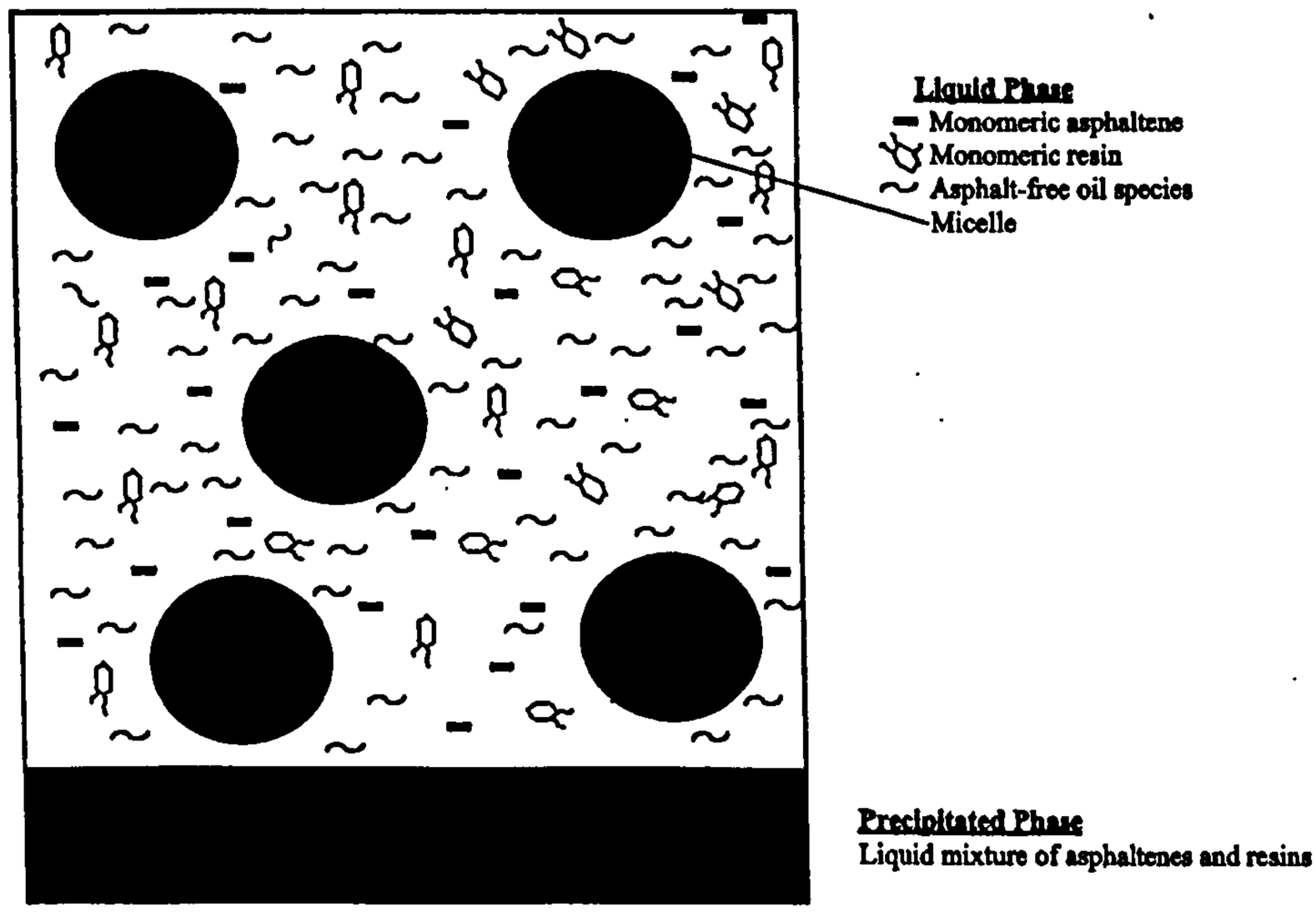

Figure 2.3. Schematic representation of crude system (26).

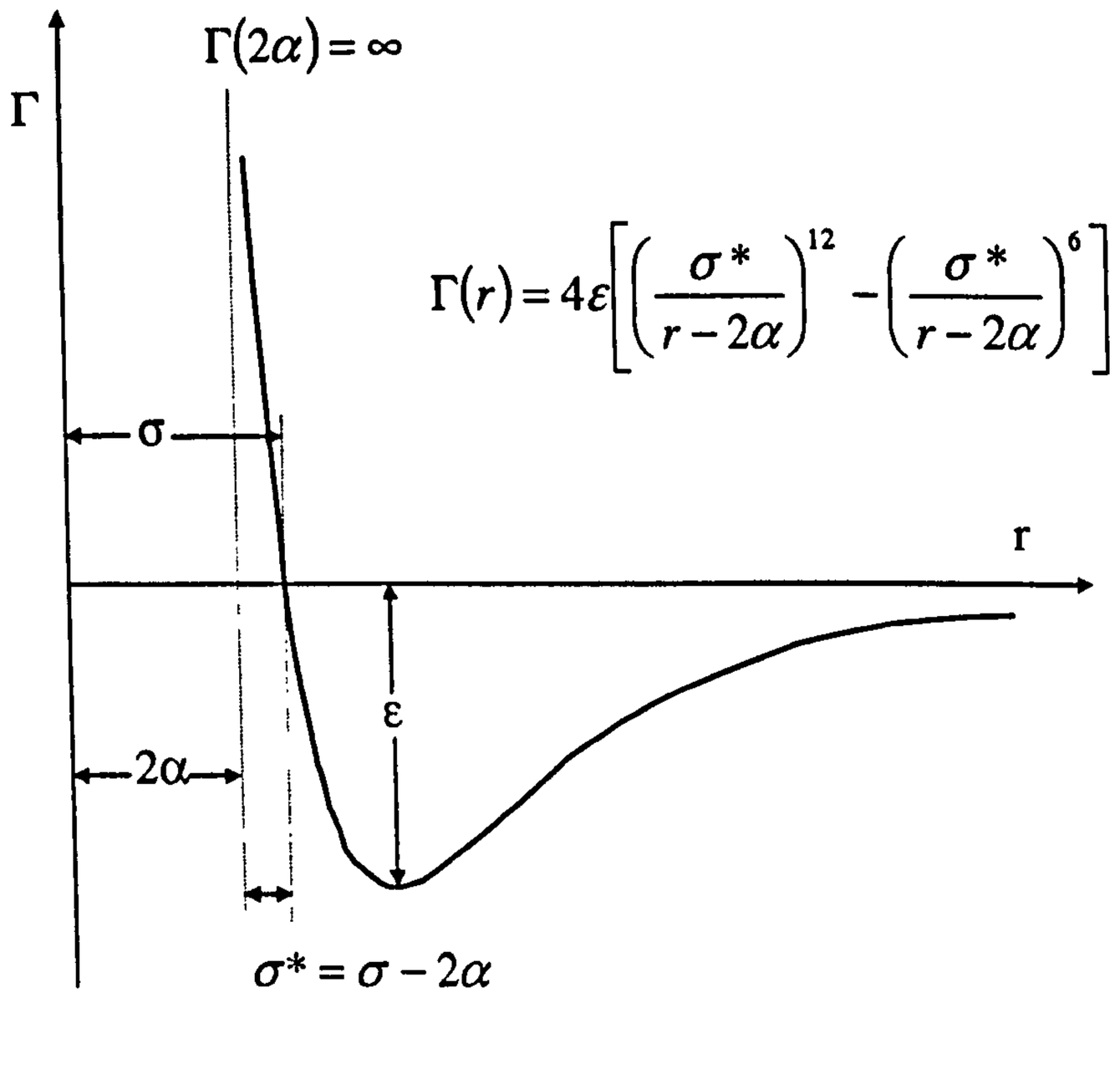

Figure 2.4. Potential function in the Kihara model.

REFERENCES

1. Sloan, E. D. Clathrate Hydrates of Natural Gases. 2nd ed., Marcel Dekker Inc., New York, 1998.
2. Jeffrey, G. A. Hydrate Inclusion Compounds, Chapter 5 in: Atwood, J. L.; Davies, J. E. D.; MacNichol, D. D. Inclusion Compounds, 1, Academic Press, London, 135-191, 1984.
3. Ripmeester, J. A.; Tse, J. S.; Ratcliffe, C. I.; Powell, B. M. A New Clathrate Hydrate Structure. *Nature* 1987, *325*, 135-135.
4. Cole, W. A.; Goodwin, S. P. Flash Calculations for Gas Hydrates: A Rigorous Approach. *Chem. Eng. Sci.* 1990, *45(3)*, 569-573.
5. Avlonitis, D. Thermodynamics of Gas Hydrate Equilibria; Ph.D. Thesis, Department of Petroleum Engineering, Heriot-Watt University, Edinburgh, 1992.
6. Michelsen, M. L. The Isothermal Flash Problem. Part-I. Stability. *Fluid Phase Equilibria* 1982, *9*, 1-19.
7. Michelsen, M. L. The Isothermal Flash Problem. Part-II. Phase-Split Calculation. *Fluid Phase Equilibria* 1982, *9*, 21-42.
8. Danesh, A.; Xu, D.-H.; Todd, A. C. Comparative Study of Cubic Equations of State for Predicting Phase Behaviour and Volumetric Properties of Injection Gas-Reservoir Oil Systems. *Fluid Phase Equilibria* 1991, *63*, 259-278.
9. Valderrama, J. O. A Generalised Patel-Teja Equation of State for Polar and Non Polar Fluids and Their Mixtures. *J. Chem. Eng. Japan* 1990, *23(1)*, 87-91.
10. Patel, N. C.; Teja, A. S. A New Cubic Equation of State for Fluids and Fluid Mixtures. *Chem. Eng. Sci.* 1982, *37(3)*, 463-473.
11. Avlonitis, D.; Danesh, A.; Todd, A. C. Prediction of VL and VLL Equilibria of Mixtures Containing Petroleum Reservoir Fluids and Methanol with a Cubic EoS. *Fluid Phase Equilibria* 1994, *94*, 181-216.
12. Tohidi-Kalorazi, B. Gas Hydrate Equilibria in the Presence of Electrolyte Solutions; Ph.D. Thesis, Department of Petroleum Engineering, Heriot-Watt University, Edinburgh, 1995.
13. Tohidi, B.; Danesh, A.; Todd, A. C. Modelling Single and Mixed Electrolyte Solutions and its Applications to Gas Hydrates, *Trans IChemE* 1995, *73(A)*, 464-472.
14. Aasberg-Petersen, K.; Stenby, E.; Fredenslund, Aa. Prediction of High-Pressure Gas Solubilities in Aqueous Mixtures of Electrolytes. *Ind. Eng. Chem. Res.* 1991, *30(9)*, 2180-2185.
15. Østergaard, K. Gas Hydrate Stability in the Petroleum Industry and its Application in Gas-Liquid Separation; Ph.D. Thesis, Department of Petroleum Engineering, Heriot-Watt University, Edinburgh, 2000.
16. Smith, J. M.; Van Ness, H. C. Introduction to Chemical Engineering Thermodynamics, 4th ed., McGraw-Hill Inc., New York, 1987.
17. Anderson, F. E.; Prausnitz, J. M. Inhibition of Gas Hydrates by Methanol. *AIChE J.* 1986, *32(8)*, 1321-1333.

18. van der Waals, J. H.; Platteeuw, J. C. Clathrate Solutions. *Adv. Chem. Phys.* 1959, *2(1)*, 1-57.

19. Parrish, W. R.; Prausnitz, J. M. Dissociation Pressures of Gas Hydrates Formed by Gas Mixtures. *Ind. Eng. Chem. Proc. Des. Dev.* 1972, *11(1)*, 26-35.

20. Holder, G. D.; Corbin, G.; Papadopoulos, K. D. Thermodynamic and Molecular Properties of Gas Hydrates from Mixtures Containing Methane, Argon, and Krypton. *Ind. Eng. Chem. Fundam.* 1980, *19*, 282-286.

21. Mehta, A. P.; Sloan, E. D. A Thermodynamic Model for Structure-H Hydrates. *AIChE J.* 1994, *40(2)*, 312-320.

22. Dharmawardhana, P. B.; Parrish, W. R.; Sloan, E. D. Experimental Thermodynamic Parameters for the Prediction of Natural Gas Hydrate Dissociation Conditions. *Ind. Eng. Chem. Fundam.* 1980, *19*, 410-414.

23. Mckoy, V.; Sinanoğlu, O. Theory of Dissociation Pressures of Some Gas Hydrates. *J. Chem. Phys.* 1963, *38*, 2946.

24. Kihara, T. Virial Coefficients and Models of Molecules in Gases. *Reviews of Modern Physics* 1953, *25(4)*, 831-843.

25. Scott, R.L.; Magat, M. The Thermodynamics of High-Polymer Solutions: The Free Energy of Mixing of Solvents and Polymers of Heterogeneous Distribution. *The Journal of Chemical Physics* 1945, *13/5*, 172-177.

26. Firoozabadi, A. Thermodynamics of Hydrocarbon Reservoirs, McGraw-Hill, 1999.

CHAPTER 3

WATER CONTENT OF NATURAL GASES

3.1. INTRODUCTION

Natural gases are generally saturated with water at reservoir conditions. During production, transportation and processing, some of the dissolved water in the vapour phase may condense. The condensed water may contribute to corrosion and two phase flow problems, gas hydrates and/ or ice formation under specific temperature and pressure conditions. The formation of gas hydrates and/or ice could results in pipeline blockage and shutdown.

Therefore, accurate knowledge of phase behaviour in water –gas systems is crucial to the design and operation of natural gas pipelines and production/ processing facilities. On the other hand, oil and gas producers have been faced with a growing challenge to reduce atmospheric emissions of acid gases produced from sour hydrocarbon pools due to environmental regulations. When these gases are extracted, one of the options for their disposal is disposal by injection into an underground zone. As acid/sour gases are normally saturated with water in gas treatment/ gas injection units, a comprehensive coverage of the many design considerations requires knowledge of the phase equilibrium in water –gas systems.

However, most of experimental data on water content for hydrocarbons and non-hydrocarbon gases (e.g., nitrogen, carbon dioxide and hydrogen sulphide) at low temperature conditions are scarce and often rather dispersed. It seems that achieving equilibrium at low temperature conditions, especially near and inside hydrate forming

conditions is a very slow process and requires a long time. At rather low temperatures and high pressures conditions, the water content of a gas is indeed very low. It is well known that the determination of water traces in gases is one of the most difficult problems of trace analyses, and their accurate measurements require specialised techniques.

To give a qualified estimate of the amount of water in the gas phase, predictive methods are required. General methods of calculation include the use of:

1) Empirical or semi – empirical equations and plots of water content versus pressure and temperature and corrections for the presence of acid gases such as hydrogen sulphide and carbon dioxide or heavy hydrocarbons and salts (e.g. Ideal model, Ideal model + Poynting correction, Bukacek correlation (1), Sharma – Campbell method (2-4), Robinson et al. chart (5-7), Maddox et al. correlation (8), Wichert – Wichert correlation (9), McKetta-Wehe chart (10) and Ning et al. correlation (11)).

2) Thermodynamic models which are based on equality of chemical potential of various components in different phases.

The main advantage of empirical or semi – empirical correlations and charts is the availability of input data and the simplicity of the calculations, which can be performed by using charts or hand-held calculators. The correlations / charts have still kept their popularity among engineers in the petroleum industry. Although most available thermodynamic models could be installed on typical laptop computers, there seem to be a need for simple, yet robust, predictive methods for quick estimation of water content of natural gases.

The available correlations and charts are generally based on limited data and with limited application. In general, the available correlations / charts can predict water content of gases with good accuracy at high temperature conditions. While in predicting water content at low temperature conditions, the available methods have lower accuracy and need further verification at low temperature conditions. In fact, during the development of the original correlations / charts, experimental data describing the phase equilibrium in water – hydrocarbons systems for temperatures typically lower than 298.15 K were not available. Due to this shortcoming, water content for low temperatures calculated by the correlations / charts might not be accurate.

To develop new correlations / charts and to improve the accuracy of the estimated water content of gases, experimental data are required (which could also be used for validation of correlations / charts). Unfortunately, most of the water content data for hydrocarbons and for non-hydrocarbon gases (e.g. N_2, CO_2 and H_2S) at low temperature conditions are often inconsistent. These types of uncertainties can lead to large deviations for correlations, when using these scattered data for regressing.

The aim of this work is to study phase equilibria in water – natural gas systems at low concentrations of water. For this purpose, a review is made on the existing predictive methods in the open literature.

A thermodynamic model based on the Valderrama modification of the Patel and Teja equation of state (*VPT - EoS*) (12) with the non density dependent (*NDD*) mixing rules (13) is used for predicting phase equilibrium. In this model, the fugacity of ice is calculated by correcting the saturation fugacity of water at the same temperature by an exponential factor (the Poynting correction). The hydrate phase is modelled by the

solid solution theory of van der Waals and Platteeuw (14). To evaluate the performance of the model, the results are compared with some reliable experimental data from the literature. The results are in good agreement demonstrating the reliability of the model used for this work.

Then, a semi-empirical approach based on equality of fugacity in equilibrium phases for estimating the water content of natural gases is developed. To evaluate the capability of the approach, the results are compared with literature data as well as other predictive tools. The results are in good agreement demonstrating the capability of the approach developed in this work.

3.2. LITERATURE REVIEW

Many thermodynamic models and correlations/charts are available, which can calculate phase equilibrium in water – hydrocarbon systems. Thermodynamic models use different approaches in order to model the fluid. ice and gas hydrates phases. For example, some thermodynamic models use activity coefficient and Henry's constant approaches for modelling the aqueous phase, however other models use equation of state approach. Although thermodynamic models are useful tools in phase behaviour calculations, they may not be available easily. Correlations and charts are more simple tools and because of their ease of use, they are of interest to engineers in petroleum industry. Various correlations and charts with different capabilities have been reported for estimating the water content / water dew point of gases. The original correlations / charts are normally applicable to dry and sweet gases. Generally, these correlations / charts have been developed for the liquid water - vapour (L_w-V) region and interpolating the results to the hydrate - vapor (H-V) and ice - vapour (I-V) regions may

be questionable (See Figure 3.1). In this section, a review of the most famous correlations and charts in the natural gas industry are presented:

- The *Ideal* model (Raoult's law) is expressed by the following expression:

$$y_w = \frac{(1-x_g)P_w^{sat}}{P} \tag{3.1}$$

where y, x , and P are the mole fraction in the vapour phase, mole fraction in the liquid phase and pressure, respectively, and subscripts w and g relate to water and gas and the superscript *sat* relates to the saturation state. In this equation, the gas solubility in the water x_g can be ignored for hydrocarbons, as hydrocarbons are weakly soluble in water and solubility will decrease by increasing the molecular weight of hydrocarbons, however for acid gases (CO_2 and H_2S) the solubility can be significant, even at relatively low pressure (15), (16). In this case, the water content can be expressed by the following expression:

$$y_w = \frac{P_w^{sat}}{P} \tag{3.2}$$

The above relation assumes the water content of a gas equals to the ratio of the water vapour pressure and total pressure of the system.

A more accurate form of the *Ideal* model can be expressed by taking into account the *Poynting* correction:

$$y_w = \frac{P_w^{sat}}{P}\exp\left(\frac{v_w^L(P-P_w^{sat})}{RT}\right) \tag{3.3}$$

where v, R and T are molar volume, universal gas constant and temperature of the system, respectively and the superscript L stands for the liquid state . The *Ideal model*

and its *Poynting correction* are simple tools for predicting the water content of natural gases. However, these methods can be used at low-pressure conditions (Typically up to 1.4 MPa (15)).

- *Bukacek* (1) developed a method similar to the *ideal* model, which only requires information on the water vapour pressure and the temperature and pressure of the system. This correlation is one of the most used methods in the natural gas industry for calculating the water content of dry and sweet natural gases. This correlation in *American Engineering units* is given as follows (15,16):

$$y_w = 47484 \frac{P_w^{sat}}{P} + B \tag{3.4}$$

$$log_{10}(B) = \frac{-3083.87}{459.6 + t} + 6.69449 \tag{3.5}$$

where water content (y_w) and t are in *lbm/MMscf* and temperature in *°F*. As can be seen, this correlation uses an ideal contribution and a deviation factor. The above relation is reported to be accurate for temperatures between 288.15 and 511.15 K and for pressures from 0.1 to 69 MPa (15, 16). This correlation is accurate to about ± 5% within the stated range (15-17), as this is about as accurate as water content can be measured.

- *Sharma and Campbell* (2-4) provided a relatively complicated method in order to calculate the equilibrium water content of sweet and sour gases in the L_W-V region. In this method, the water content is calculated as below:

$$y_w = k \left(\frac{f_w^{sat}}{f_g}\right)^Z \tag{3.6}$$

where k, Z and f are a correction factor, the compressibility factor and the fugacity, respectively and subscript g refers to the gas phase. The compressibility factor Z should

be calculated using a suitable method. The correction factor k can be calculated from a figure (provided by the authors) or by the following equation:

$$k=(\frac{P_w^{sat}}{P})(\frac{f_w^{sat}/P_w^{sat}}{f_w/P})(\frac{P}{P_w^{sat}})^{0.0049} \quad (3.7)$$

where $f_w{}^{sat}$ and f_w are fugacity of water at saturation conditions (T and $P_w{}^{sat}$) and the fugacity of water at pressure and temperature of the system (T and P). They provided a chart for calculating the fugacity of water. As mentioned before, this method is relatively complicated, however Campbell (4) mentioned that the consistency of the results of this method is high.

- *Behr* (18) proposed the following equation for pressure ranging from 1.379 to 20.679 MPa:

$$y_w = exp(A_0+A_1(1/T)^2+A_2(1/T)^3+A_3(lnP)+A_4(lnP)^2+A_5(lnP)^3+A_6(lnP/T)^2+A_7(lnP/T)^3)$$

where y_w is in *lbm/MMscf* and A_0 to A_7 are constants based on fitting the natural gas dew point versus the water content data of *Bukacek* (1).

- Later *Kazim* (19) proposed an analytical expression for calculating the water content of sweet natural gases. The expression in *American Engineering units* is:

$$y_w = A \times B^t \quad (3.9)$$

$$A = \sum_{i=1}^{4} a_i(\frac{p-350}{600})^{i-1} \quad (3.10)$$

$$B = \sum_{i=1}^{4} b_i(\frac{p-350}{600})^{i-1} \quad (3.11)$$

where y_w is in *lbm/MMscf* and p is the pressure in *psia* and a_is and b_is are constants reported in the original publication. These two correlations are similar as in which, they originate from regression methods to express the water content of natural gases as a function of temperature and pressure and require many constants, which may reduce their applications for calculating the water content of natural gases in comparison with the *Bukacek* (1) correlation.

Several charts have been reported in order to calculate the equilibrium water content of gases. The most commonly used is the *McKetta – Wehe* (10) chart, which is used for sweet natural gases containing over 70% methane and small amounts of heavy hydrocarbons (10, 20). This chart was first published in 1958 (10) and was based on experimental data available at that time (10). Gas Processors Associations (*GPA*) and Gas Processors Supplier Associations (*GPSA*) have reproduced this chart for many years. In this chart the water content of a sweet gas is presented in a semi – logarithmic plot versus temperature at different pressures. Two correction factors have been provided in order to take into account the presence of heavy hydrocarbons in the gas phase and salts in the liquid water. In this chart, meta-stable L_W –V equilibrium is assumed rather than H–V equilibrium in the hydrate formation region with limited justification (21). However the actual water content in the H –V region is lower than the calculated water content by assuming L_W –V equilibrium. Furthermore, reading the water content from this semi – logarithmic chart may be slightly difficult. If used with care, this chart can calculate the water content of sweet gases with less than 5% error (15).

- *Ning et al.* (11) proposed the following correlation based on the *McKetta – Wehe* (10) chart (15-16):

$$y_w = e^{a_0 + a_1 T + a_2 T^2} \tag{3.12}$$

For the above equation, a complicated figure and table have been provided in order to calculate the pressure dependent coefficients a_0, a_1 and a_2 for pressures up to 100 MPa. It seems that this correlation is not a simple tool due to the complicated dependency of coefficients to the pressure. Their correlation takes into account the effect of gas gravity by the following correction factor (15):

$$F_{HC} = 1.01532 + 0.011(T-273.15) - 0.0182\, SG_g - 0.0142\, SG_g (T-273.15) \tag{3.13}$$

$$y_{w,heavy} = F_{HC} y_{w,light} \tag{3.14}$$

where F and SG are correction factor due to presence of heavy hydrocarbons and gas gravity and subscripts *HC*, *heavy* and *light* relate to hydrocarbon, heavy and light components, respectively.

The above correlations / charts (except Sharma and Campbell method (2-4)) assume that the water content of dry and sweet natural gases is independent of the gas composition. However, when acid gases and heavy hydrocarbons and/or salts are present in the system, their accuracy is reduced and some corrections should be used in addition to the above correlations / charts.

Both hydrogen sulphide and carbon dioxide contain more water at saturation than methane or sweet natural gas mixtures and the relative amounts vary considerably with temperature and pressure (10). Water content of carbon dioxide and hydrogen sulphide plays an important role in phase equilibria calculations, e.g., enhanced oil recovery (*EOR*) processes, corrosion prevention, flow assurance, gas hydrates inhibition, etc.

There are some methods for estimation of water content due to the presence of acid gases in the gas phase. The correlations should be applied when the gas mixture contains more than 5% hydrogen sulphide and/ or carbon dioxide, especially at high pressures (10).

Several graphs are reported for estimating the water content of pure carbon dioxide (10, 16, 22-27) and pure hydrogen sulphide (10, 16, 24, 28). There are also other graphs for estimating the water content of different mixtures containing acid gases (5-10, 26).

The *Robinson et al.* (5-7), *Maddox et al.* (8) and *Wichert – Wichert* (9) methods correct the water content of sweet gases due to the presence of acid gases.

Robinson et al. (5-7) reported a series of charts to estimate the water content of sour natural gases. These charts were calculated based on an equation of state based model. They used an equivalent mole fraction for H_2S for their charts, which is calculated by the following expression (6-7):

$$z_{H2S}^{equi} = z_{H2S} + 0.75\, z_{CO2} \qquad (3.15)$$

where z is the mole fraction in the natural gas, the subscripts CO_2 and H_2S refer to carbon dioxide and hydrogen sulphide, respectively and the superscript *equi* refers to equivalent H_2S. This method is applicable for $z_{H2S}^{equi} < 0.4$ (mole fraction), $283.15 < T < 450.15$ K and $2.07 < P < 69$ MPa. In addition, using these charts is slightly difficult due to the need for interpolations.

In *Maddox et al.* (8) method, the water content of sour gases is calculated using the following expression:

$$y_w = y_{w,HC} \times z_{HC} + y_{w,CO2} \times z_{CO2} + y_{w,H2S} \times z_{H2S} \quad (3.16)$$

where subscript *HC* refers to hydrocarbon. In the above equation, the contribution to the sweet gas can be calculated using an appropriate correlation or chart. The acid gas contributions can be calculated by either the corresponding charts or equations. The above correlation is applicable to acid gas concentrations of less than 40 mole % and a pressure range of $0.7 < P < 20.7$ MPa, and a temperature range of $300.15 < T < 344.15$ K for CO_2 and $300.15 < T < 411.15$ K for H_2S.

Wichert and *Wichert* (9) proposed a new chart based on temperature, pressure and equivalent H_2S content in order to calculate a correction factor (F_{sour}). They used definition of *Robinson et al.* (6-7) for the equivalent H_2S content. Using this correction factor, the water content of sour natural gases can be calculated by using the following expression:

$$y_{w,sour} = F_{sour} y_{w,sweet} \quad (3.17)$$

In the above equation, the subscripts *sour* and *sweet* relate to the sour and sweet natural gases. The *McKetta – Wehe* (10) chart is recommended for calculating y_{sweet} in the above equation. This method is applicable for $z_{H2S}^{equi} < 0.55$ (mole fraction), $283.15 < T < 450.15$ K and $1.4 < P < 69$ MPa. In addition, using this method is easier than the method suggested by *Robinson et al.* (5-7), as there is no need for interpolation.

In addition, determining the water content in acid/sour gases is a very complex topic. According to *GPSA* (10), an accurate determination of water content requires a careful study of the existing literature and available experimental data.

Figure 3.1 shows a typical pressure –temperature diagram for water – hydrocarbon system (29). As can be seen; the *I-V* equilibrium for sweet natural gases with very low nitrogen content can be reached at relatively low-pressure conditions. The maximum

pressure at which the *I-V* equilibrium can be reached is around 2.563 MPa, which corresponds to hydrate formation conditions for methane at around quadruple point. The *Poynting* correlation can be used for estimating the water content of sweet natural gases with very low nitrogen content in equilibrium with ice. *Katz* (30) also reported a chart in temperature and pressure range of $222.04 < T < 273.15$ K and $0.1 < P < 2.757$ MPa for calculating the water content of natural gases in equilibrium with ice.

The water content of natural gases in equilibrium with gas hydrates is lower (typically less than 0.001 mole fraction (21)) than the water content of natural gases in equilibrium with meta-stable liquid water and therefore difficult to measure, as hydrate formation is a time consuming process and water content of gases in the hydrate region is a strong function of composition (10, 21). In other word, a gas phase saturated with water can form gas hydrates in the *H-V* region from a strict thermodynamic stand point, however the question of the accumulation of a hydrate phase is a question of kinetics, dependent upon the time necessary for hydrate nuclei to attain a critical size (21). This time may be in excess of that available for laboratory study, but may occur in processes, which operate over extended periods of days, months or years (22). On the other hand, limited experimental data have been reported in this region. Therefore, a comprehensive correlation / chart for calculating water content of gases in equilibrium with gas hydrates would be problematic (21). Few mathematical relations/ charts for this region have been developed in the literature (15, 21, 31-35). Where experimental data is limited, utilization of a thermodynamic based model can provide an estimate of water content in equilibrium with hydrates.

In addition, in many standards, the *Bukacek* (1) correlation and the *McKetta–Wehe* (10) chart are recommended to estimate the water content of sweet natural gases in equilibrium with liquid water. However, *Bukacek* (1) correlation and *McKetta–Wehe* (10) chart may not describe real phase behaviour in water – hydrocarbon systems at low temperature conditions. In other words, the *Bukacek* (1) correlation should be used at temperatures higher than 288.15 K (15, 16) and the water contents obtained from the *McKetta–Wehe* (10) chart at temperatures below hydrate formation conditions correspond to the meta-stable $L_W - V$ equilibrium rather than H-V equilibrium.

3.3 DESCRIPTION OF THE THERMODYNAMIC MODEL

A detailed description of the model is given in Chapter-2. Briefly, a thermodynamic model based on uniformity of fugacity of each component throughout all the phases (13, 36) is extended to model the equilibrium conditions. The *VPT – EoS* (12) with *NDD* mixing rules (13) is used to determine component fugacities in fluid phases. This combination has proved to be a strong tool in modelling systems with polar as well as non-polar compounds (13). The fugacity of ice is rigorously calculated by correcting the saturation fugacity of water at the same temperature by using the Poynting correction. The hydrate phase is modelled using the solid solution theory of van der Waals and Platteeuw (14). The Kihara model for spherical molecules is applied to calculate the potential function for compounds forming hydrate phases. These parameters are taken from Tohidi-Kalorazi (36).

Figure 3.1 shows a typical pressure –temperature diagram for water - hydrocarbon system (pure gas and water as limiting component). As can be seen, for H-V equilibria, the temperature must be below the three-phase liquid water-hydrate-vapour (L_w-H-V) or

ice- hydrate-vapour (*I-H-V*) temperature at a given pressure. Alternatively the pressure must be above the three-phase L_w-*H-V* or *I-H-V* pressure at a given temperature (21). Consequently, for ice-vapour (*I-V*) equilibrium the temperature must be above the *I-V-H* temperature at a given pressure or the pressure must be below the *I-H-V* pressure at a given temperature. Also, for liquid water- vapour (L_w-*V*) equilibrium the temperature must be above the L_w-*V-H* temperature at a given pressure or the pressure must be below the L_w-*H-V* pressure at a given temperature.

3.4. SEMI-EMPIRICAL APPROACH

The main advantage of this method is the availability of input data and the simplicity of the calculations, which can be performed by using hand-held calculators.

The vapour – liquid equilibrium (*VLE*) of a system is calculated, using the following equation:

$$f_i^V = f_i^L \qquad i = 1, N \tag{3.18}$$

where N is the number of components. The equality of fugacities can be calculated using the following relationship:

$$y_i \phi_i P = x_i \gamma_i P_i^{sat} \exp \int_{P_i^{sat}}^{P} \frac{v_i^L dP}{RT} \tag{3.19}$$

In the intermediate pressure range, liquid water is an incompressible fluid and gas solubility is very small comparing to unity for hydrocarbons and some gases like nitrogen (solubility of hydrocarbons in water are, in general, considerably less than water in hydrocarbons (10)) and to an approximation activity coefficient of water can be taken unity. However, the non-ideality of the liquid phase and gas solubility become

important at high pressure conditions. Therefore, the mole fraction of water in the gas phase can be estimated, using the following equation:

$$y_w=\frac{(1-x_g)P_w^{sat}}{\phi_w P}\exp(\frac{v_w^L(P-P_w^{sat})}{RT}) \quad (3.20)$$

As can be seen, water content is determined primarily by the fugacity coefficient of water (ϕ_w) in the gas phase, temperature and pressure. In other word, the non-ideality of the gas phase is the critical factor determining water content in the intermediate pressure range. The fugacity coefficient of water (ϕ_w) in the gas phase up to intermediate pressures may be calculated as below:

$$\phi_w=exp(BP+CP^2) \quad (3.21)$$

where B and C are a function of temperature. The following relations for B and C seem to be satisfactory:

$$B=a+\frac{b}{T} \quad (3.22)$$

$$C=c+\frac{d}{T} \quad (3.23)$$

where a, b, c and d are constants and can be calculated for every water – gas system by regressing the water content data for that system. To estimate vapour pressure and molar volume of water in equation (3.20), the relations reported by *Daubert* and *Danner* (37) and *McCain* (17) are used, respectively:

$$P_w^{sat}=10^{-6}exp(73.649-7258.2/T-7.3037ln(T)+4.1653\times10^{-6}T^2) \quad (3.24)$$

$$v_w^L=18.015/\rho_w \quad (3.25)$$

$$\rho_w=62.368/D_w \quad (3.26)$$

$$D_w=(1+\Delta V_{wt}) \quad (3.27)$$

$$\Delta V_{wt}=-1.0001\times10^{-2}+1.33391\times10^{-4}t+5.50654\times10^{-7}t^2 \quad (3.28)$$

where, T, t, p, P_w^{sat}, v_w^L are in K, ^oF, $psia$, MPa and $ft^3/lbmol$ respectively and ρ_w, D_w and ΔV_{wt} are water density in lb_m/ft^3, formation volume factor, volume change due to temperature, respectively. Equations (3.24) – (3.28) are valid at $t < 260\ ^oF$, and $p <$ 5000 psia even over a wide range of salt concentration (38). To find constants a, b, c, and d in equations 3.22 and 3.23, water content data are used as input for a multi-dimension regression procedure, in order to reduce average absolute deviation (AAD) between experimental and calculated data.

The above approach can be used for estimating water content of gases in equilibrium with ice. For this purpose, the following relations for molar volume of ice and ice vapour pressure can be used (36):

$$v_w^I=(19.655+0.0022364\times(T-273.15))/10^3 \quad (3.29)$$

$$\log_{10}(P_w^{sub})=-1032.5576407/T+51.0557191\times\log(T)-0.0977079751\times T+$$

$$7.035711316\times10^{-5}\times T^2-98.5115496 \quad (3.30)$$

where superscript I and sub refer to ice and sublimation, respectively. In the above equations, T, v_w^I and P_w^{sub} are in K, $m^3/kgmol$ and $mmHg$, respectively.

3.5. ESTIMATION OF WATER CONTENT IN SOUR GASES

It is necessary to be able to estimate the equilibrium water contents of sour gases as a function of system temperature, pressure and composition. This will enable the engineers to calculate the amount of water condensed as a result of changes in the system conditions. The literature review shows that almost all the existing tools for estimating the water contents of sour gases are graphical methods and in most cases an interpolation is necessary in order to calculate the water content. Therefore, it was

decided to develop an analytical method, without any need for graphical techniques, for calculating the water content of sour gases. The developed method could significantly simplify the calculations procedure and facilitate the use of hand held calculators.

In order to develop a new correction factor for taking into account the effect of acid gases, *Robinson et al.*'s (6-7) definition of equivalent H_2S mole fraction (equation 3.15) is used. Considering the fact that the water content of an acid/sour gas is a function of temperature, pressure and acid gas/ equivalent H_2S mole fraction, the following correction factor is suggested for taking into account the effect of acid gases on the water content:

$$F_{sour}=1-z_{H2S}^{equi}[c_1(\frac{T}{T_0})+c_2(\frac{T}{T_0})(\frac{P}{P_0})+c_3(\frac{P}{P_0})] \quad (3.31)$$

In the above equation, F_{sour} is a correction factor due to the presence of acid gases, P and T are pressure and temperature of the system, respectively and z_{H2S}^{equi} is equivalent mole fraction of acid gases, which is calculated using equation 3.15. P_0 and T_0 are reference pressure (atmospheric pressure) and reference temperature (273.15 K), respectively and c_1-c_3 are constants. The water content of sour gases is then calculated by multiplying the new correction factor and the water content of the corresponding sweet gas (equation 3.17).

3.6. RESULTS AND DISCUSSIONS

3.6.1. Thermodynamic model

A preliminary study shows that most of the existing *EoS* were developed at relatively high temperature conditions. Therefore, the *EoS* may not cover low temperature conditions (29). Different attempts have been made to solve this problem. Some investigators developed new alpha – functions for appropriate *EoS*, particularly Peng –

Robinson *(PR) EoS* and some of them relaxed the alpha function for water, in order to improve the predicted water fugacity. Exact prediction of the water vapour pressure has an important effect on the phase behaviour of wet gases (29). The calculated results significantly depend on the temperature dependency of the alpha – function. This function is generally developed as a function of reduced temperature and acentric factor. Anderko (39) mentioned that the acentric factor is not a characteristic parameter for polar substances. This fact may lead to undesired results, when using the acentric factor in the alpha – function for the polar substances. To improve the predicted water fugacity in this study, the alpha function for water in the *VPT – EoS* (12), $\alpha_w(T_r)$, is relaxed, using experimental water vapour pressure data in the range of 258.15 to 374.15 K, as implemented by Tohidi – Kalorazi (36).

The model is then used to predict the water content of gases. As mentioned earlier, at rather low temperatures and high pressures conditions, the water content of a gas is indeed very low. It is well known that the determination of water traces in gases is one of the most difficult problems of trace analyses, and their accurate measurements require very specialised techniques. In general, measuring gas solubility in water is easier than water content measurement of natural gases. A preliminary study shows that using only gas solubility data in tuning thermodynamic models can lead to accurate predictions of water content data and therefore less need to measure water solubility in the gas phase. Therefore, only gas solubility data are used for tuning binary interaction parameters in the present study. The binary interaction parameters are reported in Table 3.1. Figures 3.1-3.23 and Tables 3.1-3.24 show the results.

3.6.1.1. Water content of nitrogen

There are some disagreements among the predictions and data describing the influence of nitrogen on water content / water dew point. According to Campbell (4), nitrogen shows lower values of equilibrium water content than methane, due to lower solubility in water. Experimental results obtained by Althaus (29) indicate that outside the hydrate region of methane, the measured water content for the methane – water system is slightly higher than that of nitrogen-water system. Inside the hydrate region of methane, the water content of methane is lower than that of nitrogen. In the light of the above conflicting data it would be desirable to check the influence of nitrogen on water content, particularly inside and outside hydrate formation region. Figure 3.23 shows the model predictions for water content of nitrogen and methane, respectively. Comparing the water contents for the methane – water and nitrogen – water systems shows that the water content for the methane – water system is slightly higher than that of nitrogen-water system outside the hydrate region of methane. Inside the hydrate region of methane, the water content of methane is lower than that of nitrogen. The differences between the water contents of both gases increase with decreasing temperatures, when the distance to the hydrate boundary of methane becomes larger. This means that the statement of Campbell (4), that nitrogen shows lower values of water content than methane, may not be confirmed. A direct comparison of the predicted water contents shows that only for temperatures of and above approximately 283.15 K always higher water contents are predicted for methane.

3.6.1.2. Water dew point

Determining the water dew point of gases is one of the most important quality parameters of gases. It is of interest to be able to estimate water dew points of gases at

given pressures and water contents. Most of the existing correlations have been developed for estimation of the water content of gases and a simple determination of the water dew point from given water content often is not easy. In addition, the dew point can be estimated from the water content by iteration, when using these correlations.

The correlation of *Bukacek* (1) is one of the most used correlations in the natural gas industry for calculating the water content / water dew point of sweet gases. The above relation is reported to be accurate for temperatures between 288.15 and 511.15 K and for pressures from 0.1 to 69 MPa (15). Some tests by Carroll (15) indicate that within the stated range, this correlation is accurate to about ± 5%, which is comparable to the *McKetta – Wehe* chart (10).

In Table 3.24, the water dew point of methane has been estimated using the *Bukacek* (1) correlation and also the model. According to Althaus (29), the dew point temperature of gases can be predicted with an accuracy of $\pm$ 2 K. As can be seen, the model predictions are in good agreement with those calculated using *Bukacek* (1) correlation with less than 2 K absolute difference.

3.6.2. Semi-empirical approach

In order to find the constants *a*, *b*, *c* and *d* for methane-water system, the data reported in Table 3.14 are used. As can be seen, the temperature range is from 273.15 K to 377.59 K, and the pressures are up to 13.81 MPa, respectively. The *AAD%* among all the experimental and calculated data is 4.43 %. These constants are reported in Table 3.15. On the other hand, the saturated water content of a natural gas depends on pressure, temperature and composition. The effect of composition increases with

pressure and is particularly important if the gas contains carbon dioxide and hydrogen sulphide. For lean and sweet natural gases containing over 70 mole % methane and small amounts of heavy hydrocarbons, the effect of composition can be ignored and the water content can be assumed a function of temperature and pressure. Therefore, the constants *a, b, c* and *d* for methane – water system can be used with a good approximation for dry and sweet natural gases – water system.

These constants can also be used for predicting the water content of methane and dry and sweet natural gases in the *I – V* region. Table 3.16 shows a comparison between the experimental and predicted water content of methane in this region. The agreements between the experimental and predicted data are satisfactory and the *AAD%* among all the experimental and predicted data is 2.78 %.

In Table 3.4 and 3.17, the capabilities of this approach are tested with data from the literature. As it can be observed for all references not used in the tuning of *a, b, c* and *d* parameters, the predictions of this approach are in acceptable agreement with the reported results (less than 13% absolute deviation). It is particularly noticeable that the influence of the gas composition/gas gravity (in all of these cases the gas gravity is close to the one of methane, 0.554) is negligible and even high concentrations of nitrogen (10.35 %) has little effect on the quality of the predictions. However, this latest assumption is true if the gas is mainly composed of methane and light hydrocarbons and therefore its gas gravity is close to that of pure methane. The presence of heavy hydrocarbons in natural gases decreases the water content. To take into account the effect of gas composition, the correction factor of *McKetta-Wehe* (10) chart can be used.

McKetta-Wehe (10) have suggested a correction factor as a function of gas gravity and temperature for taking into account the effect of heavy hydrocarbons. This correction factor is well represented by the following equation:

$$F_{hh}=1+b_1(\gamma\text{-}0.554)+b_2(\gamma\text{-}0.554)\left(\frac{T}{T_0}\right)+b_3(\gamma\text{-}0.554)^2\left(\frac{T}{T_0}\right)^2 \qquad (3.32)$$

where F_{hh} is correction factor to take into account the effect of heavy hydrocarbons, γ stands for gas gravity, T and T_0 represent temperature of the systems and reference temperature (273.15 K), respectively and b_1. b_3 are constants. These constants are tabulated in Table 3.18.

The presence of high quantities of nitrogen in natural gases can shift the hydrate phase boundaries to higher pressures. To estimate water content in systems composed mainly of nitrogen, it is advised to use the values of the *a, b, c* and *d* parameters in Table 3.15 for the L_w-V region, as the water contents for the methane and nitrogen systems in this region are nearly identical (29). Table 3.19 shows a comparison between experimental and predicted water content of nitrogen in equilibrium with liquid water.

Dissolved solids (salts) in the water can change water properties such as reducing the water vapour pressure and changing water density and therefore reducing the water content of natural gases. To take into account the presence of salts, the extrapolation of the salinity correction factor in *McKetta-Wehe* (10) chart to high salt concentrations is believed to under-predict the water content of a gas in equilibrium with brine (38). The graphical correlation of Katz (30) for the salinity correction factor is recommended instead (38). The graphical correlation, developed from water vapour pressure depression due to the presence of salt, can be expressed as (17, 38):

$$F_{salt}=1-4.920\times10^{-3}w_{salt}-1.7672\times10^{-4}w_{salt}^{2} \quad (3.33)$$

where w is the weight percent of salt in brine and subscript *salt* refers to salt.

The semi-empirical predictive method developed in this work can predict water content of natural gases near hydrate forming conditions. It is recommended to use this approach at temperature and pressure ranging 243.15 – 377.59 K and 0.1-13.81 MPa, as the experimental data at these ranges have been used to optimise the constants. Therefore, using this approach at higher pressures and temperatures may result in unreliable predictions as at these conditions, water may be compressible liquid, equation (3.21) for fugacity coefficient may not be acceptable, the solubilities of gases in water may not be negligible and also activity coefficient of water may not be taken unity. Using this approach for pure CO_2 and/or H_2S is not recommended. In addition, using more reliable water content data, especially at low temperature conditions in the future, can increase the accuracy of this approach.

As mentioned earlier, sour natural gases will contain higher water content than sweet natural gases. The effect of acid gases has not been taken into account, as in equation 3.20 the gas solubility in the water phase is assumed to be negligible (which may not be true if high concentrations of acid gases are present). However at low pressure conditions (up to 0.5 MPa) this approach as well as some other correlations can be used, as the solubilities of acid gases are relatively small. Table 3.20 shows the predictions of this approach for water content of some sour natural gases with low and intermediate concentrations of acid gases. As it can be seen, at low and intermediate concentrations of acid gases, this approach is capable of predicting the water content with reasonable accuracy (AAD = 8.4%). It should be noted that measuring the water content of gases especially at low temperature conditions is very difficult and an

accuracy of 10% is generally acceptable. The presence of acid gases can be taken into account, using equation 3.31.

In order to find constants of the correction factor (equation 3.31), a variety of water content data for sour gases generated by the model described in section 3.3 for different concentrations of methane/acid gas and at different temperatures and pressures are used rather than experimental data, as according to GPSA (10), an accurate determination of water content in such systems requires a careful study of the existing experimental data. These data are then employed as input for a multi-dimensional regression procedure. The objective function is defined as the *AAD* between the water content determined by the thermodynamic model and the water content calculated by the tested equation. The optimised values for constants c_1-c_3 in equation 3.31 along with the application ranges of this correction factor are reported in Tables 3.21 and 3.22, respectively. Table 3.23 shows the predictions of this approach for water content of some sour natural gases. As it can be seen, the agreement is acceptable (AAD = 4.9%), demonstrating the reliability of the method developed in the present work.

3.7. CONCLUSIONS

Accurate knowledge of phase behaviour in water-natural gas systems especially at low temperature conditions is necessary for industrial applications. For this purpose, a review was conducted on the existing methods for predicting water content / water dew point of gases (pages 39-48). The investigation showed that most of the existing predictive methods have been developed at high temperature conditions.

A thermodynamic model based on the Valderrama modification of the Patel-Teja equation of state and non-density mixing rules was developed to estimate the water

content/ water dew point of gases (pages 48-49). The results were in acceptable agreement with independent data, demonstrating the reliability of the model developed in this work. Furthermore, the study showed that using only gas solubility data in tuning binary interaction parameters can lead to accurate predictions of water content data (pages 52-53).

A semi – empirical approach based on equality of fugacity concept was proposed for estimating the water content of natural gases in temperature range 243.15 – 377.59 K and pressures up to 13.81 MPa (section 3.4). The results of the predictivė method developed in this work are in good agreement with the experimental data and other predictive methods. The developed approach was able to estimate water content of a natural gas containing up to 10% nitrogen. The presence of carbon dioxide as a minor component of the natural gas was also taken into account and no degradation of the prediction was observed for small amount of carbon dioxide.

The study on the most popular methods of estimating the water content of sour gases in the literature showed a need for developing new tools. In order to take into account the presence of acid gases, a new analytical correction factor was developed and the results of the model were used for tuning parameters of the new approach (section 3.5). Good agreement between the predictions of this approach and independent data demonstrated the reliability of the new predictive method for estimating the water content of sour gases.

TABLES

Table 3.1. *BIP*s between natural gas main component and water for the *VPT-EoS* (12) and *NDD* mixing rules (13).

System	k_{w-hc}	l_{w-hc}^{0}	$l_{w-hc}^{1}\times10^{4}$
Methane-Water	0 .5044	1.8302	51.72
Ethane-Water	0.5442	1.5629	35.23
Propane-Water	0.6512	1.8137	37.71
n-Butane-Water	0.5800	1.6885	33.57
Nitrogen-Water	0.4788	2.6576	65.10
Hydrogen Sulphide-Water	0.1231	0.3785	16.95
Carbon Dioxide-Water	0.1965	0.7232	23.74

Table 3.2. Experimental (40) and calculated methane mole fractions in the liquid phase of the methane - water system.

T/K	P_{exp}/MPa	$x_{exp}\times10^{3}$	$x_{cal}\times10^{3}$	Δx %
275.11	0.973	0.399	0.361	9.52
275.11	1.565	0.631	0.567	10.14
275.11	2.323	0.901	0.815	9.54
275.11	2.820	1.061	0.969	8.67
283.13	1.039	0.329	0.327	0.61
283.12	1.810	0.558	0.553	0.90
283.13	2.756	0.772	0.812	-5.18
283.13	5.977	1.496	1.561	-4.34
298.16	0.977	0.238	0.238	0.00
298.16	2.542	0.613	0.589	3.92
298.15	5.922	1.238	1.233	0.40
298.13	15.907	2.459	2.498	-1.59
313.11	1.025	0.204	0.205	-0.49
313.11	2.534	0.443	0.486	-9.71
313.11	7.798	1.305	1.295	0.77
313.11	17.998	2.325	2.346	-0.90

Table 3.3. Experimental and predicted water contents (mole fraction × 1000) in water + methane system.

P /MPa	*T* /K	Experimental (41)	This Model	Ideal Model	Poynting Correction	BukacekCorrelation [1]	AQUAlibrium Model [15]	*AD*%, This Model	*AD*%, Ideal Model	*AD*%, Poynting Correction	*AD*%, Bukacek Correlation[1]	*AD*%, AQUAlibrium Model [15]
1.147	282.98	1.143	1.114	1.058	1.067	1.15	1.112	2.54	7.44	6.65	0.61	2.71
1.005	283.08	1.240	1.272	1.216	1.225	1.308	1.277	2.58	1.94	1.21	5.48	2.98
1.003	283.15	1.260	1.280	1.224	1.233	1.316	1.286	1.59	2.86	2.14	4.44	2.06
1.000	288.11	1.780	1.775	1.701	1.714	1.819	1.783	0.28	4.44	3.71	2.19	0.17
1.005	288.15	1.770	1.771	1.697	1.710	1.815	1.779	0.06	4.12	3.39	2.54	0.51
2.051	293.01	1.170	1.230	1.131	1.148	1.279	1.241	5.13	3.33	1.88	9.32	6.07
0.992	293.01	2.410	2.434	2.338	2.355	2.486	2.445	1.00	2.99	2.28	3.15	1.45
0.510	293.01	4.640	4.642	4.547	4.564	4.695	4.654	0.04	2.00	1.64	1.19	0.30
0.990	293.11	2.400	2.454	2.357	2.374	2.506	2.465	2.25	1.79	1.08	4.42	2.71
0.563	297.97	5.690	5.694	5.571	5.594	5.756	5.71	0.07	2.09	1.69	1.16	0.35
1.697	298.00	1.959	1.979	1.852	1.875	2.037	1.993	1.02	5.46	4.29	3.98	1.74
0.608	298.01	5.193	5.295	5.171	5.194	5.357	5.31	1.96	0.42	0.02	3.16	2.25
2.846	298.01	1.218	1.236	1.105	1.128	1.290	1.25	1.48	9.28	7.39	5.91	2.63
1.010	298.11	3.270	3.258	3.132	3.155	3.318	3.272	0.37	4.22	3.52	1.47	0.06
1.030	303.11	4.400	4.278	4.115	4.145	4.346	4.296	2.77	6.48	5.80	1.23	2.36
0.990	308.11	5.820	5.883	5.675	5.714	5.961	5.907	1.08	2.49	1.82	2.42	1.49
1.090	313.12	7.340	7.032	6.766	6.817	7.117	7.061	4.20	7.82	7.13	3.04	3.80

Table 3.4. Experimental (42) and predicted water contents (mole fraction) in methane – water and gas mixture – water system.

T /K	P /MPa	Experimental water content	Semi –empirical approach		Thermodynamic model	
			Predicted water content	AD %	Predicted water content	AD %
CH_4 - H_2O						
277.8	0.491	1.73E-03	1.77E-03	2.3	1.77E-03	2.3
277.8	1.081	8.30E-04	8.30E-04	0.0	8.28E-04	0.2
277.8	2.196	4.36E-04	4.31E-04	1.1	4.29E-04	1.6
277.8	3.136	3.21E-04	3.16E-04	1.6	3.14E-04	2.2
279.3	1.178	8.61E-04	8.49E-04	1.4	8.47E-04	1.6
282.9	0.493	2.64E-03	2.51E-03	4.9	2.50E-03	5.3
282.9	0.688	1.83E-03	1.81E-03	1.1	1.81E-03	1.1
283.0	1.081	1.22E-03	1.18E-03	3.3	1.18E-03	3.3
282.9	1.458	9.26E-04	8.87E-04	4.2	8.84E-04	4.5
283.0	2.822	5.30E-04	4.91E-04	7.4	4.89E-04	7.7
283.0	4.374	3.13E-04	3.40E-04	8.6	3.38E-04	8.0
287.7	0.993	1.85E-03	1.74E-03	5.9	1.74E-03	5.9
287.7	1.985	9.33E-04	9.12E-04	2.3	9.09E-04	2.6
287.7	2.393	7.75E-04	7.71E-04	0.5	7.67E-04	1.0
292.7	0.976	2.52E-03	2.43E-03	3.6	2.43E-03	3.6
292.7	2.690	9.26E-04	9.49E-04	2.5	9.44E-04	1.9
292.7	2.735	9.08E-04	9.35E-04	3.0	9.31E-04	2.5
292.7	3.667	7.03E-04	7.25E-04	3.1	7.21E-04	2.6
297.6	1.008	3.10E-03	3.17E-03	2.3	3.17E-03	2.3
297.5	2.342	1.44E-03	1.43E-03	0.7	1.43E-03	0.7
297.9	3.675	1.00E-03	9.87E-04	1.3	9.82E-04	1.8
297.6	3.865	8.76E-04	9.29E-04	6.1	9.25E-04	5.6
Gas mixture - H_2O						
278.1	0.501	1.82E-03	1.78E-03	2.2	1.78E-03	2.2
277.8	1.721	5.25E-04	5.38E-04	2.5	5.35E-04	1.9
282.9	0.521	2.43E-03	2.37E-03	2.5	2.37E-03	2.5
282.8	1.076	1.17E-03	1.17E-03	0.0	1.17E-03	0.0
282.8	1.235	1.04E-03	1.03E-03	1.0	1.03E-03	1.0
282.8	1.868	7.00E-04	7.01E-04	0.1	6.97E-04	0.4
282.8	3.028	4.44E-04	4.56E-04	2.7	4.53E-04	2.0
292.8	0.503	4.66E-03	4.65E-03	0.2	4.64E-03	0.4
292.8	0.986	2.44E-03	2.42E-03	0.8	2.42E-03	0.8
292.9	1.785	1.38E-03	1.38E-03	0.0	1.39E-03	0.7
303.1	0.511	8.47E-03	8.46E-03	0.1	8.45E-03	0.2
303.9	1.068	4.30E-03	4.33E-03	0.7	4.32E-03	0.5
303.1	2.415	1.98E-03	1.93E-03	2.5	1.93E-03	2.5
303.0	3.661	1.27E-03	1.33E-03	4.7	1.32E-03	3.9
322.0	0.526	2.26E-02	2.26E-02	0.0	2.26E-02	0.0
321.8	1.103	1.06E-02	1.09E-02	2.8	1.09E-02	2.8
322.0	1.924	6.44E-03	6.46E-03	0.3	6.46E-03	0.3
321.9	3.114	3.96E-03	4.13E-03	4.3	4.13E-03	4.3
321.8	4.174	3.05E-03	3.17E-03	3.9	3.17E-03	3.9
332.6	0.510	3.97E-02	3.87E-02	2.5	3.88E-02	2.3
332.7	1.523	1.34E-02	1.34E-02	0.0	1.35E-02	0.7
333.0	2.915	7.22E-03	7.40E-03	2.5	7.44E-03	3.0
332.9	4.902	4.53E-03	4.64E-03	2.4	4.67E-03	3.1
347.3	0.567	6.89E-02	6.66E-02	3.3	6.70E-02	2.8
347.1	1.534	2.53E-02	2.50E-02	1.2	2.52E-02	0.4
347.3	2.660	1.51E-02	1.50E-02	0.7	1.51E-02	0.0
347.2	4.115	9.86E-03	1.00E-02	1.4	1.01E-02	2.4
361.2	0.954	6.98E-02	6.96E-02	0.3	7.05E-02	1.0
361.4	1.740	4.01E-02	3.91E-02	2.5	3.98E-02	0.7
361.3	3.050	2.36E-02	2.29E-02	3.0	2.33E-02	1.3
361.0	4.599	1.52E-02	1.55E-02	2.0	1.59E-02	4.6

Table 3.5. Experimental (43) and calculated ethane mole fraction in the aqueous phase of the ethane - water system.

T/K	P/MPa	$x_{exp} \times 10^3$	$x_{cal} \times 10^3$	AD %
274.26	0.393	0.2237	0.2329	4.11
274.26	0.4922	0.2841	0.288	1.37
278.06	0.4004	0.205	0.2157	5.22
278.04	0.6128	0.3106	0.322	3.67
278.07	0.8126	0.4143	0.4163	0.48
283.12	0.473	0.225	0.2248	0.09
283.1	0.8122	0.3676	0.3714	1.03
283.1	1.2232	0.53	0.5325	0.47
288.08	0.4844	0.203	0.2067	1.82
288.08	1.0426	0.4227	0.4185	0.99
288.06	2.0801	0.7411	0.7392	0.26
293.33	0.382	0.1464	0.1483	1.30
293.31	1.01	0.369	0.3681	0.24
293.3	1.852	0.6073	0.6154	1.33
293.3	2.963	0.8647	0.8631	0.19
293.31	3.632	0.9696	0.9696	0.00
298.3	0.4486	0.1676	0.1579	5.79
298.37	0.8992	0.2972	0.303	1.95
298.35	1.377	0.4498	0.4421	1.71
298.42	2.021	0.6068	0.6054	0.23
298.32	2.7539	0.7699	0.7615	1.09
298.31	4.1297	0.9592	0.9635	0.45
303.19	0.373	0.1341	0.1214	9.47
303.21	0.719	0.2396	0.2274	5.09
303.21	1.093	0.346	0.3338	3.53
303.22	1.598	0.4719	0.4644	1.59
303.23	2.299	0.6295	0.6219	1.21
303.22	2.932	0.7415	0.7414	0.01
303.22	3.977	0.8827	0.8922	1.08
313.17	0.439	0.1337	0.1219	8.83
313.19	0.965	0.2623	0.2579	1.68
313.19	1.497	0.3841	0.3822	0.49
313.19	1.987	0.4799	0.4853	1.13
313.19	2.492	0.583	0.5806	0.41
313.19	3.088	0.6887	0.6793	1.36
313.18	4.669	0.8703	0.8717	0.16
323.17	0.397	0.0983	0.0964	1.93
323.19	0.947	0.2231	0.2239	0.36
323.19	1.989	0.4336	0.4337	0.02
323.2	3.03	0.5877	0.6047	2.89
323.18	3.963	0.7279	0.7277	0.03
323.2	4.838	0.8154	0.8182	0.34
343.08	0.44	0.0854	0.0853	0.12
343.06	1.503	0.272	0.2849	4.74
343.06	2.895	0.4997	0.5012	0.30
343.06	4.952	0.7376	0.738	0.05

Table 3.6. Experimental and predicted water mole fractions in the vapour phase of the ethane - water system.

T/K	P/MPa	y_{exp}	y_{prd}	AD %
Coan and King (23)				
298.15	2.442	0.00142	0.001324	6.76
	2.969	0.00111	0.001081	2.61
	3.597	0.0009	0.000871	3.22
	3.607	0.00093	0.000868	6.67
323.15	2.28	0.00563	0.005571	1.05
	2.969	0.00432	0.004286	0.79
	2.969	0.00432	0.004286	0.79
	2.969	0.00437	0.004286	1.92
	3.577	0.00354	0.003551	0.31
	3.627	0.00354	0.003501	1.10
348.15	2.33	0.0175	0.017173	1.87
	2.371	0.0169	0.016881	0.11
	3.03	0.0132	0.013275	0.57
	3.627	0.0109	0.011124	2.06
373.15	2.594	0.0414	0.041156	0.59
	2.928	0.0367	0.036582	0.32
	2.989	0.036	0.035856	0.40
	3.638	0.0296	0.02963	0.10
Song and Kobayashi (44)				
288.65	3.421	0.000525	0.000497	5.33
294.45	3.876	0.00065	0.000616	5.22
299.85	4.345	0.000716	0.000729	1.80
303.75	4.714	0.000736	0.000792	7.61
Althaus (29)				
278.15	0.5	0.001754	0.00176	0.37
283.15	0.5	0.002443	0.002477	1.41
283.15	1.5	0.00081	0.000834	2.99
288.15	1.5	0.001123	0.001159	3.20
288.15	2	0.000833	0.000869	4.38
288.15	2.5	0.000664	0.000691	4.11
293.15	1.5	0.001547	0.00159	2.75
293.15	2	0.001193	0.001194	0.11
293.15	2.5	0.000917	0.000952	3.79
293.15	3	0.00075	0.000784	4.58
Mohammadi et al. (41)				
282.93	0.506	0.002442	0.002412	1.23
288.11	1.859	0.001031	0.000933	9.51
292.95	1.049	0.002204	0.002237	1.50
293.1	1.926	0.001305	0.001236	5.29
293.1	2.99	0.000832	0.000784	5.77

Table 3.7. Experimental (45) and calculated propane mole fractions in the aqueous phase of the propane - water system.

T/K	P_{exp}/MPa	$x_{exp} \times 10^4$	$x_{cal} \times 10^4$	AD %
277.62	0.378	2.235	1.946	12.93
278.09	0.357	2.061	1.816	11.89
278.09	0.357	2.107	1.816	13.81
278.09	0.398	2.208	2.005	9.19
278.09	0.445	2.439	2.218	9.06
280.14	0.395	2.027	1.851	8.68
280.14	0.447	2.245	2.070	7.80
280.14	0.504	2.461	2.304	6.38
280.14	0.557	2.694	2.515	6.64
283.06	0.401	1.796	1.696	5.57
283.06	0.46	2.028	1.921	5.28
283.06	0.522	2.266	2.150	5.12
283.06	0.612	2.555	2.470	3.33
288.13	0.488	1.733	1.718	0.87
288.13	0.697	2.347	2.346	0.04
288.13	0.596	2.080	2.051	1.39
288.13	0.39	1.423	1.401	1.55
293.13	0.399	1.229	1.229	0.00
293.13	0.8	2.249	2.272	1.02
293.13	0.699	2.023	2.028	0.25
293.13	0.599	1.756	1.774	1.03
293.13	0.5	1.510	1.510	0.00
298.12	0.401	1.037	1.071	3.28
298.12	0.493	1.244	1.296	4.18
298.12	0.58	1.438	1.500	4.31
298.12	0.675	1.650	1.714	3.88
298.12	0.812	1.938	2.007	3.56
298.12	0.92	2.144	2.224	3.73
308.13	0.399	0.770	0.825	7.14
308.13	0.61	1.158	1.221	5.44
308.13	0.848	1.525	1.629	6.82
308.13	1.003	1.755	1.873	6.72
308.13	1.191	2.007	2.146	6.93
323.13	0.425	0.598	0.635	6.19
323.13	0.65	0.897	0.947	5.57
323.13	0.898	1.199	1.263	5.34
323.13	1.156	1.485	1.563	5.25
323.13	1.396	1.728	1.815	5.03
323.13	1.665	1.957	2.066	5.57
338.15	0.403	0.449	0.461	2.67
338.15	0.697	0.766	0.787	2.74
338.15	0.997	1.094	1.091	0.27
338.15	1.302	1.370	1.370	0.00
338.15	1.632	1.621	1.640	1.17
338.15	2.008	1.899	1.907	0.42
338.15	2.292	2.082	2.080	0.10
353.18	0.404	0.368	0.366	0.54
353.18	0.696	0.646	0.642	0.62
353.18	0.972	0.917	0.884	3.60
353.18	1.431	1.317	1.246	5.39
353.18	2.061	1.745	1.665	4.58
353.18	2.483	2.006	1.897	5.43
353.18	3.082	2.270	2.158	4.93
368.16	0.41	0.321	0.296	7.79
368.16	1.028	0.891	0.803	9.88
368.16	1.433	1.203	1.095	8.98
368.16	1.94	1.586	1.419	10.53
368.16	2.495	1.989	1.723	13.37
368.16	2.997	2.236	1.952	12.70
368.16	3.503	2.482	2.141	13.74
368.16	3.915	2.601	2.262	13.03

Table 3.8. Experimental and predicted water mole fractions in the vapour phase of the propane - water system.

T / K	P_{exp} / MPa	Experimental water content	Predicted water content	AD%
Kobayashi and Katz (46)				
310.93	0.703	0.009540	0.008905	6.66
310.93	0.972	0.006960	0.006501	6.59
338.71	1.006	0.026490	0.024450	7.70
338.71	1.496	0.017020	0.015790	7.23
338.71	1.992	0.012000	0.011190	6.75
360.93	1.310	0.049670	0.047690	3.99
360.93	2.130	0.029100	0.027660	4.95
360.93	3.205	0.017220	0.015900	7.67
Song and Kobayashi (47)				
281.95	0.621	0.002000	0.001718	14.10
285.25	0.679	0.002028	0.001950	3.85
292.65	0.819	0.002668	0.002568	3.75
299.65	0.897	0.003494	0.003576	2.35

Table 3.9. Experimental (48) and calculated nitrogen mole fraction in the aqueous phase in nitrogen - water system.

T/K	P_{exp}/MPa	$x_{exp}\times10^3$	$x_{cal}\times10^3$	AD %
274.19	0.979	0.176	0.1704	3.18
274.19	1.9	0.3248	0.3248	0.00
274.18	3.006	0.5112	0.5039	1.43
274.18	3.837	0.6365	0.6337	0.44
274.19	4.868	0.795	0.7892	0.73
274.21	5.993	0.9626	0.9523	1.07
274.26	6.775	1.0733	1.0613	1.12
278.15	0.971	0.1552	0.1559	0.45
278.21	1.763	0.286	0.2789	2.48
278.19	2.99	0.4683	0.4631	1.11
278.19	3.99	0.6127	0.6073	0.88
278.16	4.934	0.7394	0.7395	0.01
278.05	5.9	0.8711	0.872	0.10
278.17	6.916	1.0149	1.0033	1.14
283.12	1.012	0.1439	0.1481	2.92
283.13	2.413	0.3441	0.3447	0.17
283.13	4.877	0.6684	0.6694	0.15
283.18	5.825	0.7971	0.7868	1.29
283.16	7.16	0.9538	0.9479	0.62
288.11	0.966	0.1318	0.1299	1.44
288.09	2.395	0.3158	0.3149	0.28
288.11	4.042	0.5168	0.5178	0.19
288.11	5.444	0.6829	0.6829	0.00
288.11	7.003	0.8609	0.8585	0.28
293.12	0.984	0.1195	0.1223	2.34
293.08	2.511	0.3025	0.3054	0.96
293.09	3.964	0.47	0.4719	0.40
293.09	5.655	0.657	0.657	0.00
293.09	6.945	0.7884	0.7925	0.52
298.07	1.004	0.1139	0.1164	2.19
298.1	2.233	0.259	0.2544	1.78
298.1	3.717	0.4111	0.4149	0.92
298.08	4.745	0.5206	0.5222	0.31
298.04	6.967	0.7457	0.7446	0.15
308.23	1.04	0.1033	0.1066	3.19
308.18	2.196	0.2152	0.2222	3.25
308.18	4.18	0.4	0.4126	3.15
308.19	7.032	0.655	0.6701	2.31
323.13	0.915	0.0843	0.0817	3.08
323.13	2.031	0.1846	0.1802	2.38
323.13	3.542	0.3028	0.3095	2.21
323.13	4.957	0.417	0.4266	2.30
323.14	7.043	0.5926	0.5926	0.00
342.99	0.992	0.0771	0.0783	1.56
342.92	2.424	0.1929	0.1922	0.36
342.98	4.956	0.3896	0.3854	1.08
342.98	6.941	0.5354	0.5303	0.95
362.9	1.001	0.0739	0.0733	0.81
362.9	1.9	0.1458	0.1428	2.06
363	3.396	0.2521	0.2558	1.47
362.92	4.776	0.3578	0.3575	0.08
363.02	6.842	0.5147	0.5053	1.83

Table 3.10. Experimental and predicted water mole fraction in the gas phase of the nitrogen - water system.

T/K	P/MPa	Experimental Data	Predicted Data	AD %
Rigby and Prausnitz (49)				
298.15	2.249	0.001529	0.001521	0.52
	3.090	0.001149	0.001138	0.96
	3.870	0.000941	0.000933	0.85
323.15	2.109	0.006260	0.006220	0.64
	3.742	0.003680	0.003662	0.49
	5.982	0.002420	0.002428	0.33
	7.700	0.001956	0.001969	0.66
348.15	4.221	0.010090	0.010113	0.23
	6.115	0.007210	0.007269	0.82
	8.972	0.005230	0.005252	0.42
373.15	5.717	0.019940	0.020022	0.41
	7.948	0.015030	0.014974	0.37
	10.152	0.012180	0.012163	0.14
Namiot and Bondareva (50)				
310.95	1.380	0.005020	0.004963	1.14
	3.100	0.002360	0.002326	1.44
	6.550	0.001220	0.001215	0.41
	10.340	0.000850	0.000852	0.24
	13.790	0.000690	0.000695	0.72
366.45	0.340	0.233000	0.236873	1.66
	1.380	0.060500	0.059820	1.12
	3.100	0.027700	0.027572	0.46
	6.550	0.013700	0.013933	1.70
	13.790	0.007470	0.007490	0.27
Althaus (29)				
273.15	0.500	0.001245	0.001249	0.32
	1.500	0.000427	0.000434	1.64
	4.000	0.000171	0.000181	5.85
	6.000	0.000127	0.000130	2.36
	8.000	0.000106	0.000106	0.00
	10.000	0.000091	0.000091	0.00
278.15	0.500	0.001780	0.001781	0.06
	1.500	0.000601	0.000618	2.83
	6.000	0.000178	0.000184	3.37
	8.000	0.000151	0.000149	1.32
	10.000	0.000122	0.000128	4.92
283.15	0.500	0.002504	0.002504	0.00
	1.500	0.000838	0.000868	3.58
	4.000	0.000354	0.000358	1.13
	6.000	0.000248	0.000256	3.23
	8.000	0.000205	0.000206	0.49
	10.000	0.000176	0.000176	0.00
293.15	1.500	0.001632	0.001645	0.80
	4.000	0.000654	0.000673	2.91
	6.000	0.000467	0.000479	2.57
	8.000	0.000375	0.000383	2.13
	10.000	0.000326	0.000326	0.00

Table 3.11. Experimental (51) (y_{2exp}) and predicted (y_{2prd}) water contents (mole fraction) in the nitrogen + water system.

T/K	P/MPa	$y_{2exp}\times10^4$	Literature model (51)		This Model	
			$y_{2prd}\times10^4$	*AD %*	$y_{2prd}\times10^4$	*AD %*
282.86	0.607	20.40	20.20	1.0	20.30	0.5
282.99	1.799	7.14	7.23	1.3	7.24	1.4
282.99	3.036	4.46	4.51	1.1	4.50	0.9
283.03	4.408	3.17	3.29	3.8	3.27	3.2
293.10	0.558	42.50	42.00	1.2	42.60	0.2
293.19	1.828	13.60	13.60	0.0	13.70	0.7
293.10	2.991	8.44	8.61	2.0	8.66	2.6
293.10	4.810	5.58	5.72	2.5	5.73	2.7
304.02	0.578	79.30	77.10	2.8	78.70	0.8
304.36	1.257	37.00	37.00	0.0	37.70	1.9
304.51	2.539	18.80	19.30	2.7	19.60	4.3
304.61	4.638	11.20	11.40	1.8	11.50	2.7
313.30	0.498	153.00	148.00	3.3	152.00	0.7
313.15	1.246	60.90	60.20	1.1	61.60	1.1
313.26	2.836	27.80	28.00	0.7	28.50	2.5
313.16	4.781	17.50	17.50	0.0	17.80	1.7
322.88	0.499	240.00	241.00	0.4	248.00	3.3
323.10	1.420	87.20	88.20	1.1	90.40	3.7
322.93	3.397	39.60	38.70	2.3	39.50	0.3
322.93	4.841	29.20	28.30	3.1	28.80	1.4
332.52	0.461	427.00	414.00	3.0	426.00	0.2
332.45	1.448	134.00	135.00	0.7	139.00	3.7
332.52	2.454	85.50	82.10	4.0	84.30	1.4
332.52	4.358	48.80	48.60	0.4	49.80	2.0
342.31	0.425	719.00	696.00	3.2	718.00	0.1
342.31	0.462	658.00	641.00	2.6	661.00	0.5
342.39	1.466	219.00	208.00	5.0	214.00	2.3
342.42	2.899	103.00	109.00	5.8	112.00	8.7
342.31	4.962	66.60	66.70	0.2	68.40	2.7
351.87	0.540	849.00	822.00	3.2	848.00	0.1
352.12	1.480	335.00	310.00	7.5	320.00	4.5
351.92	2.957	162.00	159.00	1.9	164.00	1.2
351.95	4.797	111.00	102.00	8.1	105.00	5.4
363.00	0.555	1260.00	1240.00	1.6	1280.00	1.6
363.08	4.874	161.00	155.00	3.7	160.00	0.6

Table 3.12. Experimental (52) and calculated H_2S mole fractions in the aqueous phase of H_2S - H_2O systems.

T /K	P /MPa	$x_{exp} \times 10^3$	$x_{cal} \times 10^3$	AD %
298.16	0.503	9.120	9.318	2.2
298.16	0.690	12.784	12.693	0.7
298.16	0.797	14.693	14.588	0.7
308.2	0.483	6.689	7.144	6.8
308.2	0.763	10.688	11.201	4.8
308.2	1.193	17.089	17.259	1.0
308.2	1.748	24.735	24.737	0.0
308.2	2.175	30.364	30.213	0.5
308.2	2.483	34.008	33.999	0.0
318.21	0.507	5.815	6.154	5.8
318.21	1.053	12.496	12.666	1.4
318.21	1.507	17.873	17.883	0.1
318.21	2.024	23.896	23.597	1.3
318.21	2.139	24.717	24.836	0.5
318.21	2.570	29.590	29.351	0.8
318.21	3.094	35.070	34.568	1.4
328.28	0.497	4.963	5.053	1.8
328.28	1.008	10.046	10.264	2.2
328.28	1.498	14.891	15.117	1.5
328.28	1.978	19.500	19.696	1.0
328.28	2.468	24.410	24.224	0.8
328.28	3.034	29.503	29.215	1.0
328.28	3.475	33.560	32.847	2.1
338.34	0.509	4.354	4.412	1.3
338.34	0.536	4.588	4.650	1.4
338.34	1.053	9.226	9.244	0.2
338.34	1.688	14.708	14.708	0.0
338.34	2.215	19.151	19.095	0.3
338.34	2.796	24.200	23.738	1.9
338.34	3.370	28.820	28.176	2.2
338.34	3.962	31.830	31.702	0.4

Table 3.13. Experimental (52) and predicted water mole fractions in the vapour phase of H_2S - H_2O systems.

T /K	P /MPa	$y_{1,exp} \times 10^3$	Predicted water content $\times 10^3$	AD %
298.16	0.503	6.53	6.643	1.7
298.16	0.690	4.70	4.943	5.2
308.2	0.503	10.46	11.781	12.6
308.2	0.762	7.19	7.987	11.1
308.2	0.967	5.77	6.432	11.5
308.2	1.401	4.38	4.655	6.3
308.2	1.803	3.64	3.789	4.1
308.2	2.249	3.20	3.208	0.3
318.21	0.518	21.28	19.470	8.5
318.21	0.999	11.30	10.580	6.4
318.21	1.053	11.16	10.091	9.6
318.21	1.519	7.44	7.338	1.4
318.21	1.944	5.92	6.002	1.4
318.21	2.531	4.70	4.931	4.9
318.21	2.778	4.61	4.630	0.4

Table 3.14. Experimental data used for developing this approach in the $L_W - V$ region.

Reference	T_{min} /K	T_{max} /K	P_{min} /MPa	P_{max}/MPa	Number of Points	AAD%
Althaus (29)	273.15	293.15	0.5	10	17	4.43
Rigby and Prausnitz (49)	298.15	373.15	2.35	9.35	12	1.07
Yokoyama et al. (53)	298.15	323.15	3	8	6	3.03
Gillespie and Wilson (24)	323.15	348.15	1.379	13.786	6	2.25
Kosyakov et al. (54)	273.16	283.16	1.01	6.08	5	7.52
Olds et al. (55)	310.93	377.59	2.67	13.81	11	8.65

Table 3.15. Constants *a*, *b*, *c* and *d* in equations (3.22) and (3.23) for methane – water system.

Constant	Value
a	0.069355849
b	-30.90480919
c	-0.000765359
d	0.317895764

Table 3.16. Comparison between the experimental data and the predictions of this approach in the *I – V region*.

Reference	T /K	P /MPa	Water Content Experimental (mole fraction)	Water Content This Work (mole fraction)	AD%
Althaus (29)	253.15	0.500	0.00021	0.00021	0.00
	258.15	1.500	0.00011	0.00012	9.09
	258.15	0.500	0.00031	0.00034	9.68
	263.15	1.500	0.00019	0.00019	0.00
	263.15	0.500	0.00052	0.00053	1.92
	268.15	1.500	0.00028	0.00029	3.57
	268.15	0.500	0.00083	0.00083	0.00
Kosyakov et al. (54)	263.15	1.013	0.00028	0.00027	3.57
	253.15	1.013	0.00011	0.00011	0.00
	243.15	1.013	0.00004	0.00004	0.00

Table 3.17*a*. Comparison between the predictions of this approach and *Bukacek* (1) correlation for water content of different natural gases (*NG*).

T /K	P /MPa	SG_g	Experimental Water Content	Predicted Water Content, This Work	AD %	Predicted Water Content, Bukacek (1)	AD %
NG1 (29)							
273.15	0.500	0.5654	1.169E-03	1.25E-03	6.93	1.24E-03	6.07
273.15	1.500	0.5654	4.26E-04	4.39E-04	3.05	4.62E-04	8.45
278.15	0.500	0.5654	1.68E-03	1.79E-03	6.55	1.82E-03	8.33
278.15	1.500	0.5654	6.05E-04	6.25E-04	3.31	6.53E-04	7.93
283.15	1.500	0.5654	8.42E-04	8.78E-04	4.28	9.11E-04	8.19
283.15	6.000	0.5654	2.51E-04	2.68E-04	6.77	2.97E-04	18.33
288.15	1.500	0.5654	1.16E-03	1.22E-03	5.17	1.25E-03	7.76
288.15	6.000	0.5654	3.56E-04	3.69E-04	3.65	4.02E-04	12.92
288.15	10.000	0.5654	2.50E-04	2.60E-04	4.00	2.88E-04	15.20
NG2 (29)							
273.15	0.500	0.598	1.19E-03	1.25E-03	5.04	1.24E-03	4.20
278.15	0.500	0.598	1.68E-03	1.79E-03	6.55	1.82E-03	8.33
278.15	1.500	0.598	5.99E-04	6.25E-04	4.34	6.53E-04	9.02
288.15	1.500	0.598	1.16E-03	1.22E-03	5.17	1.25E-03	7.76
288.15	4.000	0.598	4.68E-04	5.09E-04	8.76	5.44E-04	16.24
288.15	6.000	0.598	3.56E-04	3.69E-04	3.65	4.02E-04	12.92
293.15	6.000	0.598	4.65E-04	5.00E-04	7.53	5.39E-04	15.91
293.15	10.000	0.598	3.26E-04	3.50E-04	7.36	3.83E-04	17.48
NG3 (29)							
273.15	0.500	0.628	1.20E-03	1.25E-03	4.17	1.24E-03	3.33
278.15	0.500	0.628	1.72E-03	1.79E-03	4.07	1.82E-03	5.81
283.15	1.500	0.628	8.26E-04	8.78E-04	6.30	9.11E-04	10.29
288.15	1.500	0.628	1.15E-03	1.22E-03	6.09	1.25E-03	8.70
NG4 (29)							

273.15	0.500	0.6326	1.19E-03	1.25E-03	5.04	1.24E-03	4.20
278.15	0.500	0.6326	1.71E-03	1.79E-03	4.68	1.82E-03	6.43
278.15	1.500	0.6326	5.91E-04	6.25E-04	5.75	6.53E-04	10.49
283.15	1.500	0.6326	8.50E-04	8.78E-04	3.29	9.11E-04	7.18
288.15	1.500	0.6326	1.17E-03	1.22E-03	4.27	1.25E-03	6.84
288.15	4.000	0.6326	4.85E-04	5.09E-04	4.95	5.44E-04	12.16
293.15	6.000	0.6326	4.70E-04	5.00E-04	6.38	5.39E-04	14.68
293.15	8.000	0.6326	3.62E-04	4.06E-04	12.15	4.41E-04	21.82
NG_5 (29)							
273.15	0.500	0.6672	1.16E-03	1.25E-03	7.76	1.24E-03	6.90
278.15	0.500	0.6672	1.69E-03	1.79E-03	5.92	1.82E-03	7.69
283.15	1.500	0.6672	8.36E-04	8.78E-04	5.02	9.11E-04	8.97
288.15	1.500	0.6672	1.17E-03	1.22E-03	4.27	1.25E-03	6.84
NG_6 (29)							
273.15	0.500	0.6395	1.22E-03	1.25E-03	2.46	1.24E-03	1.64
278.15	0.500	0.6395	1.72E-03	1.79E-03	4.07	1.82E-03	5.81
278.15	1.500	0.6395	6.03E-04	6.25E-04	3.65	6.53E-04	8.29
283.15	1.500	0.6395	8.55E-04	8.78E-04	2.69	9.11E-04	6.55
288.15	1.500	0.6395	1.16E-03	1.22E-03	5.17	1.25E-03	7.76
288.15	6.000	0.6395	3.49E-04	3.69E-04	5.73	4.02E-04	15.19
NG_7 (29)							
278.15	0.500	0.8107	1.76E-03	1.79E-03	1.70	1.82E-03	3.41
Synthetic mixture containing 96.94 mole % of methane and 3.06 mole % of ethane (29)							
278.15	1.500	0.569	6.12E-04	6.25E-04	2.12	6.53E-04	6.70
288.15	4.000	0.569	4.94E-04	5.09E-04	3.04	5.44E-04	10.12
288.15	6.000	0.569	3.52E-04	3.69E-04	4.83	4.02E-04	14.20
288.15	8.000	0.569	2.86E-04	3.00E-04	4.90	3.31E-04	15.73
288.15	10.000	0.569	2.48E-04	2.60E-04	4.84	2.88E-04	16.13

Table 3.17*b*. Composition (mole%) of different natural gases (29).

Gas / Gravity / Component	0.5654 (NG_1)	0.598 (NG_2)	0.628 (NG_3)	0.6326 (NG_4)	0.6672 (NG_5)	0.6395 (NG_6)	0.8107 (NG_7)
Helium	0.015	0.028	-	0.152	0.004	0.043	0.038
Nitrogen	0.840	1.938	0.912	4.863	0.800	10.351	1.499
Carbon Dioxide	0.109	0.851	-	0.167	1.732	1.291	25.124
Methane	98.197	93.216	88.205	86.345	84.339	83.847	70.144
Ethane	0.564	2.915	8.360	6.193	8.724	3.460	2.520
Propane	0.189	0.715	1.763	1.550	3.286	0.657	0.394
i-Butane	0.029	0.093	0.293	0.214	0.311	0.093	0.067
n-Butane	0.038	0.135	0.441	0.314	0.584	0.126	0.074
C_5	0.014	0.058	0.027	0.130	0.163	0.067	0.054
C_{6+}	0.007	0.049	-	0.064	0.049	0.069	0.118

Table 3.18. Constants b_1-b_3 in equation 3.32.

Constant	Value
b_1	0.17006
b_2	-0.15241
b_3	-0.04515

Table 3.19. Experimental and predicted water content of nitrogen in the $L_W - V$ region.

Reference	T_{min} /K	T_{max} /K	P_{min} /MPa	P_{max}/MPa	Number of Points	AAD%
Maslennikova et al. (56)	298.15	373.15	5	10	12	6.09
Sidorov et al. (57)	373.15	373.15	5.066	10.133	2	3.19
Althaus (29)	273.15	293.15	0.5	10	22	5.91
Rigby and Prausnitz (49)	298.15	373.15	2.109	10.152	13	1.65

Table 3.20. Comparison between experimental water content data of different sour gases (with low and intermediate concentrations of acid gases) and predictions of the approach developed in this work (Values are in mole fraction).

T /K	P/ MPa	Gas Composition (mole fraction)			Experimental	Predictions, This Work	AD%
		Methar	CO_2	H_2S			
GPA Engineering Databook (10)							
311.15	13.800	0.89	0.11	-	8.08E-04	7.63E-04	5.57
311.15	13.800	0.8	0.2	-	8.08E-04	7.63E-04	5.57
327.15	10.300	0.92	-	0.08	2.21E-03	1.98E-03	10.41
344.15	6.900	0.89	0.11	-	5.67E-03	5.64E-03	0.53
344.15	6.900	0.8	0.2	-	5.59E-03	5.64E-03	0.89
344.15	6.900	0.83	-	0.17	5.79E-03	5.64E-03	2.59
344.15	9.430	0.725	-	0.275	4.90E-03	4.39E-03	10.41
Lukacs and Robinson (58)							
344.26	2.468	0.79	-	0.21	1.50E-02	1.41E-02	6.00
344.26	4.212	0.81	-	0.19	9.30E-03	8.67E-03	6.77
344.26	6.376	0.71	-	0.29	6.90E-03	6.05E-03	12.32
344.26	6.962	0.83	-	0.17	6.16E-03	5.62E-03	8.77
344.26	9.595	0.725	-	0.275	5.20E-03	4.35E-03	16.35
344.26	9.616	0.84	-	0.16	4.75E-03	4.34E-03	8.63
Ng et al. (59)							
322.04	1.379	0.75[+]	0.0625	0.1875	9.367E-03	8.87E-03	5.31
322.04	1.379	0.75[+]	0.1875	0.0625	8.74E-03	8.87E-03	1.49
322.04	10.339	0.75[+]	0.1875	0.0625	1.871E-03	1.56E-03	16.62
322.04	10.339	0.75[+]	0.0625	0.1875	1.814E-03	1.56E-03	14.00
366.48	1.379	0.75[*]	0.1875	0.0625	5.93E-02	5.93E-02	0.00
366.48	1.379	0.75[*]	0.0625	0.1875	5.9674E-02	5.93E-02	0.63
366.48	4.136	0.75[+]	0.1875	0.0625	2.9922E-02	2.09E-02	30.15
366.48	10.339	0.75[*]	0.1875	0.0625	1.1179E-02	9.45E-03	15.47
366.48	10.339	0.75[*]	0.0625	0.1875	1.0448E-02	9.45E-03	9.55
366.48	10.339	0.75[+]	0.1875	0.0625	1.0053E-02	9.45E-03	6.00

[*] *This mixture consists of methane and propane with a molar ratio equal to 95:5*
[+] *Composition of this mixture is 90 % methane, 6 % ethane, 2.5 % propane, 0.6 % i-butane and 0.9 % n-butane*

Table 3.21. Constants of equation 3.31.

Constant	Value
c_1	0.03185
c_2	0.01538
c_3	-0.02772

Table 3.22. Application ranges of equation 3.31.

Acid gas	T/ K	P/ MPa	Maximum concentration of acid gas/ mole%
H_2S	310-420	0.5-40	30
CO_2	310-420	0.5-40	50
$CO_2 + H_2S$	310-420	0.5-35	15% H_2S and 35% CO_2

Table 3.23. Comparison between experimental water content data of different sour gases and predictions of the correlation developed in this work (Values are in mole fraction).

T /K	P/ MPa	Gas Composition (mole fraction)			Experimental	Predictions, This Work	AD%
		Methar	CO_2	H_2S			
GPA Engineering Databook (10)							
311.15	13.800	0.89	0.11	-	8.08E-04	8.48E-04	4.95
311.15	13.800	0.8	0.2	-	8.08E-04	9.18E-04	13.61
327.15	10.300	0.92	-	0.08	2.21E-03	2.12E-03	4.07
344.15	6.900	0.89	0.11	-	5.67E-03	5.89E-03	3.88
344.15	6.900	0.8	0.2	-	5.59E-03	6.09E-03	8.94
344.15	6.900	0.83	-	0.17	5.79E-03	6.15E-03	6.22
344.15	9.430	0.725	-	0.275	4.90E-03	5.28E-03	7.76
Lukacs and Robinson (58)							
344.26	2.468	0.79	-	0.21	1.50E-02	1.46E-02	2.67
344.26	4.212	0.81	-	0.19	9.30E-03	9.17E-03	1.40
344.26	6.376	0.71	-	0.29	6.90E-03	6.90E-03	0.00
344.26	6.962	0.83	-	0.17	6.16E-03	6.13E-03	0.49
344.26	9.595	0.725	-	0.275	5.20E-03	5.25E-03	0.96
344.26	9.616	0.84	-	0.16	4.75E-03	4.86E-03	2.32
Ng et al. (59)							
322.04	1.379	0.75[+]	0.0625	0.1875	9.367E-03	9.06E-03	3.28
322.04	1.379	0.75[+]	0.1875	0.0625	8.74E-03	9.04E-03	3.43
322.04	10.339	0.75[+]	0.1875	0.0625	1.871E-03	1.86E-03	0.59
322.04	10.339	0.75[+]	0.0625	0.1875	1.814E-03	1.90E-03	4.74
366.48	1.379	0.75[*]	0.1875	0.0625	5.93E-02	5.99E-02	1.01
366.48	1.379	0.75[*]	0.0625	0.1875	5.9674E-02	6.00E-02	0.55
366.48	4.136	0.75[+]	0.1875	0.0625	2.9922E-02	2.19E-02	26.81
366.48	10.339	0.75[*]	0.1875	0.0625	1.1179E-02	1.08E-02	3.39
366.48	10.339	0.75[*]	0.0625	0.1875	1.0448E-02	1.10E-02	5.28
366.48	10.339	0.75[+]	0.1875	0.0625	1.0053E-02	1.08E-02	7.43

[*] *This mixture consists of methane and propane with a molar ratio equal to 95:5*
[+] *Composition of this mixture is 90 % methane, 6 % ethane, 2.5 % propane, 0.6 % i-butane and 0.9 % n-butane*

Table 3.24. Estimation of water dew point temperature (K) of methane using *Bukacek* (1) correlation and this model.

P/MPa	Water Content / mg/Nm^3	Bukacek (1) correlation	This model	Absolute Difference
15	319.97	298.15	299.3	1.15
10	404.99	298.15	299.48	1.33
5	660.14	298.15	299.22	1.07
2	1426.58	298.15	298.71	0.56
13	211.82	289.15	290.66	1.51
9	261.81	289.15	290.77	1.62
4	464.99	289.15	290.29	1.14
2	830.96	289.15	289.83	0.68

FIGURES

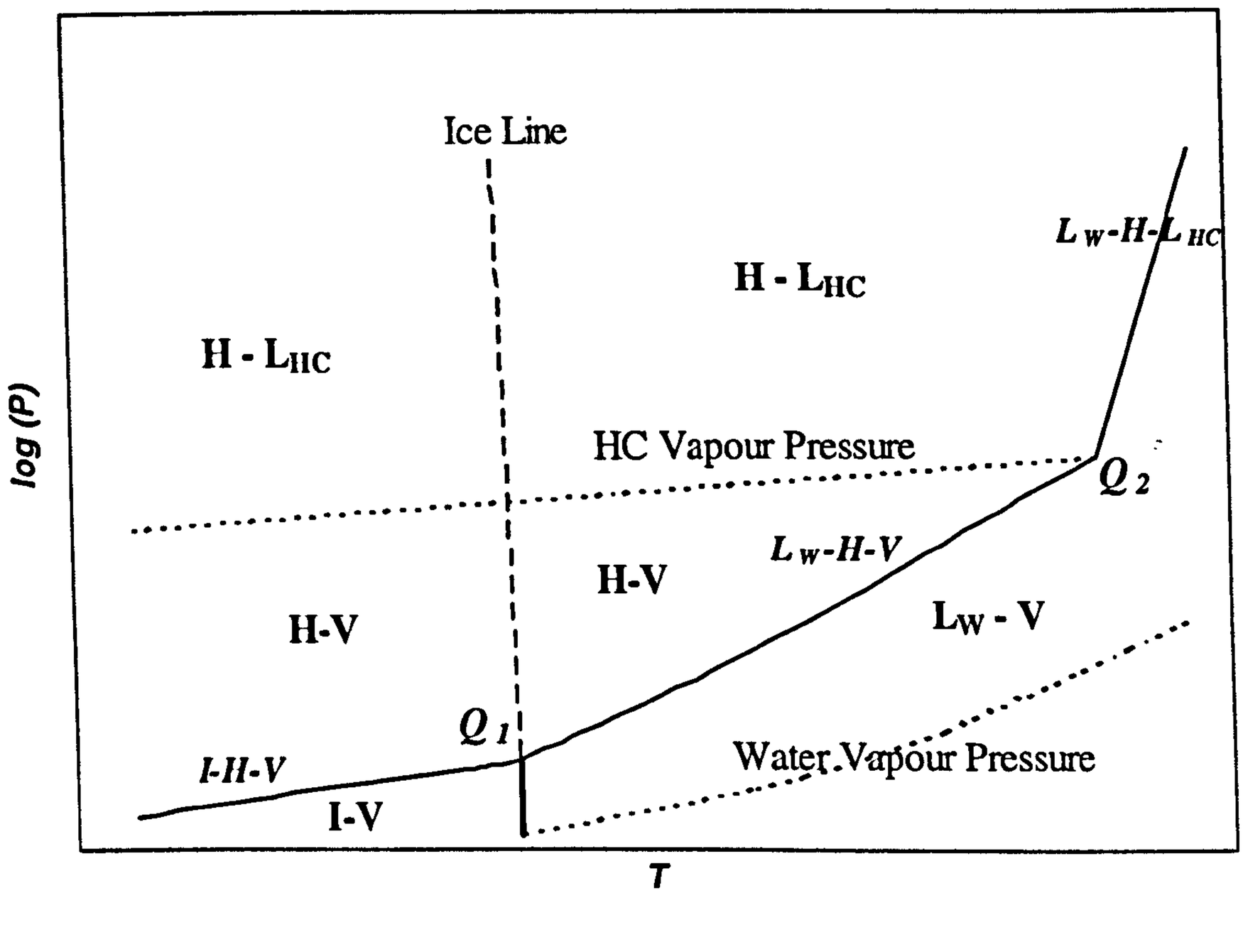

Figure 3.1. Typical pressure – temperature diagram for a water (limiting reactant) – single (pure) hydrocarbon system (29).

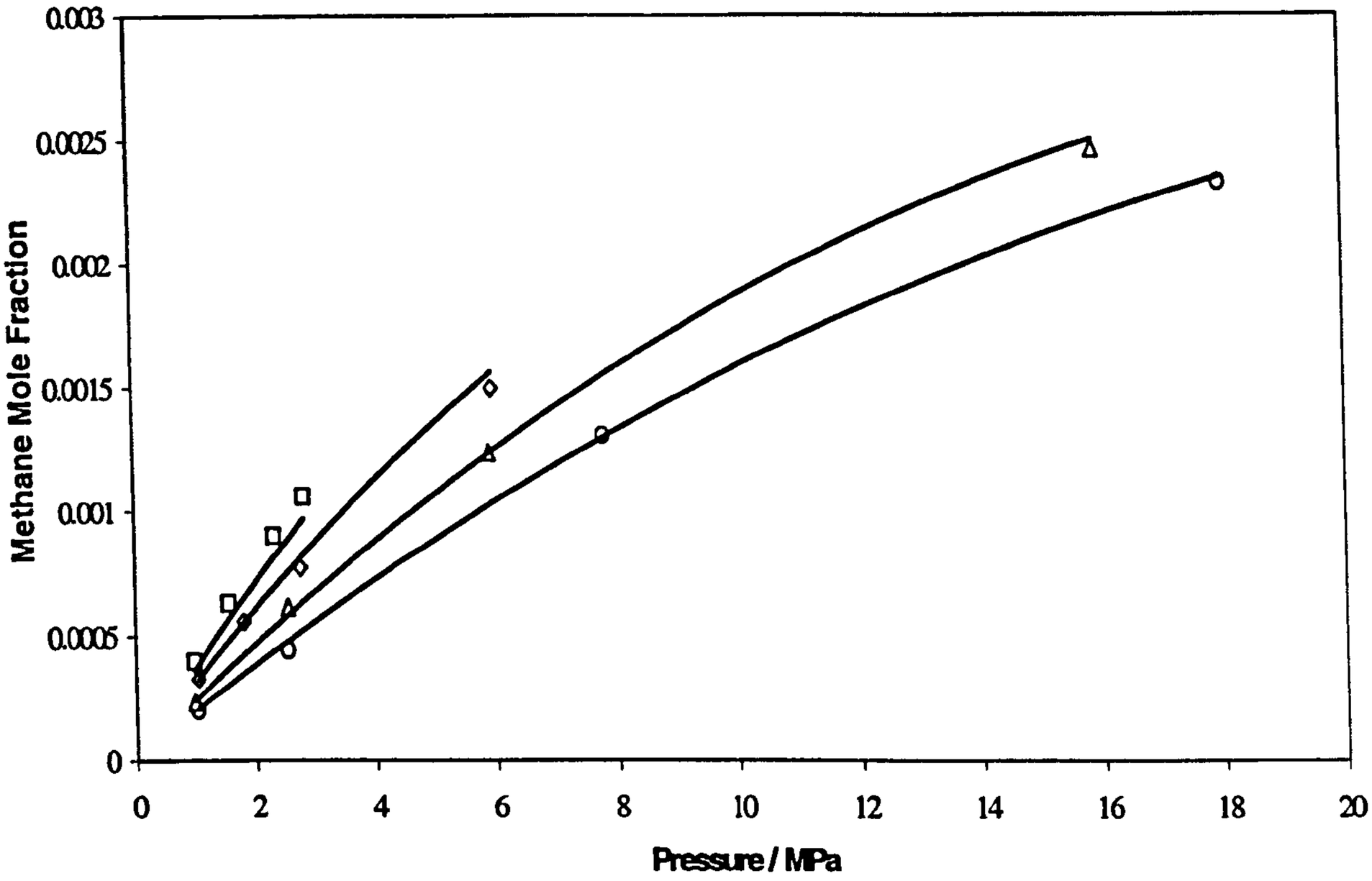

Figure 3.2. Methane mole fraction in water rich phase in the methane – water binary system as a function of pressure at various isotherms:

Experimental data (40): □, 275.11 K; ◇, 283.12 & 283.13 K; Δ, 298.13, 298.15 & 298.16 K; ○, 313.11 K. Solid lines, calculated with the VPT-EoS (12) and NDD mixing rules (13).

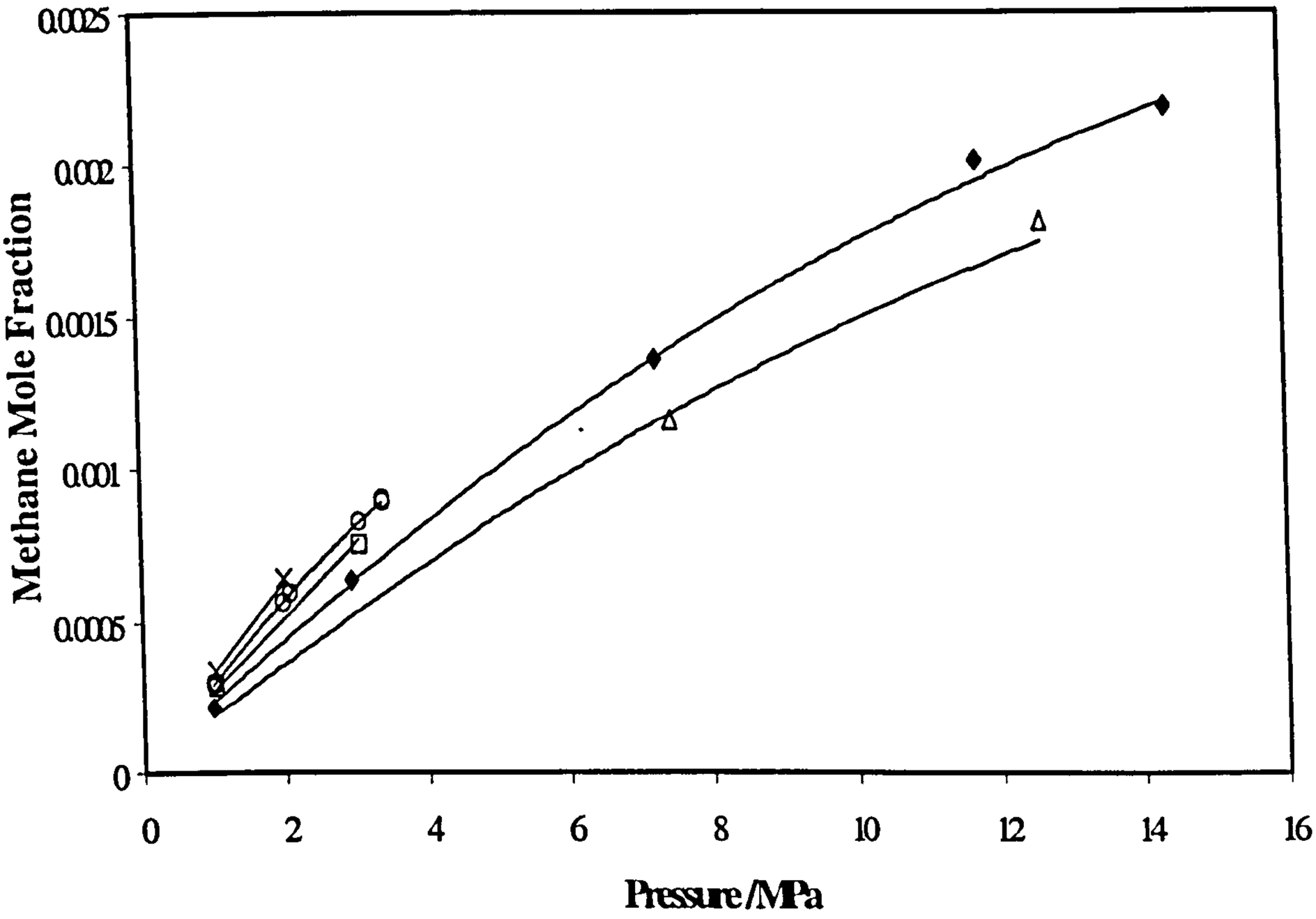

Figure 3.3. Methane solubilities in the gas mixture (94 mole% methane + 4 mole% ethane + 2 mole% n-butane) - water system as a function of pressure at various isotherms:

Experimental data (40): ×, 278.14 & 278.15 K ; ○, 283.14, 283.15 & 283.16 K ; □, 288.16 & 288.17 K; ♦, 298.14 K; Δ, 313.12 K; Solid lines, calculated with the VPT-EoS (12) and NDD mixing rules (13).

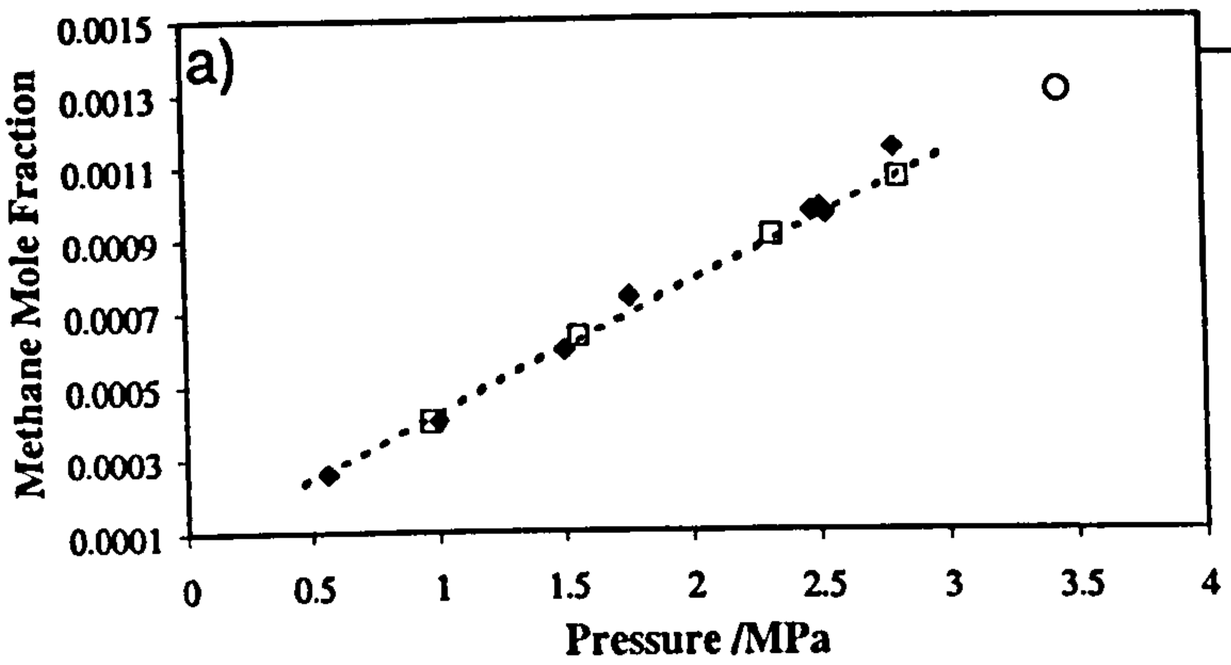

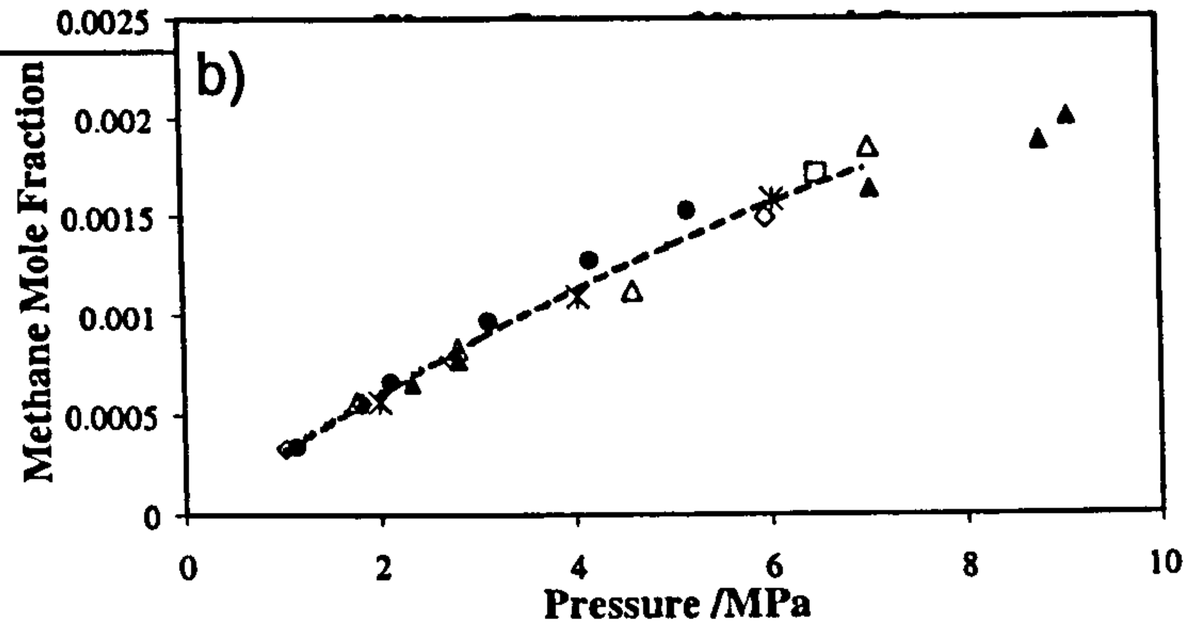

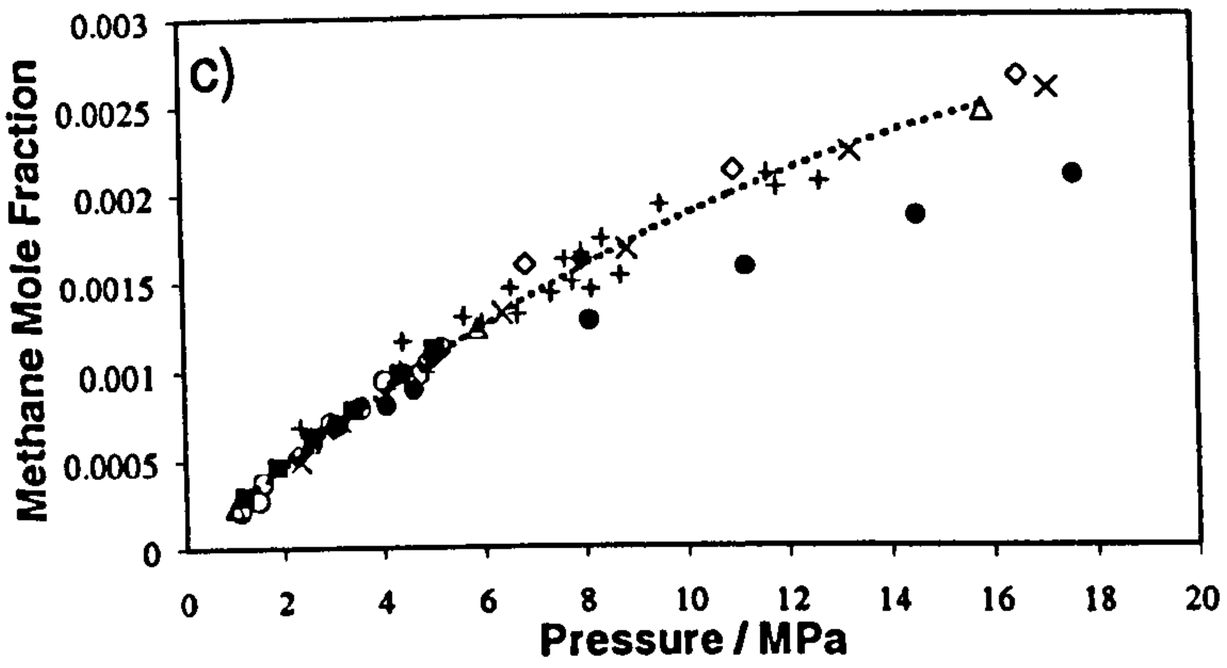

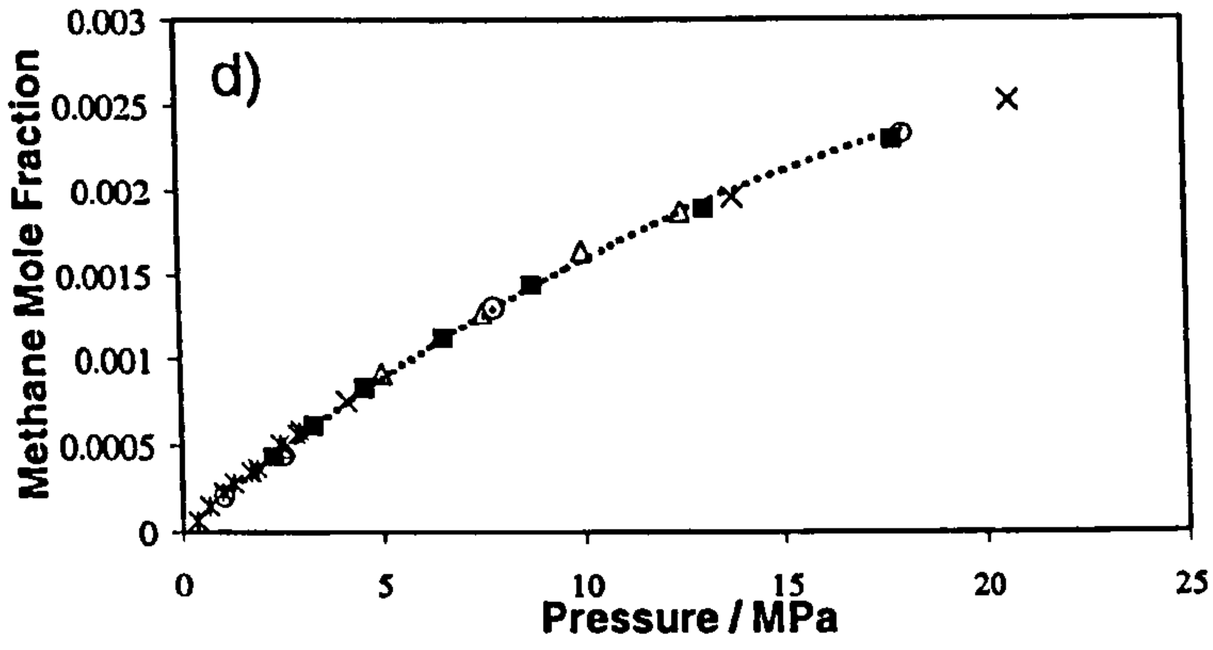

Figure 3.4. Comparison of experimental methane solubilities in water in the methane – water binary system:

a) □, 275.11 K; ○, 274.15 K from (60); ♦, 274.29 K from (61).
b) ◇, 283.13 K; ●, 283.15 K from (62); Δ, 283.2 K from (61); ∗, 283.2 K from (63); ▲, 285.65 K from (61).
c) Δ, 298.15 K; ▲, 298.15 K from (64); ×, 298.15 K from (65); Δ, 298.15 from (66); +, 298.1 from (67); ●, 298.15 K from (68); ♦ ; 298.2 K from (69); ■, 298.15 from (53); ○, 298.15 K from (70); ♦, 298.15 K from (53); ◇, 298.15 K from (71).
d) ○, 313.11 K; ×, 310.93 from (72); ■, 310.93 from (66); Δ, 313.2 K from (73);

Dashed lines, calculated with the VPT-EoS (12) and NDD mixing rules (13).

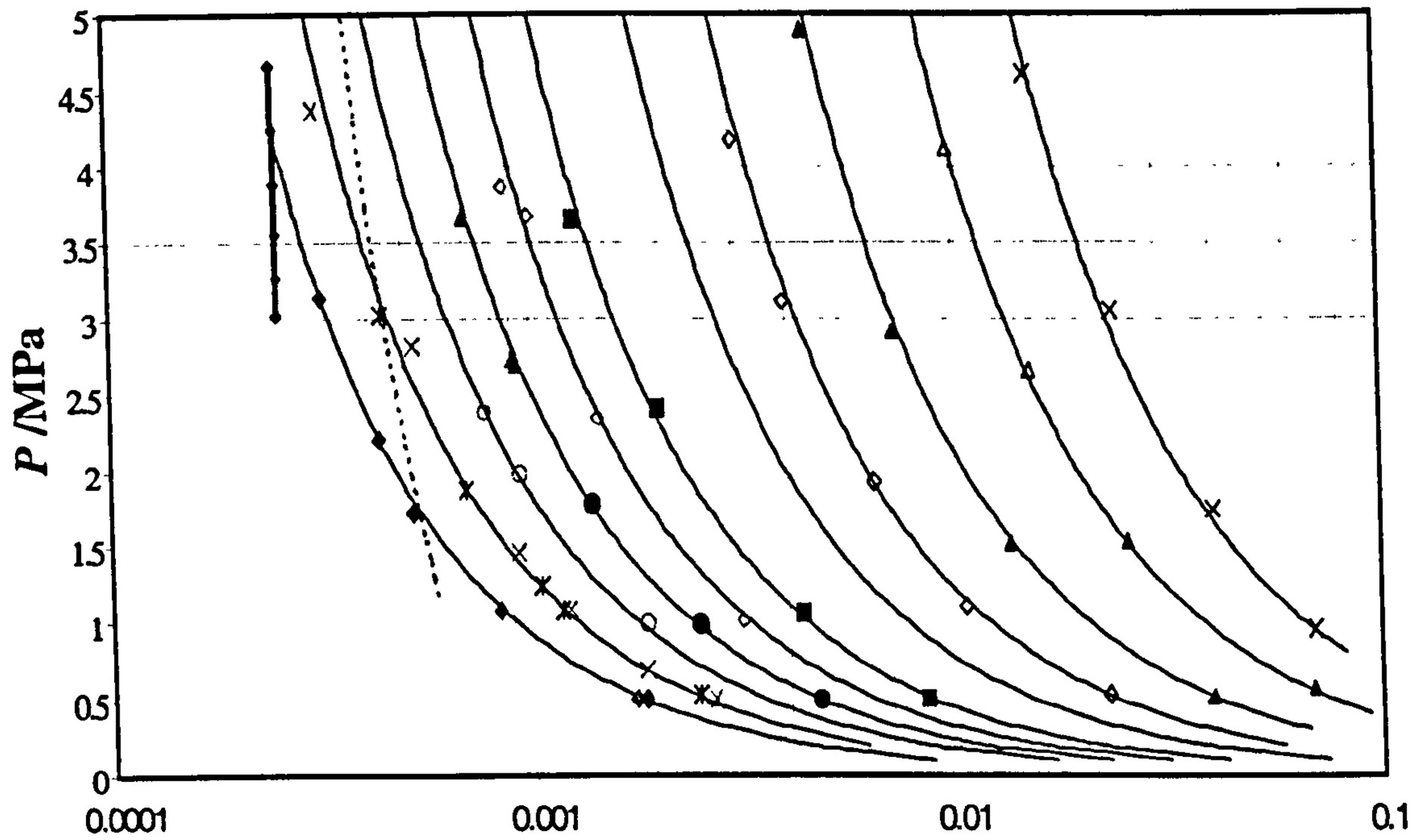

Figure 3.5. Water content (mole fraction) in the gas (or vapour) phase of the methane – water and methane – ethane – *n*-butane – water systems:

CH_4 - H_2O: ♦, 277.8 K; ×, 282.9 K; ▲, 287.7 K; ○, 292.7 K; ◇, 297.6 K. CH_4 – C_2H_6 – n-C_4H_{10} - H_2O: ◆, 278.1 K; ✱, 282.8 K; ●, 292.8 K; ■, 303.1 K; ◇, 321.9 K; ▲, 332.9 K; △, 347.2 K; × , 361.2 K (Experimental data from 42). Dashed line: Water content at mixture hydrate forming conditions. Thick solid line: Water content at methane hydrate forming conditions.

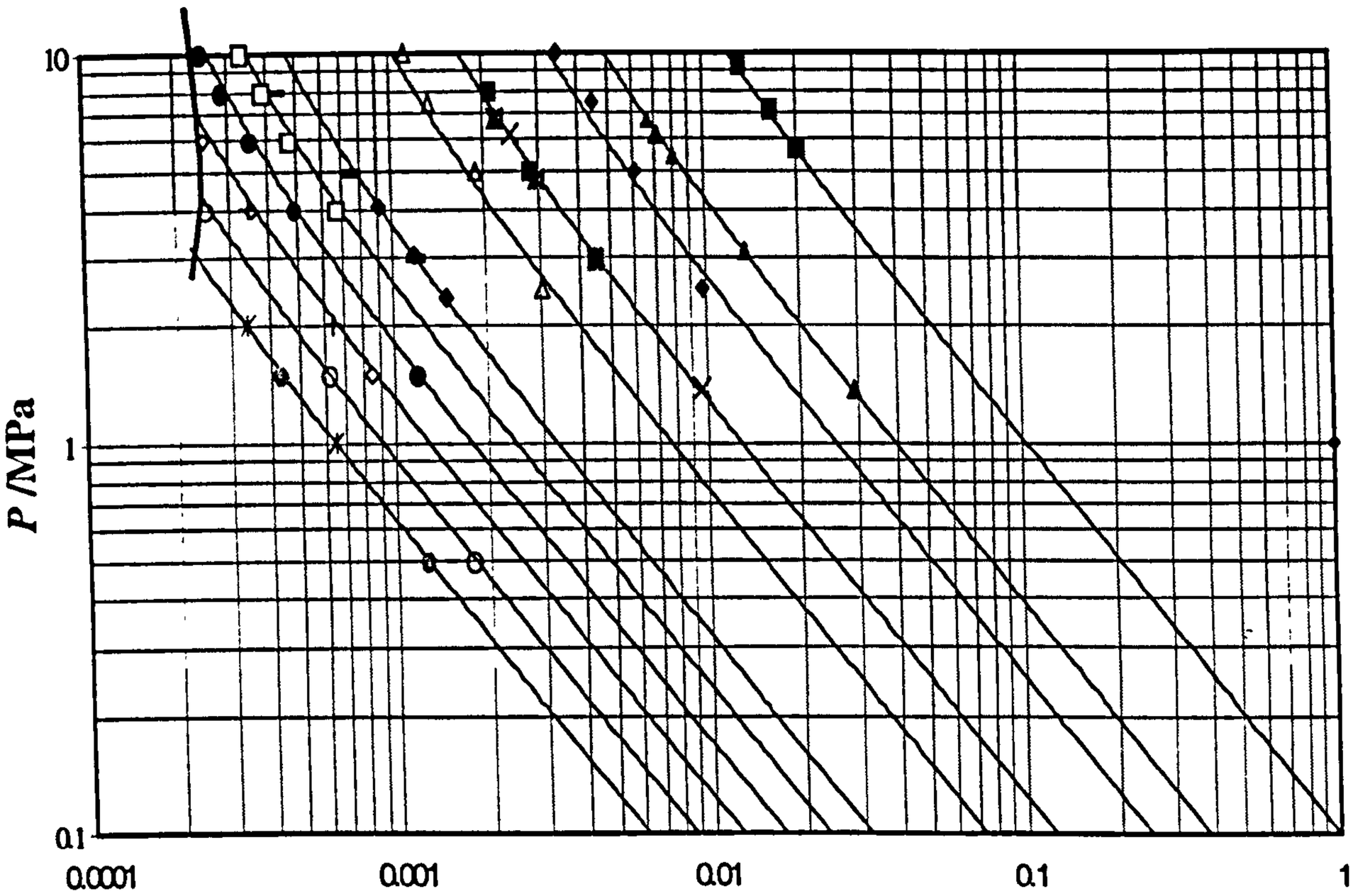

Figure 3.6. Water content (mole fraction) in the gas (or vapor) phase of the methane – water system:

Solid line: Water content in the gas phase; Thick solid line: Water content in the gas phase at Methane hydrate dissociation conditions; ●, 273.15 K from Althaus (29); ✱, 273.15 K from Kosyakov et al. (54); ○, 278.15 K from Althaus (29); ◇, 283.15 K from Althaus (29); + ,283.15 K from Kosyakov et al. (54); ●, 288.15 K from Althaus (29); □, 293.15 K from Althaus (29); ◆, 298.15 K from Rigby and Prausnitz (49); —, 298.15 K from Yokoyama et al. (53); △, 313.15 K from Yarym-Agaev et al (69); ✱, 323.15 K from Rigby and Prausnitz (49); ■, 323.15 K from Yokoyama et al. (53); ×, 323.15 K from Gillespie and Wilson (24); ▲, 348.15 K from Gillespie and Wilson (24); ▲, 348.15 K from Rigby and Prausnitz (49); ■, 373.15 K from Rigby and Prausnitz (49).

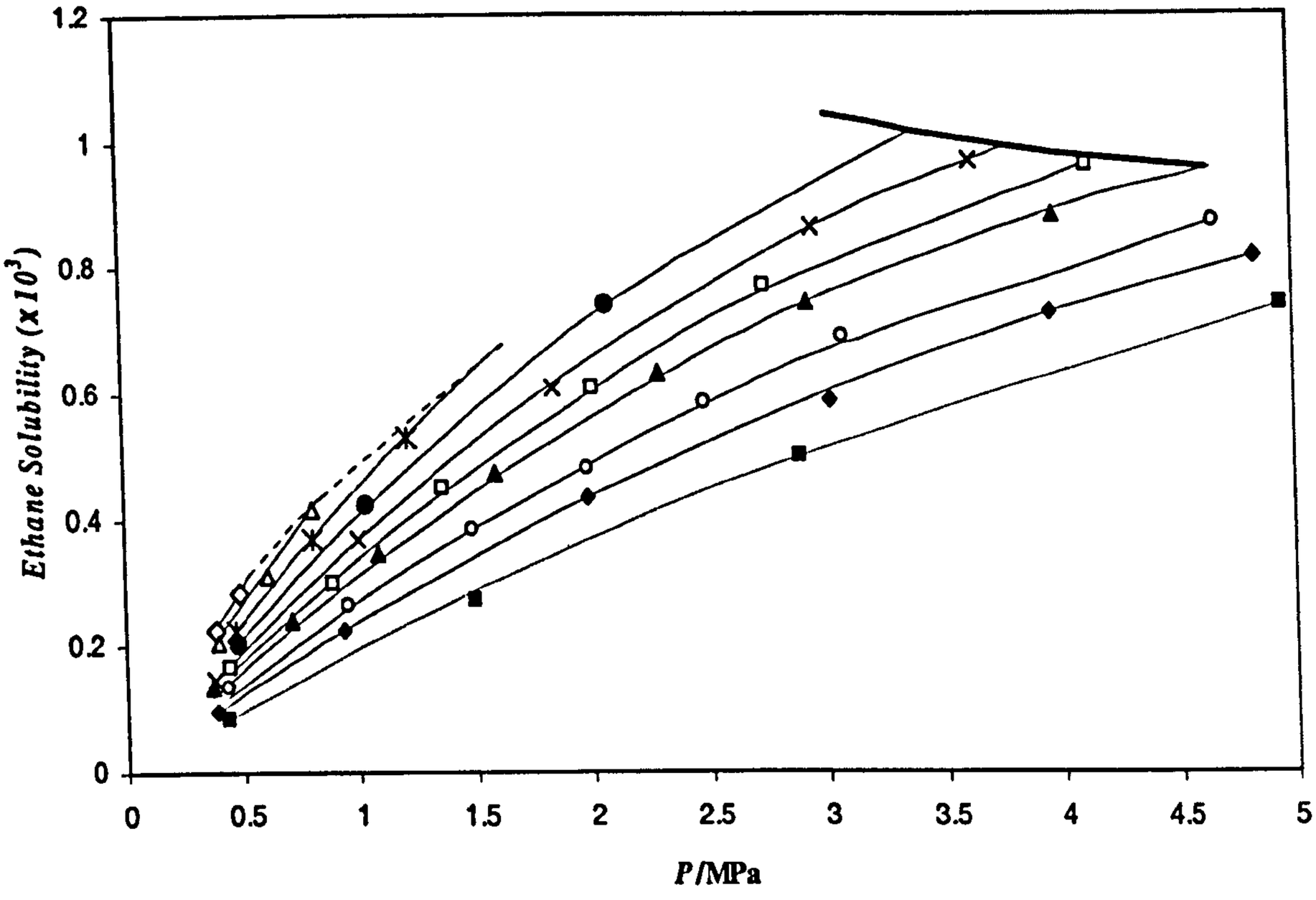

Figure 3.7. Experimental and calculated ethane solubility (mole fraction) in the aqueous phase as a function of pressure at various temperatures:

Experimental data (43): ◇, 274.26 K; Δ, 278.06 K; *, 283.11 K; ●, 288.07 K; ×, 293.31 K; □, 298.35 K; ▲, 303.22 K; ○, 313.19 K; ♦, 323.19 K; ■, 343.06 K. Solid curves, calculated with the VPT-EoS (12) and NDD mixing rules (13). Bold solid curve: Ethane vapour pressure (VLL three phase line); Dashed curve: Hydrate phase boundary.

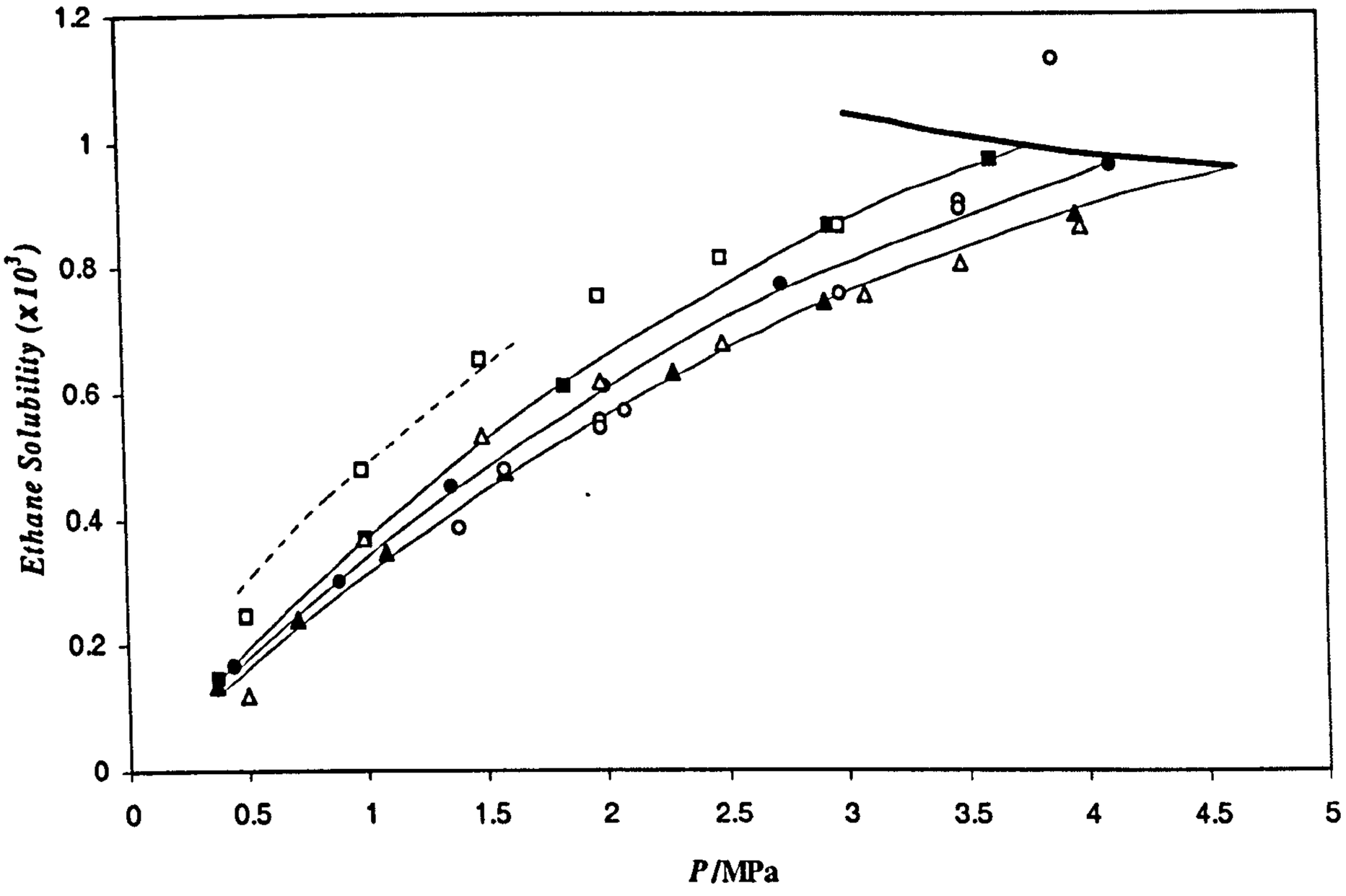

Figure 3.8. Comparison of experimental ethane solubilities (mole fraction) in water: □, 293.2 K, from (63); ■, 293.31 K, from (43); ○, 298.15 K, from (71); ●, 298.35 K, from (43); Δ, 303.2 K, from (63); ▲, 303.22 K, from (43). Solid curves, calculated with the VPT-EoS (12) and NDD mixing rules (13). Bold solid curve: Ethane vapour pressure (VLL three phase line); Dashed curve: Hydrate phase boundary.

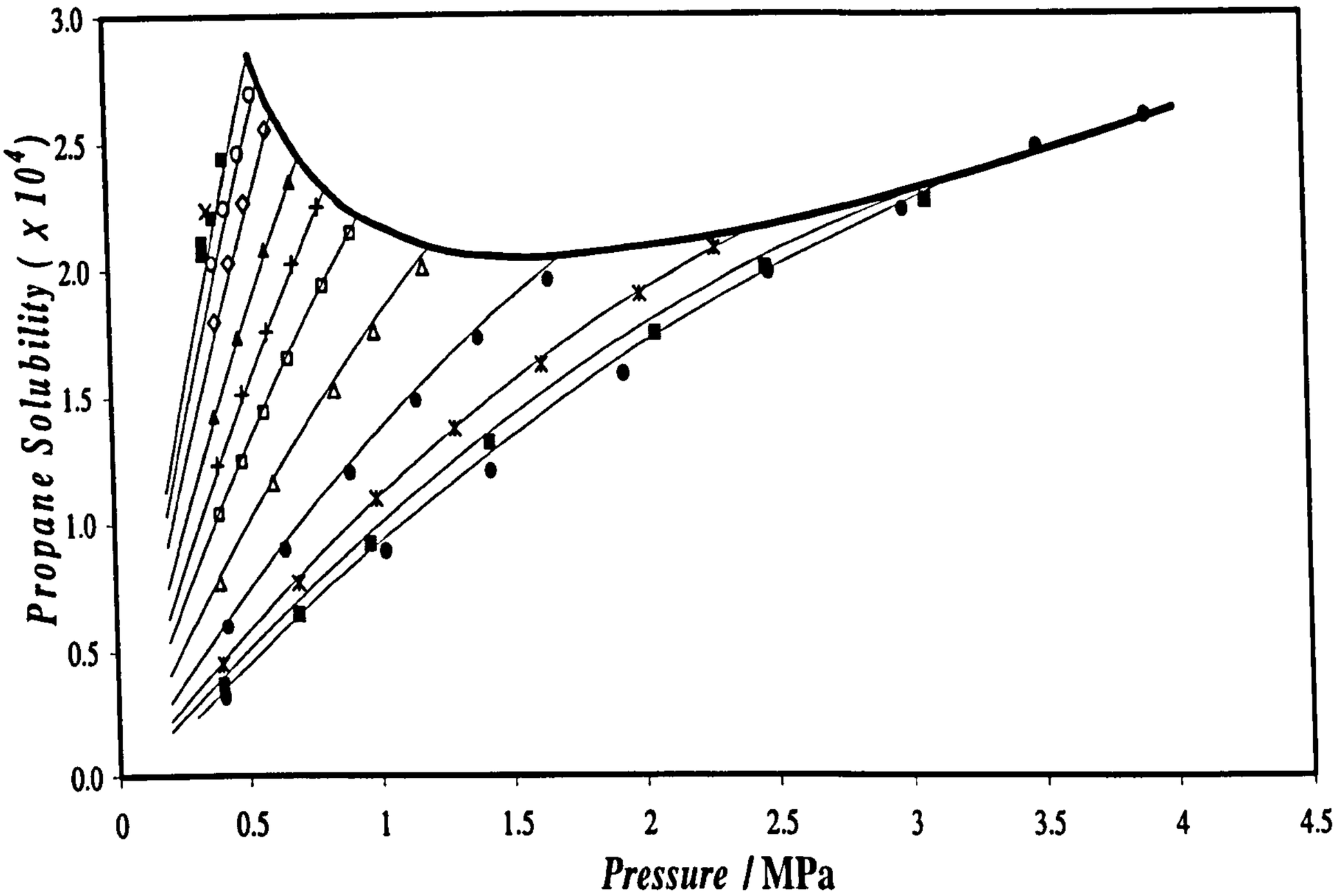

Figure 3.9. Propane mole fraction in the aqueous phase as a function of pressure at various temperatures:

Experimental data (45): ×, 277.62 K; ■, 278,09 K; ○, 280.14 K; ◇, 283.06 K; ▲, 288.13 K; +, 293.13 K; □, 298.12 K; Δ, 308.13 K; ●, 323.13 K; *, 338.15 K; ■, 353.18 K; ●, 368.16 K. Thin Solid lines, calculated with the VPT-EoS (12) and NDD mixing rules (13). Bold Solid line: VLL three phase line, delimiting the vapour-liquid and liquid-liquid coexistence regions

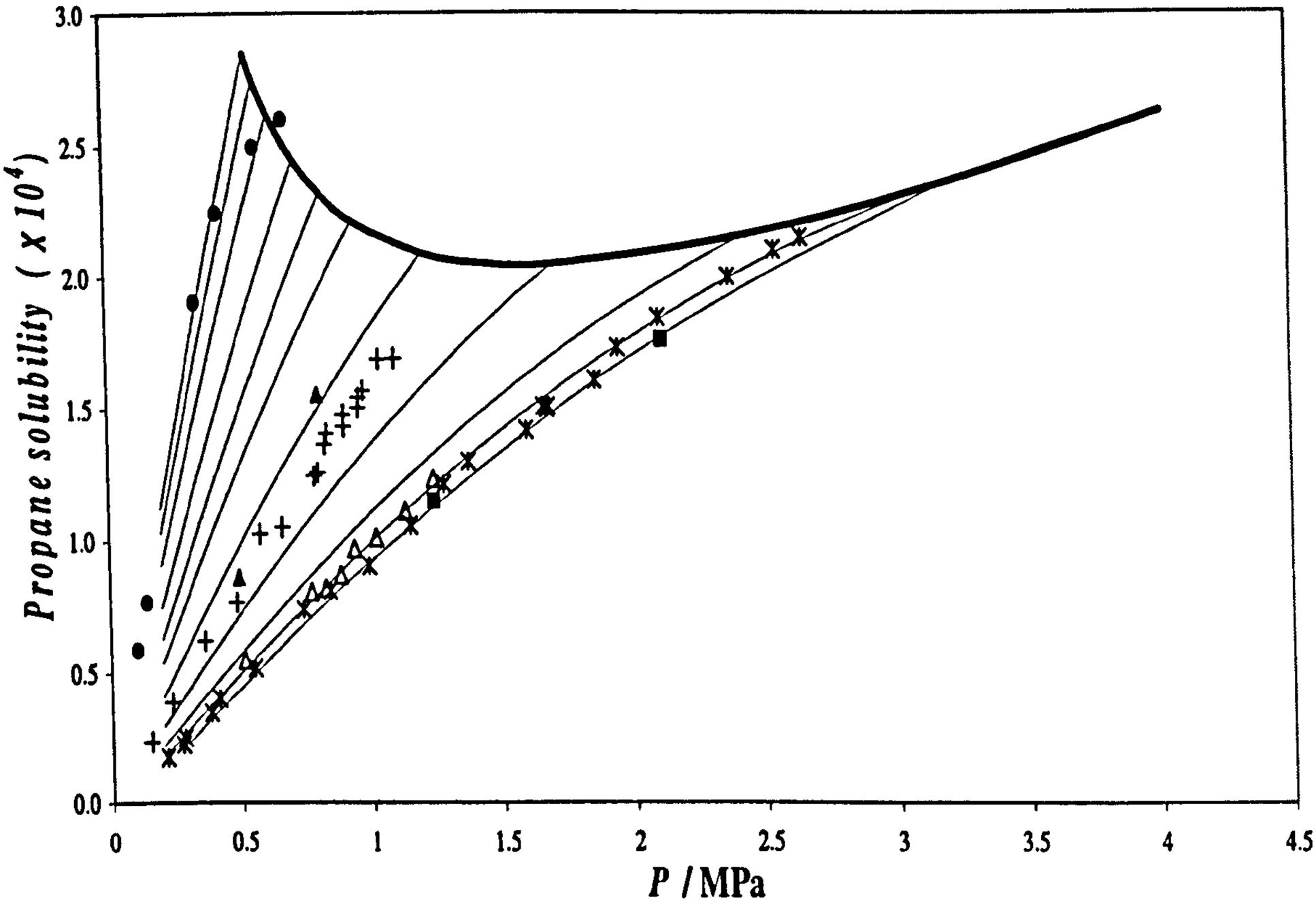

Figure 3.10. Comparison of experimental propane solubilities in water:

•, 288.71 K from (74); ▲, 310.93 K from (46); +, 310.93 from (74); △, 344.26 K from (75); ∗, 344.26 K from (74); ■, 349.82 K from (46). Solid lines, calculated with the VPT-EoS (12) and NDD mixing rules (13) at 278.09 K, 280.14 K; 283.06 K,. 288.13 K, 293.13 K, 298.12 K, 308.13 K, 323.13 K, 338.15 K, 353.18 K and 368.16 K (from left to right). Bold Solid line: VLL three phase line, delimiting the vapour-liquid and liquid-liquid coexistence regions.

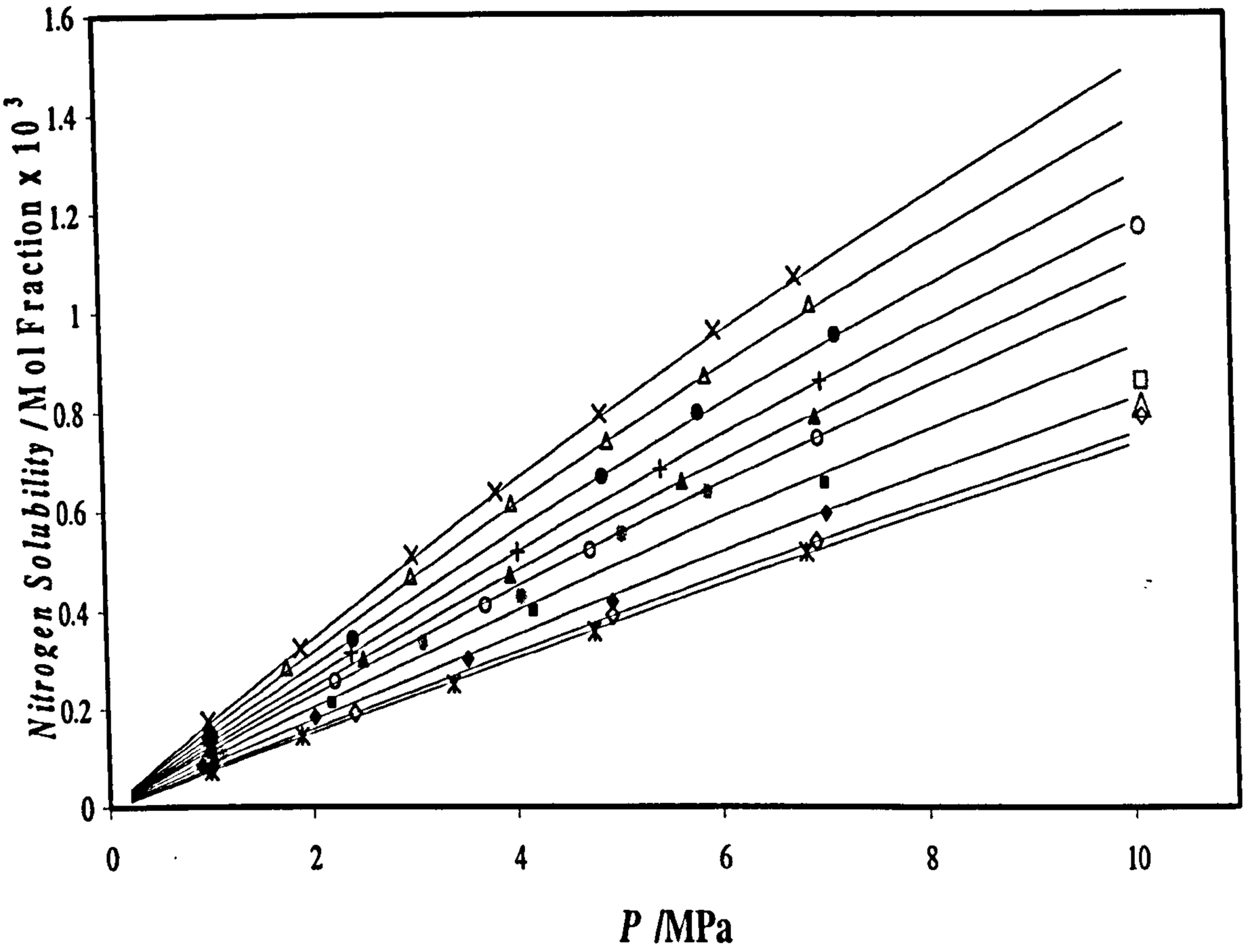

Figure 3.11. Nitrogen mole fraction in water rich phase as a function of pressure at various temperatures:

×, 274.2 K; △, 278.2 K; ●, 283.1 K; +, 288.1 K; ▲, 293.1 K; ○, 298.1 K; ■, 308.2 K; ♦, 323.1 K; ◇, 343.0 K; ✱, 363.0 K: From (48); ●, 303.1 K from (76) ; ○, 273.1 K from (77); □, 298.1 K from (77); △, 324.6 K from (78); ◇, 338.1 K from (79); Solid lines, calculated with the VPT-EoS (12) and NDD mixing rules (13).

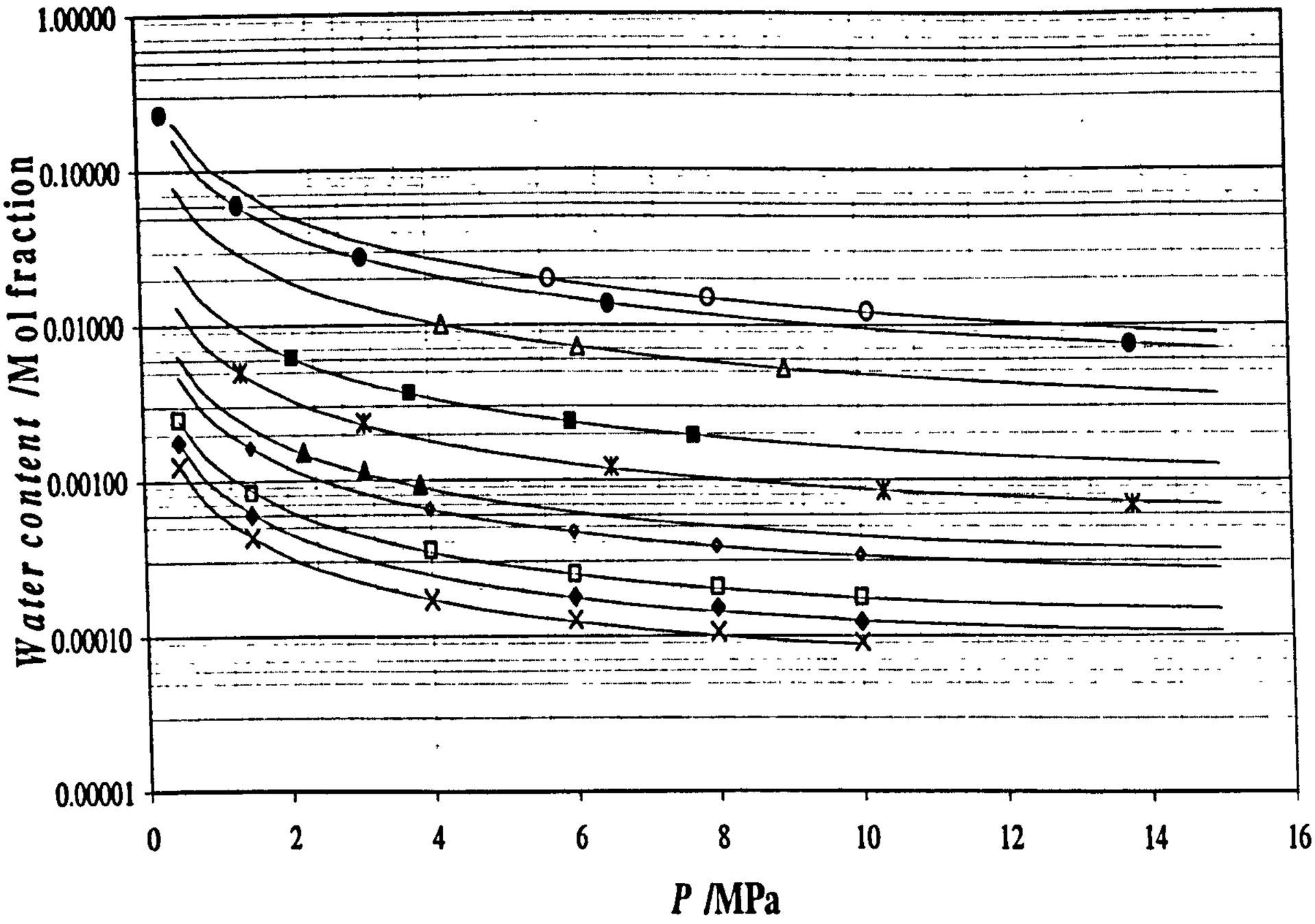

Figure 3.12. Water content in the gas phase of the nitrogen – water system:

×, 273.15 K from (29); ♦, 278.15 K from (29); □, 283.15 K from (29); ◇, 293.15 K from (29); ▲, 298.15 K from (49); ∗, 310.9 K from (50); ■, 323.15 K from (49); △, 348.15 K from (49); ●, 366.95 K from (50); ○, 373.15 K from (49); Solid lines, calculated with the VPT-EoS (12) and NDD mixing rules (13).

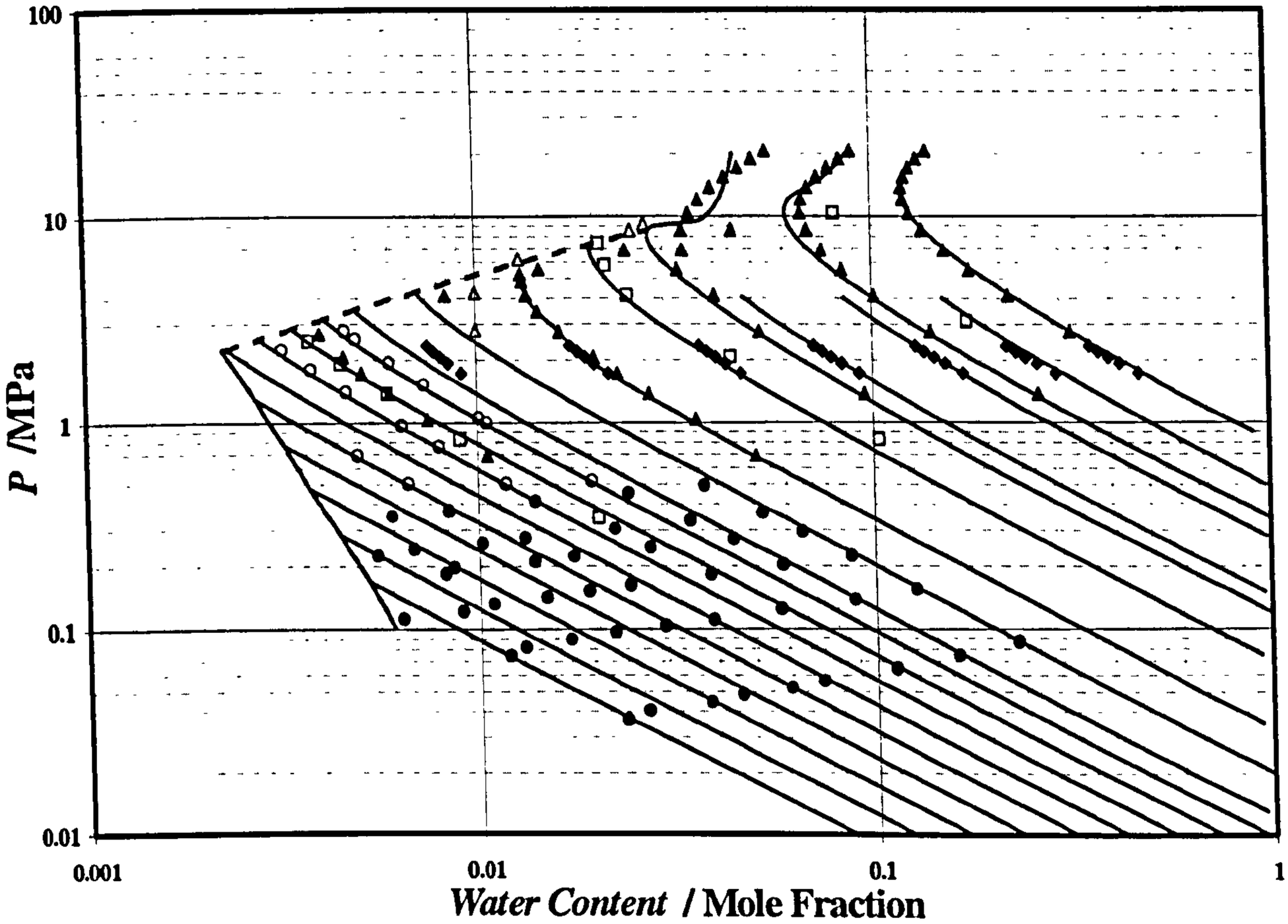

Figure 3.13. Experimental data on the water content of vapour phase:

Dashed line, hydrogen sulphide + water liquid-liquid locus; Grey solid line, hydrate dissociation line; ○, from (52); ●, data from (80); ×, data from (81); ◆, data from (82); ▲, data from (28); □, data from (24); △, data from (83).

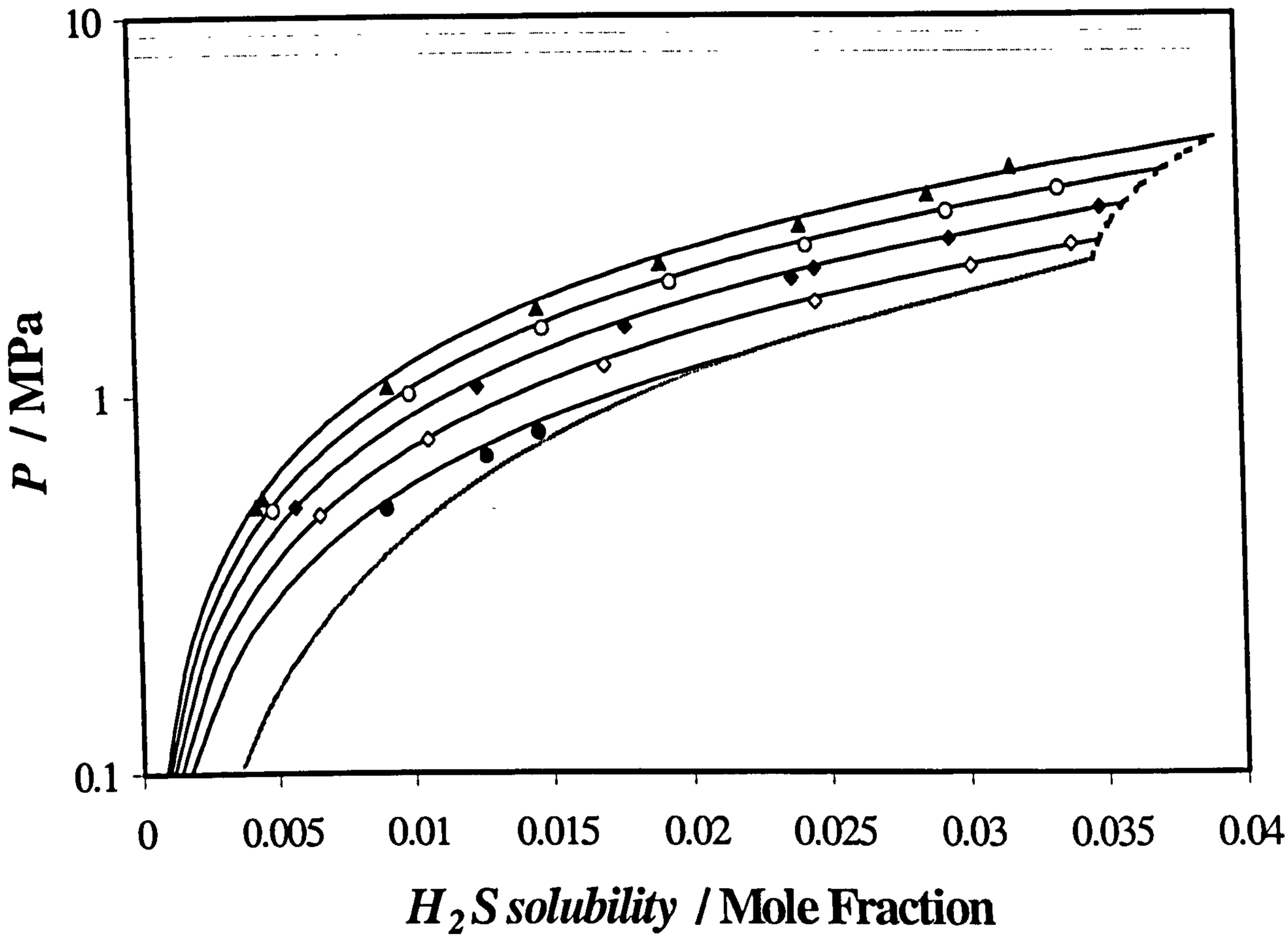

Figure 3.14. H_2S solubility in water:

Dashed line, hydrogen sulphide + water liquid-liquid locus; Grey solid line, hydrate dissociation line; Experimental data (52): ●, 298.16 K; ◇, 308.2 K; ◆, 318.21 K; ○, 328.28 K; ▲, 338.34 K.

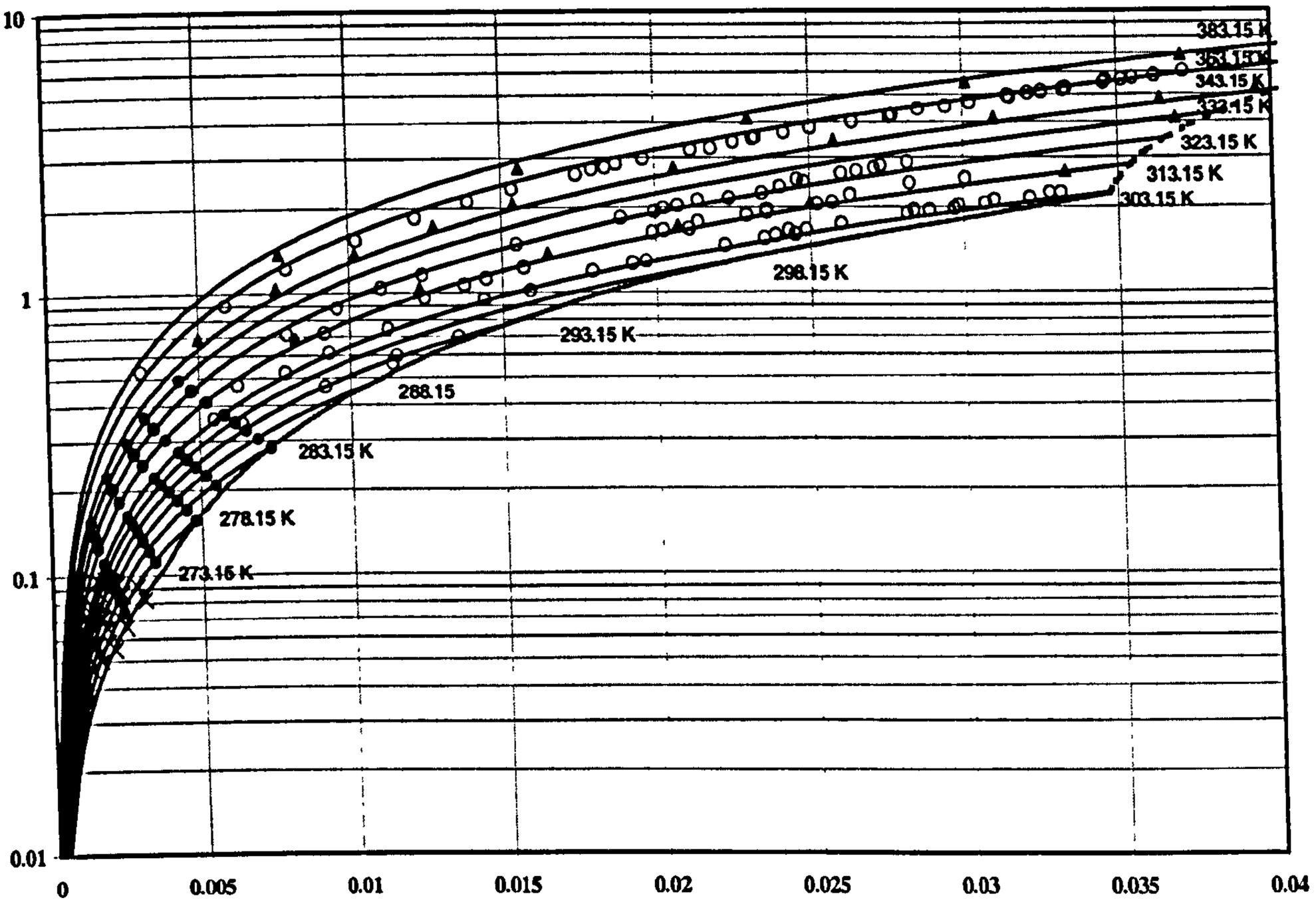

Figure 3.15. Selected literature data, H_2S solubility in water:

Dashed line, hydrogen sulphide + water liquid-liquid locus; Grey solid line, hydrate dissociation line; ●, data from (80); ×, data from (81); ◆, data from (82); ○, data from (84); ▲, data from (28).

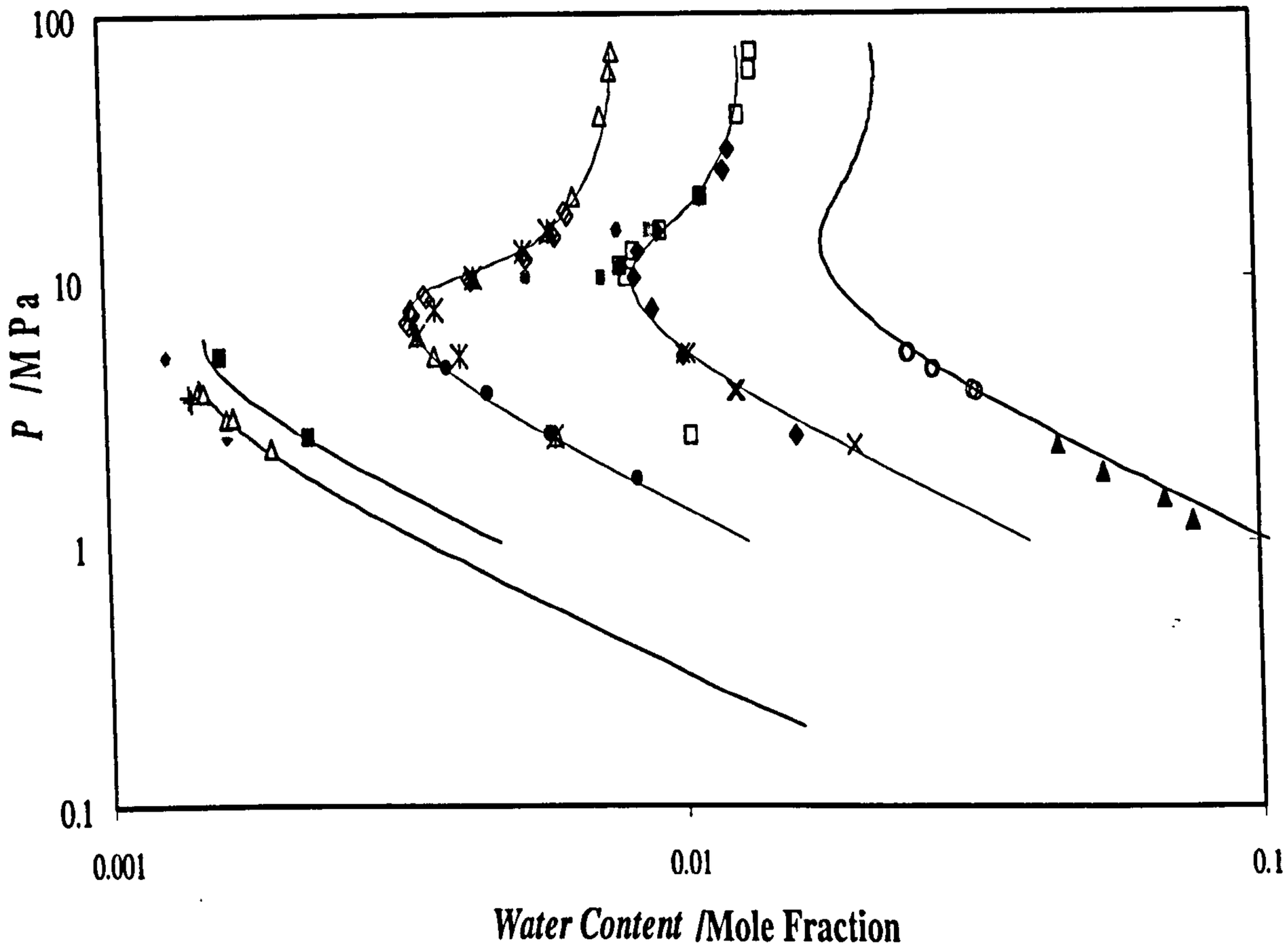

Figure 3.16. Water content in the gas (or vapour) phase in carbon dioxide – water systems:

(♦) 298.15 K from (22); (▲) 298.15 K from (23); (+) 298.15 K from (85); (■) 304.19 K from (22); (Δ) 323.15K from (22); (∗) 323.15 K from (57); (●) 323.15 K from (23); (◇) 323.15 K from (86); (●) 323.15 K from (87); (□) 348.15 K from (22); (♦) 348.15 K from (57); (×) 348.15 from (23); (■) 348.15 from (87); (○) 373.15 K from (23); (▲) 373.15 K from (88); Solid curves, predicted with the VPT-EoS (12) and NDD mixing rules (13).

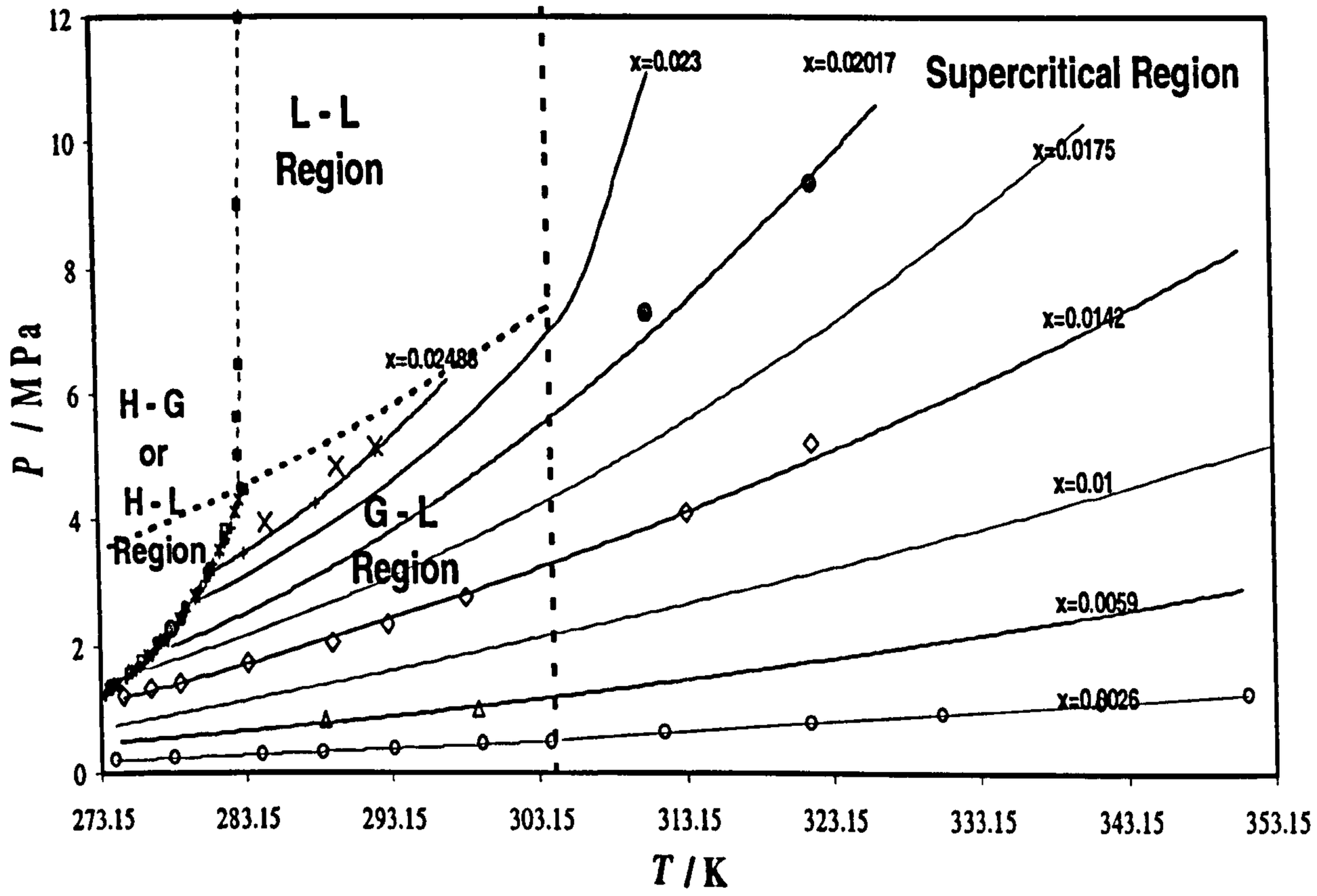

Figure 3.17. Carbon dioxide solubility data in water from 273.15 to 353.15 K:

Experimental data (89): (○) x_{CO2}=0.00262; (Δ) x_{CO2}=0.0059; (◇) x_{CO2}=0.0142; (●), x_{CO2}=0.02017; (×) x_{CO2}=0.02488; Solid curves calculated using the VPT-EoS (12) and NDD mixing rules (13).

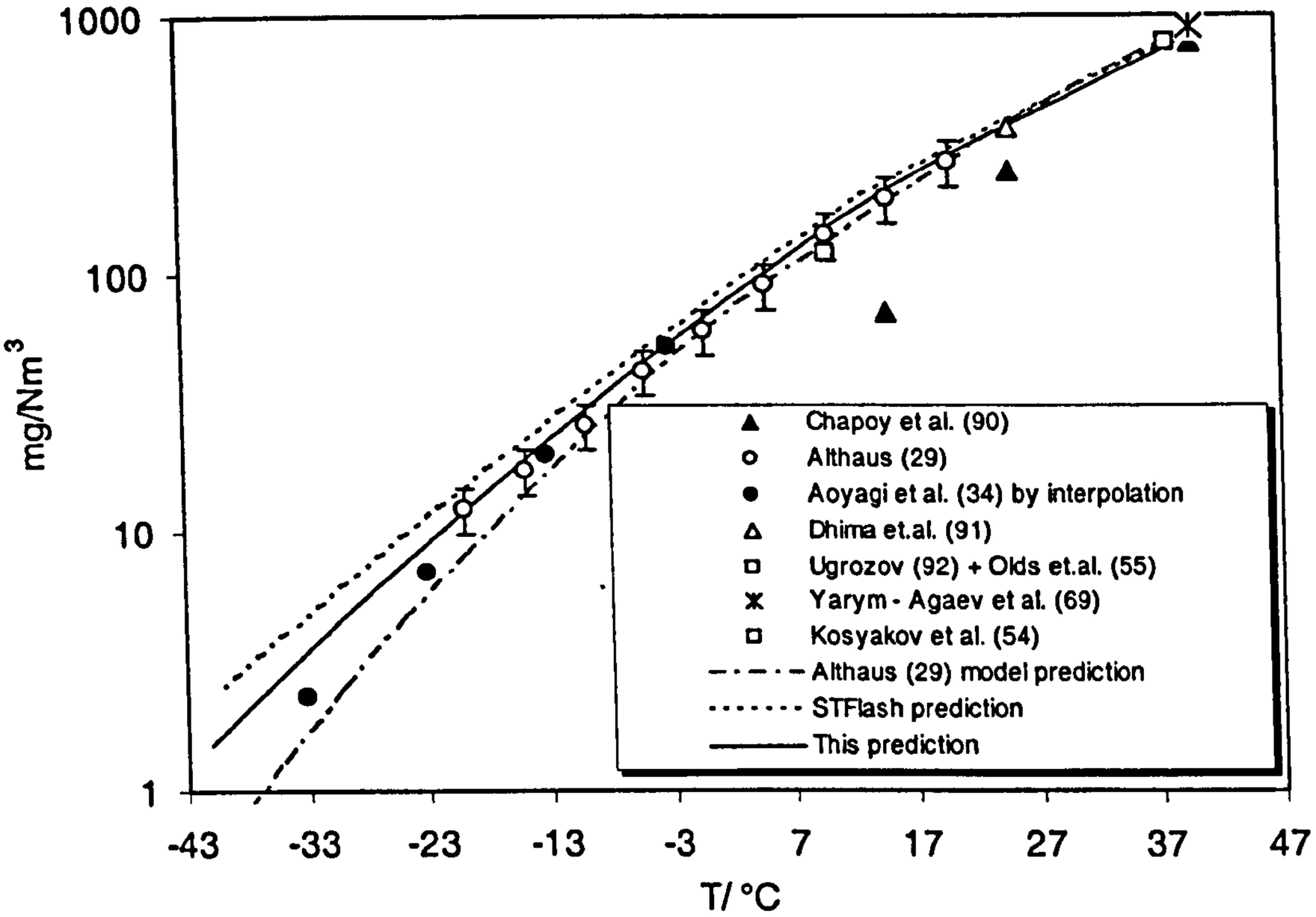

Figure 3.18 Water content of methane at 10 MPa (All water content values in "mg/Nm^3" are based on the dry gas mixture).

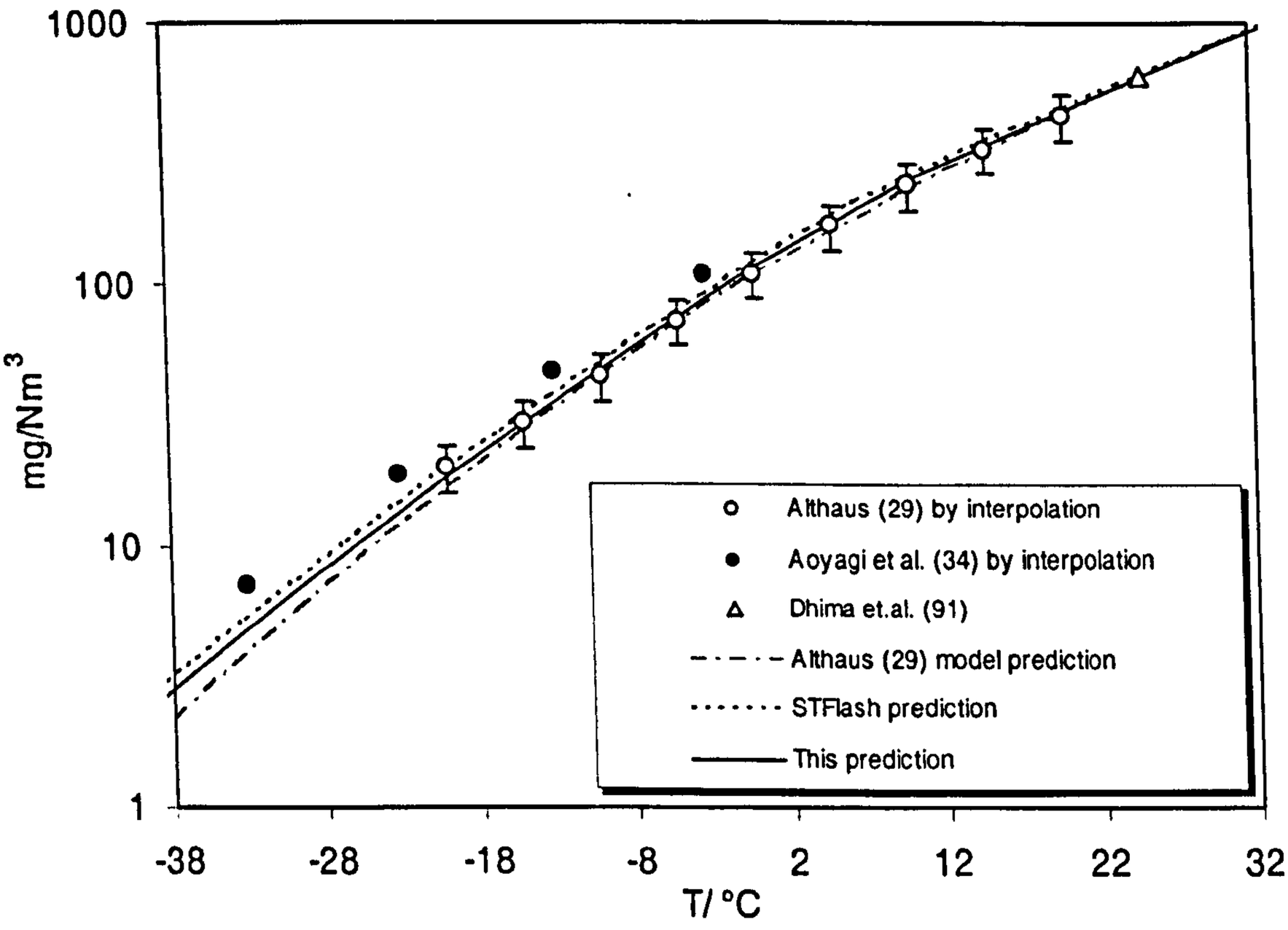

Figure 3.19 Water content of methane at 5 MPa.

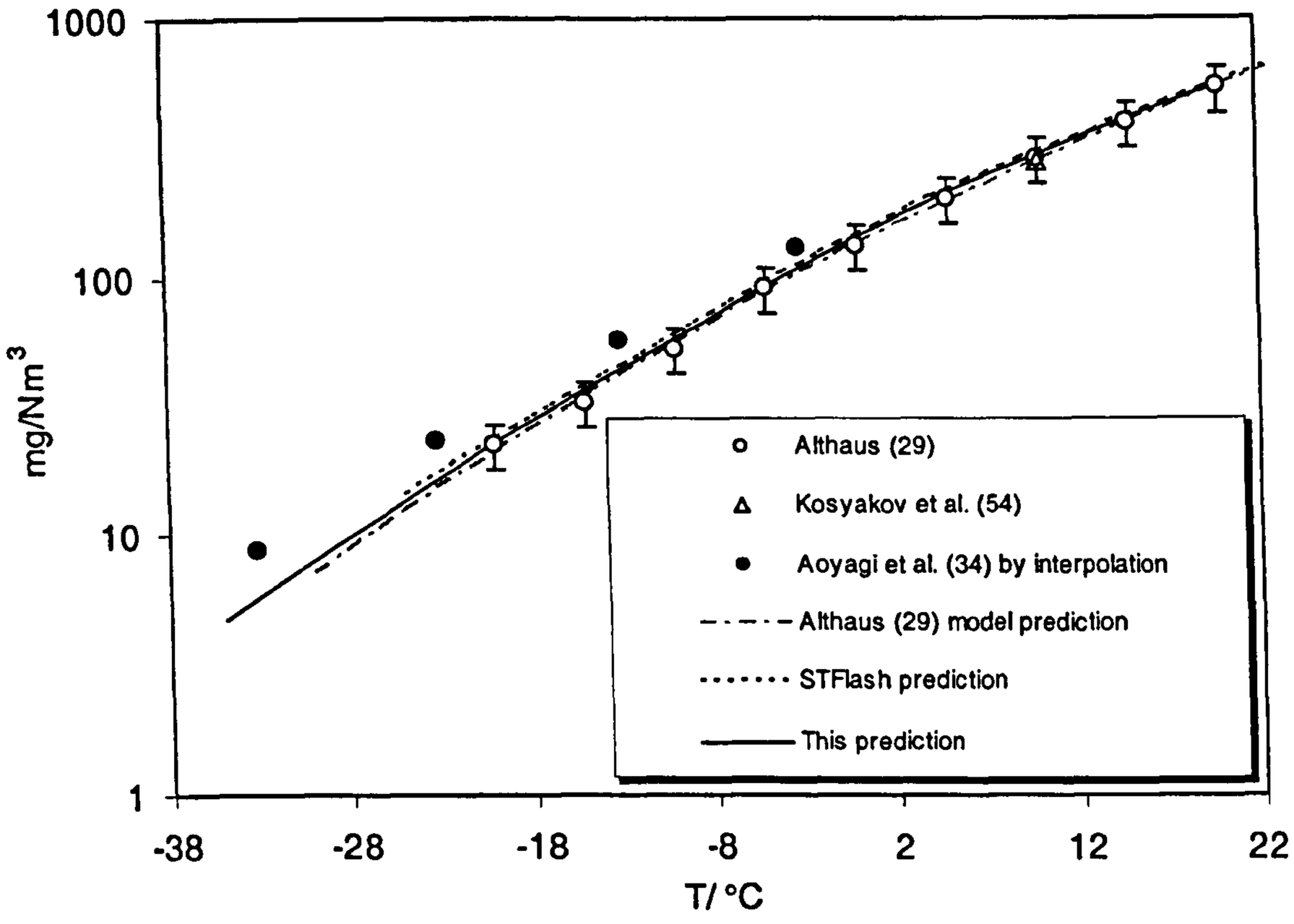

Figure 3.20 Water content of methane at 4 MPa.

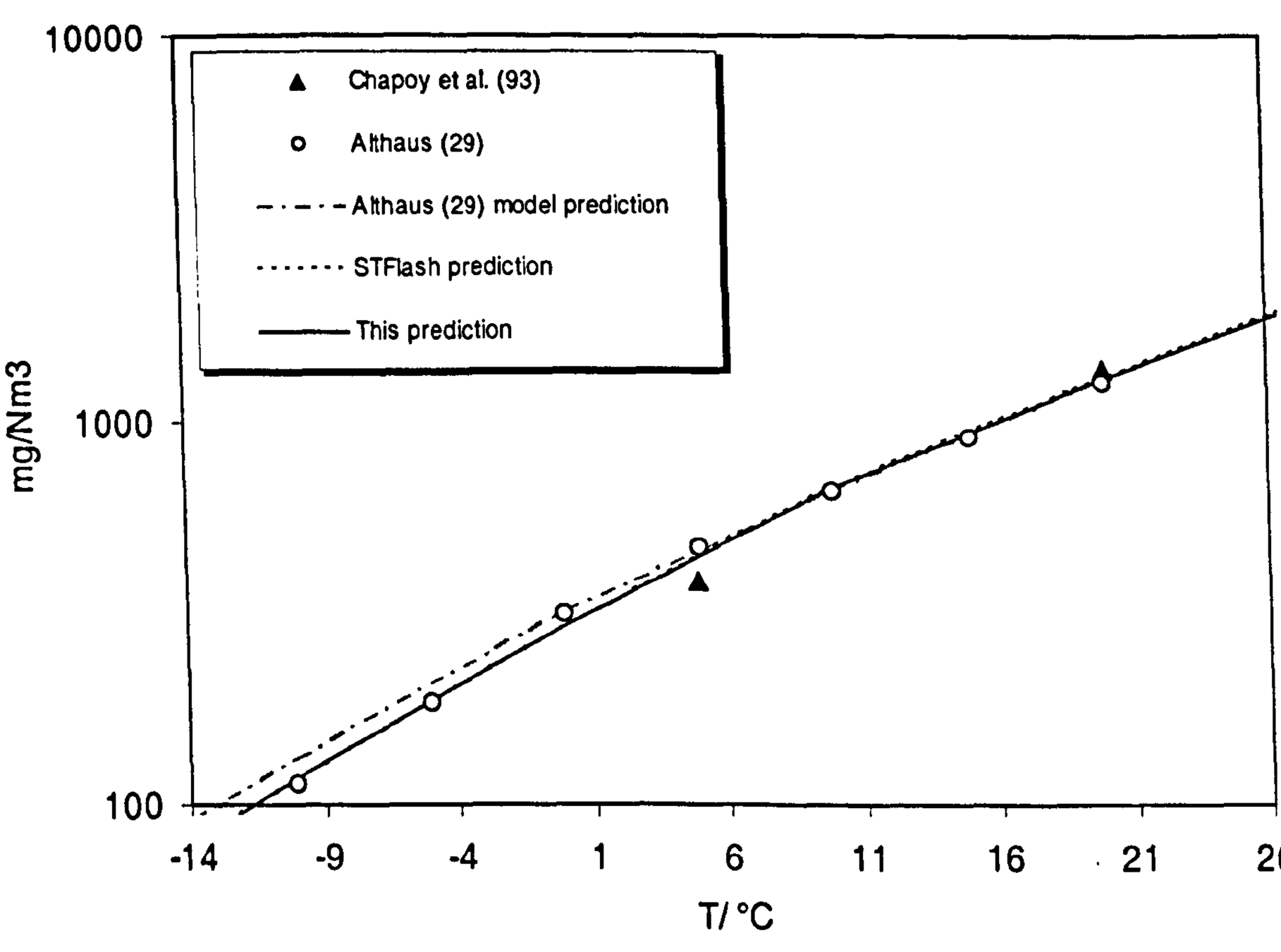

Figure 3.21 Water content of ethane at 1.5 MPa.

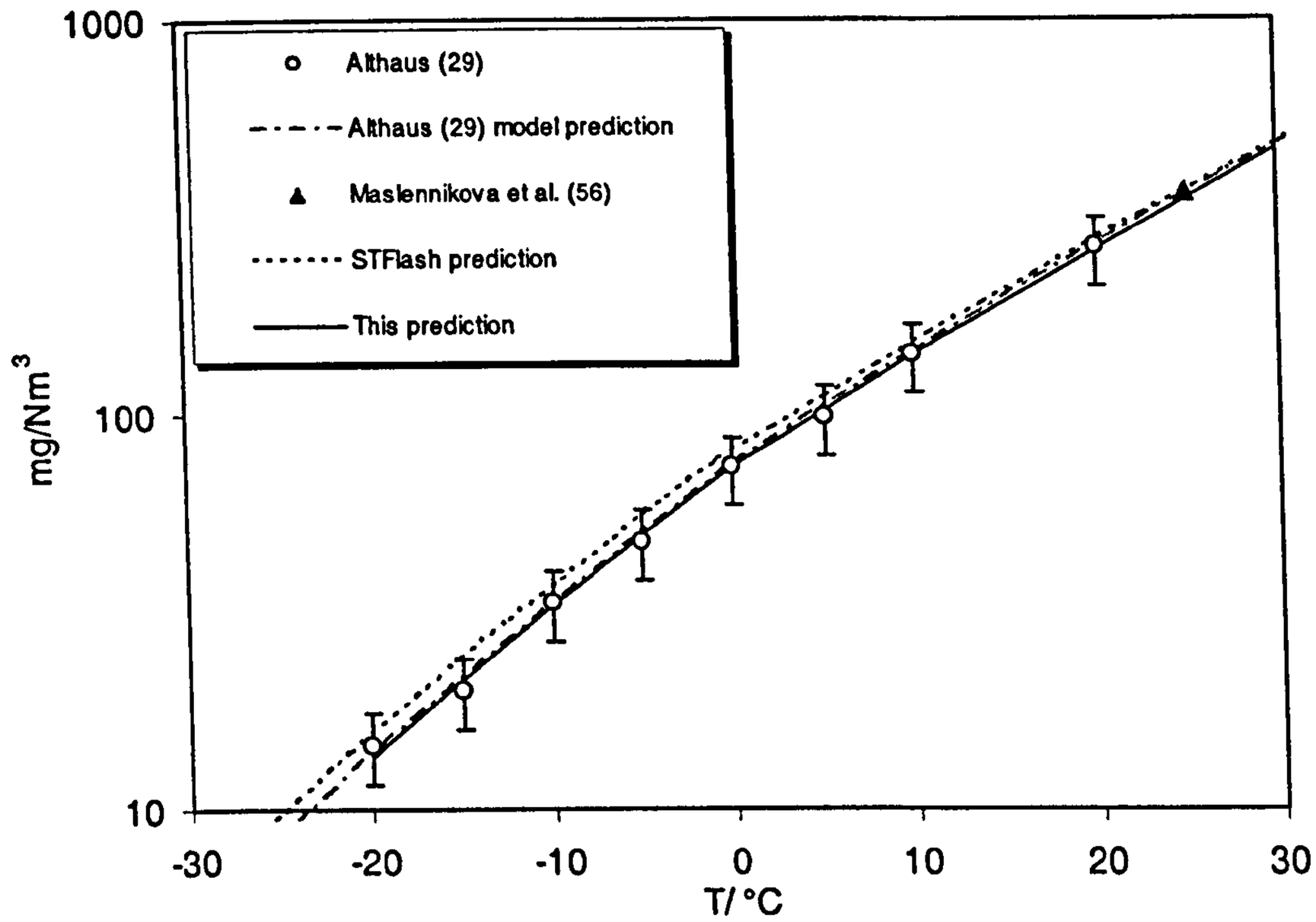

Figure 3.22 Water content of nitrogen at 10 MPa.

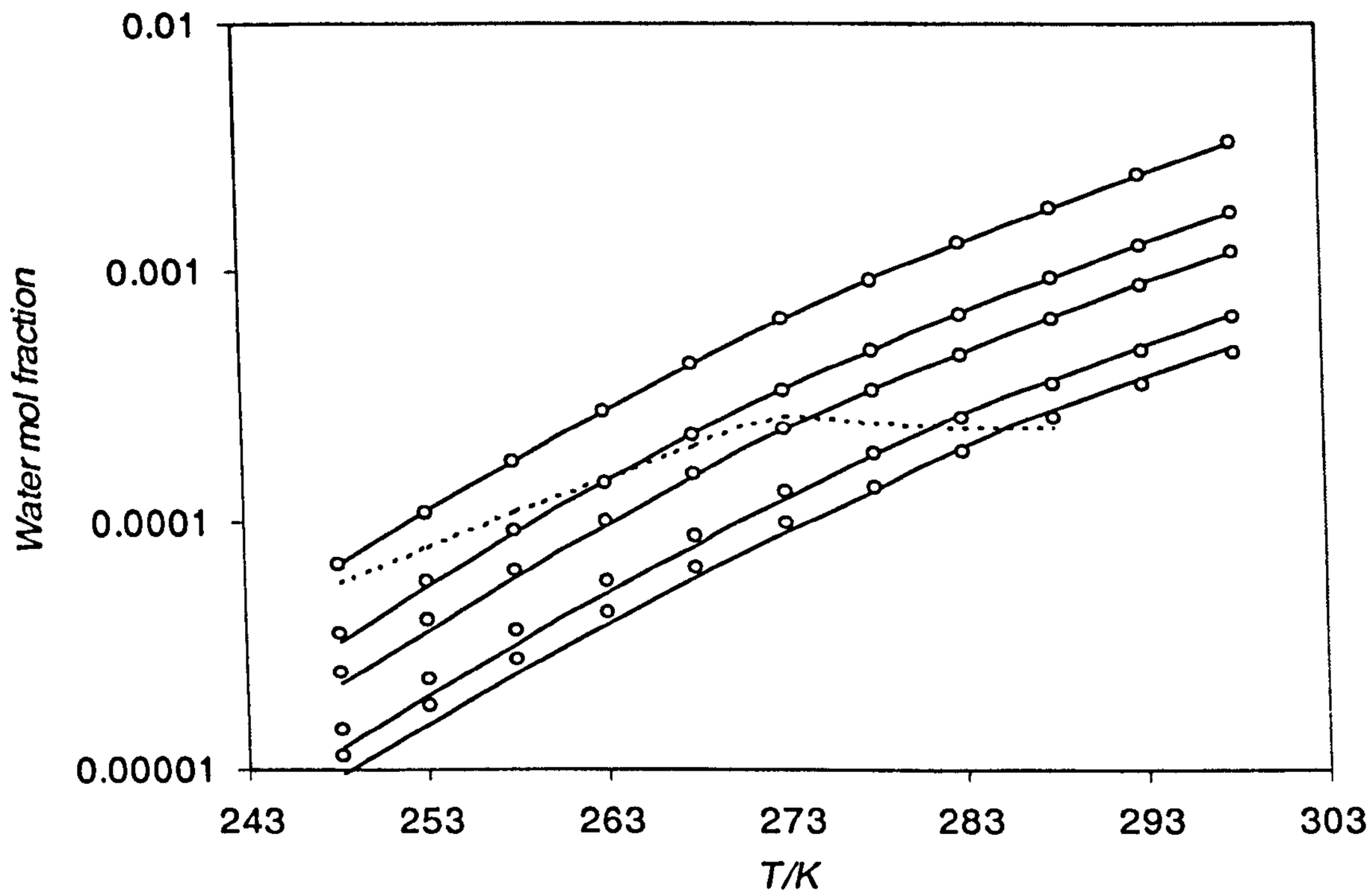

Figure 3.23 Water content of nitrogen and methane at different pressures and temperatures:

Solid lines: Predicted water content of methane, Points: Predicted water content of nitrogen, Dashed lines: Methane hydrate phase boundary; From left to right: 1, 2, 3, 6 and 8 MPa isobar lines.

REFERENCES

1. Bukacek, R. F. Equilibrium Moisture Content of Natural Gases. *Institute of Gas Technology, Research Bulletin 8.* 1955 (Quoted in ref. 15 and 16).

2. Sharma, S. Equilibrium Water Content of Gaseous Mixtures. PhD Thesis, University of Oklahoma, 1969.

3. Sharma, S.; Campbell, J. M. Predict natural-gas water content with total gas usage. *Oil & Gas J.* 4 Aug 1969, 136-137.

4. Campbell, J. M. Gas Conditioning and Processing. Volume 1: The Basic Principles; Campbell Petroleum Series, Oklahoma, 1994.

5. Robinson, J. N.; Moore, R. G.; Heideman, R. A.; Wichert, E. Estimation of the Water Content of Sour Natural Gases. *SPE J.* August 1977, 281-286.

6. Robinson, J. N.; Wichert, E.; Moore, R. G.; Heidemann, R. A. Charts help estimate H_2O content of sour gases. *Oil & Gas J.* 6 February 1978, 76-78.

7. Robinson, J. N.; Moore, R. G.; Heidemann, R. A.; Wichert, E. Estimation of the Water Content of Sour Natural Gas. *Laurance Reid Gas Conditioning Conference*, 1980, Norman, OK.

8. Maddox, R. N.; Lilly, L. L.; Moshfeghian, M.; Elizondo, E. Estimating Water Content of Sour Natural Gas Mixtures. *Laurance Reid Gas Conditioning Conference*, 8 March 1988, Norman, OK.

9. Wichert, G. C.; Wichert, E. Chart estimates water content of sour natural gas. *Oil & Gas J.* 29 March 1993, 61-64.

10. GPSA Engineering Data Book; 11th ed. Tulsa, OK, 1998.

11. Ning, Y.; Zhang, H.; Zhou, G. Mathematical simulation and program for water content chart of natural gas. *Chem. Eng. Oil Gas* 2000, *29*, 75-77 (in Chinese, Quoted in ref. 15).

12. Valderrama, J. O. A generalized Patel-Teja equation of state for polar and non-polar fluids and their mixtures. *J. Chem. Engng Japan* 1990, *23*, 87-91.

13. Avlonitis, D.; Danesh, A.; Todd, A. C. Prediction of VL and VLL equilibria of mixtures containing petroleum reservoir fluids and methanol with a cubic EoS. *Fluid Phase Equilib.* 1994, *94*, 181-216.

14. van der Waals, J. H., Platteeuw, J. C. Clathrate Solutions. Adv. Chem. Phys. 1959, 2, 1.

15. Carroll, J. J. Natural Gas Hydrates: A Guide for Engineers; Gulf Professional Publishing, 2003.

16. Carroll, J. J. The Water Content of Acid Gas and Sour Gas from 100 ° to 220 °F and Pressures to 10000 psia. *Presented at the 81st Annual GPA Convention*, Dallas, Texas, 11-13 March 2002.

17. McCain, W. D. Jr. The Properties of Petroleum Fluids. second edition, Pennwell Publishing Company, Tulsa, OK, 1990.

18. Behr, W. R. Correlation eases absorber-equilibrium-line calculations for TEG-natural gas dehydration. *Oil & Gas J.* 7 Nov 1983, 96-98.

19. Kazim, F. M. A. Quickly calculate the water content of natural gas. *Hydrocarbon Processing,* March 1996, 105-108.

20. Arnold, K.; Stewart, M. Surface Production Operations. Volume 2: Design of Gas-Handling Systems and Facilities; Second Edition, Gulf Publishing Company, Houston, Texas, 1999.

21. Sloan, E. D. Jr. Clathrate Hydrates of Natural Gases. Second Edition, Marcel Dekker, Inc., New York, 1998.

22. Wiebe, R.; Gaddy, V. L. Vapor Phase Composition of Carbon Dioxide-Water Mixtures at Various Temperatures and at Pressures to 700 Atmospheres. *J. Am. Chem. Soc.* February 1941, *63*, 475-477.

23. Coan, C. R.; King, A. D. Jr. Solubility of Water in Compressed Carbon Dioxide, Nitrous Oxide, and Ethane. Evidence for Hydration of Carbon Dioxide and Nitrous Oxide in the Gas Phase. *J. Am. Chem. Soc.* 21 April 1971, *93(8),* 1857 - 1862.

24. Gillespie, P. C.; Wilson, G. M. Vapor–Liquid and Liquid–Liquid Equilibria: Water–Methane, Water–Carbon Dioxide, Water–Hydrogen Sulfide, Water–nPentane, Water–Methane–nPentane. GPA Research Report 48, Tulsa, OK, April 1982.

25. Song, K. Y.; Kobayashi, R. The Water Content of CO_2 – rich Fluids in Equilibrium with Liquid Water and/ or Hydrates. GPA Research Report 99, Tulsa, OK, June 1986.

26. Song, K. Y.; Kobayashi, R. Water Content Values of a CO_2 – 5.31 Mol Percent Methane Mixture. GPA Research Report 120, Tulsa, OK, January 1989.

27. King, M. B.; Mubarak, A.; Kim, J. D.; Bott, T. R. The Mutual Solubilities of Water with Supercritical and Liquid Carbon Dioxide. *The Journal of Supercritical Fluids* 1992, *5*, 296 – 302.

28. Selleck, F. T.; Carmichael, L. T.; Sage, B. H. Phase Behavior in the Hydrogen Sulfide - Water System. *Ind. Eng. Chem.* September 1952, *44(9)*, 2219 – 2226.

29. Althaus, K. *Fortschritt - Berichte VDI* 1999, Reihe 3, 350. (in German), Oellrich, L. R.; Althaus, K. GERG – Water Correlation (GERG Technical Monograph TM14) Relationship Between Water Content and Water Dew Point Keeping in Consideration the Gas Composition in the Field of Natural Gas. *Fortschritt - Berichte VDI* 2000, Reihe 3- Nr. 679 (in English).

30. Katz, D. L.; Cornell, D.; Kobayashi, R.; Poettmann, F. H.; Vary, J. A.; Elenbaas J. R.; Weinaug, C. F. Handbook of Natural Gas Engineering. McGraw-Hill Book Company, 1959.

31. Kobayashi, R.; Song, K. Y.; Sloan, E. D. Petroleum Engineering Handbook. Chapter 25: Phase Behavior of Water/Hydrocarbon Systems, Society of Petroleum Engineers, Richardson, Texas, 1987.

32. Sloan, E. D.; Khoury, F. M.; Kobayashi, R. Water Content of Methane Gas in Equilibrium with Hydrates. *Ind. Eng. Chem. Fundam.* 1976, *15(4)*, 318- 323.

33. Song, K. Y.; Kobayashi, R. Measurement and Interpretation of the Water Content of a Methane-Propane Mixture in the Gaseous State in Equilibrium with Hydrate. *Ind. Eng. Chem. Fundam.* 1982, *21(4)*, 391-395.

34. Aoyagi, K.; Song, K. Y.; Kobayashi, R.; Sloan, E. D.; Dharmawardhana P. B. (I). The Water Content and Correlation of the Water Content of Methane in Equilibrium with Hydrates (II). The Water Content of a High Carbon Dioxide Simulated Prudhoe Bay Gas in Equilibrium with Hydrates. GPA Research Report 45, Tulsa, OK, December 1980.

35. Aoyagi, K.; Song, K. Y.; Sloan, E. D.; Dharmawardhana, P. B.; Kobayashi, R. Improved Measurements and Correlation of the Water Content of Methane Gas in Equilibrium with Hydrate. *58th Annual GPA Convention* 1979, Denver, CO, March.

36. Tohidi-Kalorazi, B. Gas Hydrate Equilibria in the Presence of Electrolyte Solutions. Ph.D. Thesis, Heriot-Watt University, 1995.

37. Daubert, T. E.; Danner, R. P. DIPPR Data Compilation Tables of Properties of Pure Compounds. AIChE, New York, 1985 (Quoted in ref. 38).

38. Danesh, A. PVT and Phase Behaviour of Petroleum Reservoir Fluids. Elsevier Science B.V. 1998.

39. Anderko, A. *Fluid Phase Equilibria* 1990, *61*, 145-225.

40. Chapoy, A.; Mohammadi, A.H.; Richon, D.; Tohidi, B. Gas solubility measurement and modeling for methane – water and methane – ethane – *n*-butane - water systems at low temperature conditions. *Fluid Phase Equilibria* 2004, *220*, 113–121.

41. Mohammadi, A.H.; Chapoy, A.; Richon, D.; Tohidi, B. Experimental Measurement and Thermodynamic Modeling of Water Content in Methane and Ethane Systems. *Ind. Eng. Chem. Res.* 2004, *43*, 7148-7162.

42. Chapoy, A.; Mohammadi, A. H.; Tohidi, B.; Richon, D. Estimation of water content for methane+water and methane+ethane+n-buthane systems using a new sampling device. *J. Chem. Eng. Data* 2005, *50*, 1157-1161.

43. Mohammadi, A.H.; Chapoy, A.; Tohidi, B.; Richon, D. Measurements and Thermodynamic Modeling of Vapor-Liquid Equilibria in Ethane –Water Systems from 274.26 to 343.08 K. *Ind. Eng. Chem. Res.* 2004, *43*, 5418-5424.

44. Song, K. Y.; Kobayashi, R. Water Content of Ethane, Propane, and Their Mixtures in Equilibrium with Liquid Water or Hydrates. GPA, Tulsa, OK, Research Report 132, December 1991.

45. Chapoy, A.; Mokraoui, S.; Valtz, A.; Richon, D.; Mohammadi, A. H.; Tohidi, B. Solubility Measurement and Modeling for the System Propane-Water from 277.62 to 368.16 K. *Fluid Phase Equilib.* 2004, *226*, 213-220.

46. Kobayashi, R., Katz D. L., *Ind. Eng. Chem.* February 1953, *45/2*, 440-451.

47. Song, K. Y., Kobayashi R., *Fluid Phase Equilib.* 1994, *95*, 281 - 298.

48. Chapoy, A.; Mohammadi, A. H.; Tohidi, B.; Richon, D. Gas solubility measurement and modeling for nitrogen–water system from 274.18 K up to 363.02 K. *J. Chem. Eng. Data* 2004, *49*, 1110-1115.

49. Rigby, M.; Prausnitz, J. M. Solubility of Water in Compressed Nitrogen, Argon, and Methane. *J. Phys. Chem.* January 1968, *72(1)*, 330-334.

50. Namiot, A. Yu.; Bondareva, M. M. Rastvorimost' gazov v vode (Solibility of Gases in Water), Moscow: Gostekhizdat, 1959 (Quoted in: Ugrozov, V. V. Equilibrium Compositions of Vapor-Gas Mixtures over Solutions. *Zh. Fiz. Khim.* 1996, *70(7)*, 1328-1329 (in Russian)).

51. Mohammadi, A.H.; Chapoy, A.; Tohidi, B.; Richon, D. Water Content Measurement and Modeling in the Nitrogen + Water System. *J. Chem. Eng. Data* 2005, *50*(2), 541 - 545.

52. Chapoy, A.; Mohammadi, A. H.; Tohidi, B.; Valtz, a.; Richon, D. Experimental Measurement and Phase Behavior Modeling of Hydrogen Sulfide + Water Systems. *Ind. Eng. Chem. Res.* 2005, *44*, 7567-7574 (Also: *Ind. Eng. Chem. Res.* 2005, 44, 10021).

53. Yokoyama, C.; Wakana, S.; Kaminishi, G. I.; Takahashi, S. Vapor - Liquid Equilibria in the Methane - Diethylene Glycol - Water System at 298.15 and 323.15 K. *J. Chem. Eng. Data* 1988, *33*, 274 – 276.

54. Kosyakov, N. E. *et al. Vopr Khim. Tekhnol.* 1982, *47*, 33 (in Russian, Data from Dortmund Data Base).

55. Olds, R. H.; Sage, B. H.; Lacey, W. N. Phase Equilibria in Hydrocarbon Systems. Composition of the Dew-Point Gas of the Methane-Water System. *Ind. Eng. Chem.* October 1942, *34(10)*, 1223 - 1227.

56. Maslennikova, V. Ya.; Vdovina, N. A.; Tsiklis, D. S. Solubility of Water in Compressed Nitrogen. *Russian Journal of Physical Chemistry* (*Zh. Fiz. Khim.* : *In Russian*) 1971, *45(9)*, 1354.

57. Sidorov, I. P.; Kazarnovsky, Y. S.; Goldman, A. M. *Tr. Gosudarst. Nauch.-Issled. I Proekt. Inst. Azot. Prom.* 1953, *1*, 48 (Data from Dortmund Data Base).

58. Lukacs, J.; Robinson, D. B. Water Content of Sour Hydrocarbon Systems. *SPE J.* December 1963, 293 –297.

59. Ng, H.-J.; Chen, C.-J.; Schroeder, H. Water Content of Natural Gas Systems Containing Acid Gas. GPA Research Report 174, Tulsa, OK, January 2001.

60. Song, K. Y.; Fneyrou, G.; Martin, R.; Lievois, J.; Kobayashi, R., *Fluid Phase Equilibria* 1997, *128*, 249-260.

61. Lekvam, K.; Bishnoi, P.R., *Fluid Phase Equilibria* 1997, *131*, 297-309.

62. Wang, Y.; Han, B.; Yan, H.; Liu, R., *Thermochim. Acta.* 1995, *253*, 327-334.

63. Wang, L.-K.; Chen, G-J.; Han, G-H.; Guo, X-Q.; Guo, T-M., *Fluid Phase Equilibria* 2003, *5180*, 1–12.

64. Culberson, O. L.; Horn, A. B.; Mc Ketta, J. J., *Trans. AIME* 1950, *189*, 1-6.

65. Culberson, O. L.; Mc Ketta, J. J., *Trans. AIME* 1951, *192*, 223-226.

66. Abdulgatov, I. M.; Bazaev, A. R.; Ramazanova, A. E. *J. Chem. Therm.* 1993, *25*, 249-259.

67. Yang, S. O.; Cho, S. H.; Lee, H.; Lee, C. S., *Fluid Phase Equilibria* 2001, *185*, 53-63.

68. Michels, A.; Gerver, J.; Bijl, A., *Physica III* 1936, 3819-3822.

69. Yarym-Agaev, N. L.; Sinyavskaya, R. P.; Koliushko, I. I.; Levinton, L.Ya., *Zh. Prikl. Khim.* 1985, *58*, 165-168 (in Russian).

70. Toplak, G. J., MS thesis, University of Pittsburgh, Pittsburgh, PA. 1989.

71. Y. S. Kim, S. K. Ryu, S. O. Yang and C. S. Lee, *Ind. Eng. Chem. Res.* 42 (2003) 2409-2414.

72. Sultanov, R. G.; Skripka, V. G.; Namiot, A. Y., *Gaz. Prom.* 1971, *16*, 6-7.

73. Cramer, S. D., *Ind. Eng. Chem. Pr. Des. Dev.* 1984, *23*, 533-538.

74. Azarnoosh, A.; McKetta, J. J., *Petrol. Refiner.* 1958, *37*, 275-278.

75. Wehe, A. H.; McKetta, J. J., *Anal. Chem.* 1961, *33/2*, 291-293.

76. Smith, N. O.; Kelemen, S.; Nagy, B. *Geochim. Cosmochim. Acta.* 1962, *26*, 921-926 (Data from Dortmund Data Base).

77. Goodman, J. B.; Krase, N. W. Solubility of Nitrogen in Water at High Pressures and Temperatures. *Ind. Eng. Chem.* April 1931, *23(4)*, 401-404.

78. O'Sullivan, T. D.; Smith, N. O.; Nagy, B. *Geochim. Cosmochim. Acta.* 1966, *30*, 617-619 (Data from Dortmund Data Base).

79. Saddington, A.W.; Krase, N.W. Vapor-Liquid Equilibria in the System Nitrogen–Water. *J. Am. Chem. Soc.* February 1934, *56(2)*, 353-361.

80. Wright, R. H.; Maass, O. *Canadian Journal of Research* 1932, *6*, 94 –101.

81. Clarke, E. C. W.; Glew, D.N. Aqueous non electrolyte solutions. Part VIII. Deuterium and hydrogen sulfide solubilities in deuterium oxide and water. *Can. J. Chem. Eng.* 1971, *49*, 691-698.

82. Burgess, M.P.; Germann, R.P. Physical properties of hydrogen sulfide water mixtures. *AIChE J.* 1969,*15*, 272-275,

83. Carroll, J. J.; Mather, A. A. The solubility of hydrogen sulphide in water from 0 to 90°C and pressures up to 1 MPa. *Geochimica et Cosmochimica Acta* 1989, *53*, 1163-1170.

84. Lee, J.I.; Mather, A. E. Solubility of hydrogen sulphide in water. *Ber. Besunges. Phys.* 1977, *81*, 1021-1023.

85. Nakayama, T.; Sagara, H.; Arai, K.; Saito, S. High pressure liquid - liquid equilibria for the system of water, ethanol and 1,1-difluoroethane at 323.2 K. *Fluid Phase Equilib.* 1987, *38*, 109-127.

86. Briones, J.A.; Mullins, J.C.; Thies, M.C.; Kim, B.-U. Ternary phase equilibria for acetic acid-water mixtures with supercritical carbon dioxide. *Fluid Phase Equilib.* 1987, *36*, 235-246.

87. D'Souza, R.; Patrick, J.R.; Teja, A.S. High pressure phase equilibria in the carbon dioxide – n-Hexadecane and carbon dioxide-water systems. *Can. J. Chem Eng.* 1988, *66*, 319-323.

88. Müller, G.; Bender, E.; Maurer, G. Das Dampf-Flüssigkeitsgleichgewicht des ternären systems ammonik-kolhendioxid wasser bei hohen wassergehalten im bereich zwischen 373 und 473 K. *Ber. Bunsenges. Phys. Chem.* 1988, 92,148-160.

89. Chapoy, A.; Mohammadi, A.H.; Chareton, A.; Tohidi, B.; Richon, D. Measurement and Modeling of Gas Solubility and Literature Review of the Properties for the Carbon Dioxide-Water System. *Ind. Eng. Chem. Res.* 2004, *43*, 1794 - 1802.

90. Chapoy, A.; Coquelet, C.; Richon D. Solubility measurement and modeling of water in the gas phase of the methane/water binary system at temperatures from 283.08 to 318.12 K and pressures up to 34.5 MPa. *Fluid Phase Equilib.* 2003, *214*, 101-117.

91. Dhima, A.; Noll, O.; Valtz, A.; Richon, D. Solubility of water in gaseous methane near the hydrate formation conditions. *Presented at 18th European Seminar on Applied Thermodynamics*, Kutna Horna, Czech Republic, 8-11th June 2000.

92. Ugrozov, V.V., *Zh.Fiz.Khim.* 1996, *70*, 1328-1329 (in Russian, Data from Dortmund Data Base).

93. Chapoy, A.; Coquelet, C.; Richon, D. Measurement of the water solubility in the gas phase of the ethane + water binary system near hydrate forming conditions. *J. Chem. Eng. Data* 2003, *48*, 957-966.

CHAPTER 4

WATER CONTENT OF NATURAL GASES

FURTHER INVESTIGATION OF HYDRATE-VAPOUR EQUILIBRIA

4.1 INTRODUCTION

Production, transportation and processing of natural gases in relatively cold regions has renewed interest in determining the water content in the gas, which is necessary to form hydrates at a specified temperature and pressure. From a strict thermodynamic standpoint, a gas phase (with dissolved water) can form hydrates at the hydrate-vapour boundaries without a free water phase. The question of the accumulation of a hydrate phase is a question of kinetics, dependent upon the time necessary for hydrate nuclei to attain a critical size and form a gas hydrates phase. This time may be in excess of that available for laboratory study but may occur in processes, which operate over extended periods of days, months or years (1).

Therefore, the determination of water content in gas at equilibrium with hydrates is difficult, because of the very low concentration of water in the gaseous phase. The experimental work done to describe the water content of gas in equilibrium with hydrates in the two-phase region are limited in accuracy due to two factors: the fact that metastable liquid water may extend well into the gas-hydrate region and the experimental restraint that the existing analysis methods require large amounts of gas in equilibrium with hydrates. Literature survey reveals the availability of few sets of experimental data for water content of gases in equilibrium with hydrates and all other data represent metastable liquid water – gas equilibrium. Therefore, few predictive

methods for the water content of gases in equilibrium with hydrates have been reported in the literature as these methods are generally based on experimental data.

The aim of this work is to develop the capability of our previously reported semi – empirical approach, which is based on equality of water fugacity in equilibrium phases, for estimating the water content of natural gases in equilibrium with hydrates. The main advantage of this method is the availability of input data and the simplicity of the calculations, which can be performed by using hand-held calculators.

Hence, a quick review is made of the existing methods (for the hydrate region) available in the open literature to show the need for a simple and robust predictive method for estimation of water content of natural gases in equilibrium with hydrates. In order to develop the approach, experimental data for water content of methane and a gas mixture containing methane (94.69 mole%) and propane (5.31%) are used. However further experimental work is necessary for developing new predictive methods inside the hydrate region. The capability of this approach is compared with predictions of a recommended predictive tool. It will be shown that the results of this method are in close agreement demonstrating the capability of the new approach developed in this work for estimating the water content of natural gases in equilibrium with gas hydrates.

4.2 EXPERIMENTAL DATA AND PREDICTIVE METHODS

There is a paucity of accurate equilibrium data in the gas-hydrate region due to the difficulty in analysing low water concentrations in the gas and due to the unusual metastability of liquid water in the gas-hydrate region (The water content of a gas in equilibrium with hydrates is lower than that of the same gas in equilibrium with meta-stable liquid water). Most of the available experimental data inside the hydrate region do not warrant thermodynamic equilibrium, *i.e.* these data are not in equilibrium with

hydrates. The establishment of gas-hydrate equilibrium constitutes the principle problems associated with properly conducting the tests. Another serious problem is the sampling and analysis of the gas phase for the small equilibrium or concentrations of water. Also, another problem is to maintain a constant composition in the gas mixtures by enriching or adding gas(s), which is depleted preferentially during the course of hydrate formation. Furthermore, it is necessary to decompose and recrystallise the hydrate phase to ensure that the hydrate crystal is indeed in equilibrium with the gas phase (2).

Among the data reported for *gaseous systems* in the literature, those reported by Sloan et al. (3), Aoyagi et al. (4) and Song et al. (5) for water content of methane, Song and Kobayashi (2) for water content of a mixture of methane (94.69 mole%) and propane (5.31%) and Song and Kobayashi (6) for water content of carbon dioxide and also a mixture of carbon dioxide and methane seem to be equilibrium points (1). On the other hand, the only recommended correlation (See Sloan (1) and Kobayashi et al. (7)) was presented by Kobayashi et al. (7). Carroll (8) also presented a chart for estimating the water content of methane in equilibrium with hydrates and then extended its application to gases with higher specific gravities, using simple assumptions. In the following, a review is made on the methods proposed by Kobayashi et al. (7) and Carroll (8).

4.2.1. Kobayashi et al.'s method

Kobayashi et al. (7) presented the following complicated algorithm to calculate the water content of methane-rich gases in equilibrium with gas hydrates. In order to calculate the water content of vapour in equilibrium with hydrates at a given temperature and pressure, the six steps below should be followed:

1) Calculate the metastable water content y_{MS} at the temperature and pressure of interest. This may be done via an appropriate Figure, such as the McKetta-Wehe chart or by the following equation for pressures between 1.378 and 13.789 MPa and for temperatures between 233.15 and 322.04 K:

$$y_{MS} = exp[C_1+C_2/T+C_3(lnP)+C_4/T^2+C_5(lnP)/T+C_6(lnP)^2] \quad (4.1)$$

where:

y_{MS}: metastable water content

T: temperature

P: pressure

C_i: constants whose values are given in a table.

2) Calculate the three-phase (L_w-H-V) temperature at the given pressure and water free composition, using an appropriate method. Obtain a temperature difference ΔT by subtracting the temperature of interest from the calculated three-phase temperature.

3) Calculate the displacement from the metastable water content (Δy_w) at the above ΔT and pressure of interest using the following equation for methane and a 94.69 mole% methane + 5.31 mole% propane mixture:

$$\Delta y_W = exp[C_1 + C_2(lnP) + C_3(ln\Delta T) + C_4(lnP)^2 + C_5(lnP)\,(ln\Delta T) + C_6(ln\Delta T)^2 + C_7(lnP)^3 + C_8(lnP)^2(ln\Delta T) + C_9(lnP)(ln\Delta T)^2 + C_{10}(ln\Delta T)^3 + C_{11}(lnP)^4 + C_{12}(lnP)^3(ln\Delta T) + C_{13}(lnP)^2(ln\Delta T)^2 + C_{14}(lnP)(ln\Delta T)^3 + C_{15}(ln\Delta T)^4] \quad (4.2)$$

Constants for the above equation are reported in a table, reported by the authors for methane, with a regression of the methane data in the pressure range between 3.447

and 10.342 MPa and the temperature range of 239.81 to 269.81 K. The constants for the mixture were generated in the pressure range of 3.447 and 10.342 MPa, and in the temperature range of 234.26 to 277.59 K.

4) Calculate the Δy_w for the gas composition of interest by a linear interpolation between the Δy_w for methane (gravity 0.552) and the Δy_w for the mixture containing 5.31% propane (gravity 0.603), using gravity as an interpolation parameter.

5) Calculate the equilibrium water content by subtracting the Δy_w value obtained in Step 4 from the metastable water value obtained in Step 1.

6) Consider the range of the data used to determine the regression constants of above equations to determine whether the answer obtained in Step 5 is within the bounds of the correlation.

As can be seen, the above method requires different steps and it is not easy to use it.

4.2.2. Carroll's method

Carroll (8) showed that if one examines the correction chart on the McKetta-Wehe chart, it is easy to conclude that the gravity correction is unity in the range of temperature encountered with hydrate formation (that is, there is no gravity correction). However, it has been observed that gas gravity does affect the water content. Song and Kobayashi (2) measured the water content of a mixture of methane (94.69 mole%) and propane (5.31%), which has a gas gravity of 0.6053, in equilibrium with a hydrate. These data encouraged Carroll (8) to make some interpretation of the effect of gas gravity on the water content of a gas in equilibrium with a hydrate. Carroll (8) plotted a figure of experimental data of Song and Kobayashi (2) along with curves based on the

water content of methane in equilibrium with hydrates reported by Aoyagi et al. (4), where the mixture data were at consistently lower water content than those for pure methane. A close examination of this plot revealed that the difference in the logarithm of the water content is approximately independent of the temperature. However, there appears to be a pressure dependence, albeit a weak one. Carroll (8) used a regression procedure and assumed that the water content is a linear function of the gas gravity. However, Carroll's (8) method shows higher values of water content for gases with higher gas gravities, which is not in agreement with those reported experimentally where the water content decreases, when increasing the gas gravity.

Carroll's (8) method requires a semi-logarithmic chart for estimating the water content of methane, which is not easy to read and can introduce a source of error. In addition, Carroll's (8) method gives higher values of water content for gases with higher gas gravities, which is not in agreement with those reported experimentally where the water content decreases, when increasing the gas gravity.

Because these correlations/charts are based on limited information, they should be used with some caution and the thermodynamic based approaches are more suitable for this region. Unfortunately, more experimental data are not available at present to compare the results of these methods for water content of gases.

4.3 SEMI – EMPIRICAL APPROACH

A preliminary study shows that exact prediction of water content of methane has an important effect on determination of water content of natural gas. As mentioned earlier, using semi-logarithmic charts for estimating the water content of methane, considering the associated difficulties in reading the values, can introduce a source of error. Our previous study showed that mathematical relations based on thermodynamic concepts

can be used for this purpose, *i.e.*, these methods can be based on equality of water fugacities:

The gas–hydrate equilibrium of a system is calculated, by equating the fugacities of water in the gas phase, f_w^g, and in the hydrate phase, f_w^H:

$$f_w^g = f_w^H \tag{4.3}$$

The fugacity of water in the hydrate phase, f_w^H, is related to the chemical potential difference of water in the filled and empty hydrate by the following expression:

$$f_w^H = f_w^{MT} exp\frac{\mu_w^H - \mu_w^{MT}}{RT} \tag{4.4}$$

where f_w^{MT} is the fugacity of water in the hypothetical empty hydrate phase, $\mu_w^H - \mu_w^{MT}$ represents the chemical potential difference of water in the filled and empty hydrate, R and T stand for universal gas constant and temperature.

The solid solution theory of van der Waals – Platteeuw (9) can be employed for calculating $\frac{\mu_w^H - \mu_w^{MT}}{RT}$:

$$\frac{\mu_w^H - \mu_w^{MT}}{RT} = -\sum_i \nu_i \ln(1 + C_i f_{CH_4}) = \sum_i \ln(1 + C_i f_{CH_4})^{-\nu_i} \tag{4.5}$$

where ν_i is the number of cavities of type i per water molecule in a unite hydrate cell (The values of ν_i have been reported in Sloan (1)), C_i stands for the Langmuir constant for methane's interaction with each type cavity and f_{CH4} is the fugacity of methane in the gas phase. For simple gas hydrates, f_{CH4} can be set to P, with a good approximation (Sloan (1), Carroll (8)). Therefore,

$$exp(\frac{\mu_w^H - \mu_w^{MT}}{RT}) = \prod_i (1 + C_i P)^{-\nu_i} \tag{4.6}$$

The Langmuir constants accounting for the interaction between the gas and water molecules in the cavities were reported by Parrish and Prausnitz (10) for a range of temperatures. The integration procedure was followed in obtaining the Langmuir constants for lower temperatures using the Kihara potential function with a spherical core according to the study by McKoy and Sinanoğlu (11). The Langmuir constants are consistent with initial hydrate data. However, since the experimental conditions go far below the initial hydrate formation conditions, the assumptions that are evidently valid at the initial hydrate formation conditions may be invalid elsewhere. Nevertheless, until experimental occupation numbers as a function of temperature, pressure, composition etc., are obtained, there can be no independent check of this assumption as discussed by Davidson (12). In this work, the Langmuir constants for methane's interaction with each type of cavities have been determined as a function of temperature, which are expressed from statistical mechanics as well as from data at the three-phase line by Parrish and Prausnitz (10):

for pentagonal dodecahedra (Small cavity):

$$C_{small} = \frac{3.7237 \times 10^{-3}}{T} exp(\frac{2.7088 \times 10^{3}}{T}) \tag{4.7}$$

for tetrakaidecahedra (Large cavity):

$$C_{large} = \frac{1.8373 \times 10^{-2}}{T} exp(\frac{2.7379 \times 10^{3}}{T}) \tag{4.8}$$

where T is in *Kelvin* and C has units of reciprocal *atmospheres*.

The fugacity of water in the empty lattice can be expressed as:

$$f_w^{MT} = P_w^{MT} \varphi_w^{MT} exp \int_{P_w^{MT}}^{P} \frac{v_w^{MT} dP}{RT} \tag{4.9}$$

where P_w^{MT}, φ_w^{MT}, v_w^{MT} and P are the vapour pressure of the empty hydrate lattice, the correction for the deviation of the saturated vapour of the pure (hypothetical) lattice from ideal behaviour, the partial molar volume of water in the empty hydrate given by von Stackelberg and Müller (13) (Quoted in Sloan (1)) and pressure, respectively and the exponential term is a Poynting type correction. The concept in the above equation of universal empty hydrate vapour pressure for each structure, prompted Dharmawardhana et al. (14) to calculate the P_w^{MT} from a number of simple hydrate three-phase ice-vapour-hydrate equilibrium, which represent the upper concentration limit of the method. By equating the fugacity of water in the hydrate phase to that of pure ice at the three-phase line, Dharmawardhana et al. (14) obtained the following equation for the vapour pressure of the empty hydrate structure I:

$$P_w^{MT} = exp(17.440 - \frac{6003.9}{T}) \qquad (4.10)$$

where P_w^{MT} is in *atmospheres* and T in *Kelvin*. The non-ideality of water vapour pressure of the empty hydrate at saturation seems to be negligible due to the small quantity (typically, 10^{-2} to 10^{-4} atm). However, they have been corrected for pressure by Poynting effect. Again, the vapour pressures of the empty hydrate lattice are consistent with initial hydrate data. However, since the experimental conditions go far below the initial hydrate formation conditions, the assumptions that are evidently valid at the initial hydrate formation conditions may be invalid deep inside the hydrate stability zone.

The equation 4.9 may be simplified by two assumptions: (1) that the hydrate partial molar volume equals the molar volume and is independent of pressure and (2) that P_w^{MT} is relatively small (on the order of *0.01 atm*), so that $\varphi_w^{MT} = 1$. Therefore,

$$f_w^{MT} = P_w^{MT} exp \frac{v_w^{MT}(P - P_w^{MT})}{RT} \tag{4.11}$$

The fugacity of water in the gas phase is expressed by:

$$f_w^g = y_w \varphi_w^g P \tag{4.12}$$

where y_w is the water content of gas phase and φ_w^g is the fugacity coefficient of water in the gas phase.

Using the above equations, the following expression is obtained for estimating the water content of methane in equilibrium with gas hydrates:

$$y_w = \frac{P_w^{MT}}{\phi_w^g P} \times \exp[\frac{v_w^{MT}(P - P_w^{MT})}{RT}] \times [(1 + C_{small} P)^{-v_{small}} \times (1 + C_{large} P)^{-v_{large}}] \tag{4.13}$$

In the above equation,

$v_w^{MT} = 0.022655$ m^3/kgmol (von Stackelberg and Müller (13))

$v_{small} = \frac{1}{23}$ (Sloan (1))

$v_{large} = \frac{3}{23}$ (Sloan (1))

The fugacity coefficient of water (ϕ_w^g) in the gas phase may be calculated as below:

$$\phi_w^g = exp(BP + CP^2 + DP^3) \tag{4.14}$$

where B-D are a function of temperature. The following relations for B-D seem to be satisfactory:

$$B = a + \frac{b}{T} \tag{4.15}$$

$$C = c + \frac{d}{T} \tag{4.16}$$

$$D = e + \frac{f}{T} \tag{4.17}$$

where *a-f* are constants and can be calculated for water – methane system by regressing the water content data.

The water contents in the gaseous mixtures of hydrocarbons, in general, show much lower values than that in the pure methane gas. The reasons for this behaviour are (2): The shift in the initial hydrate formation condition (The higher the initial hydrate formation conditions, the greater will be the distance between the stable and metastable equilibrium values at a given pressure and temperature, as shown by Aoyagi et al. (4)), differences in the hydrate crystal filling characteristics of the molecules and the possibility of the coexistence of structures I and II under the high-pressures and low-temperatures. Song and Kobayashi (2) also observed some large deviations in the predictions at low temperatures near the envelope and recommended the use of experimental measurements at these temperatures rather than the predicted values.

According to Figure-4.1, examination of the water content data of methane and a mixture of methane (94.69 mole%) and propane (5.31%) reveals that the difference in the logarithm of the water content is approximately independent of the temperature, which is in good agreement with that observed by Carroll (2).

Assuming that the water content is a linear function of the gas gravity, the following equation for estimating the water content of a gas mixture is proposed:

$$ln\left(\frac{y_{w,CH_4}}{y_{w,\gamma}}\right) = -2.1851 + 4.0813\gamma - 0.2221P + 0.4149P\gamma \tag{4.18}$$

P, is in *MPa* and the gas gravity, γ, is dimensionless. Therefore, equation 4.11 can be used along with equation 4.16 for estimating the water content of sweet natural gases in equilibrium with gas hydrates.

4.4 RESULTS AND DISCUSSIONS

In order to find constants *a-f*, the data reported in Table 4.1 and plotted in Figure 4.2 are used. As can be seen, the temperature range is from 196 K to 270 K, and the pressures are up to 10.34 MPa, respectively. The *AAD%* among all the experimental and calculated data is 7.4 %. These constants are reported in Table 4.2.

Table 4.3 and Figure 4.3 show a comparison between the predictions of this approach and experimental data reported for water content of a mixture of methane (94.69 mole%) and propane (5.31 mole%) in equilibrium with gas hydrates. As can be seen, the predictions are in close agreement with the experimental data.

In order to further evaluate the performance of the new approach, the results are compared with the results of Kobayashi et al.'s (7) method for estimating the water content of a gas whose gravity is *0.575*.

Example: Determine the water content of a gas in ppm (mole) whose gravity is 0.575 in equilibrium with hydrate at 6.895 MPa and 260.04 K.

Answer: Answer: Kobayashi et al. (1987): 32.1 ppm (ref. 1)

This work: 29.2 ppm

As can be seen, the water contents are in close agreement (Average deviation = 9%) demonstrating the ability of this approach for predicting the water content of natural gases in equilibrium with gas hydrates. Unfortunately, more experimental data are not available to compare the predicted results with them.

In summary, the predictive method developed in this work can predict water content of sweet natural gases inside hydrate forming conditions. Its recommended to use this approach for estimating the water content of sweet natural gases at 234.2 K to 277.6 K, and the pressures up to 10.34 MPa, as the experimental data of methane (94.69 mole%)

and propane (5.31%) at these ranges have been used to find the constants. Using this approach for pure CO_2 is also recommended. In addition, using more reliable water content data in the future can increase the accuracy of this approach.

4.5. CONCLUSIONS

A review was made on the existing predictive methods for determining the water content of natural gases in equilibrium with gas hydrates (section 4.2). The review showed a need for developing a simple and more robust method. Then, a semi–empirical approach based on equality of fugacity concept was proposed for estimating the water content of sweet natural gases in equilibrium with gas hydrates (section 4.3). The results of the predictive method were in close agreement with the results of a previously reported predictive method, demonstrating the capability of the new approach for estimating the water content of sweet natural gases.

TABLES

Table 4.1.*a* Water content of methane in equilibrium with gas hydrates (Experimental data from Aoyagi et al. (4)).

P/MPa	T/K	Mole fraction		AD%
		Experimental	Calculated	
3.45	240	1.23E-05	1.15E-05	6.5
3.45	250	3.22E-05	3.21E-05	0.3
3.45	260	7.82E-05	8.32E-05	6.4
3.45	270	1.78E-04	2.01E-04	12.9
6.9	240	5.60E-06	5.66E-06	1.1
6.9	250	1.55E-05	1.53E-05	1.3
6.9	260	3.96E-05	3.83E-05	3.3
6.9	270	9.44E-05	8.97E-05	5.0
10.34	240	2.72E-06	2.70E-06	0.7
10.34	250	8.46E-06	8.46E-06	0.0
10.34	260	2.42E-05	2.42E-05	0.0
10.34	270	6.42E-05	6.42E-05	0.0

Table 4.1.*b*. Water content of methane in equilibrium with gas hydrates (Experimental data from Song et al. (5)).

P/MPa	T/K	Mole fraction		AD%
		Experimental	Calculated	
3.45	270	1.73E-04	2.01E-04	16.2
3.45	254	4.24E-05	4.74E-05	11.8
3.45	240	1.17E-05	1.15E-05	1.7
3.45	224	2.17E-06	1.82E-06	16.1
3.45	213	5.48E-07	4.37E-07	20.3
3.45	196	6.32E-08	3.52E-08	44.3
6.9	260	4.16E-05	3.83E-05	7.9
6.9	254	2.07E-05	2.23E-05	7.7
6.9	246	9.48E-06	10.4E-06	9.7
6.9	230	2.08E-06	1.92E-06	7.7
6.9	213	2.32E-07	2.42E-07	4.3
6.9	204	6.95E-08	7.04E-08	1.3
6.9	202	5.26E-08	5.27E-08	0.2

Table 4.2. Constants *a-f* in the semi-empirical approach.

Constant	Value
a	-0.19108
b	-13.59073
c	0.17963
d	-36.84950
e	-0.01721
f	4.00814

Table 4.3. Water content of a mixture of methane (94.69 mole%) and propane (5.31 mole%) in equilibrium with gas hydrates (Experimental data from Song and Kobayashi (2)).

P/MPa	T/K	Experimental		Calculated	
		Mole fraction	sp.gr	Mole fraction	AD%
2.07	234.2	6.86E-06	0.606	6.41E-06	6.6
2.07	246.2	2.43E-05	0.606	2.41E-05	0.8
2.07	251.7	4.15E-05	0.606	4.23E-05	1.9
2.07	260.1	8.52E-05	0.606	9.56E-05	12.2
2.07	266.5	1.62E-04	0.606	1.72E-04	6.2
2.07	277.2	4.27E-04	0.606	4.30E-04	0.7
3.45	234.2	3.47E-06	0.606	4.10E-06	18.2
3.45	246.2	1.39E-05	0.606	1.49E-05	7.2
3.45	252.1	2.75E-05	0.606	2.68E-05	2.5
3.45	263.2	7.88E-05	0.606	7.53E-05	4.4
3.45	274.7	1.88E-04	0.606	2.01E-04	6.9
6.89	234.2	1.92E-06	0.606	1.88E-06	2.1
6.89	246.2	7.03E-06	0.606	6.50E-06	7.5
6.89	252.1	1.23E-05	0.606	1.15E-05	6.5
6.89	260	2.54E-05	0.606	2.35E-05	7.5
6.89	263.2	3.58E-05	0.606	3.11E-05	13.1
6.89	276.2	10.4E-05	0.606	9.04E-05	13.1
10.34	234.2	1.15E-06	0.606	0.74E-06	35.7
10.34	246.2	3.75E-06	0.606	3.07E-06	18.1
10.34	252.1	7.33E-06	0.606	5.88E-06	19.8
10.34	260.1	1.47E-05	0.606	1.35E-05	8.2
10.34	266.5	2.68E-05	0.606	2.55E-05	4.9
10.34	277.6	8.12E-05	0.606	7.11E-05	12.4

FIGURES

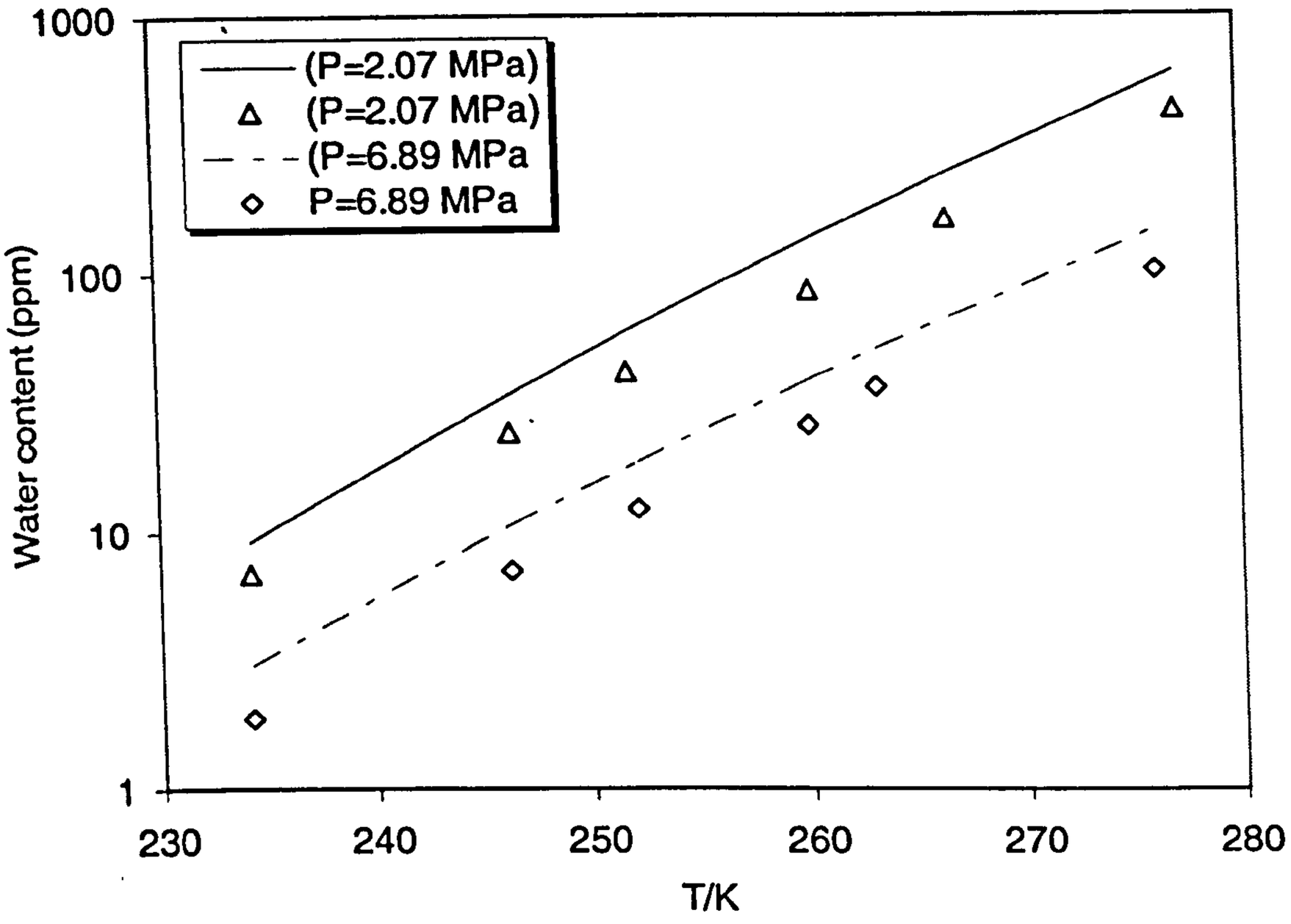

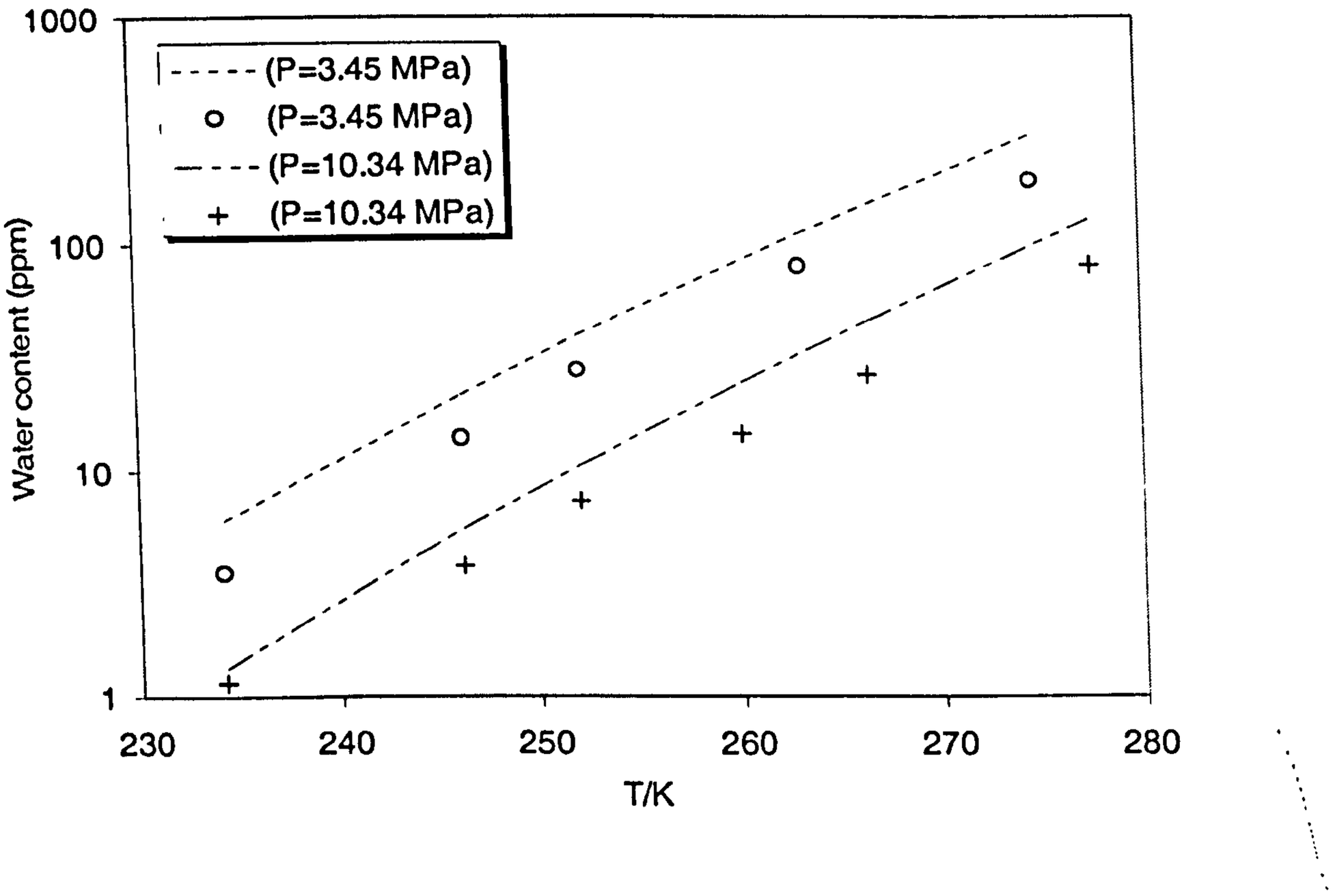

Figure 4.1. Water content of methane (solid and dashed lines, calculated using equation 4.13) and a mixture of methane (94.69 mole%) and propane (5.31%) (Points, experimental data from Song and Kobayashi (2)) in equilibrium with gas hydrates.

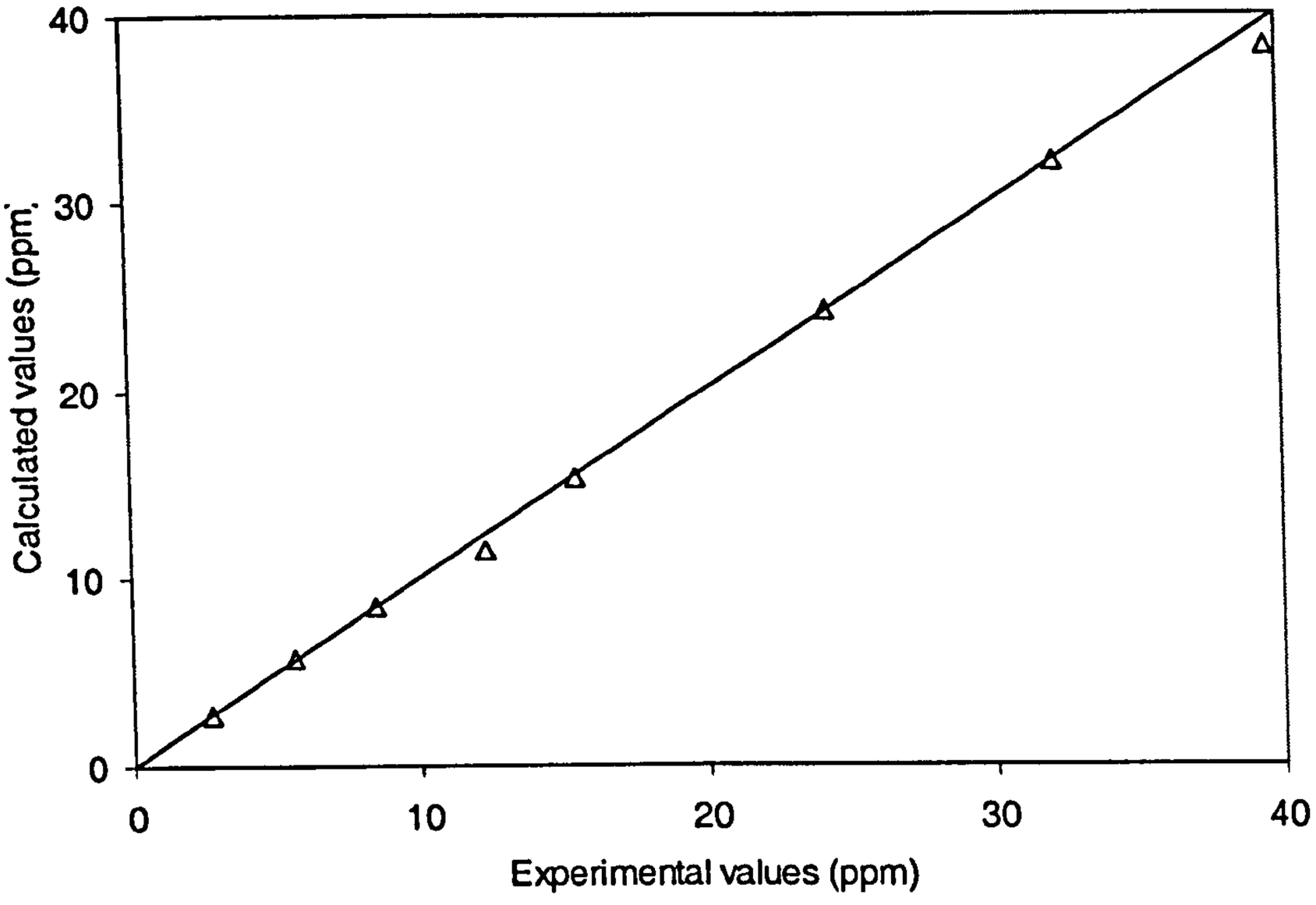

Figure 4.2.*a*. Experimental and calculated water content of methane in equilibrium with gas hydrates (Experimental data from Aoyagi et al. (4)).

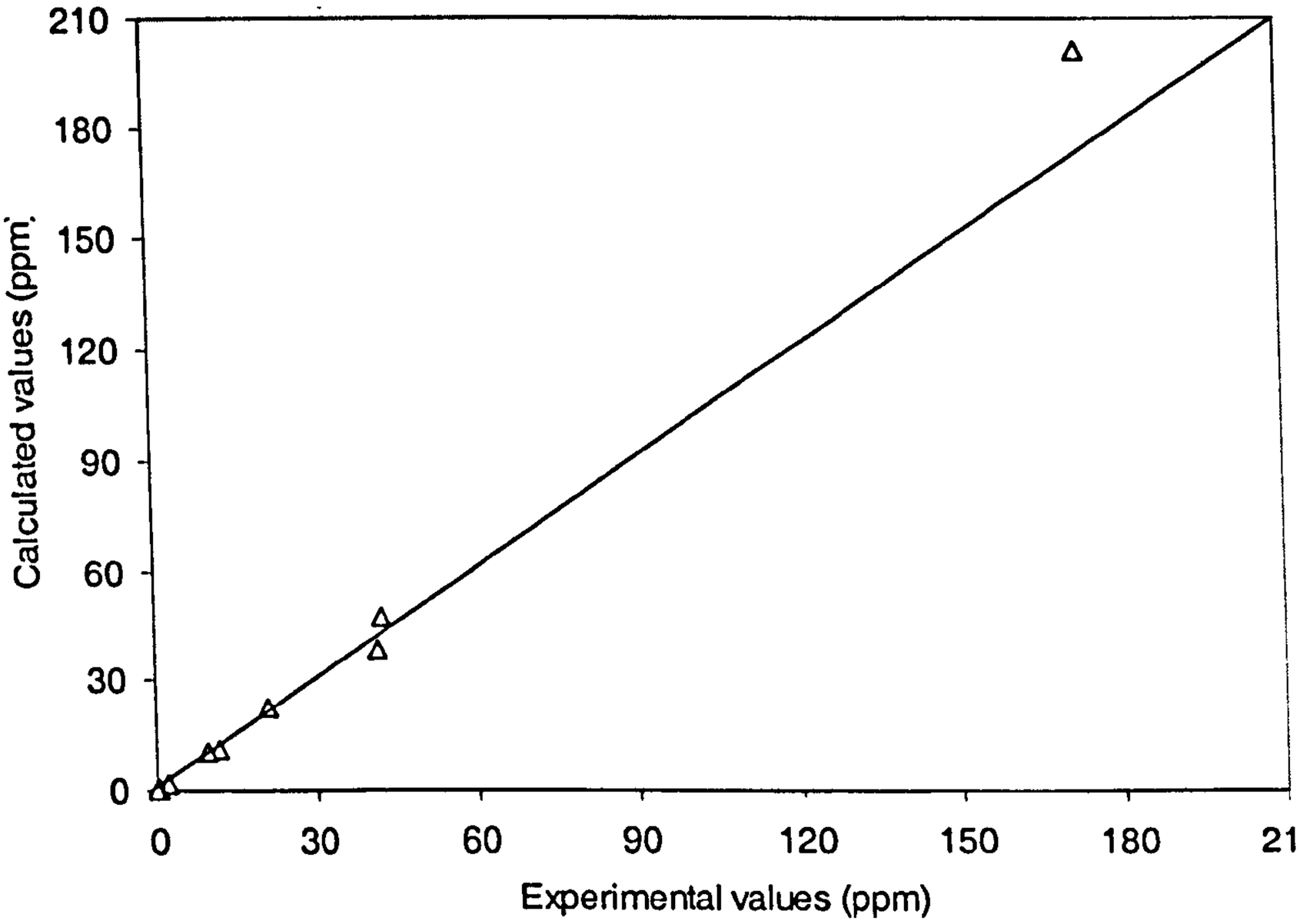

Figure 4.2.*b*. Experimental and calculated water content of methane in equilibrium with gas hydrates (Experimental data from Song et al. (5)).

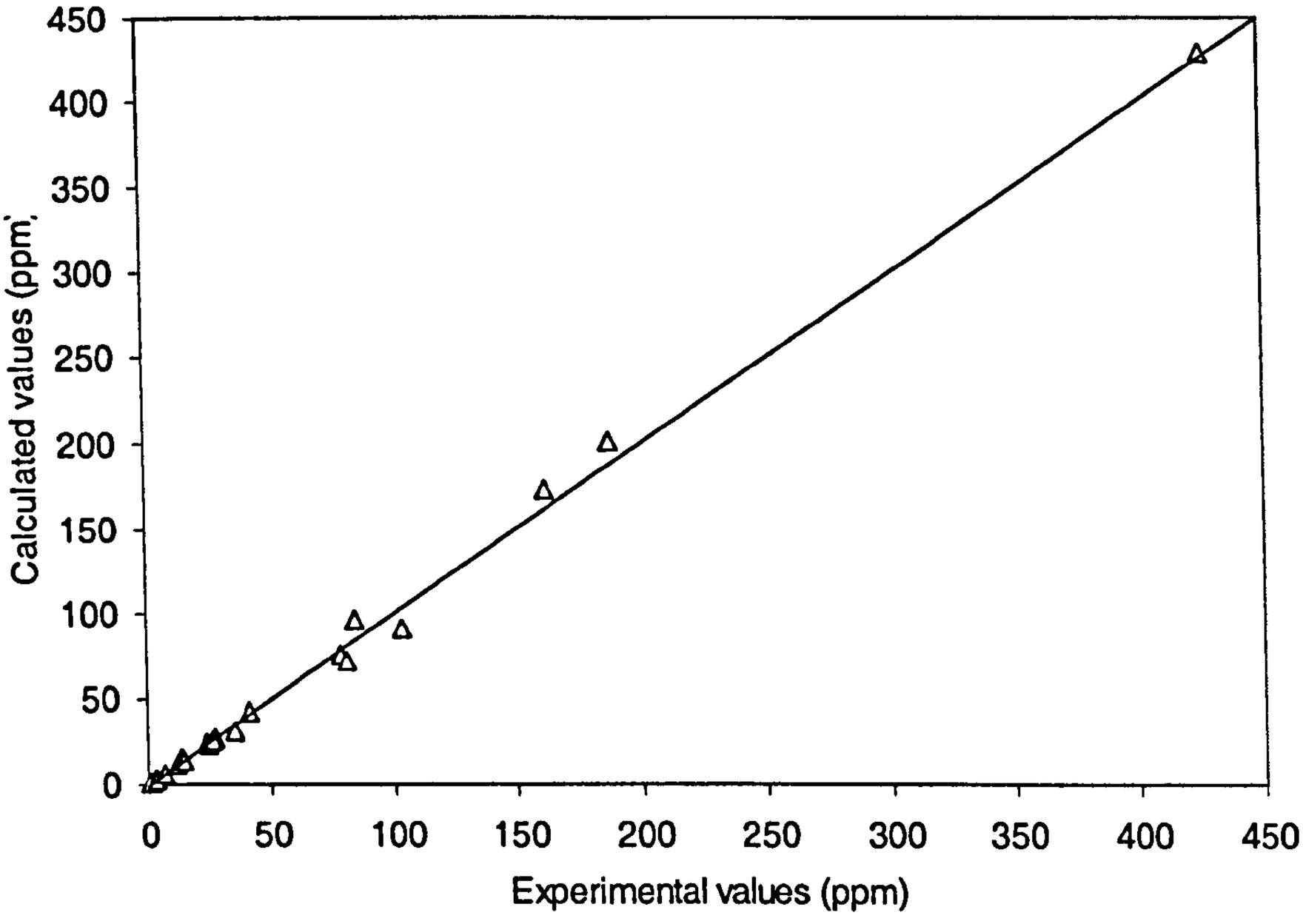

Figure 4.3. Experimental and calculated water content of a mixture of methane (94.69 mole%) and propane (5.31%) in equilibrium with gas hydrates (Experimental data from Song and Kobayashi (2)).

REFERENCES

1. Sloan, E. D. Clathrate Hydrates of Natural Gases. Second Edition, Marcel Dekker. Inc., New York, 1998.

2. Song, K. Y.; Kobayashi, R. Measurement and Interpretation of the Water Content of a Methane-Propane Mixture in the Gaseous State in Equilibrium with Hydrate. *Ind. Eng. Chem. Fundam.* 1982, *21(4)*, 391-395. Also: Song, K. Y.; Kobayashi, R. Measurement & Interpretation of the Water Content of a Methane-5.31 mol% Propane Mixture in the Gaseous State in Equilibrium with Hydrate. GPA Research Report 50, Tulsa, OK, January 1982.

3. Sloan, E. D.; Khoury, F. M.; Kobayashi, R. Water Content of Methane Gas in Equilibrium with Hydrates. *Ind. Eng. Chem. Fundam.* 1976, *15(4)*, 318- 323.

4. Aoyagi, K.; Song, K. Y.; Kobayashi, R.; Sloan, E. D.; Dharmawardhana, P. B. (I). The Water Content and Correlation of the Water Content of Methane in Equilibrium with Hydrates (II). The Water Content of a High Carbon Dioxide Simulated Prudhoe Bay Gas in Equilibrium with Hydrates. GPA Research Report 45, Tulsa, OK, December 1980. Also: Aoyagi, K.; Song, K. Y.; Sloan, E. D.; Dharmawardhana, P. B.; Kobayashi, R. Improved Measurements and Correlation of the Water Content of Methane Gas in Equilibrium with Hydrate. 58th Annual GPA Convention, Denver, CO, 1979.

5. Song, K. Y.; Yarrison, M.; Chapman W. Experimental low temperature water content in gaseous methane, liquid ethane, and liquid propane in equilibrium with hydrate at cryogenic conditions. *Fluid Phase Equilibria* 2004, *224*, 271–277.

6. Song, K. Y.; Kobayashi, R. The Water Content of CO_2 – rich Fluids in Equilibrium with Liquid Water and/ or Hydrates", GPA Research Report 99, Tulsa, OK, June 1986.

7. Kobayashi, R.; Song, K. Y.; Sloan, E. D. Petroleum Engineering Handbook, Chapter 25: Phase Behavior of Water/Hydrocarbon Systems", Society of Petroleum Engineers, Richardson, Texas, 1987.

8. Carroll, J. J. Natural Gas Hydrates: A Guide for Engineers. Gulf Professional Publishing, 2003.

9. van der Waals, J. H.; Platteeuw, J. C. Clathrate solutions. *Adv. Chem. Phys.*1959, 2, 1.

10. Parrish, W.R.; Prausnitz, J.M. Dissociation pressures of gas hydrate formed by gas mixture. *Ind. Eng. Chem. Process. Des. Develop.* 1972, *11*, 26-34.

11. McKoy, V.; Sinanoğlu, O. Theory of dissociation pressures of some gas hydrates. *J. Chem. Physics* 1963, *38(12)*, 2946-2956.

12. Davidson, D. W. Water: A Comprehensive Treatise. Frank, F., Ed.; Plenum Press: New York, 1973.

13. von Stackelberg, M.; Müller, H. R. Feste Gashydrate. *Z. für Elektrochemie*, 1954, *58*, 25 (Quoted in ref. 10).

14. Dharmawardhana, P.B.; Parrish, W.R.; Sloan, E.D. Experimental thermodynamic parameters for the prediction of natural gas hydrate dissociation conditions. *Ind. Eng. Chem. Fundam.* 1980, *19*, 410-414 (Quoted in ref. 1).

CHAPTER-5

THERMODYNAMIC MODELLING OF MIXED SALT AND CHEMICAL INHIBITOR

5.1. INTRODUCTION

Salts and/or organic inhibitors are generally used to inhibit hydrate formation in drilling fluids and oil/gas production, transportation and processing. Hydrate formation in drilling fluids represents a relatively new challenge resulting from deepwater offshore drilling. Potential problem areas can involve both safety and economic factors including plugging well choke and kill-lines, blowout preventers (*BOP*s) and drill-strings (1). To inhibit hydrate formation during deepwater drilling, high salinity drilling fluids with or without organic inhibitors are commonly used (2).

On the other hand, the application of extended subsea networks and transportation of unprocessed well-streams are amongst favourable options for reducing field development and operational costs. These pipelines will convoy a mixture of multiphase fluids, including mixed electrolyte produced water and liquid and gaseous hydrocarbons and may therefore be prone to hydrate formation, which potentially can block the pipe and lead to serious operational problems. These can be avoided by either operating outside the hydrate region or transporting hydrates as slurry. The economics of the first option is largely dependent on the accurate determination of the hydrate phase boundary, whereas the amount of hydrates to be transferred could be the main factor in the success of the second option (3).

A good knowledge of the behaviour of these complex systems is essential for safe and economical design and operation of associated fields, pipelines and production/processing facilities and for avoiding the risk of hydrate formation.

Many models have been developed that are able to predict the phase equilibria of mixtures containing both electrolyte and non-electrolyte compounds. This is usually done by either introducing complex mixing rules to an equation of state or by coupling the equation of state (short-range interactions) with a Debye-Hückel (*D-H*) electrostatic term (long-range interactions). The available models are normally developed for electrolyte solutions in the absence of organic inhibitors (e.g., alcohols).

However, in cases where the inhibition effect of the produced saline water is not adequate for avoiding gas hydrate formation, organic inhibitors (e.g., methanol, glycol) are added to the pipelines, resulting in a system containing both salts and organic inhibitors. In these cases, it is necessary to take into account the hydrate inhibition effect of combined salts and organic inhibitors. The simplest possible solution is to assume that the combined effect of salts and organic inhibitors on the water activity is the sum of their separate effects. Nasrifar et al. (4) showed that additivity of activities could be assumed if the interaction between the salt and organic inhibitor is neglected. Later, Jager et al. (5) suggested that theoretical models must properly account for the interaction of all species in the aqueous solution in order to predict the effect of mixed inhibitors correctly.

In this work, a thermodynamic model based on combination of the Valderrama modification of the Patel-Teja equation of state (*VPT-EoS*) (6) with non-density dependent mixing rules (*NDD*) (7) and a modification of a *D-H* electrostatic term (8)

is extended to modelling the phase behaviour of electrolyte solutions containing organic inhibitors by taking into account interaction of all species in the aqueous solution and by correcting the system properties, such as, dielectric constant, density and molecular weight. The *VPT-EoS* (6) with *NDD* (7) is also used to model the vapour phase. The previously reported binary interaction parameters (*BIP*) are used in this *EoS* (3). The hydrate phase is modelled by the solid solution theory of van der Waals and Platteeuw (9) using the previously reported Kihara potential parameters (3). The performance of the model is evaluated using some hydrate dissociation data in the literature. Then, a literature review is made on the existing correlation with the aim of developing a new empirical predictive method based on the results of the model to predict hydrate inhibition effects of single and mixed thermodynamic inhibitors. Predictions are found to be in acceptable agreement with the independent data, demonstrating the reliability of the predictive methods developed in this work.

5.2. THERMODYNAMIC MODEL

When salt is present, the fugacities of non-electrolyte components in the aqueous phase are calculated by combining an *EoS* with the *D-H* electrostatic term to take into account the effect of electrolyte (8):

$$\ln \phi_i = \ln \phi_i^{EoS} + \ln \gamma_i^{EL} \qquad i = 1,2,...,n \tag{2.24}$$

where n is the number of non-electrolyte components, ϕ_i is the fugacity coefficient of non-electrolyte component i in the aqueous solution, ϕ_i^{EoS} is the fugacity coefficient of non-electrolyte component i using an *EoS*, neglecting the electrostatic effect, and

γ_i^{EL} is the contribution of the electrostatic term. Using the *D-H* activity model, the second term in equation 2.24 can be calculated from (8):

$$\ln \gamma_i^{DH} = \frac{2AM_m h_{is}}{B^3} f\left(BI^{1/2}\right) \tag{2.25}$$

where M_m is the salt-free mixture molecular weight determined as a molar average, and h_{is} is the binary interaction parameter between the dissolved salt and a non-electrolyte component. The function $f\left(BI^{1/2}\right)$ is obtained from (8):

$$f\left(BI^{1/2}\right) = 1 + BI^{1/2} - \frac{1}{\left(1 + BI^{1/2}\right)} - 2\ln\left(1 + BI^{1/2}\right) \tag{2.26}$$

where I is the ionic strength based on molality of salt in *pure water*. The parameters A and B are given by (8):

$$A = \frac{1.327757 \cdot 10^5 d_m^{1/2}}{\left(\eta_m T\right)^{3/2}} \tag{2.27}$$

$$B = \frac{6.359696 d_m^{1/2}}{\left(\eta_m T\right)^{1/2}} \tag{2.28}$$

where d_m is the density of the salt-free mixture and η_m is the salt-free mixture dielectric constant, which can be calculated for a mixture of salt and water from (8):

$$\eta_m = x_w \eta_w \tag{2.29}$$

x_w and η_w are the salt-free mole fraction and dielectric constant of water, respectively. The dielectric constants of dissolved non-electrolyte components have been neglected, relative to that of water.

Tohidi-Kalorazi (3) presented values for the binary interaction parameter, h_{ws}, between water and dissolved salt for several salts. He expressed h_{ws} as a function of

salt concentration and temperature using two sets of experimental data, i.e., vapour pressure depression of water in the presence of salt at 373.15 K and freezing point depression of water in the presence of salt, to calculate constants $\bar{a}-\bar{e}$ in the binary interaction parameter:

$$h_{ws}=(\bar{a}+\bar{b}T+\bar{c}W+\bar{d}W^2+\bar{e}TW)/1000 \tag{5.1}$$

where T is the temperature in Kelvin and W is the salt concentration relative to water.

To extend this model for a mixture of salt and organic inhibitor, the values of M_m, d_m, η_m are obtained from:

$$\eta_m=(x_w\eta_w+x_{al}\eta_{al})(1-\bar{k}_{w-al}) \tag{5.2}$$

$$M_m=\sum_{i=1}^{n}x_iM_i \tag{5.3}$$

$$d_m=\frac{M_m}{\sum_{i=1}^{n}\frac{x_i}{d_i'}} \tag{5.4}$$

where $\bar{k}_{w-al}$, M_i, d_i', and x_i are an interaction parameter in dielectric constant mixing rule of salt-free mixture, the molecular weight, molar density, and salt-free mole fraction of non-electrolyte components, respectively. The subscripts *w* and *al* relate to the water and inhibitor (alcohol), respectively.

To obtain the values for the binary interaction parameter between organic inhibitor and dissolved salt, the experimental data of boiling point elevation in the presence of salt and organic inhibitor are used. It should be noted that water freezing point depression data couldn't be used for the optimization of the binary interaction parameters between organic inhibitors and salts, as ice is a pure compound and does not contain any salt and/or organic inhibitor.

5.3. EMPIRICAL CORRELATION

The main advantage of empirical or semi-empirical correlations and charts is the availability of input data and the simplicity of the calculations, which can be performed by using charts or spread sheets. The correlations / charts have still kept their popularity among engineers in the petroleum industry. Although most available thermodynamic models could be installed on typical laptop computers, there seems to be a need for simple, yet robust, predictive methods for quick estimation of hydrate inhibition effect of thermodynamic inhibitors.

The existing correlations and charts are generally based on limited data and with limited application. For example, experimental data on gas hydrate formation in drilling and completion fluids are limited and in many cases inconsistent. Available predictive methods for hydrate formation in these fluids are generally empirical correlations based on limited data and with restricted applications. For predicting hydrate formation conditions in drilling and completion fluids, available empirical methods have a much lower accuracy by almost one order of magnitude. In production, transportation and processing, the available correlations / charts can predict hydrate inhibition effect of organic inhibitors and some salts with defined limitations.

The aim of this work is to develop a new correlation based on the concept of water freezing point depression due to the presence of salt and/or organic inhibitor for predicting hydrate inhibition effect of inhibitors. For this purpose a review is made on the most important existing correlations. Then, the predictions of the new correlation are compared with some independent data. The predicted results are in good

agreement with the experimental data, demonstrating the reliability of this correlation for predicting hydrate inhibition effect of thermodynamic inhibitors.

5.4. REVIEW OF THE EXISTING CORRELATION

As a first approximation, the temperature depression for hydrate inhibition might be considered to be similar to the depression of the freezing/melting point of water/ice by an equivalent mass fraction of the inhibitor. However, Nielsen and Bucklin (10) derived an equation indicating that the hydrate depression temperature will always be less than the freezing point depression temperature by around 0.6-0.7 K, depending on the hydrate structure (1).

The Hammerschmidt (11) equation is a relatively simple and widely used expression to approximate the hydrate depression temperature, which has been used over half a century by the industry. Sloan (1) and Carroll (12) have conducted a comprehensive study of this correlation. The Hammerschmidt (11) equation was based on more than 100 experimental determinations of equilibrium temperatures lowering in a given natural gas-water system in the inhibitor concentration range of 5-25 wt.% in the aqueous phase (1). The equation was used to correlate data for alcohols and ammonia inhibitors. It is based on the law of freezing point depression stating that the depression in freezing point is directly proportional to the weight of a dissolved substance in a given amount of solvent. The hydrate depression temperature is approximated by the following equation:

$$\Delta T = \frac{1297W}{100M - MW} \tag{5.5}$$

where, ΔT, M and W are hydrate depression in K, molecular weight of the inhibitor and wt.% of the inhibitor in the aqueous liquid, respectively. The concentration in the above equation is on an organic inhibitor plus water basis, i.e., it does not include the other components in the stream (12). To use this equation with *American Engineering Units*, 1297 is replaced by 2335 and ΔT is in °F.

Equation (5.5) is applicable to non-associating compounds such as most organic materials and ammonia. For salts, a correction must be made, because they dissociate (to different degree) when dissolved in water:

$$Mo = \frac{M}{\alpha(n-1)+1} \tag{5.6}$$

where, Mo, M, α and n are corrected molecular weight to be used in equation (5.5), molecular weight from chemical formula, degree of ionisation (dissociation) and number of ions formed from each molecule of the solute, respectively.

Over the years, some have proposed making constant *1297* as a function of the organic inhibitor in order to improve predictions of this correlation. Townsend and Reid (13) suggested that the Hammerschmidt (11) equation adequately represents depressions up to 60 wt.% for ethylene glycol and up to 75 wt.% for diethylene glycol if the constant *1297* is changed to *2222*. Pieroen (14) and Nielsen and Bucklin (10) presented derivations to show the theoretical validity of the Hammerschmidt (11) equation. The latter work suggested that the equation applies only to typical natural gases, and to methanol concentrations less than 0.20 mole fraction (typically for systems operating at temperatures above 250 K). It may easily be shown (15) that the Hammerschmidt (11) equation should not apply to high concentrations of an inhibitor, which might vaporize. Nixdorf and Oellrich (16) have shown that the

Hammerschmidt (11) equation under-predicts in natural gas systems inhibited with triethylene glycol. Due to a cancellation of errors, the equation (without modification) is applicable for aqueous ethylene glycol concentrations to about 0.40 mole fraction (typically for system operation to 233 K) (1). Carroll (12) has recently shown that this correlation is limited to concentrations of about 30 wt.% for methanol and ethylene glycol and only to about 20 wt.% for other glycols. Other improvements have been made by Pedersen et al. (17); Arnold and Stewart (18); *GPSA* Engineering Data Book (19). Table 5.1 shows some suggested coefficients for the Hammerschmidt (11) equation. Unfortunately, no information on the gas composition and no listing of the individual experimental data were provided. The assumption is normally made that the gases used by Hammerschmidt (11) were methane-rich (1).

Nielsen and Bucklin (10) used first principles to present an improved version of the Hammerschmidt (11) correlation and to develop another equation for estimating hydrate inhibition of methanol solutions up to a wider range. It is based on the law of freezing point depression and is applicable at inhibitor mole fractions as high as 0.8 (88 wt%). The equation was originally developed for prediction of gas hydrate formation in connection with installation and operation of turbo-expander plants, using high concentrations of methanol and the authors suggested that the above equation might be used for design of methanol hydrate control systems operating as low as 166.5 K. However, the equation is actually independent of the choice of inhibitor. The equation involves only the properties of water and the concentration of the inhibitor. Therefore, theoretically it can be used for any non-ionic inhibitor (12). This correlation is given by the following equation:

$$\Delta T = -72 \ln(1-x) \qquad (5.7)$$

where ΔT is in K and x is the mole fraction of methanol. This correlation and the Hammerschmidt (11) correlation predict the same inhibiting effect for a given inhibitor solution at low concentration. Although the Nielsen-Bucklin (10) correlation has a wider range of applicability than the Hammerschmidt (11) correlation, it has not gained wide acceptance (12).

Carroll (12) included an activity coefficient term to account for the type of the inhibitor:

$$\Delta T=-72ln[\gamma_w(1-x)] \tag{5.8}$$

where γ_w is the activity coefficient of water, which is calculated by using the two-suffix Margules model:

$$\Delta T=-72\,[bx^2+ln(1-x)] \tag{5.9}$$

where b is the Margules coefficient. It is believed that this equation is sufficiently accurate over a wide range of inhibitor concentrations (12). Carroll (12), even presented a graphical version of this correlation in order to determine the temperature depression for a given inhibitor (methanol, ethylene glycol and tri- ethylene glycol) concentration and vice versa. Table 5.2 shows the Margules coefficient for various inhibitors. In this table, the Margules coefficient for ethanol was set equal to that for methanol, due to limited reliable data in the literature for ethanol. For the same reason, the value for the Margules coefficient used for di-ethylene glycol is the average of the values for ethylene glycol and tri-ethylene glycol (12). This equation is reported to be good for high concentrations of methanol or ethylene glycol (12).

As mentioned earlier, produced waters normally contain salts and it is important to be able to estimate the effect of salts in the produced water on the hydrate formation, as the presence of salts in the water will also decrease the temperature at which hydrates

form. McCain (20, 21) provided a relation for predicting hydrate inhibition effect of salts:

$$\Delta T = AW + BW^2 + CW^3 \tag{5.10}$$

$$A_1 = 2.20919 - 10.5746\bar{\gamma}_g + 12.1601\bar{\gamma}_g^2 \tag{5.11}$$

$$B_1 = -0.106056 + 0.722692\bar{\gamma}_g - 0.85093\bar{\gamma}_g^2 \tag{5.12}$$

$$C_1 = 0.00347221 - 0.0165564\bar{\gamma}_g + 0.019764\bar{\gamma}_g^2 \tag{5.13}$$

where ΔT is in $^{\circ}F$, W is the salinity in *wt.%* and the coefficients A_1, B_1 and C_1 are functions of the gas gravity, $\bar{\gamma}_g$. The above correlation is based on $0.55 < \bar{\gamma}_g < 0.68$ and $W < 20\%$. Later, Carroll (12) used this correlation to generate some figures, which are useful for rapid approximation of the inhibition effect of salts. It is believed that the above correlation agrees with the data of Deaton and Frost (22) exactly when the results are rounded to the nearest whole degree Fahrenheit (21).

Ouar et al. (23) were able to determine a linear regression for the non-interacting effects of drilling mud components over a small range of concentrations for 17 drilling muds. The following equation may be used to determine the depression of hydrate formation temperature in drilling muds, relative to that for pure water (1):

$$\Delta T = \sum_{i=1}^{9} C_i X_i \tag{5.14}$$

where X_i is the inhibitor concentration (vol.%) and the coefficients C_i are obtained from fitting data. Table 5.3 shows coefficients and range of variables for this equation. This equation represents a first approximation and when high accuracy is required, the computer methods should be used (1). Potential users are cautioned to note both the concentration range of each variable (X_i in vol.%) in this equation and the low value of the regression coefficients.

Later, Yousif and Young (2) proposed a correlation, which is intended to obtain an estimate of the hydrate point suppression of a specific drilling fluid. The following equation can be used to estimate the suppression in the hydrate formation temperature using mixtures of salts and glycerol:

$$\Delta T = 112.3x + 2011.6x^2 - 6505.0x^3 \tag{5.15}$$

where ΔT is hydrate depression temperature in °F and x represents mole fraction of inhibitor/salt in the aqueous liquid. In determining the mole fraction of the salt(s) in a mixture of salts and glycerol, the molecular weights of salts is corrected to take into account the association of the solvated salts and their interaction with the glycerol:

$$Mo = \frac{M}{\alpha(n-1)+1} \tag{5.6}$$

where Mo is apparent molecular weight of salt i in the aqueous solution that contains salts and glycerol, M is molecular weight from chemical formula, n stands for number of ions that results from the salts, α represents the degree of ionization for the salt mixture, which is calculated from:

$$\frac{1}{\alpha} = \sum \frac{1}{\alpha_i} + 1 \tag{5.16}$$

where α_i is the degree of ionization of salt i. The authors presented following correlations for sodium chloride, sodium bromide, potassium chloride, and calcium chloride:

$$\alpha_{NaCl} = -3.635028\times10^{-5}W^3 + 1.813359\times10^{-3}W^2 - 0.044152W + 0.974734 \tag{5.17}$$

$$\alpha_{NaBr} = -2.573254\times10^{-5}W^3 + 1.345127\times10^{-3}W^2 - 0.034563W + 0.993063 \tag{5.18}$$

$$\alpha_{KCl} = -1.574001\times10^{-4}W^3 + 3.987148\times10^{-3}W^2 - 0.057379W + 1.011077 \tag{5.19}$$

$$\alpha_{CaCl2} = -1.692509\times10^{-7}W^3 + 6.211715\times10^{-4}W^2 - 0.029771W + 0.957757 \qquad (5.20)$$

where, W is concentration of salt in weight percent (wt%) and maximum concentrations are given in Table 5.4.

This correlation includes higher concentrations of inhibitors than the original Hammerschmidt (11) correlation. However, Østergaard et al. (24) indicated that the correlation by Yousif and Young (2) has proven to be inaccurate in estimating the inhibition effect, when tested on independent experimental data. It is believed that some of the discrepancies observed between the predictions by the correlation and the experimental data at some salt/organic inhibitor concentrations are partly due to inaccurate experimental data (25).

"An important recent development is the consideration of under-inhibited systems, as reported by Austvik et al. (26), Yousif et al. (27) and Gjertsen et al. (28) (Quoted in ref. 1). At under-inhibited conditions for methanol, ethylene glycol and salt, hydrates coated the pipe wall more than cases without thermodynamic inhibitors, both in field and in laboratory studies. This is a morphology effect, yet the result of pipeline plugging may be worse in under-inhibited systems than if no thermodynamic inhibitor were added" (Quoted in ref. 1).

Generally, these methods predict *hydrate depression temperature* due to the presence of salt or organic inhibitor. That is, first the hydrate formation temperature in the presence of distilled water should be predicted using an appropriate predictive method like that reported by Østergaard et al. (29) or other predictive methods. The hydrate dissociation temperature in the absence of salt or organic inhibitor is corrected using the above methods. These methods also assume that the inhibition effect of salt or

organic inhibitor is independent of the system pressure. A preliminary study shows that this assumption could be good enough for engineering purposes and it is safe to ignore the effect of pressure on the inhibition effect of salts or organic inhibitors. This is in good agreement with that reported by Makogon (30) that the inhibition effect is a function (albeit much smaller) of pressure. Furthermore, these methods assume that the temperature depression is independent of both the nature of the hydrate former present and the type of hydrate formed. That is, the temperature depression in a 25 wt.% methanol solution is the same for a methane hydrate (Structure I) and also for a propane hydrate (Structure II) (12), which may be good enough for engineering purposes.

On the other hand, as mentioned by Carroll (12), the Hammerschmidt (11) and Nielsen-Bucklin (10) equations have some characteristics that make them desirable. In addition to their simplicity, they exhibit the correct limiting behaviour. In the limit, as the inhibitor approaches zero concentration, ΔT approaches zero. In the other limit, as one approaches pure inhibitor, the equation predicts large ΔT – no hydrate formation. Therefore, the new correlation should have these limits. In addition, Nielsen and Bucklin (10) showed that the Hammerschmidt (11) equation is a limiting case for their correlation. Thus, the new equation should have the Nielsen and Bucklin (10) (and hence the Hammerschmidt (11)) equation as a low concentration limit. Finally, the equation should have a firm basis in theory such that it can be extrapolated to conditions where no data exist. With this in mind, the new correlation was developed, as detailed below.

5.5. CONSTRUCTION OF A NEW CORRELATION

The new correlation for estimating hydrate inhibition effects of thermodynamic inhibitors is based on correction of freezing point depression of water due to the presence of salt and/or organic inhibitor. The condition for equilibrium between the aqueous solution and the ice is:

$$\mu_{ice}=\mu_w \tag{5.21}$$

where μ is chemical potential and subscript w stands for water. Assuming the solution is non-ideal and then defining equation for a non-ideal solution gives:

$$\mu_w=\mu_{pure,w}+RT\,ln\,(\gamma_w x_w) \tag{5.22}$$

where T, R and γ represent temperature, universal gas constant and activity coefficient, respectively. Therefore, the temperature T at the freezing point of the solution must satisfy:

$$ln(\gamma_w x_w)=(\mu_{ice}-\mu_{pure,w})/RT \tag{5.23}$$

Replacing the chemical potentials with quantities that are easier to measure directly (or look up in the literature), and taking the derivative of both sides with respect to temperature at constant pressure,

$$dln(\gamma_w x_w)/dT=-(\mu_{ice}-\mu_{pure,w})/RT^2 + ((\partial\mu_{ice}/\partial T)_P + (\partial\mu_{pure,w}/\partial T)_P)/RT \tag{5.24}$$

where subscript P stands for pressure and since

$$\mu_i=H_i - T\,S_i,\ \text{and}\ (\partial\mu_i/\partial T)_p = -S_i, \tag{5.25}$$

where H, S represent the molar enthalpy and entropy, respectively, then

$$dln(\gamma_w x_w)/dT=-(H_{ice}-H_{pure,w})/RT^2 = \Delta H_{fus}/RT^2 \tag{5.26}$$

where ΔH_{fus} is the molar enthalpy of fusion. Collecting all the temperature dependent terms on the right hand side and integrating from conditions in pure water to those in the solution,

$$dln(\gamma_w x_w)=\int_{T_0}^{T}(\frac{\Delta H_{fus}}{RT^2})dT \tag{5.27}$$

$$ln(\gamma_w x_w)=(\frac{\Delta H_{fus}}{R})(\frac{\Delta T}{TT_0}) \tag{5.28}$$

where T_0 is the freezing point of pure water. The above equation can be rearranged as below:

$$ln\gamma_w+ln(1-x_{solute})=(\frac{\Delta H_{fus}}{R})(\frac{\Delta T}{TT_0}) \tag{5.29}$$

For dilute solutions, the equation becomes much simpler. That is, the freezing point depression will be small, so T_0 is approximately equal to T. For simplicity, x_{solute} is assumed to be equal to mole fraction of organic inhibitor only. Then

$$\Delta T=-(\frac{RT_0T}{\Delta H_{fus}})[\ln(1-x_{solute})+\ln\gamma_w] \tag{5.30}$$

$$\Delta T=-a[\ln(1-x_{solute})+\ln\gamma_w] \tag{5.31}$$

where a is a constant. When electrolytes are present, the activity of water rich phase, γ_w, is calculated by combining the non-electrolyte term, $\gamma_w^{Non-Electrolyte}$, with the *Debye-Hückel* electrostatic contribution, γ_i^{EL}, for taking into the account the effect of salt:

$$\ln\gamma_w=\ln\gamma_w^{Non-Electrolyte}+\ln\gamma_w^{El} \tag{5.38}$$

Therefore,

$$\Delta T = -a[\ln(1 - x_{solute}) + \ln \gamma_w^{Non-Electrolyte} + \ln \gamma_w^{El}] \quad (5.39)$$

Employing the simplest activity coefficient model, two-suffix Margules for the non-electrolyte term, yields:

$$\ln \gamma_w^{Non-Electrolyte} = \frac{A'}{RT} x_{solute}^2 \quad (5.40)$$

Assuming the term $\frac{A'}{RT}$ is independent of the temperature and can be replaced by a constant, b, equation (5.39) becomes:

$$\Delta T = -a[\ln(1 - x_{solute}) + bx_{solute}^2 + \ln \gamma_w^{El}] \quad (5.41)$$

As it can be seen, the right hand side of the above equation consists of three terms: The first term takes into account the ideality of the system, second term represents the non-ideality of the system due to the presence of organic inhibitors and the third term non-ideality of the system due to the presence of salts.

The *Debye-Hückel* activity coefficient model can be used for expressing the third term of the right hand side of the above equation:

$$\ln \gamma_w^{EL} = \frac{2AM_m h_{ws}}{B^3} f(BI^{1/2}) \quad (2.25)$$

where M_m is the salt-free mixture molecular weight and h_{ws} is the interaction coefficient between the dissolved salt and non-electrolyte component. The function $f(BI^{1/2})$ is obtained from:

$$f(BI^{1/2}) = 1 + BI^{1/2} - \frac{1}{(1 + BI^{1/2})} - 2\ln(1 + BI^{1/2}) \quad (2.26)$$

where I is the ionic strength. The parameters A and B are given by:

$$A = \frac{1.327757 \cdot 10^5 d_m^{1/2}}{(\eta_m T)^{3/2}} \tag{2.27}$$

$$B = \frac{6.359696 d_m^{1/2}}{(\eta_m T)^{1/2}} \tag{2.28}$$

where d_m is the density of the salt-free mixture and η_m is the salt-free mixture dielectric constant. Therefore:

$$\ln \gamma_w^{EL} = ch_{ws} \left[1 + BI^{1/2} - \frac{1}{(1 + BI^{1/2})} - 2\ln(1 + BI^{1/2})\right] \tag{5.42}$$

where c is a constant. Assuming $BI^{0.5} < 1$, then $\ln \gamma_w^{EL}$ becomes a function of h_{ws}, which can be expressed as a function of weight percent of salt in the aqueous solution, W, in the following form:

$$h'_{ws} = (c'_1 W + c'_2 W^2 + c'_3 W^3) \tag{5.43}$$

where c'_1 , c'_2 and c'_3 are constants. Using the above expression, the final form of equation 5.41 is obtained as below:

$$\Delta T = - a[\ln(1 - x_{solute}) + bx_{solute}^2 + (c_1 W + c_2 W^2 + c_3 W^3)] \tag{5.44}$$

where c_1 , c_2 and c_3 are constants. In most practical cases, several salts with or without one organic inhibitor are used. The following relation can extend the above equation to mixed salts and one organic inhibitor:

$$\Delta T = - a[\ln(1 - x_{solute}) + bx_{solute}^2 + \Sigma (c_{1,i} W_i + c_{2,i} W_i^2 + c_{3,i} W_i^3)] \tag{5.45}$$

where $c_{1,i}$, $c_{2,i}$ and $c_{3,i}$ are constants. The above equation could be used for predicting the freezing point depression of aqueous solutions as well as hydrate inhibition due to the presence of salts and/or organic inhibitors. Constants c_1 - c_3 and b take into account the effect of salt and organic inhibitor, respectively. For a mixture of salt and

organic inhibitor, all constants b and c_1 - c_3 are used. However their values are different from those reported for single salt and single organic inhibitor. As it can be seen, the above correlation re-confirms the Nielsen-Bucklin (10) and Carroll (12) correlations and is a combination of Yousif-Young (2), Nielsen-Bucklin (10) and Carroll (12) correlations.

5.6. RESULTS AND DISCUSSION

5.6.1. Thermodynamic model

As mentioned earlier, the *VPT-EoS* (6) combining with *NDD* mixing rules (7) is used for calculating the first term of equation 2.24 and for calculating the fugacity of the vapour phase using the previously reported *BIP*s (3). This combination has proved to be a strong tool in modelling systems with polar as well as non-polar compounds (7).

In the second term of equation 2.24, the dielectric constant of the solvent mixture can be approximated from the pure compound values and Oster's mixing rule (31). However, a preliminary study shows that the dielectric constant of the salt-free mixture has a very important effect on model predictions. Any uncertainty can lead to large deviations between the experimental and predicted results. Therefore, equation 5.2 is used rather than Oster's mixing rule (31). In equation 5.2, $\bar{k}_{w-al}$ is tuned using the experimental data on water freezing point depression in the presence of salts and organic inhibitors. In this work, the data in Table 5.5 are used for tuning $\bar{k}_{w-al}$. This value is relatively constant for large ranges of concentrations in the aqueous phase and equals to 0.08. Tables 5.6 and 5.7 compare predicted and experimental freezing point temperatures for KCl + methanol and $CaCl_2$ + methanol aqueous solutions using the

above value of $\bar{k}_{w-at}$. Acceptable agreement between the results demonstrates the reliability of the approach used in the present work.

In equation 2.25, the binary interaction parameters between salts and non-electrolyte components (except for organic inhibitors which are the subject of this study) are set to those reported by Tohidi-Kalorazi (3) with constants $a-b$ reported in Table 5.8.

The binary interaction parameters between salts and organic inhibitors are tuned using the vapour pressure data of the system. Tables 5.9-5.11 show the data used in this work. Using an average value equal to 0.020, 0.027 and 0.007 for the binary interaction parameter between NaCl/ KCl/ $CaCl_2$ and methanol, respectively gives reasonable results for the predicted bubble point. Obviously, this value does not have any effect on the predicted freezing point/ hydrate formation conditions in the presence of salts and organic inhibitors.

In order to further evaluate the performance of the model, hydrate dissociation conditions in the presence of salts and organic inhibitors are predicted and compared with the experimental data. Limited experimental data on hydrate dissociation conditions of gases in the presence of salts and organic inhibitors have been reported in the literature. In this work, hydrate dissociation conditions of methane (5, 31) and a mixture of methane and carbon dioxide (32) in the presence of different concentrations of methanol and salt are predicted and compared to those reported in the literature. For this purpose, reliability of the model is first investigated for predicting hydrate dissociation conditions of methane and carbon dioxide in the presence of distilled water, aqueous solutions containing salt (NaCl, KCl, $CaCl_2$) and methanol aqueous solution. Figures 5.1-5.15 show all the results.

As shown in the figures, the predicted data are in acceptable agreement with the experimental data. However, this model shows some deviations at very high concentrations of methanol for data reported by Jager et al. (5). These deviations may be attributed to the uncertainties in the experimental data at high concentrations of methanol. Jager et al. (5) used two difference methods for measuring methane hydrate stability in methanol and NaCl solutions and reported that their data show some deviations at high concentrations of salt and organic inhibitor, indicating a need for generating accurate hydrate dissociation data as well as freezing point and boiling point data at high concentrations of salt and organic inhibitors.

5.6.2. Correlation

To optimise constants a, b and c_1-c_3 (Equations 5.44 and 5.45) for predicting the freezing point depression of aqueous solutions containing salts and/or organic inhibitors, the thermodynamic model was used for generating the necessary tuning data in the presence of pure water as well as various salts and/or organic inhibitors. The generated data are used as input for a multi-dimension regression procedure. The objective function is defined as the average absolute deviation (*AAD*) between the water freezing point depression temperature determined by the thermodynamic model and the depression temperature calculated by the new correlation. The results along with the *AAD* are presented in Table 5.12.

These parameters for hydrates are optimised using hydrate dissociation temperatures for methane generated in the presence of pure water as well as various salts and/or organic inhibitors using the above thermodynamic model. Parameter a is set to that reported by Nielsen-Bucklin (10) in order to reduce the number of tuning parameters. Tables 5.2, 5.13 and 5.14 report these constants for various organic inhibitors and/or

salts. A preliminary study shows that the values of constant *b* for various organic inhibitors reported by Carroll (12) are satisfactory with application ranges shown in Table 5.2. Therefore, the values of this constant are set to those reported by Carroll (12) and this constant is tuned only for glycerol.

In Tables 5.15-5.17 and Figures 5.16-5.17, the reliability of the correlation developed in this work is tested with data on some salts and/or organic inhibitors from the literature and other predictive methods. As it can be observed, for all references not used in the tuning of *b* and c_1 - c_3, the predictions of this correlation are in acceptable agreement with the experimental data. It should be noted that the effect of gas composition and pressure has been ignored in these calculations. The agreement between predictions and experimental data shows that the effect of gas composition can be ignored for engineering purposes. The expression could be further tuned with the availability of new data, in particular for a combination of salt and organic inhibitor at high concentrations and also by taking into account the effect of pressure on hydrate inhibition of salt and/or organic inhibitor.

The above correlation can also be used for estimating the location at which hydrate forms along a pipeline. Location of hydrate formation along a pipeline can be estimated by performing an energy balance calculation. For engineering purposes, the following equation (see Appendix A.2) can be used for calculating the location, $\bar{x}$, of the hydrate formation versus the equilibrium temperature, *T*:

$$\bar{x} = - \frac{\dot{m}_g C_P}{2\pi R U} ln(\frac{T - T_E}{T_I - T_E}) \qquad (5.46)$$

where $\dot{m}_g$, R', U, C_p, T_E and T_I are mass flow-rate of natural gas, pipe radius, overall-heat transfer coefficient, average heat capacity of natural gas, environment temperature and temperature at $\bar{x}=0$. Combination of equations (5.44) (Obviously, first the hydrate formation temperature in the absence of salt and/or organic inhibitor should be predicted using an appropriate predictive method) and (5.46) can yield the location of hydrate formation.

5.6.2.1. Predicting hydrate depression using freezing point data

The possibility of predicting hydrate inhibition effects of thermodynamic inhibitors from freezing point depression of the aqueous phase due to the presence of salt and/or organic inhibitor could have a real practical use, as measuring freezing point depression of aqueous phase is easier than hydrate suppression temperature, which could have a real benefit since experimental data on gas hydrate formation in some cases such as drilling and completion fluids and combination of salt and organic inhibitor are limited and in many cases inconsistent. For this purpose, hydrate suppression temperatures of methane and freezing point depression points of aqueous phase due to the presence of thermodynamic inhibitors generated by the model for the systems shown in Table 5.18 are used for developing the equation.

Figure 5.18 shows the collapse of all data onto one line, suggesting a linear relationship between hydrate suppression temperatures and freezing point depressions with a slope of 0.683 (i.e., $\Delta T_{hydrate}=0.683\times\Delta T_{ice}$). As can be seen, the hydrate suppression temperature is always less than the freezing point depression temperature, which is in good agreement with the Nielsen and Bucklin results (10) and that mentioned by Sloan (1).

In Tables 5.19 and 5.20 and Figures 5.19-5.22, the reliability of the predictive method developed in this work is tested with data on some thermodynamic inhibitors from the literature. It should be mentioned that the model results were used to predict freezing point depressions due to the presence of thermodynamic inhibitors. As can be observed, for all references not used in the tuning the predictive tool, the predictions of this approach are generally in acceptable agreement with the experimental data. It should be noted that the effect of gas composition and pressure has been ignored in these calculations. In Figures 5.19 and 5.20 the agreement between experimental and predicted hydrate dissociation conditions of methane in the presence of aqueous solutions composed of NaCl or methanol is acceptable.

Limited experimental data on hydrate dissociation conditions of gases in the presence of salt and organic inhibitor have been reported in the literature. In this work, hydrate dissociation conditions of methane (5) in the presence of different concentrations of methanol and NaCl are predicted and compared to those reported in the literature. As shown in the Figures 5.21 and 5.22, the predicted data are in acceptable agreement with the experimental data. However, this method shows some deviations at very high concentrations of methanol. These deviations may be attributed to the uncertainties in the experimental data at high concentrations of methanol, as explained earlier.

In Table 5.19, a comparison is made between predictions of this method, correlation and experimental data (32) for hydrate dissociation conditions of a gas mixture composed of 80 mole% methane and 20 mole% carbon dioxide in the presence of salt aqueous solutions. As can be seen, the agreement is acceptable, demonstrating the reliability of the approach developed in the present work. To study capability of this

method for predicting the hydrate inhibition characteristics for systems with structure II, the predictions of this approach are compared with experimental data (48) for hydrate dissociation conditions of a gas mixture composed of 95.01 mole% methane + 4.99 mole% propane in the presence of methanol solutions. The agreement between predictions and experimental data shows that the effect of gas composition and therefore hydrate structure can be ignored for engineering purposes.

5.7. CONCLUSIONS

A thermodynamic model based on combination of the Valderrama modification of the Patel-Teja equation of state with non-density dependent mixing rules and a modification of a Debye-Hückel electrostatic term (3) (equation 2.24) has been extended to mixed salts and organic inhibitors systems by taking into account the interaction of all species in the aqueous solution (equation 2.25) and correcting the properties of the aqueous phase (i.e., dielectric constant, density and molecular weight) (equations 5.2 – 5.4).

The binary interaction parameters between salts and organic inhibitors (equation 2.25, page 5.4) were adjusted using water vapour pressure data in the presence of salts and organic inhibitors. It was found that the dielectric constant mixing rule of salt-free mixture has very important effect on the results. A linear mixing rule was used for determination of dielectric constant of salt-free mixture by introducing an interaction parameter, which is tuned using water freezing point depression data in the presence of salts and organic inhibitors (equation 5.2). The predicted hydrate dissociation conditions were in acceptable agreement with the experimental data, demonstrating

the reliability of the developed model for predicting hydrate dissociation conditions in the presence of salts and organic inhibitors.

A new correlation based on correction of freezing point depression of water due to the presence of salt and/or organic inhibitor was developed for predicting hydrate inhibition effect as well as water freezing point depression of thermodynamic inhibitors (equation 5.44). The results of this correlation are in acceptable agreement with the experimental data in the literature. The expression could be further tuned with the availability of new experimental data, in particular at high concentrations of salts and/or organic inhibitors and also by taking into account the effect of pressure on hydrate inhibition effect of salts and/or organic inhibitors.

A new predictive method, which relates hydrate inhibition effects of thermodynamic inhibitors to freezing point depression of aqueous phase, was developed (Page 148). The expression with only one parameter produced encouraging results. The results of this approach are in acceptable agreement with the experimental data in the literature, demonstrating its reliability for estimating hydrate characteristics of salt(s) and/or organic inhibitor(s).

TABLES

Table 5.1. Some suggested coefficients for the Hammerschmidt (11) equation (12).

Inhibitor	Original	*GPSA* Engineering Data Book (19)	Arnold and Stewart (18)	Pedersen et al. (17)
Methanol	1297	1297	1297	1297
Ethanol	1297	-	1297	1297
Ethylene Glycol	1297	2222*	1222	1500
Di-ethylene Glycol	1297	2222	2427	2222
Tri-ethylene Glycol	1297	2222	2472	3000

* Carroll (12): The value of 2222 for ethylene glycol in the *GPSA Engineering Data Book* (19) is much too large. Better predictions are obtained using the original value of 1297. On the other hand, this large value does improve the calculations for tri-ethylene glycol.

Table 5.2. Parameter *b* in equation 5.9 for various organic inhibitors.

Organic inhibitor	Molecular weight	b	Maximum Concentration (wt.%)
Methanol	32.04	0.21	40
Ethanol	46.07	0.21	25
Ethylene Glycol	62.07	-1.25	25
Di-ethylene Glycol	106.12	-8	25
Tri-ethylene Glycol	150.17	-15	25
Glycerol	92.09	-0.25	35

Table 5.3. Coefficients and range of variables to prediction hydrate temperature depression in drilling muds (Equation 5.14, from ref. 1).

	Component of Drilling Fluid									
	Bent/ Thin/ Caustic	Barite 2-100 mm	Salt	Poly XCD	Poly PHPA	LVT Oil	Drill Solid	MeOH	H_2O	R^2
Concentration lb/BBL	14	150	50.3	1.0	1.0	29	20	28	rmdr	
Range (vol.%)	0-1.6	0-10.2	0-5.2	0-0.2	0-0.2	0-10	0-2.3	0-10		
Pressure (psig)										
400	-6.00	0.617	3.32	36.3	-32.2	0.667	3.13	0.007	-0.02	0.67
600	-5.58	0.672	3.22	33.4	-27.7	0.647	3.16	0.012	-0.02	0.71
800	-5.28	0.712	3.15	31.3	-24.4	0.633	3.19	0.016	-0.02	0.74
1000	-5.04	0.743	3.09	29.7	-21.8	0.622	3.21	0.019	-0.02	0.75
1200	-4.95	0.752	3.07	27.7	-20.1	0.632	3.30	0.035	-0.01	0.76

Table 5.4. Maximum concentrations used in the development of the equation 5.15.

Inhibitor	wt%
Glycerol	30
NaCl	26
NaBr	30.6
KCl	10
$CaCl_2$	19.22

Table 5.5. Experimental and calculated (using thermodynamic model) freezing point temperatures for aqueous solutions containing different concentrations of NaCl and methanol (Experimental data from Centre for Gas Hydrate Research, Heriot-Watt University).

MeOH (wt.%)	NaCl (wt.%)	Experimental freezing point /K	Calculated freezing point /K	$\lvert\Delta T\rvert$	AD%
2.81	3.16	269.0	269.3	0.3	0.13
4.21	4.18	267.1	267.5	0.4	0.15
6.39	6.99	263.0	263.2	0.2	0.09
7.83	8.17	260.4	260.7	0.4	0.14
11.48	7.11	258.0	258.3	0.3	0.13
12.9	6.26	257.5	257.8	0.4	0.15
10.15	10.21	255.9	256.1	0.2	0.08
10.77	12.82	252.1	251.9	0.1	0.05
12.92	12.45	250.1	249.7	0.3	0.13

Table 5.6. Experimental and predicted (using thermodynamic model) freezing point temperatures for aqueous solutions containing different concentrations of KCl and methanol (Experimental data from Centre for Gas Hydrate Research, Heriot-Watt University; Concentrations are relative to water).

MeOH (wt.%)	KCl (wt.%)	Experimental freezing point /K	Predicted freezing point /K	$\lvert\Delta T\rvert$	AD%
6.68	10.80	259.0	259.0	0	0
3.15	5.17	267.1	267.0	0.1	0.04
1.58	3.08	269.8	270.0	0.2	0.07
4.83	7.69	263.3	263.5	0.2	0.08

Table 5.7. Experimental and predicted (using thermodynamic model) freezing point temperatures for aqueous solutions containing different concentrations of $CaCl_2$ and methanol (Experimental data from Centre for Gas Hydrate Research, Heriot-Watt University; Concentrations are relative to water).

$CaCl_2$ (wt.%)	MeOH (wt.%)	Experimental freezing point /K	Predicted freezing point /K	$\lvert\Delta T\rvert$	AD%
2.79	1.60	270.1	270.2	0.1	0.04
5.47	3.43	267.1	266.3	0.8	0.30
8.64	5.15	263.8	261.5	2.3	0.87
12.34	8.74	257.2	255.5	1.7	0.66
16.61	4.19	257.5	255.2	2.3	0.89
5.56	6.37	264.1	262.6	1.5	0.57
10.19	4.03	263.6	261.5	2.1	0.80

Table 5.8. Constants in equation 5.1 for calculating the interaction parameter (3).

i) NaCl

Constant	Water	Methane	Carbon dioxide
$\bar{a}$	-11.91	256.70	215.65
$\bar{b}$	0.01037	-0.4447	-0.5179
$\bar{c}$	-0.06043	-7.447	-5.563
$\bar{d}$	-0.005814	0.08202	-0.01663
$\bar{e}$	0.0003861	0.01115	0.017379

ii) KCl

Constant	Water	Methane	Carbon dioxide
$\bar{a}$	-12.79	198.9	250.7
$\bar{b}$	0.01385	-0.4754	-0.7110
$\bar{c}$	0.05184	0.8223	-9.441
$\bar{d}$	-0.002152	-0.02731	0.003230
$\bar{e}$	0.00001436	0.00002068	0.02917

iii) $CaCl_2$

Constant	Water	Methane	Carbon dioxide
$\bar{a}$	-5.672	99.15	78.31
$\bar{b}$	0.008037	-0.1414	-0.1463
$\bar{c}$	-0.3330	-0.5017	-0.2631
$\bar{d}$	-0.001771	-0.000008176	-0.004413
$\bar{e}$	0.0005800	0.00000724	0.001597

Table 5.9. Experimental and calculated (using thermodynamic model) boiling point temperatures for aqueous solutions containing different concentrations of NaCl and methanol (Experimental data from Centre for Gas Hydrate Research, Heriot-Watt University).

MeOH (wt.%)	NaCl (wt.%)	Experimental boiling point /K	Calculated boiling point /K	$\lvert\Delta T\rvert$	AD%
4.96	4.90	367.5	369.3	1.8	0.49
7.38	16.46	365.2	366.3	1.1	0.31
9.67	0.00	364.3	365.9	1.6	0.44
10.10	10.27	362.9	364.4	1.6	0.44
14.46	14.57	359.4	359.5	0.1	0.04
16.84	15.84	357.8	356.9	0.9	0.25
25.57	5.14	355.4	355.7	0.3	0.08
30.12	0.00	354.2	355.9	1.8	0.49
28.51	12.44	352.8	349.5	3.3	0.92

Table 5.10. Experimental and calculated (using thermodynamic model) boiling point temperatures for aqueous solutions containing different concentrations of KCl and methanol (Experimental data from Centre for Gas Hydrate Research, Heriot-Watt University).

MeOH (wt.%)	KCl (wt.%)	Experimental boiling point /K	Calculated boiling point /K	$\lvert\Delta T\rvert$	AD%
2.72	5.13	368.1	369.4	1.3	0.35
6.67	10.69	362.8	364.0	1.2	0.33
11.66	16.51	357.2	357.2	0	0.00
3.06	20.06	368.1	368.9	0.8	0.22
19.20	8.46	354.2	353.6	0.6	0.17
2.11	2.70	369.4	370.2	0.8	0.22

Table 5.11. Experimental and calculated (using thermodynamic model) boiling point temperatures for aqueous solutions containing different concentrations of $CaCl_2$ and methanol (Experimental data from Centre for Gas Hydrate Research, Heriot-Watt University).

MeOH (wt.%)	$CaCl_2$ (wt.%)	Experimental boiling point /K	Calculated boiling point /K	$\lvert\Delta T\rvert$	AD%
4.81	5.45	368.3	369.4	1.1	0.30
13	11.18	362.2	363.2	1.0	0.28
16.87	16.24	359.9	359.9	0.0	0.00
9.48	18.56	365.5	365.9	0.4	0.11
10.31	5.53	363.8	365.2	1.4	0.38

Table 5.12. Parameters *a*, *b* and c_1-c_3 in equation 5.44 for various salts and/or organic inhibitors for calculating freezing point depression of aqueous solution of salts and/or organic inhibitors.

Solute	a	b	$c_1\times10^3$	$c_2\times10^4$	$c_3\times10^6$	Maximum Concentration (wt.%)
NaCl	72	0	-7.6820	-13.0017	-3.0296	20
KCl	72	0	-4.7517	-37.7099	15.5119	12
$CaCl_2$	72	0	-5.3161	-24.6841	-6.0665	30
KBr	72	0	-3.3596	-8.7563	0.6155	30
NaBr	72	0	-4.7455	-3.2733	-2.0896	30
HCOONa	72	0	-8.0062	-0.1347	-3.2235	20
HCOOK	72	0	-5.5432	-13.5274	0.2642	20
K_2CO_3	72	0	-5.3337	14.0897	-8.6013	15
Methanol	111	-0.3156	0	0	0	40
Ethanol	93.52	-3.1922	0	0	0	25
Ethylene Glycol	101.47	-1.9019	0	0	0	25
Di-ethylene Glycol	100.17	-4.6942	0	0	0	25
Tri-ethylene Glycol	102.42	-8.4162	0	0	0	25
Glycerol	116.38	-0.2151	0	0	0	35
Methanol-NaCl	72	-8.2396	-12.4744	-1.5941	-8.2589	*
Methanol-KCl	72	-8.6507	-9.8908	6.0098	-3.3563	*
EG-NaCl	72	-11.5745	-14.3564	148.1406	-93.0377	*
EG-KCl	72	-6.5383	-8.5939	-14.3106	2.1036	*
EG-$CaCl_2$	72	-2.2860	-7.2590	-25.5154	-6.6846	*

*See maximum concentration of single inhibitor

Table 5.13. Parameters c_1-c_3 in equation 5.44 for various salts.

Salt	Molecular weight	$c_1\times10^3$	$c_2\times10^4$	$c_3\times10^6$	Maximum Concentration (wt.%)
NaCl	58.44	-5.9048	-0.173489	-4.32669	20
KCl	74.55	-4.6760	-0.073968	-1.30581	12
$CaCl_2$	111	-4.0980	-1.271899	-4.54556	30
KBr	119	-3.3060	0.2421101	-1.52094	30
NaBr	102.9	-3.3133	-0.378275	-1.15134	30
HCOONa	68.01	-5.3128	-0.635029	-0.57396	20
HCOOK	84.12	-4.4457	-0.090758	-2.50809	20
HCOOCs	177.92	-1.8351	-0.313317	-0.596164	15
K_2CO_3	138.2	-4.0202	0.929050	-5.33882	15

Table 5.14. Parameters b and c_1-c_3 in equation 5.44 for various salts and organic inhibitors*.

Salt	Methanol				Ethylene glycol			
	b	$c_1\times10^3$	$c_2\times10^4$	$c_3\times10^6$	b	$c_1\times10^3$	$c_2\times10^5$	$c_3\times10^6$
NaCl	-2.90000	-6.36787	-1.14102	-2.5658	-5.6268	-8.0782	3.3702	-6.2052
KCl	-2.19163	-5.86440	0.634040	-4.6760	-5.0100	-6.7384	4.4417	-3.1174
$CaCl_2$	-3.19866	-4.35800	-2.20200	-2.6110	-2.2223	-6.5490	-0.4982	-6.5030

*See maximum concentration of single inhibitor

Table 5.15. Comparison of the predictions of this correlation (equation 5.44) with experimental data (31) for methane hydrate dissociation conditions in the presence of aqueous glycerol solutions.

wt.%	P/MPa	Experimental	Correlation	$\lvert\Delta T\rvert$
		T/K	T/K	
25	4.39	273.8	273.5	0.3
	6.91	278	278.0	0.0
	12.41	283	283.4	0.4
	20.53	286.2	287.6	1.4
50*	4.53	264.2	265.1	0.9
	6.65	267.8	268.9	1.1
	13.81	273.4	275.6	2.2
	20.53	276.2	278.8	2.6

*Higher than maximum concentration of inhibitor used for developing this method

Table 5.16. Comparison of the predictions of this correlation (equation 5.44) with experimental data (32) for hydrate dissociation conditions of a gas mixture (80 mole% methane and 20 mole% carbon dioxide) in the presence of salt aqueous solutions.

Salt	wt.%	P/MPa	T/K		$\lvert\Delta T\rvert$
			Experimental	Correlation	
NaCl	5.02	2.3	271.6	271.6	0.0
		3.26	275	274.9	0.1
		5.08	279.2	279.1	0.1
		6.98	282	281.9	0.1
	9.99	2.03	268.5	267.7	0.8
		3.1	272.1	272.1	0.0
		4.66	276.1	275.8	0.3
		6.56	279	278.9	0.1
	15	1.86	264.8	263.8	1.0
		2.88	269.1	268.2	0.9
		4.4	273.1	272.3	0.8
		7.37	276.8	276.9	0.1
		7.31	277.2	276.8	0.4
	20	2.12	262	261.3	0.7
		3.85	267.5	267.2	0.3
		5.42	270.4	270.4	0.0
	20.01*	9.15	274.3	274.9	0.6
KCl	5	2.04	271.4	270.7	0.7
		2.96	275	274.4	0.6
		4.46	278.8	278.4	0.4
		6.43	282	281.7	0.3
	10	1.83	269.2	267.8	1.4
		2.59	272.2	271.3	0.9
		3.94	275.9	275.4	0.5
		5.56	279	278.6	0.4
	15.01*	1.89	267	266.2	0.8
		2.62	270.1	269.5	0.6
		3.45	272.7	272.1	0.6
		5.63	277.1	276.7	0.4
$CaCl_2$	9.91	1.96	268.6	267.9	0.7
		2.8	272	271.5	0.5
		4.32	276	275.7	0.3
		6.08	279.1	278.8	0.3
	15	1.88	266.6	264.0	2.6
		3	269.1	268.7	0.4
		4.61	273.1	272.8	0.3
		7.09	276.9	276.7	0.2
	20	2.89	263.8	263.7	0.1
		4.3	267.6	267.6	0.0
		7.24	271.3	272.2	0.9
		9.46	273.7	274.4	0.7

*Higher than maximum concentration of inhibitor used for developing this method

Table 5.17. Comparison of the predictions [this correlation (equation 5.44) and the models (33, 34, 35) reported in the literature] with experimental data (33) for methane hydrate dissociation conditions in the presence of mixed salt–ethylene glycol (EG) aqueous solutions.

Salt	Salt (wt.%)	EG (wt.%)	P/MPa	Exp.	Model-1 (33)		Model-2 (34)*		Model-3 (35)*		Correlation	
				T/K	T/K	|ΔT|	T/K	|ΔT|	T/K	|ΔT|	T/K	|ΔT|
NaCl	15	21.3	5.068	262.3	261.8	0.5	264.7	2.4	266	3.7	260.9	1.4
			11.431	268.4	268.5	0.1	271.8	3.4	272.6	4.2	268.6	0.2
			27.758	274.3	275	0.7	278.3	4	278.4	4.1	275.9	1.6
			46.698	277.9	279	1.1	282.2	4.3	281.7	3.8	280.1	2.2
	12	30.8†	6.957	262.4	260.7	1.7	267.4	5	267.2	4.8	258.8	3.6
			13.61	267.3	266.2	1.1	273	5.7	272	4.7	264.9	2.4
			22.946	270.5	269.5	1	276.9	6.4	275.3	4.8	269.2	1.3
			46.691	275.2	274.8	0.4	282.3	7.1	279.6	4.4	274.9	0.3
KCl	10	23	4.164	265.5	265.4	0.1	269.4	3.9	267.2	1.7	263.5	2.0
			10.356	273.4	273.7	0.3	277.9	4.5	274.9	1.5	272.3	1.1
			22.76	279.1	279.9	0.8	284.1	5	280.3	1.2	278.9	0.2
			44.513	283.9	285	1.1	289.3	5.4	284.7	0.8	284.3	0.4
	8	35†	3.93	259.3	259.3	0	266.7	7.4	264.1	4.8	254.0	5.3
			9.935	267	267.7	0.7	275.5	8.5	271.5	4.5	263.0	4.0
			23.442	273	274.1	1.1	282.4	9.4	277	4	270.2	2.8
			45.05	277.6	279.1	1.5	287.6	10	281	3.4	275.5	2.1
Ave.						0.8		5.8		3.5		1.9

* Quoted in ref. 33

† Higher than maximum concentration of inhibitor used for developing this method

Table 5.18. Maximum concentrations used in the development of equation 5.44.

Inhibitor	Inhibitor (wt.%)	Salt (wt.%)
NaCl	0	23
KCl	0	13
$CaCl_2$	0	32
KBr	0	32
NaBr	0	40
HCOONa	0	30
HCOOK	0	30
MeOH	50	0
EtOH	30	0
EG	23	0
DEG	49	0
TEG	60	0
MeOH+NaCl	13	13
MeOH+KCl	13	15

Table 5.19. Comparison of the predictions of this work (i.e., $\Delta T_{hydrate}=0.683\times\Delta T_{ice}$) and correlation (equation 5.44) with experimental data (32) for hydrate dissociation conditions of a gas mixture (80 mole% methane and 20 mole% carbon dioxide) in the presence of salt aqueous solutions.

Salt	wt.%	P/MPa	T/K		|ΔT|	This work/K	|ΔT|
			Experimental	*Correlation*			
NaCl	5.02	2.3	271.6	271.6	0	271.7	0.1
		3.26	275	274.9	0.1	275.0	0.0
		5.08	279.2	279.1	0.1	279.2	0.0
		6.98	282	281.9	0.1	282.0	0.0
	9.99	2.03	268.5	267.7	0.8	267.8	0.7
		3.1	272.1	272.1	0	272.0	0.1
		4.66	276.1	275.8	0.3	275.9	0.2
		6.56	279	278.9	0.1	279.0	0.0
	15	1.86	264.8	263.8	1	264.0	0.8
		2.88	269.1	268.2	0.9	268.3	0.8
		4.4	273.1	272.3	0.8	272.4	0.7
		7.37	276.8	276.9	0.1	277.0	0.2
		7.31	277.2	276.8	0.4	277.0	0.2
	20	2.12	262	261.3	0.7	261.6	0.4
		3.85	267.5	267.2	0.3	267.4	0.1
		5.42	270.4	270.4	0	270.6	0.2
	20.01	9.15	274.3	274.9	0.6	275.1	0.8
KCl	5	2.04	271.4	270.7	0.7	270.9	0.5
		2.96	275	274.4	0.6	274.6	0.4
		4.46	278.8	278.4	0.4	278.5	0.3
		6.43	282	281.7	0.3	281.8	0.2
	10	1.83	269.2	267.8	1.4	268.0	1.2
		2.59	272.2	271.3	0.9	271.5	0.7
		3.94	275.9	275.4	0.5	275.5	0.4
		5.56	279	278.6	0.4	278.7	0.3
	15.01*	1.89	267	266.2	0.8	267.1	0.1
		2.62	270.1	269.5	0.6	270.4	0.3
		3.45	272.7	272.1	0.6	273.1	0.4
		5.63	277.1	276.7	0.4	277.7	0.6
$CaCl_2$	9.91	1.96	268.6	267.9	0.7	267.9	0.7
		2.8	272	271.5	0.5	271.5	0.5
		4.32	276	275.7	0.3	275.7	0.3
		6.08	279.1	278.8	0.3	278.8	0.3
	15	1.88	266.6	264	2.6	263.9	2.7
		3	269.1	268.7	0.4	268.6	0.5
		4.61	273.1	272.8	0.3	272.7	0.4
		7.09	276.9	276.7	0.2	276.6	0.3
	20	2.89	263.8	263.7	0.1	263.5	0.3
		4.3	267.6	267.6	0	267.3	0.3
		7.24	271.3	272.2	0.9	272.0	0.7
		9.46	273.7	274.4	0.7	274.2	0.5

Table 5.20. Comparison of the predictions of this work (i.e., $\Delta T_{hydrate}=0.683\times\Delta T_{ice}$) and correlation (equation 5.44) with experimental data (48) for hydrate dissociation conditions of a gas mixture (95.01 mole% methane + 4.99 mole% propane) in the presence of methanol solutions.

Methanol (wt.%)	P/MPa	T/K	Correlation /K	|ΔT|	This work /K	|ΔT|
10	0.532	265.5	267.0	1.5	266.8	1.3
	0.903	270.1	271.3	1.2	271.1	1.0
	1.544	274.5	275.7	1.2	275.5	1.0
	3.006	280.4	281.1	0.7	280.9	0.5
	6.95	286.9	287.2	0.3	287.0	0.1
	13.831	291.2	290.9	0.3	290.7	0.5
20	0.938	265.2	266.7	1.5	265.6	0.4
	1.772	270.5	271.9	1.4	270.9	0.4
	3.144	275.7	276.6	0.9	275.5	0.2
	6.846	281.9	282.2	0.3	281.2	0.7
	14.1	286.5	286.2	0.3	285.0	1.5

FIGURES

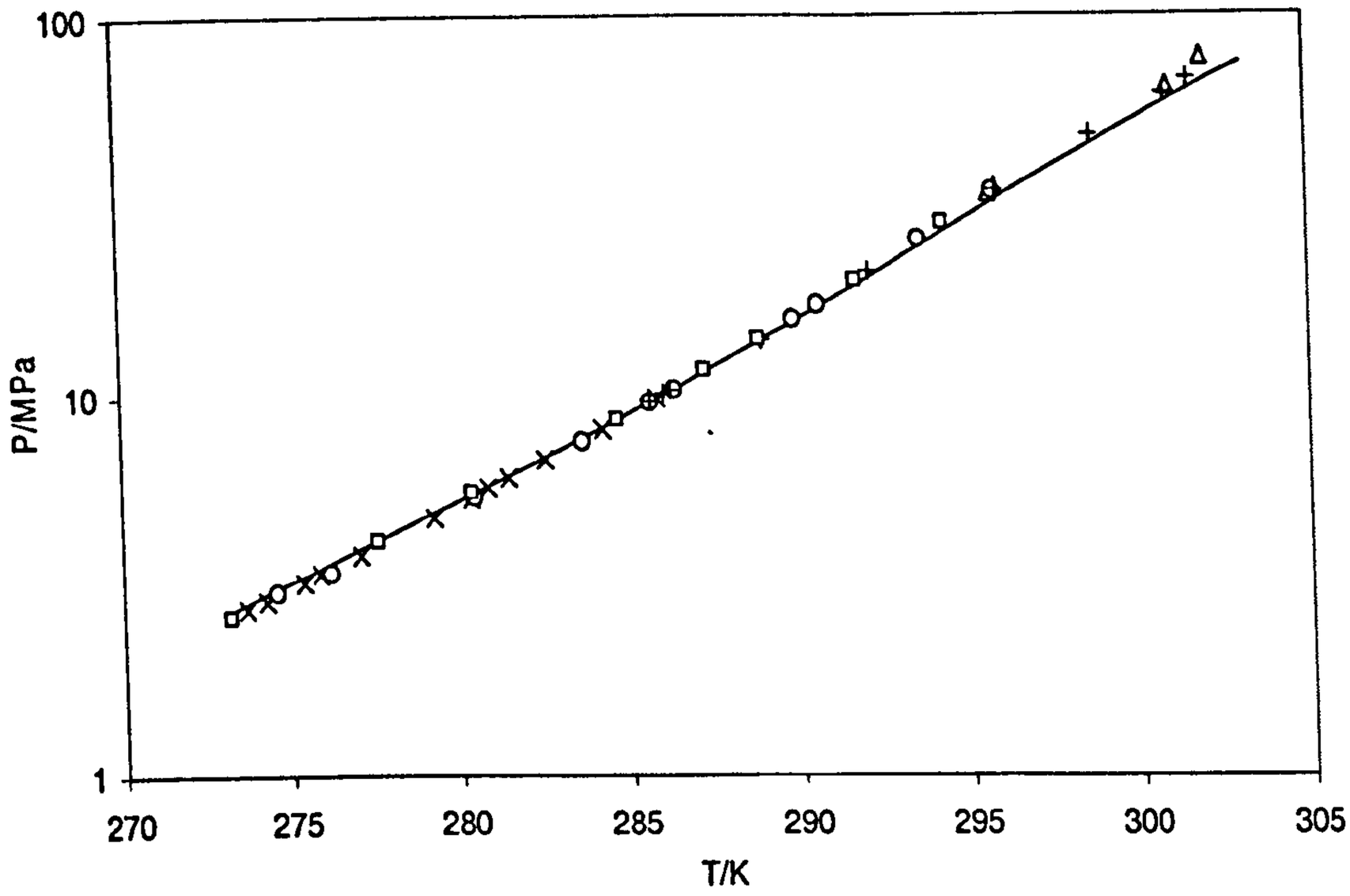

Figure 5.1. Hydrate phase boundary of methane. Experimental data: ×: Deaton and Frost (22); Δ: Kobayashi and Katz (36); +: McLeod and Campbell (37); □: Jhaveri and Robinson (38); ○: Mohammadi et al. (39); Solid curve: Model predictions.

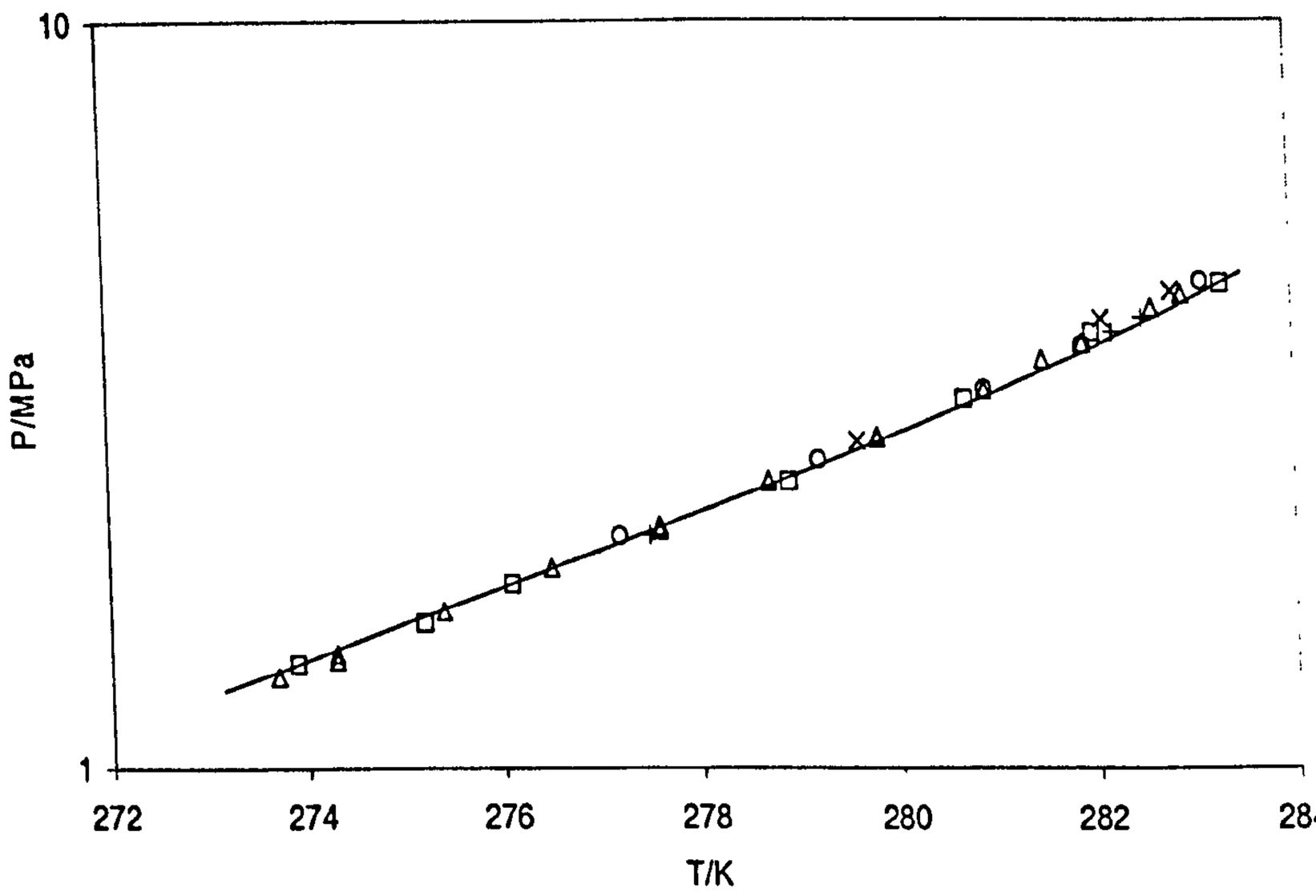

Figure 5.2. Hydrate phase boundary of carbon dioxide. Experimental data: ×: Ng and Robinson (40); Δ: Deaton and Frost (22); +: Mohammadi et al. (39); □: Robinson and Mehta (41); ○: Unruh and Katz (42); Solid curve: Model predictions.

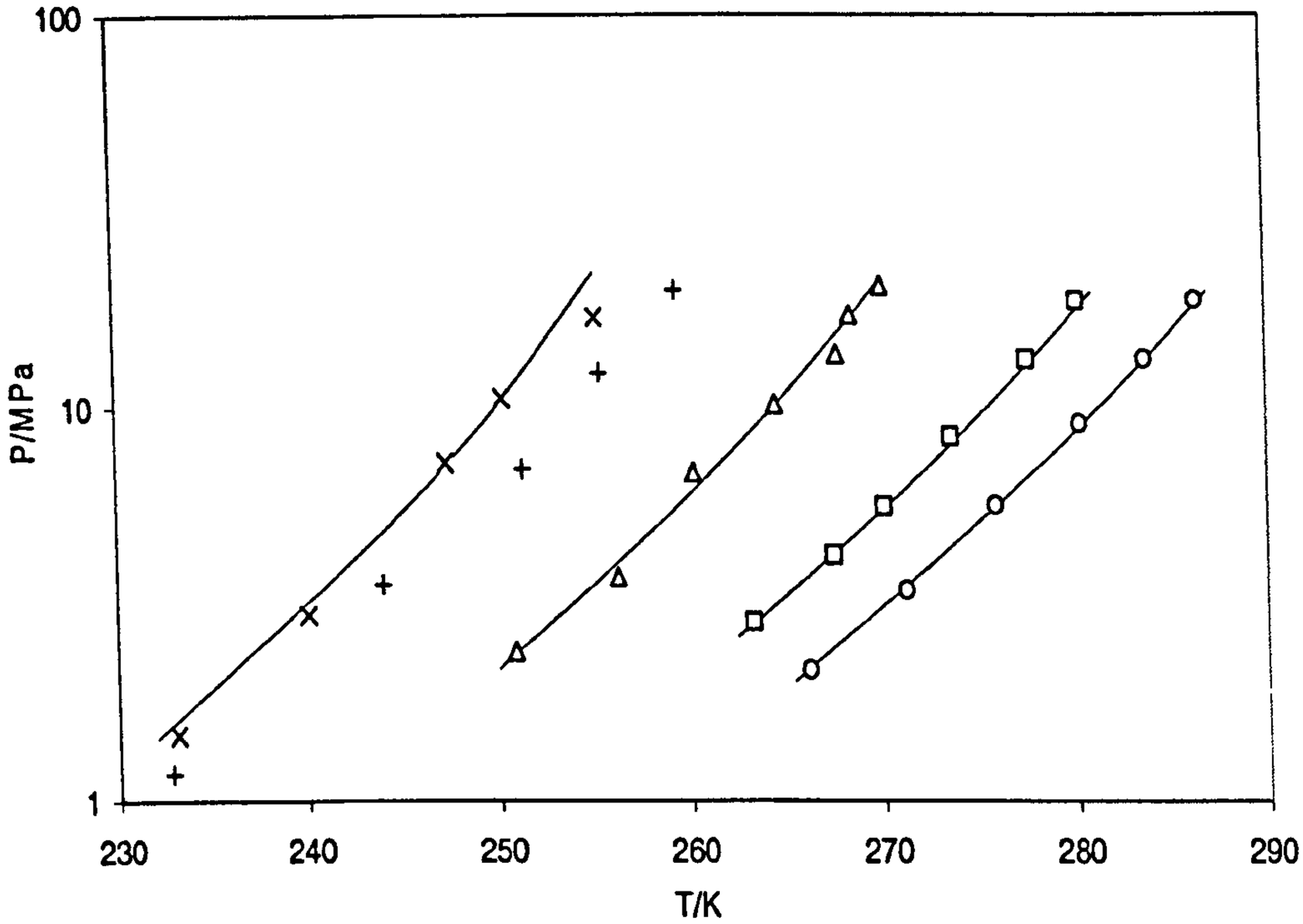

Figure 5.3. Hydrate phase boundary of methane in the presence of methanol aqueous solution. Experimental data: ○: 10 wt.% methanol (40); □: 20 wt.% methanol (40); Δ: 35 wt.% methanol (43); +:50 wt.% methanol (44); ×: 50 wt.% methanol (43); Solid curve: Model predictions.

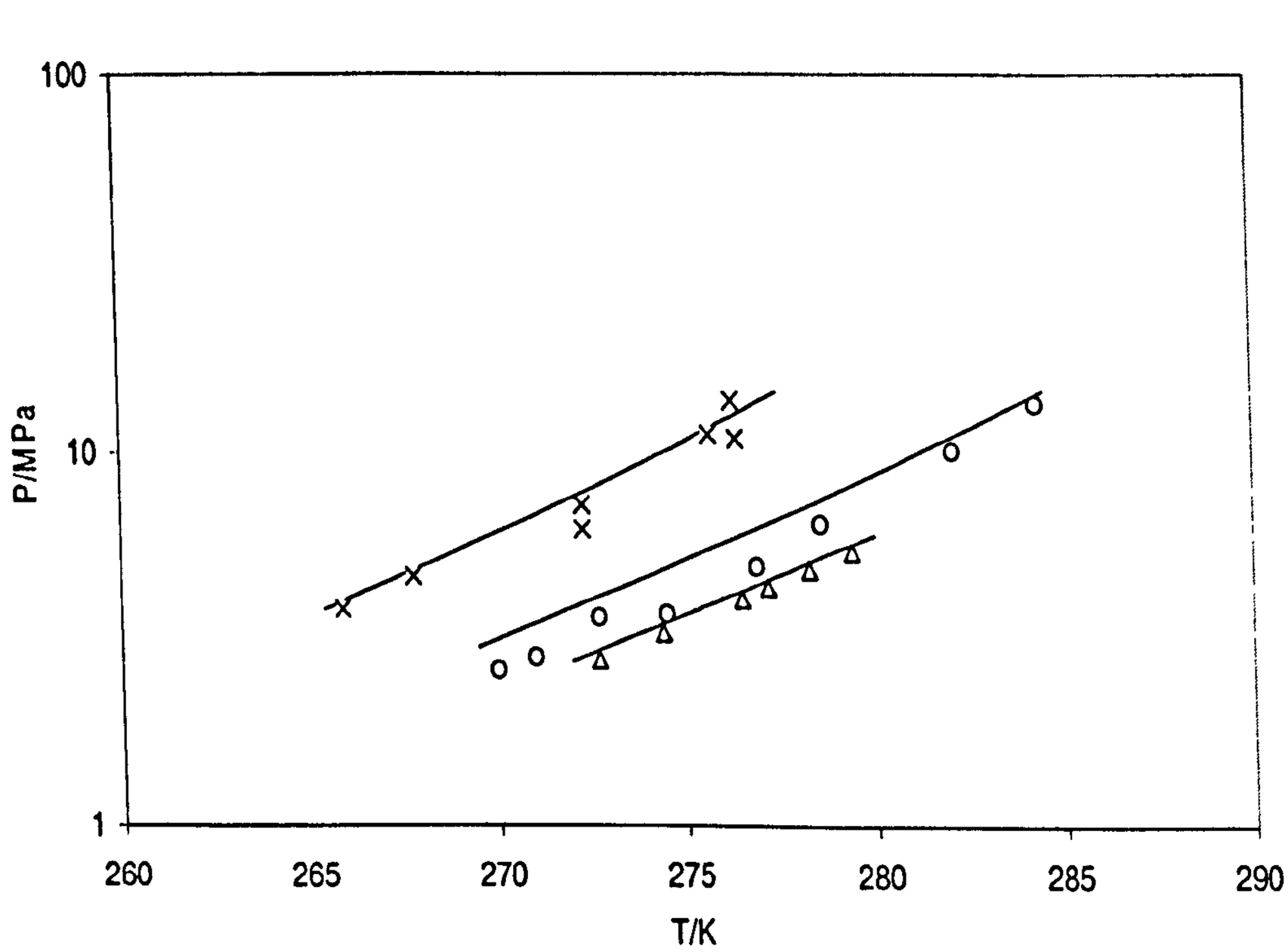

Figure 5.4. Hydrate phase boundary of methane in the presence of NaCl aqueous solution. Experimental data: Δ: 3 wt.% NaCl (45); ○: 10 wt.% NaCl (46); ×: 20 wt.% NaCl (46); Solid curve: Model predictions.

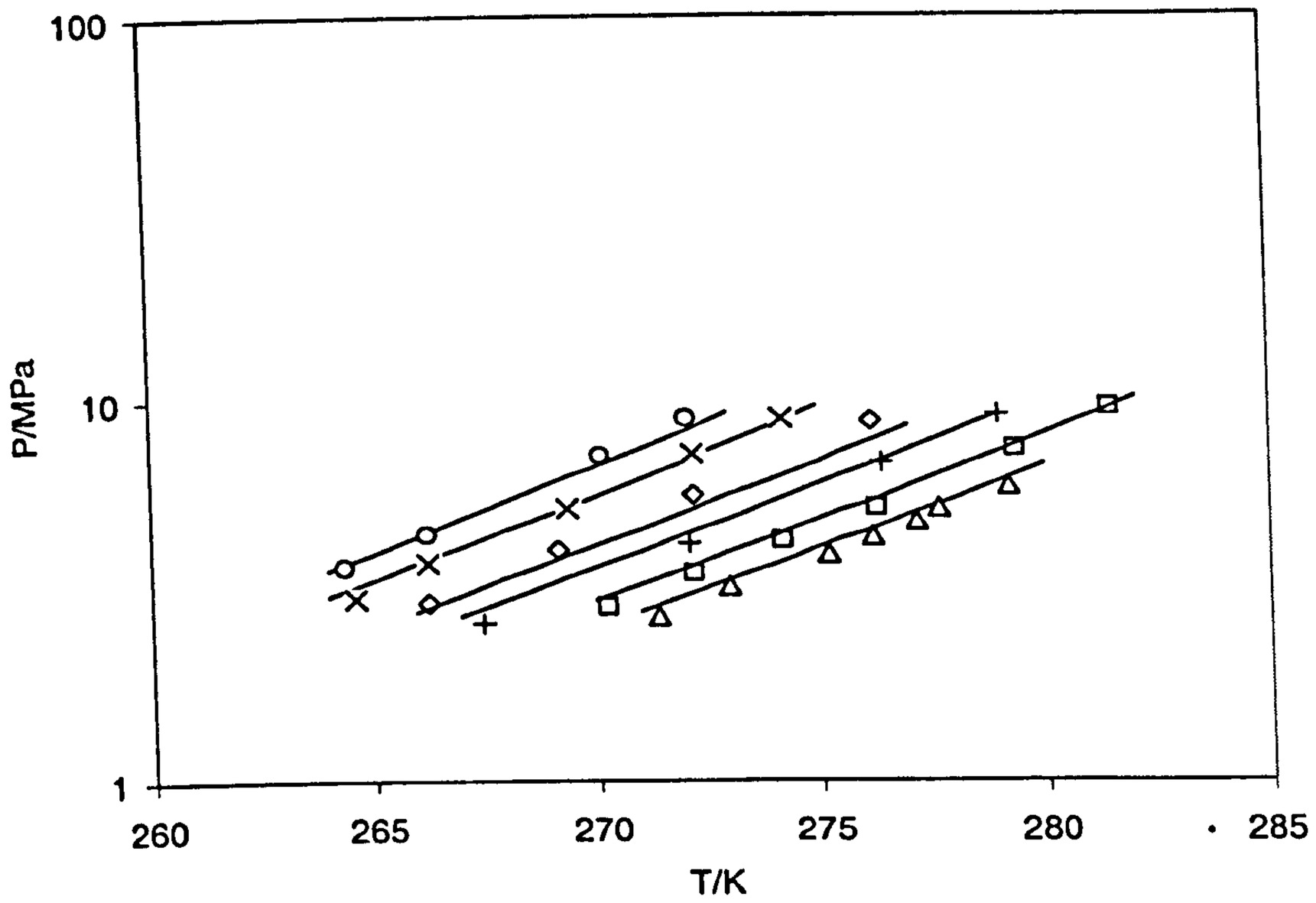

Figure 5.5. Experimental and predicted hydrate dissociation conditions of C_1 (using thermodynamic model) in the presence of aqueous solutions composed of NaCl and KCl (Experimental data from Dholabhai et al. (45), Maximum concentrations of NaCl and KCl are 15 and 15 mass%, respectively).

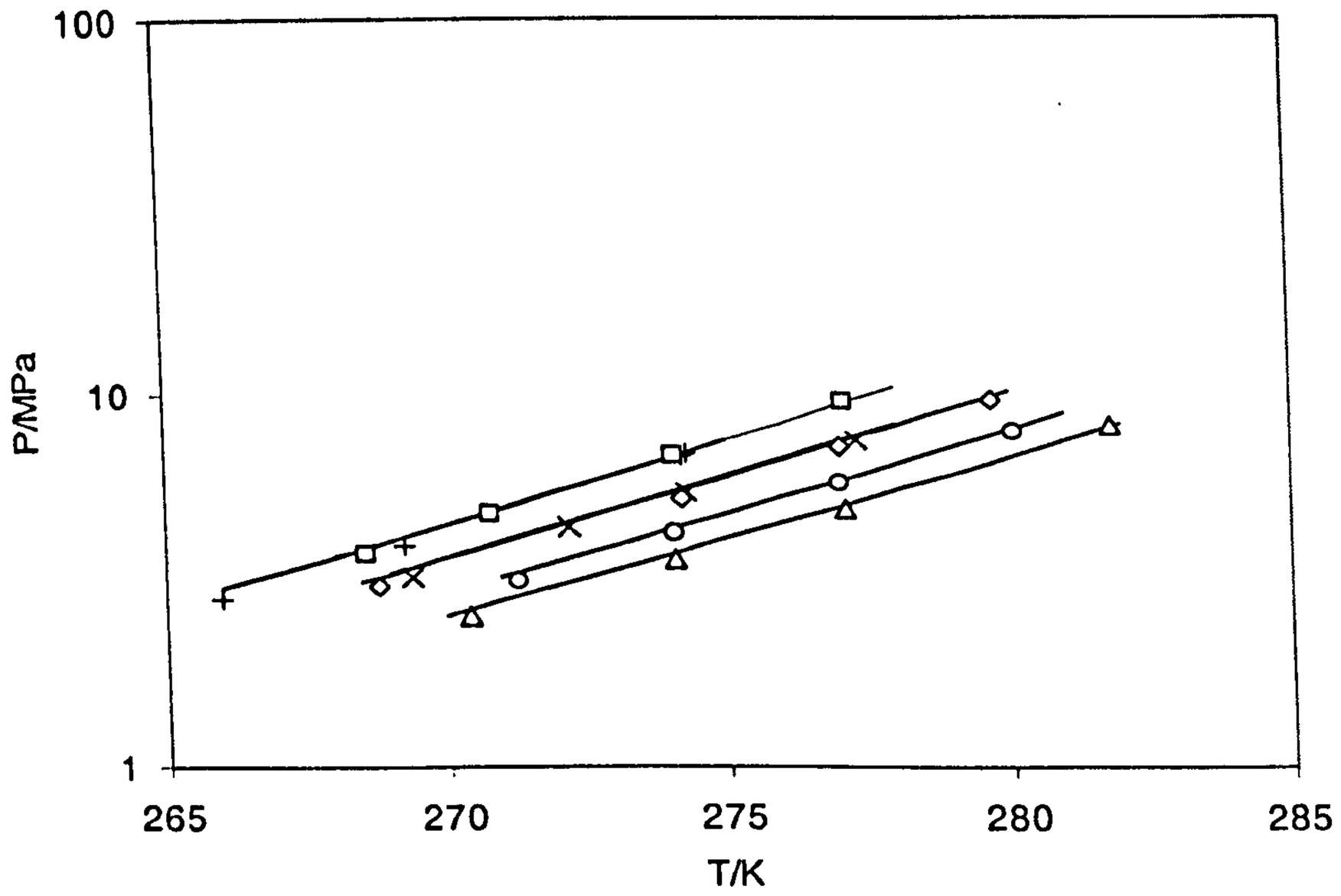

Figure 5.6. Experimental and predicted hydrate dissociation conditions of C_1 (using thermodynamic model) in the presence of aqueous solutions composed of NaCl and $CaCl_2$ (Experimental data from Dholabhai et al. (45), Maximum concentrations of NaCl and $CaCl_2$ are 10 and 10 mass%, respectively).

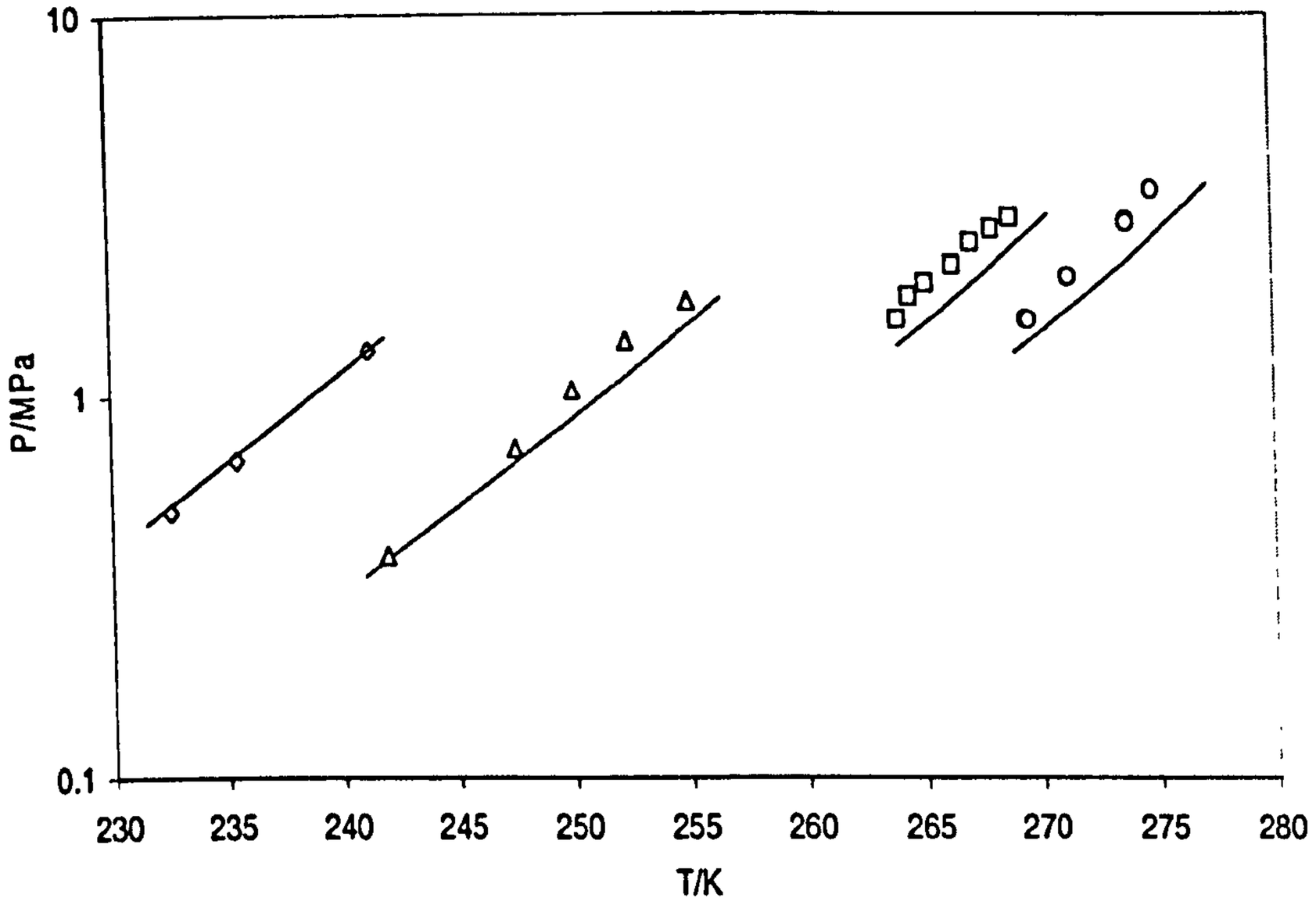

Figure 5.7. Hydrate phase boundary of carbon dioxide in the presence of methanol. Experimental data: ○: 10 wt.% methanol (40); □: 20.02 wt.% methanol (40); Δ: 35 wt.% methanol (43); ◊: 50 wt.% methanol (43); Solid curve: Model predictions.

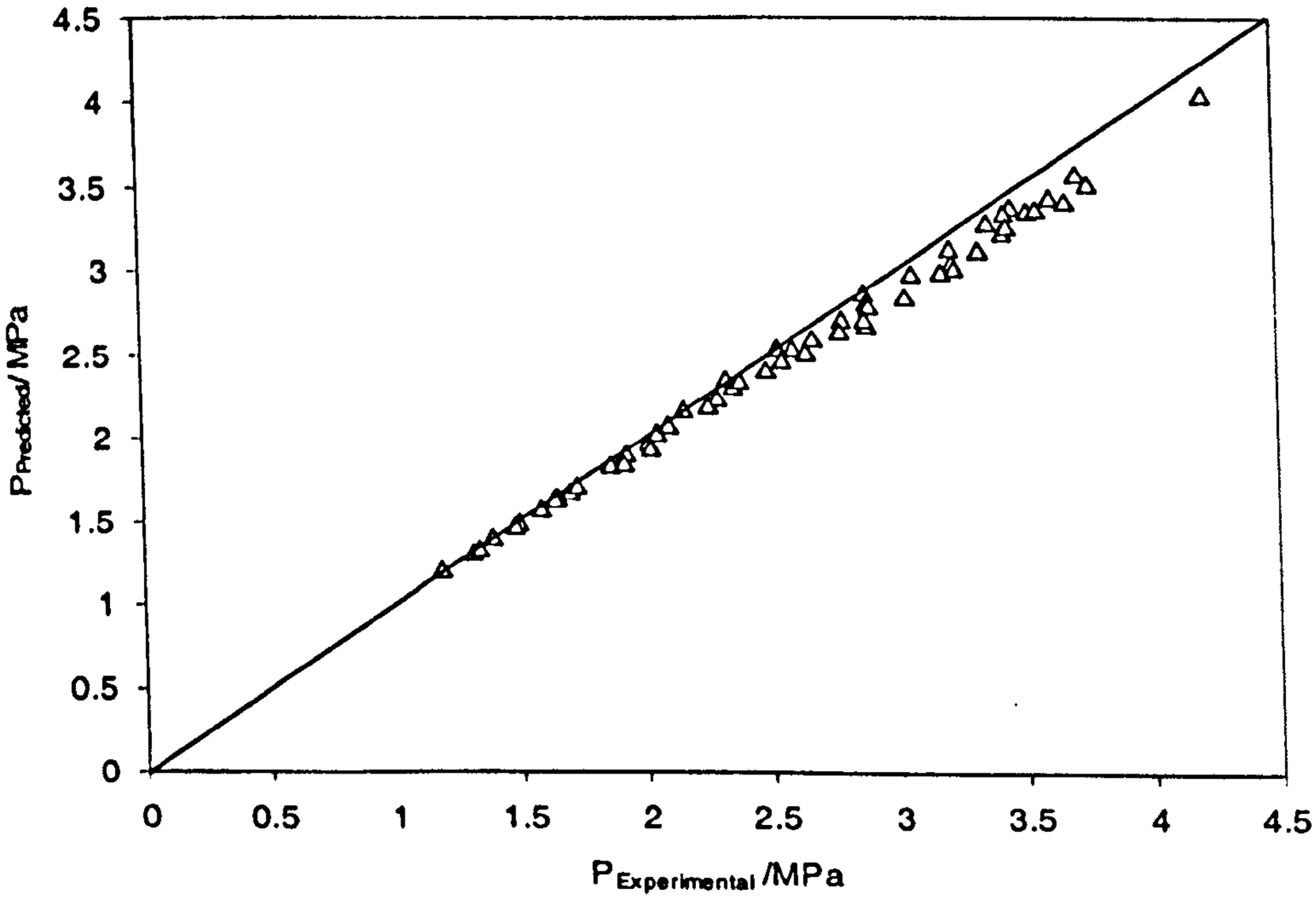

Figure 5.8. Hydrate phase boundary of carbon dioxide in the presence of NaCl. Experimental data: Δ: Vlahakis et al. (47), Maximum concentration of NaCl is 10.59 wt.%; Solid curve: Model predictions.

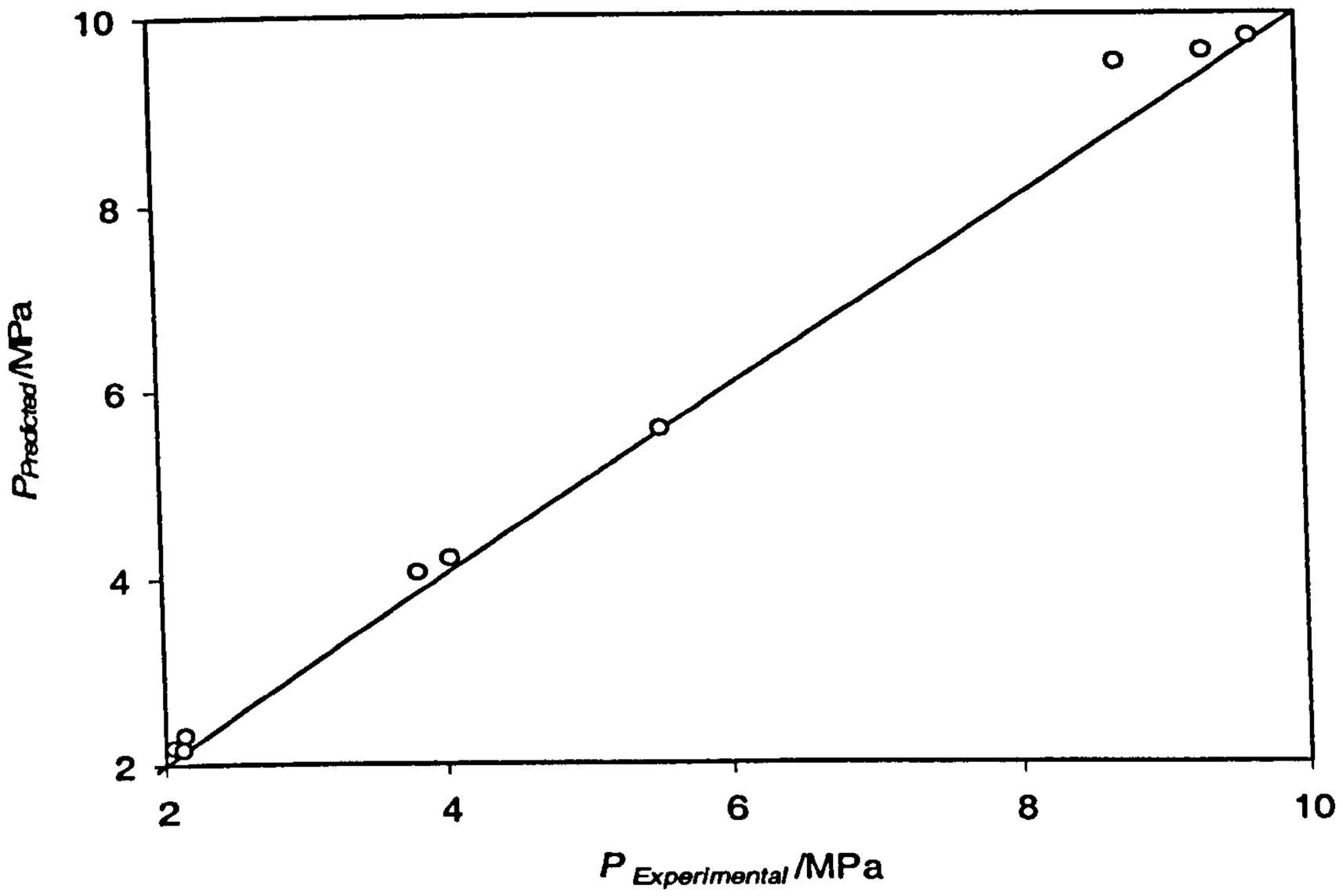

Figure 5.9. Experimental and predicted hydrate dissociation conditions (using thermodynamic model) for a gas mixture containing 80% C_1 and 20% CO_2 in the presence of aqueous solutions composed of methanol and NaCl (Experimental data from Dholabhai et al. (32); Maximum concentrations of NaCl and methanol are 15 and 9.99 mass%, respectively).

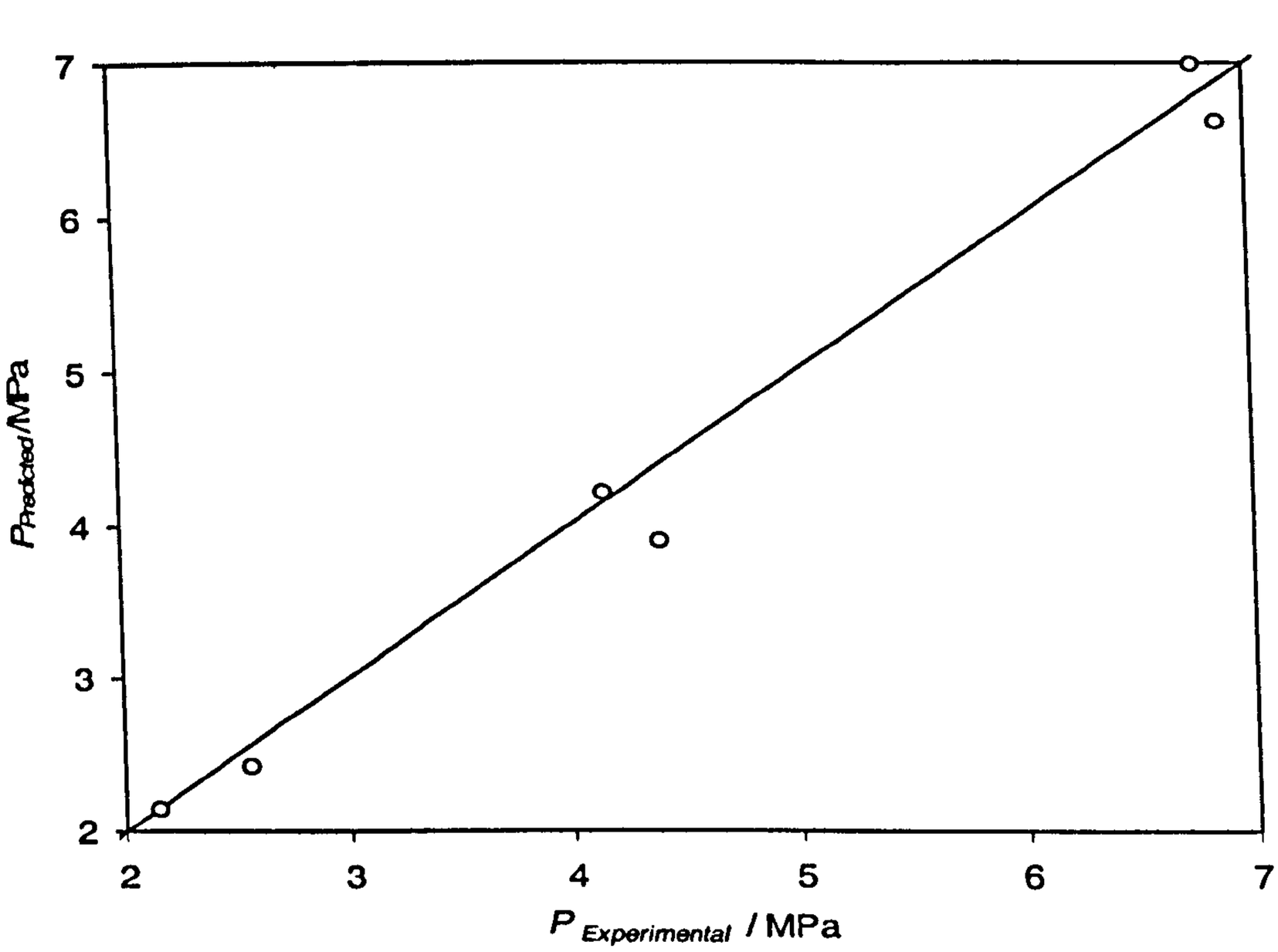

Figure 5.10. Experimental and predicted hydrate dissociation conditions (using thermodynamic model) for a gas mixture containing 50% C_1 and 50% CO_2 in the presence of aqueous solutions composed of methanol and NaCl (Experimental data from Dholabhai et al. (32); Maximum concentrations of NaCl and methanol are 10.07 and 14.99 mass%, respectively).

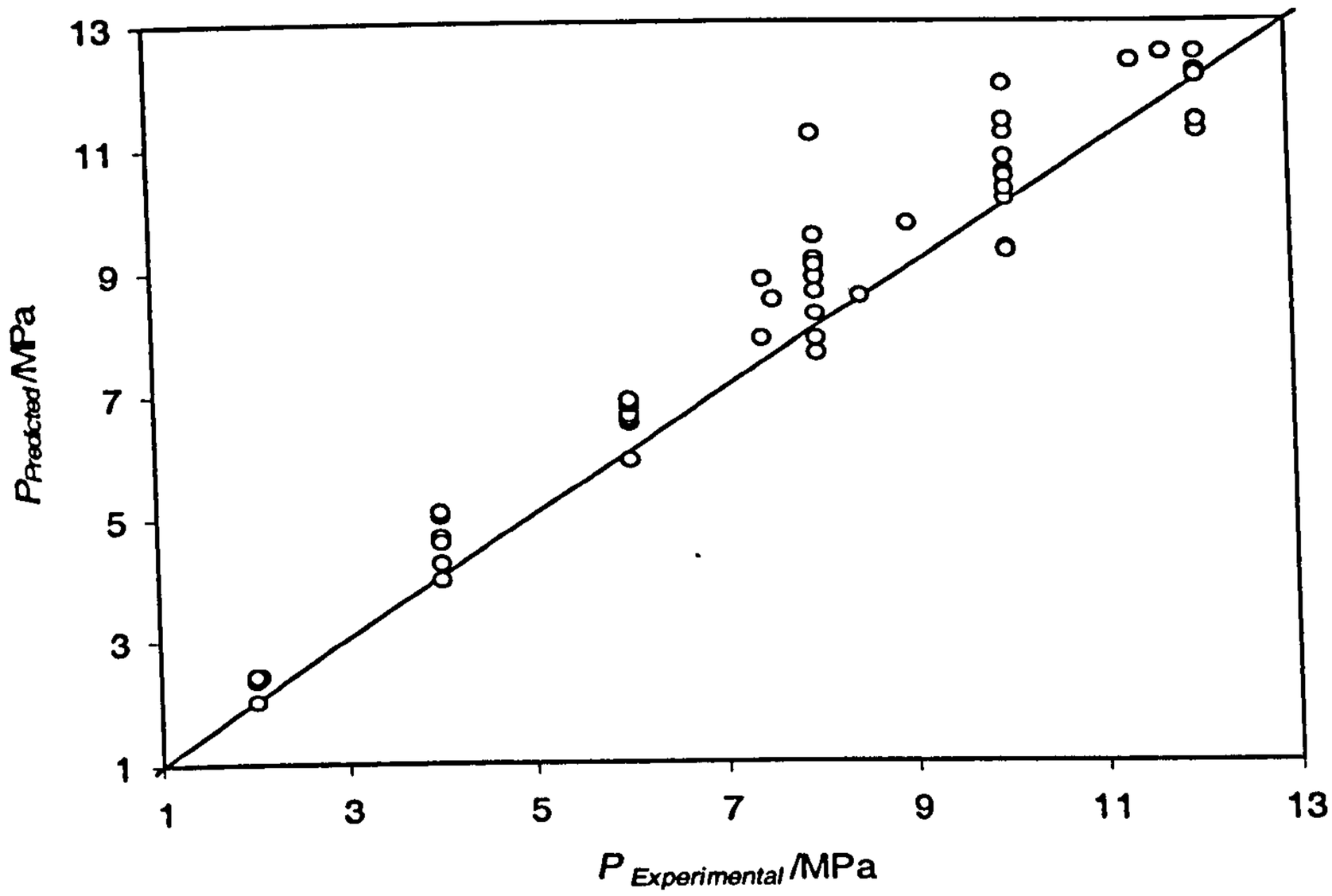

Figure 5.11. Experimental and predicted hydrate dissociation conditions of methane (using thermodynamic model) in the presence of aqueous solutions composed of methanol and NaCl (Experimental data from Jager et al. (5); Maximum concentrations of NaCl and methanol are 11.92 and 40 mass% relative to water, respectively).

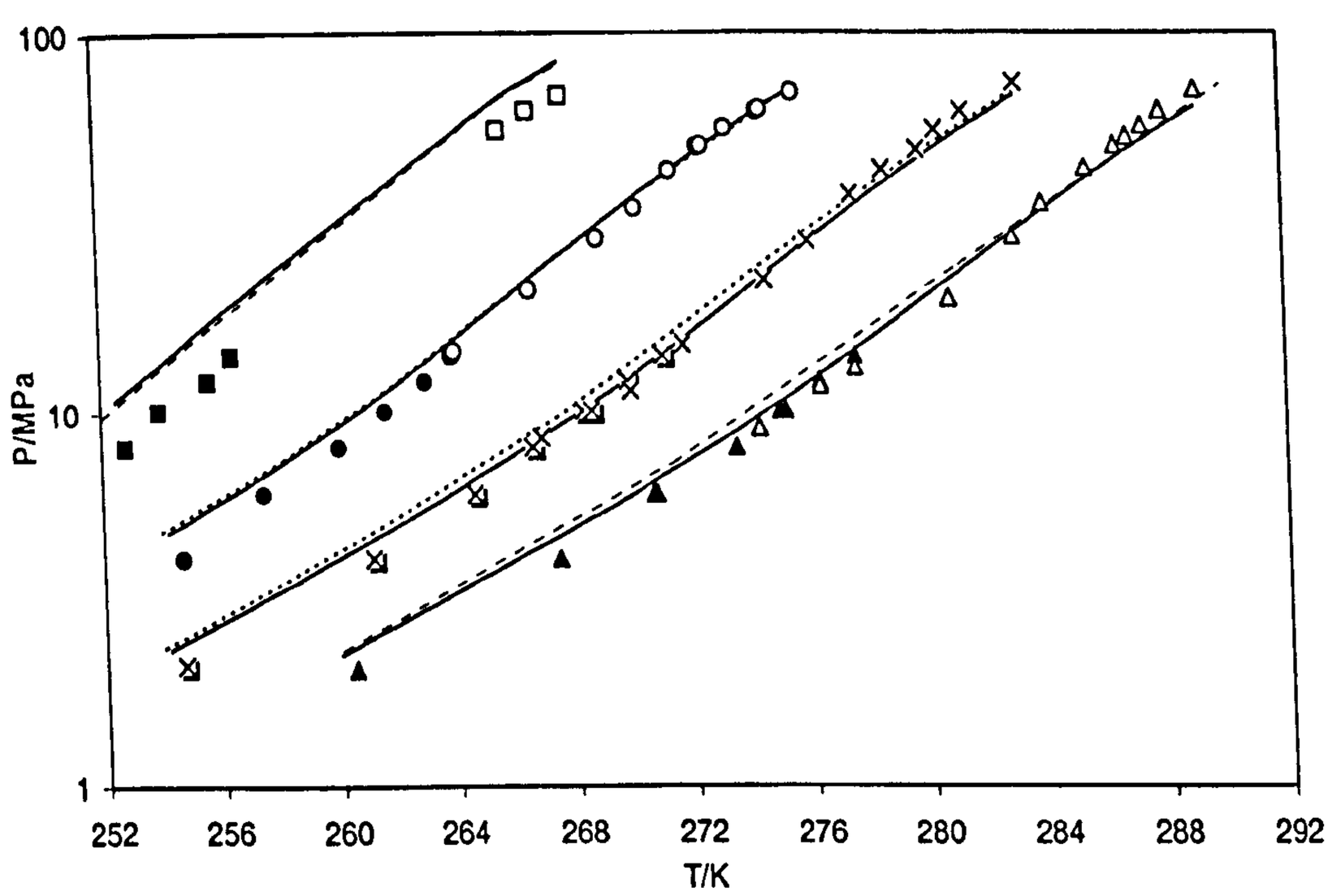

Figure 5.12. Hydrate dissociation conditions of methane in the presence of aqueous solutions composed of methanol and NaCl. Experimental data: Δ: 10 wt.% methanol and 11.92 wt.% NaCl; ×: 20 wt.% methanol and 11.92 wt.% NaCl; ○: 30 wt.% methanol and 11.92 wt.% NaCl; □: 40 wt.% methanol and 11.92 wt.% NaCl (Experimental data from Jager et al. (5); Concentrations are relative to water) Solid curve: Model predictions; Dashed curve: Predictions of *EoS* based model (33); Solid points measured by Cailletet equipment and Hollow points measured by Raman equipment (5).

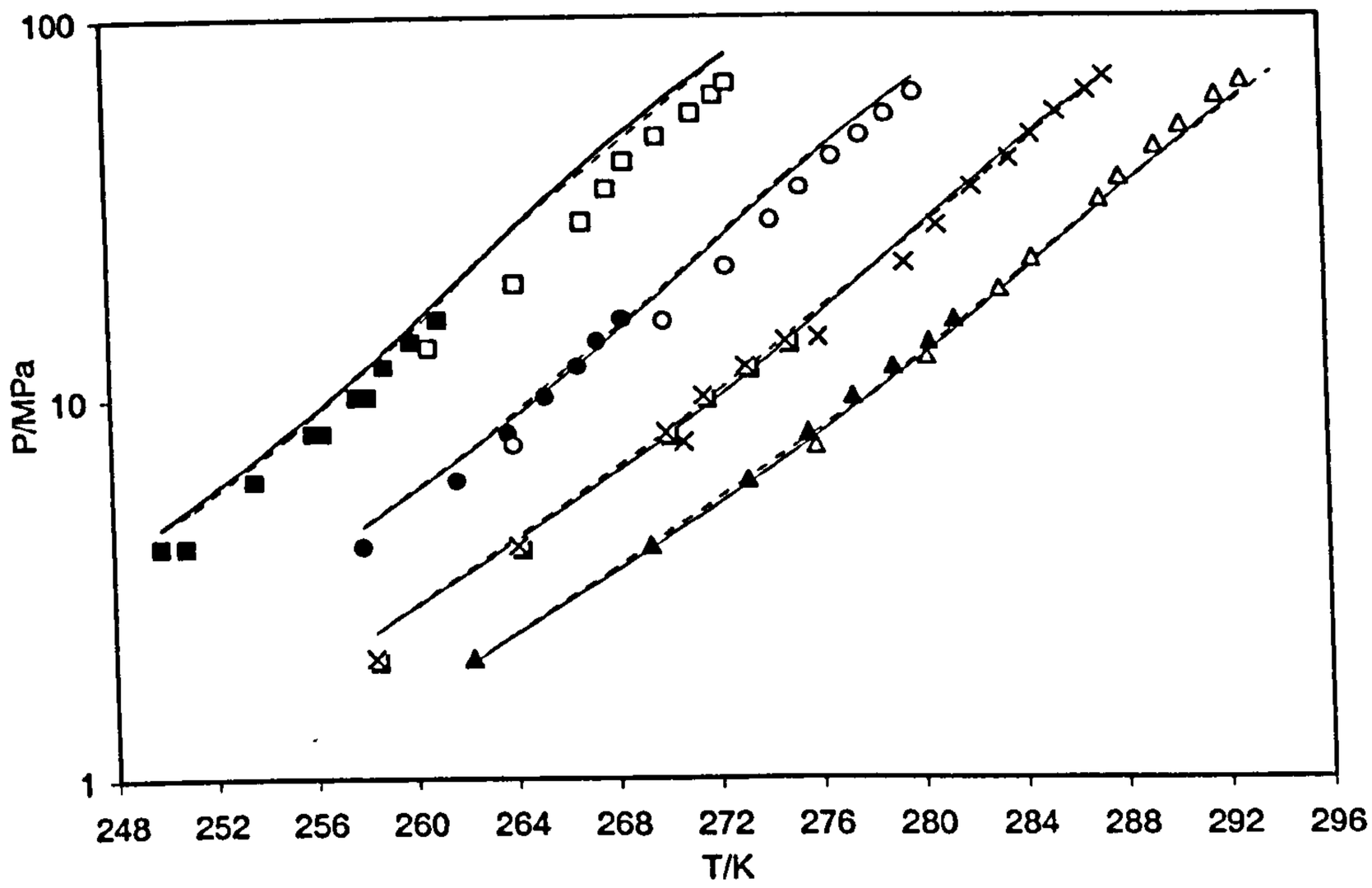

Figure 5.13. Hydrate dissociation conditions of methane in the presence of aqueous solutions composed of methanol and NaCl. Experimental data: Δ: 10 wt.% methanol and 6.22 wt.% NaCl; ×: 20 wt.% methanol and 6.22 wt.% NaCl; ○: 30 wt.% methanol and 6.22 wt.% NaCl; □: 40 wt.% methanol and 6.22 wt.% NaCl (Experimental data from Jager et al. (5); Concentrations are relative to water) Solid curve: Model predictions; Dashed curve: Predictions of *EoS* based model (33); Solid points measured by Cailletet equipment and Hollow points measured by Raman equipment (5).

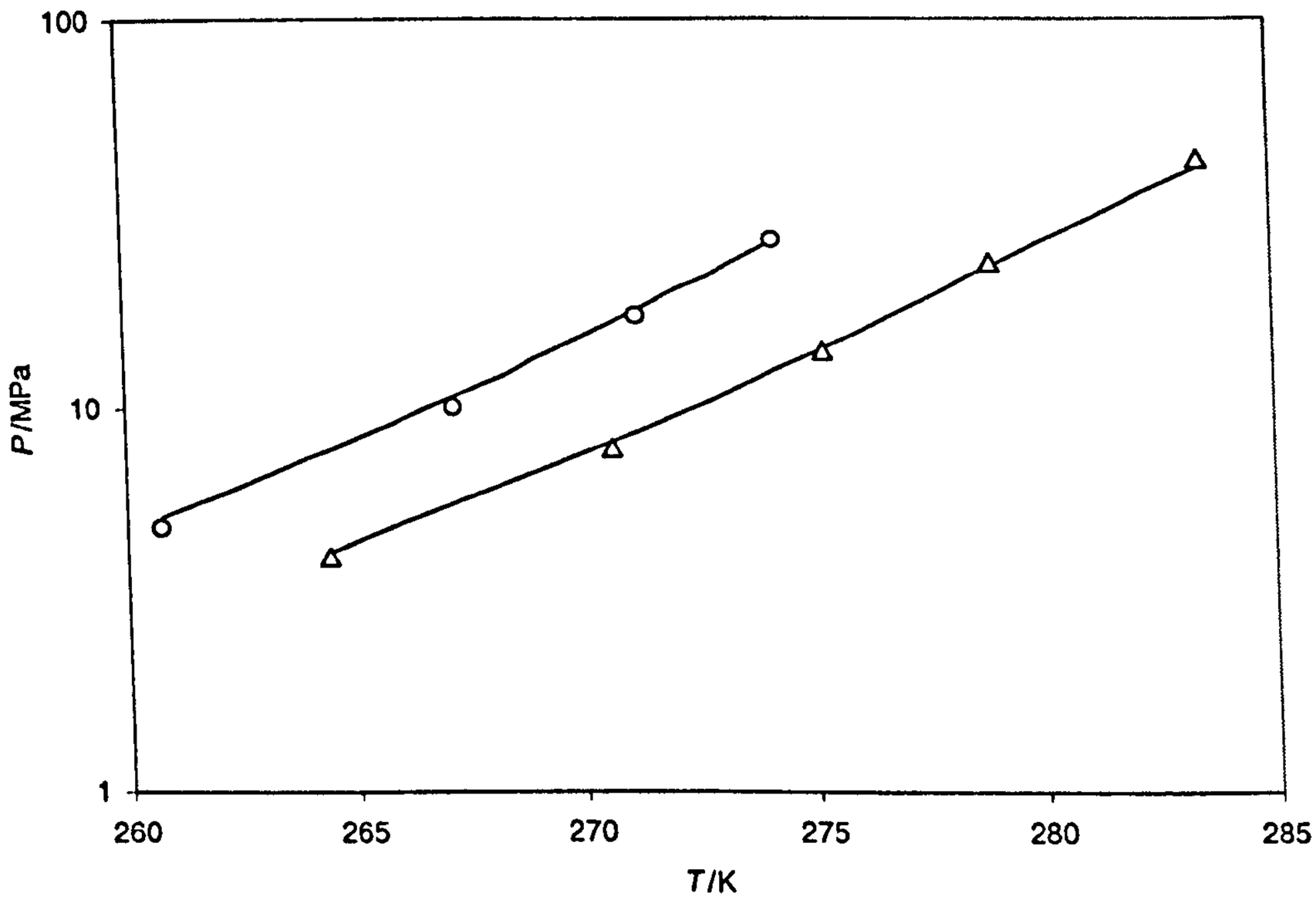

Figure 5.14. Experimental and predicted hydrate dissociation conditions of methane in the presence of aqueous solutions composed of methanol and KCl. Experimental data: Δ: 11.77 mass% KCl + 10.11 mass% methanol; ○: 9.33 mass% KCl + 17.13 mass% methanol (Experimental data from Centre for Gas Hydrate Research, Heriot-Watt University; Concentrations are relative to water) Solid curve: Model predictions.

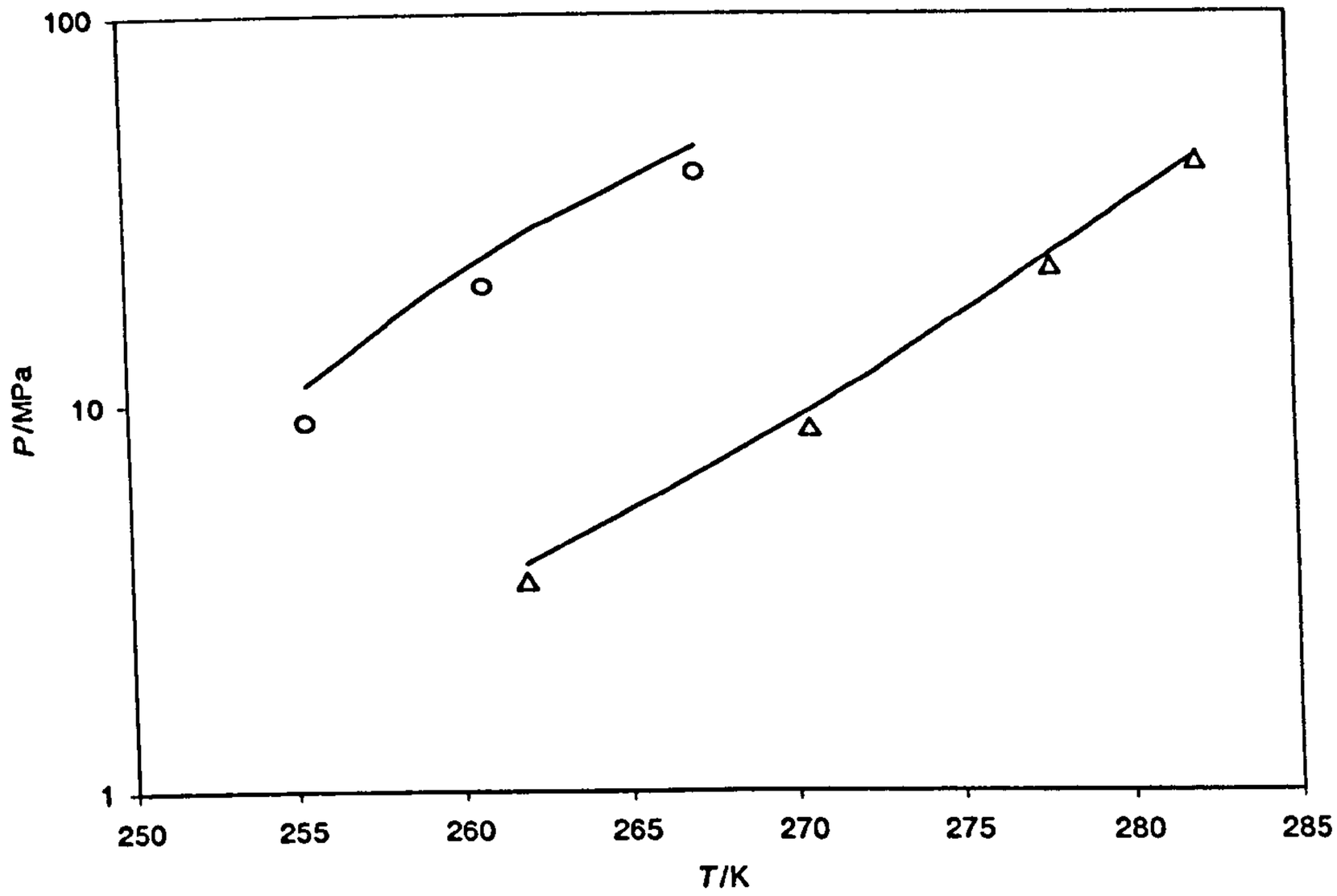

Figure 5.15. Experimental and predicted hydrate dissociation conditions of methane in the presence of aqueous solutions composed of methanol and $CaCl_2$. Experimental data: Δ: 11.8 mass% $CaCl_2$ + 16.7 mass% methanol; ○: 20 mass% $CaCl_2$ + 29.4 mass% methanol (Experimental data from Centre for Gas Hydrate Research, Heriot-Watt University; Concentrations are relative to water) Solid curve: Model predictions.

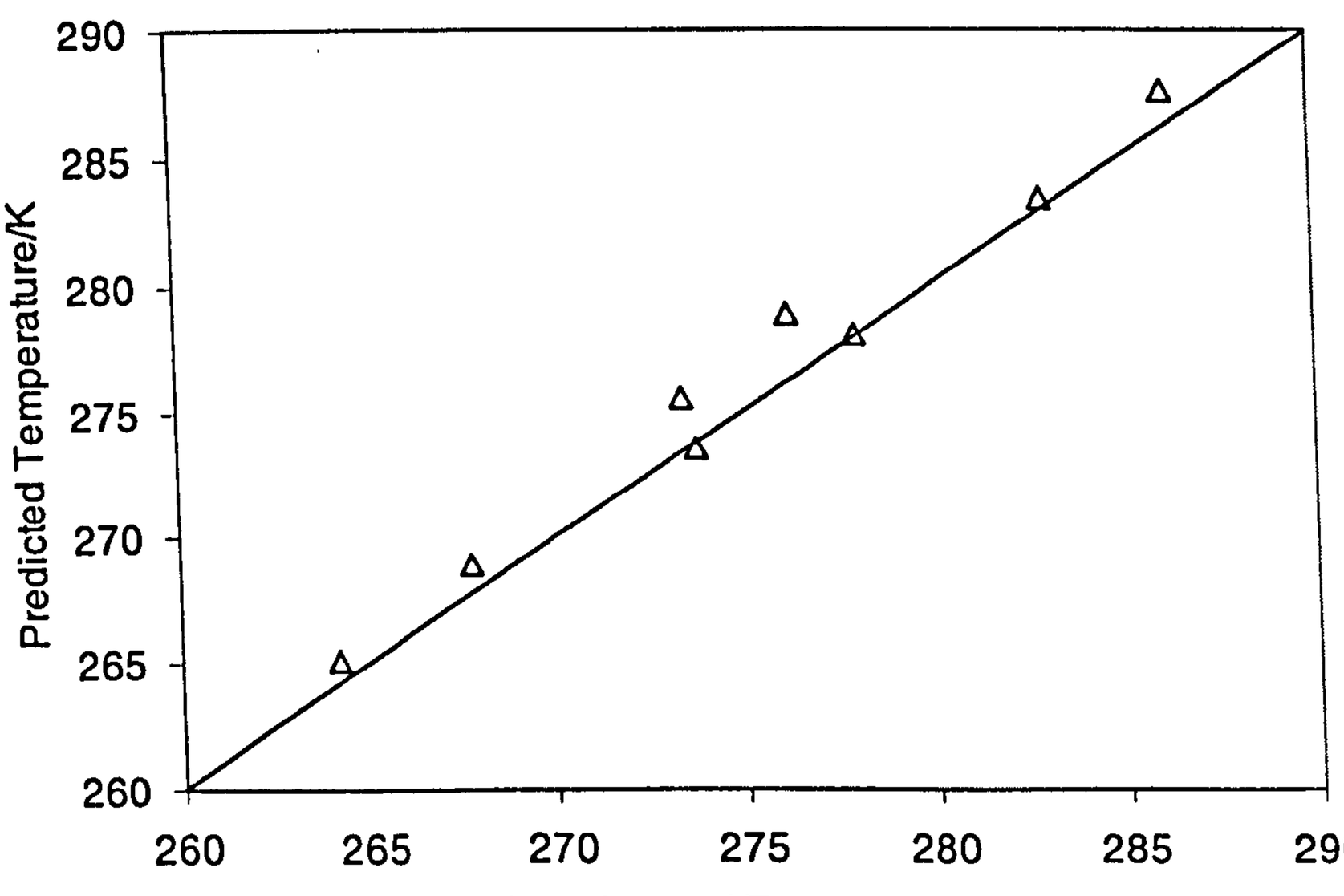

Figure 5.16. Comparison of the predictions of this correlation (equation 5.44) with experimental data (31) for methane hydrate dissociation conditions in the presence of aqueous glycerol solutions.

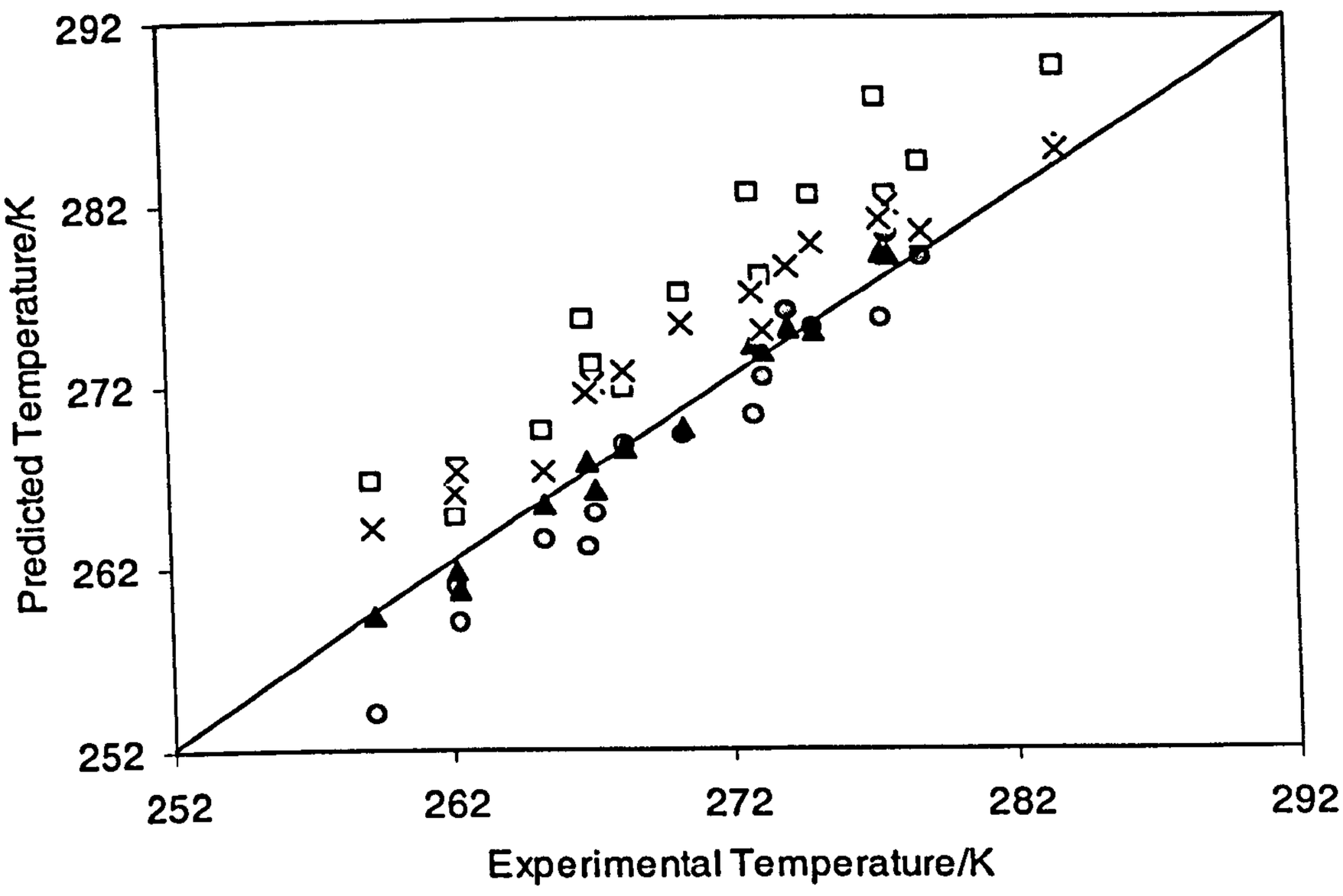

Figure 5.17. Comparison of the predictions of this correlation (equation 5.44) with experimental data (32) for hydrate dissociation conditions of a gas mixture (80 mole% methane and 20 mole% carbon dioxide) in the presence of salt aqueous solutions (Predictions: Gray ○: This correlation; ▲: Masoudi et al. (33); □: Nasrifar and Moshfeghian (4); ×: Javanmardi et al. (35)).

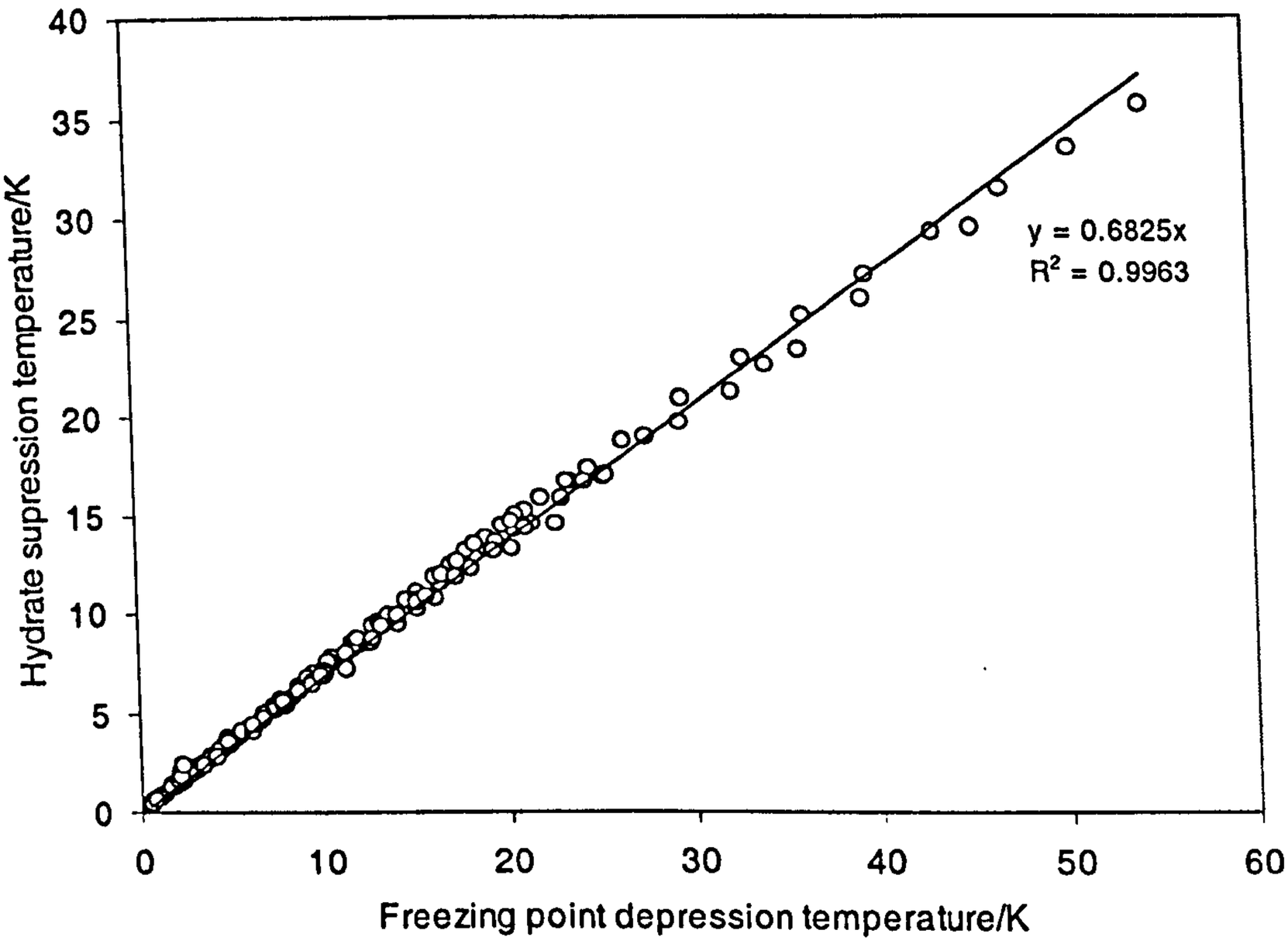

Figure 5.18. The collapse of all data generated by model onto one line suggesting linear relationship between hydrate suppression temperatures and freezing point depression points with a slope of 0.6825, which is good agreement with that mentioned by Sloan (1).

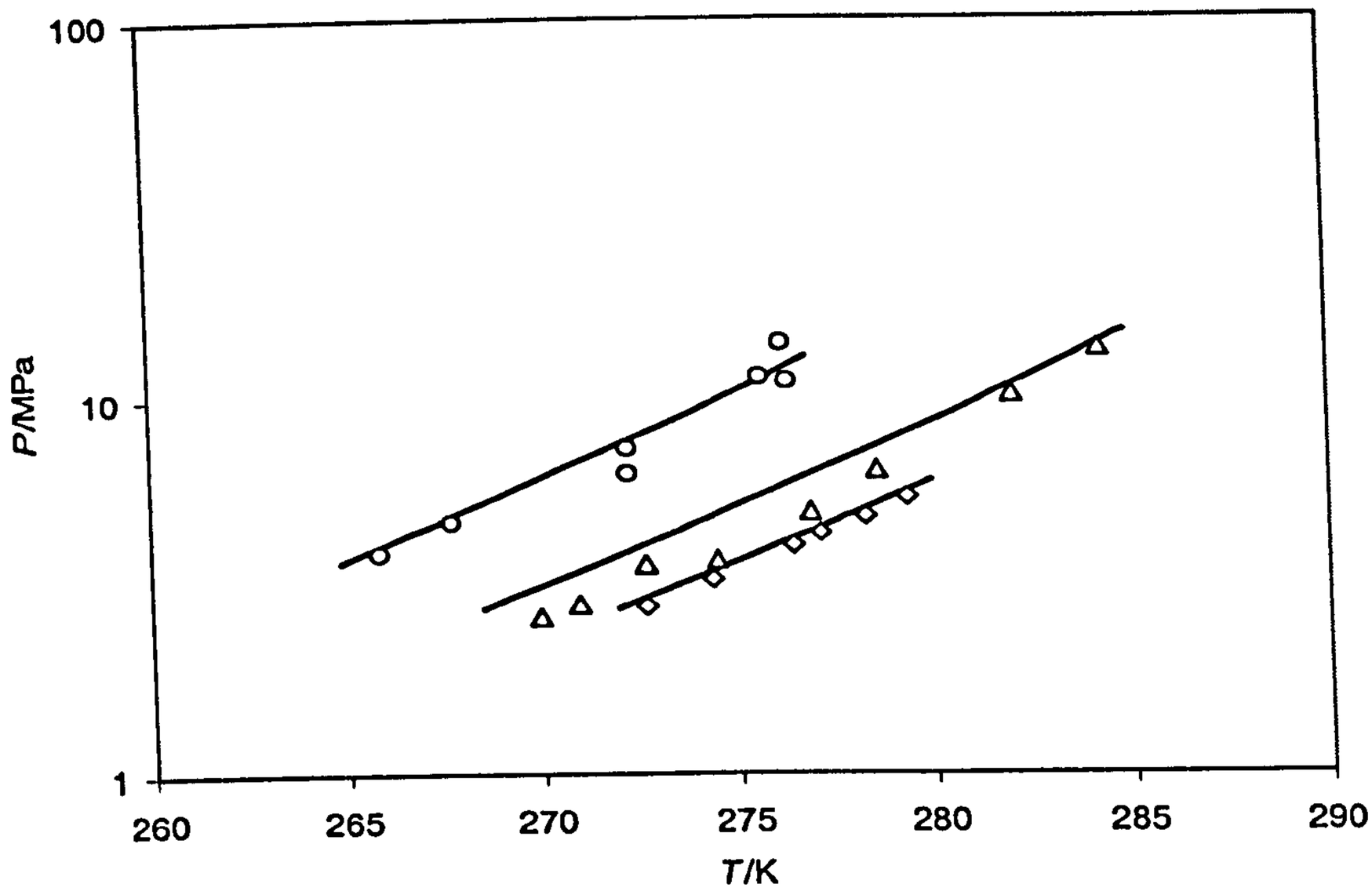

Figure 5.19. Hydrate dissociation conditions of methane in the presence of aqueous solutions composed of NaCl. Experimental data: ◊: 3 wt.% NaCl (45); Δ: 10wt.% NaCl (46); o: 20 wt.% NaCl (46); Solid curve: Predictions using $\Delta T_{hydrate}=0.683\times\Delta T_{ice}$.

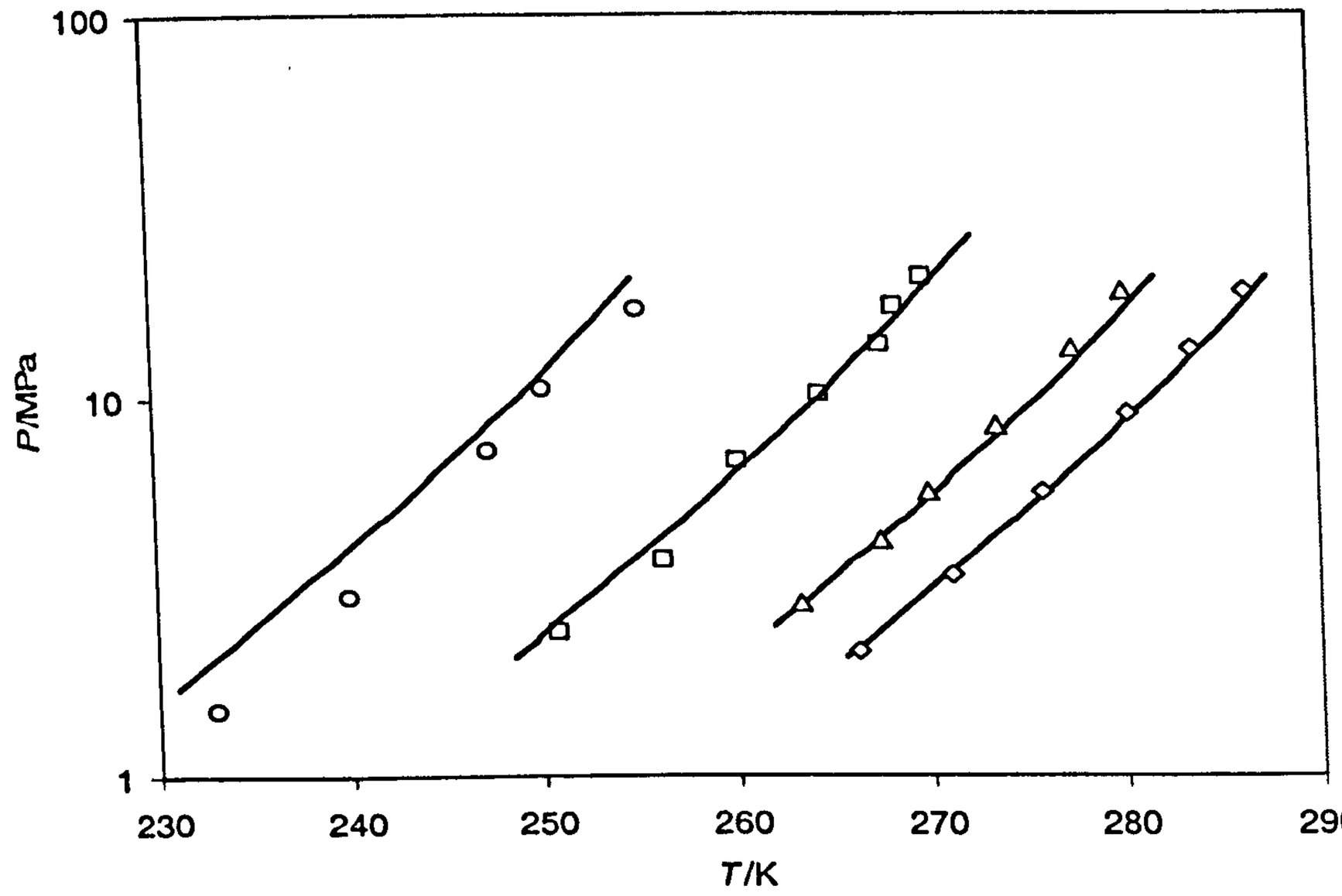

Figure 5.20. Hydrate dissociation conditions of methane in the presence of aqueous solutions composed of methanol. Experimental data: ◊: 10 wt.% methanol (40); Δ: 20wt.% methanol (40); □: 35 wt.% methanol (43); o: 50wt.% methanol (43); Solid curve: Predictions using $\Delta T_{hydrate}=0.683\times\Delta T_{ice}$.

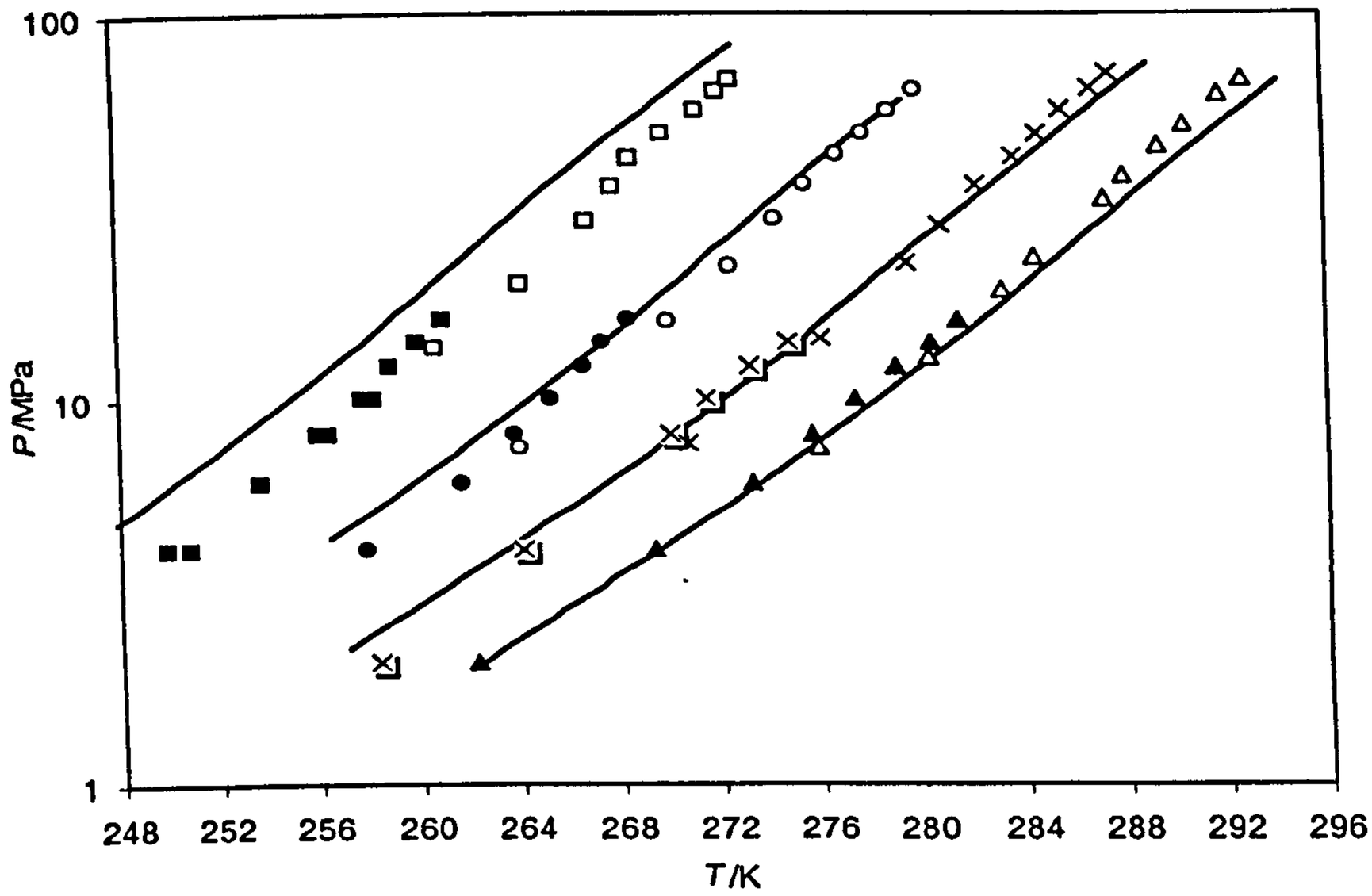

Figure 5.21. Hydrate dissociation conditions of methane in the presence of aqueous solutions composed of methanol and NaCl. Experimental data: Δ: 10 wt.% methanol and 6.22 wt.% NaCl; ×: 20 wt.% methanol and 6.22 wt.% NaCl; ○: 30 wt.% methanol and 6.22 wt.% NaCl; □: 40 wt.% methanol and 6.22 wt.% NaCl (Experimental data from Jager et al. (5); Concentrations are relative to water); Solid curve: Predictions using $\Delta T_{hydrate}=0.683\times\Delta T_{ice}$; Solid points measured by Cailletet equipment and Hollow points measured by Raman equipment (5).

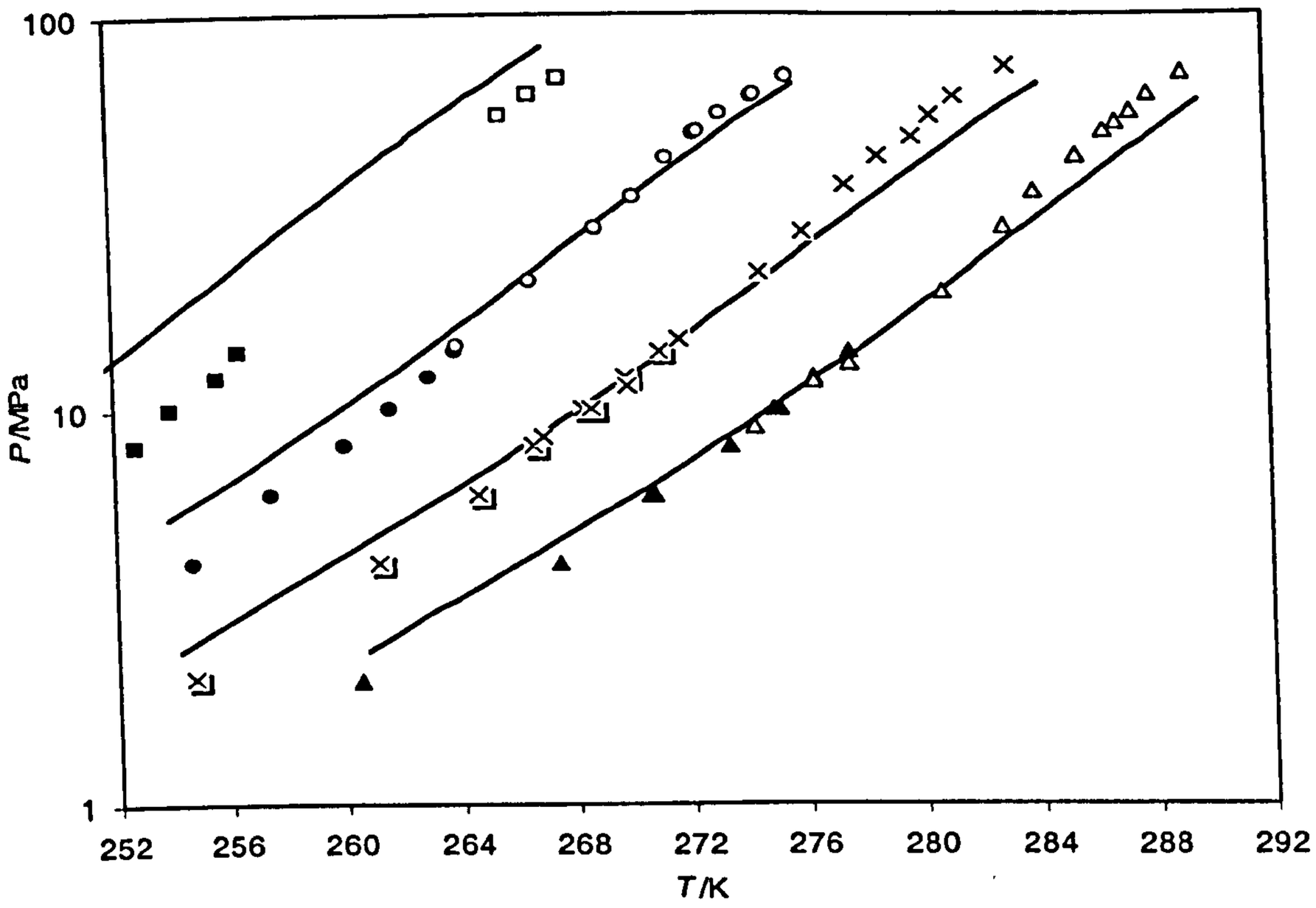

Figure 5.22. Hydrate dissociation conditions of methane in the presence of aqueous solutions composed of methanol and NaCl. Experimental data: Δ: 10 wt.% methanol and 11.92 wt.% NaCl; ×: 20 wt.% methanol and 11.92 wt.% NaCl; ○: 30 wt.% methanol and 11.92 wt.% NaCl; □: 40 wt.% methanol and 11.92 wt.% NaCl (Experimental data from Jager et al. (5); Concentrations are relative to water); Solid curve: Predictions using $\Delta T_{hydrate}=0.683\times\Delta T_{ice}$; Solid points measured by Cailletet equipment and Hollow points measured by Raman equipment (5).

REFERENCES

1. Sloan, E. D. Clathrate Hydrates of Natural Gases. Second Edition, Marcel Dekker, Inc., New York, 1998.

2. Yousif, M. H.; Young, D. B. A Simple Correlation to Predict the Hydrate Point Suppression in Drilling Fluids. *SPE/IADC 25705, The 1993 SPE/IADC Drilling Conference*, Amsterdam, The Netherlands, 1993.

3. Tohidi-Kalorazi, B. Gas hydrate equilibria in the presence of electrolyte solutions; Ph.D. thesis; Heriot-Watt University, 1995 (Also: Tohidi, B.; Danesh, A.; Todd, A. C. Modelling Single and Mixed Electrolyte Solutions and Its Applications to Gas Hydrates. *Chemical Engineering Research & Design* 1995, *73(A4)*, 464-472 & Mohammadi A.H.; Tohidi B. Prediction of Hydrate Phase Equilibria in Aqueous Solutions of Salt and Organic Inhibitor Using a Combined Equation of State and Activity Coefficient based Model. *Can J. Chem Eng*. October 2005, *83*, 865-871).

4. Nasrifar, Kh.; Moshfeghian, M.; Maddox, R.N. Prediction of Equilibrium Conditions for Gas Hydrate Formation in the Mixture of Both Electrolytes and Alcohols. *Fluid Phase Equilibria* 1998, *146*, 1-13.

5. Jager, M. D.; Peters, C. J.; Sloan, E. D. Experimental determination of methane hydrate stability in methanol and electrolyte solutions. *Fluid Phase Equilibria* 2002, *193*, 17-28.

6. Valderrama, J. O. A generalized Patel-Teja equation of state for polar and non-polar fluids and their mixtures. *J. Chem. Engng Japan* 1990, *23*, 87-91.

7. Avlonitis, D.; Danesh, A.; Todd, A. C. Prediction of VL and VLL equilibria of mixtures containing petroleum reservoir fluids and methanol with a cubic EoS. *Fluid Phase Equilibria* 1994, *94*, 181-216.

8. Aasberg-Petersen, K.; Stenby, E.; Fredenslund, Aa. Prediction of High-Pressure Gas Solubilities in Aqueous Mixtures of Electrolytes. *Ind. Eng. Chem. Res.* 1991, *30(9)*, 2180-2185.

9. van der Waals, J. H.; Platteeuw, J. C. Clathrate solutions. *Adv. Chem. Phys.* 1959, *2*, 1-57.

10. Nielsen, R. B.; Bucklin, R. W. Why not use methanol for hydrate control? *Hydrocarbon Processing* 1983, *62(4)*, 71-78.

11. Hammerschmidt, E. G. Gas Hydrate Formations, A Further Study On Their Prevention and Elimination from Natural Gas Pipe Lines. *Gas*, 1939, *15(5)*, 30-34.

12. Carroll, J. J. Natural Gas Hydrates: A Guide for Engineers. Gulf Professional Publishing, 2003.

13. Townsend, F. M.; Reid L. S. Hydrate Control in Natural Gas Systems. Laurance Reid Associates, Inc., P.O. Box 1188, Norman, OK 73070, 1978 (Quoted in ref.1).

14. Pieroen, A. P. Gas Hydrates - Approximate Relations Between Heat of Formation, Composition and Equilibrium Temperature Lowering by Inhibitors. *Recueil des Travaux Chimiques des Pays Bas* 1955, *74*, 995-1002.

15. Yamanlar, S.; Poettmann, F. H.; Sloan, E. D. Control Hydrate Formation. *Hydrocarbon Processing* 1991, *70(9)*, 155-161.

16. Nixdorf, J.; Oellrich, L. Examination of natural gas hydrates formation and its prevention under gas storage conditions. *2nd Intnl. Conf. on Natural Gas Hydrates*, 17-25, Toulouse, 2-6 June 1996 (Quoted in ref. 1).

17. Pedersen, K. S.; Fredenslund, A.; Thomassen, P. Properties of Oils and Natural Gases. Houston, TX, Gulf Publishing, 1989.

18. Arnold, K.; Stewart, M. Surface Production Operations, Vol. 2: Design of Gas-Handling Systems and Facilities, Houston, TX, Gulf Publishing, 1989.

19. GPSA Engineering Data Book; 11th ed. Tulsa, OK, 1998.

20. McCain, W. D. The Properties of Petroleum Fluids, second edition, Pennwell Publishing, Tulsa, OK, 1990.

21. McCain, W. D. Reservoir-Fluid Property Correlations-State of the Art, *SPE Reservoir Engineering*, 266-272, May 1991.

22. Deaton, W. M.; Frost, E. M. Gas Hydrates and Their Relation to the Operation of Natural Gas Pipe Lines. U.S. Bureau of Mines Monograph. 1946, *8*, 101.

23. Ouar, H.; Cha, S. B.; Wildeman, T. R.; Sloan, E. D. *Trans. I. Chem. E.*, 1992, *70(A)*, 48 (Quoted in ref.1).

24. Østergaard, K. K.; Tohidi, B.; Danesh, A.; Todd, A. C. Gas Hydrates and Offshore Drilling: Predicting the Hydrate Free Zone. *Annals of New York Academy of Sciences* 2000, *912*, 411- 419.

25. Østergaard, K. K. Gas hydrate stability in the petroleum industry and its application in gas-liquid separation. PhD Thesis, Heriot-Watt University, Edinburgh, UK, February 2000.

26. Austvik, T.; Hustvedt, E.; Meland, B.; Berge, L. I.; Lysne, D. Tommeliten Gamma Field Hydrate Experiments. *7th International Conference on Multiphase Production (Multiphase 95)*, Cannes, France, 1995.

27. Yousif, M.; Austvik, T.; Berge, L.; Lysne, D. The effects of low concentration methanol solutions on hydrate formation. *Proceedings 2nd International Conference on Natural Gas Hydrates*, Toulouse, France, 2-6 June 1996.

28. Gjertsen, L.; Austvik, T.; Urdahl, O. Hydrate Plugging in Underinhibited Systems. *The 2nd International Conference on Natural Gas Hydrates*, Toulouse, France, 2-6 June 1996.

29. Østergaard, K. K.; Tohidi, B.; Danesh, A.; Todd, A. C.; Burgass, R. W. A General Correlation for Predicting the Hydrate-Free Zone of Reservoir Fluids. *SPE Prod. & Facilities* 2000, *15(4)*, 228- 233.

30. Makagon, Y. F. Hydrates of Natural Gas, Moscow, Nedra, Izadatelstro, p. 208, 1974 (in Russian) Translated from Russian by W. J. Cieslesicz, PennWell Books, Tulsa, Oklahoma, p. 237 in Russian, 1981 (in English) (Quoted in ref. 1).

31. Franks, F. (Ed.) Water, a Comprehensive Treatise. Vol. 2, Chap. 7, Plenum Press, New York, 1973.

31. Ng, H.-J.; Robinson, D. B. New Developments in the Measurement and Prediction of Hydrate Formation For Processing Needs. *Annals of the New York Academy of Sciences* 1994, *715*, 450-462.

32. Dolabhai, P. D.; Parent, J. S.; Bishnoi, P. R. Equilibrium conditions for hydrate formation from binary mixtures of methane and carbon dioxide in the presence of electrolytes, methanol and ethylene glycol. *Fluid Phase Equilibria* 1997, *141*, 235-246. Also: Dholabhai, P. D.; Bishnoi, P. R. Hydrate Equilibrium Conditions in Aqueous-Electrolyte Solutions - Mixtures of Methane and Carbon-Dioxide. *Journal of Chemical and Engineering Data* 1994, *39(1)*, 191-194.

33. Masoudi, R.; Tohidi, B.; Anderson, R.; Burgass, R. W.; Yang, J. Experimental measurement and thermodynamic modelling of clathrate hydrate equilibria and salt solubility in aqueous ethylene glycol and electrolyte solutions. *Fluid Phase Equilibria* 2004, *219*, 157–163.

34. Nasrifar, K.; Moshfeghian, M. A model for prediction of gas hydrate formation conditions in aqueous solutions containing electrolytes and/or alcohol. *J. Chem. Thermodyn.* 2001, *33*, 999–1014.

35. Javanmardi, J.; Moshfeghian, M.; Maddox, R. N. Application and Extension of Aasberg-Petersen Model for Prediction of Gas Hydrate Formation Conditions in Mixture of Aqueous Electrolyte Solutions and Alcohol. *Can. J. Chem. Eng.* 2001, *79*, 367–373.

36. Kobayashi, R.; Katz, D. L. Methane hydrate at high pressure. *Petroleum Transactions, AIME* 1949, *186*, 66-70.

37. McLeod, H. O.; Campbell, J. M. Natural Gas Hydrates at Pressures to 10,000 psia. *J. Pet. Tech.* June 1961, 590-594.

38. Jhaveri, J.; Robinson, D. B. Hydrates in the Methane-Nitrogen System. *Can. J. Chem. Eng.* 1965, *43*, 75-78.

39. Mohammadi, A. H.; Anderson, R.; Tohidi, B. Carbon Monoxide Clathrate Hydrates: Equilibrium Data and Thermodynamic Modeling. *AIChE J.* 2005, *51(10)*, 2825-2833.

40. Ng, H.-J.; Robinson, D. B. Hydrate Formation in Systems Containing Methane, Ethane, Propane, Carbon Dioxide or Hydrogen Sulfide in the Presence of Methanol. *Fluid Phase Equilibria* 1985, *21*, 145-155.

41. Robinson, D. B.; Mehta, B. R. Hydrates in the Propane-Carbon Dioxide-Water System. *J. Can. Pet. Tech.* January-March 1971, 33-35.

42. Unruh, C. H.; Katz, D. L. Gas Hydrates of Carbon Dioxide-Methane Mixtures. *Petroleum Transactions AIME* April 1949, *186*, 83-86.

43. Robinson, D. B.; Ng, H.-J. Hydrate formation and inhibition in gas or gas condensate streams. *J. Can. Pet. Tech.* July-August 1986, 26-30.

44. Ng, H.-J.; Chen, C.-J.; Robinson, D. B. Influence of High Concentrations of Methanol on Hydrate Formation and the Distribution of Glycol in Liquid-Liquid Mixtures. Gas Processors Association (GPA) Research Report 106, April 1987.

45. Dholabhai, P. D.; Englezos, P.; Kalogerakis, N.; Bishnoi, P. R. Equilibrium Conditions for Methane Hydrate Formation in Aqueous Mixed Electrolyte Solutions. *Can. J. Chem. Eng.* 1991, *69*, 800-805.

46. Kobayashi, R.; Withrow, H. J.; Williams, G. B.; Katz, D. L. Gas Hydrate Formation with Brine and Ethanol Solutions. *Proc. 30th Ann. Convention Natural Gasoline Association of Amererica* 1951, 27–31.

47. Vlahakis, J. G.; Chen, H.-S.; Suwandi, M. S.; Barduhn, A. J. The Growth Rate of Ice Crystals: Properties of Carbon Dioxide Hydrate, A Review of Properties of 51 Gas Hydrates. Syracuse U. Research and Development Report 830, Prepared for US Department of the Interior, November 1972.

48. Ng, H.-J.; Robinson, D.B., Gas Processors Association Research Report 66 (April 1983) (Quoted in ref. 1).

CHAPTER 6

AN ACTIVITY COEFFICIENT BASED MODEL FOR MODELLING ASPHALTENE PRECIPITATION

6.1. INTRODUCTION

Crude oil composes a wide range of components. Asphaltenes are the toluene / benzene soluble fractions that precipitate from petroleum when an excess (25 to 40 times) of n-heptane / n-pentane is mixed with petroleum and waiting at least four hours before filtering (1).

Asphaltene precipitation causes fouling in the reservoir, in the well, in the pipeline and in the oil production and processing facilities. During production as the oil pressure drops above the bubble point, especially those containing high fractions of saturates, asphaltenes may precipitate. During enhanced oil recovery (*EOR*) when rich gases or carbon dioxide, are injected into the reservoir, asphaltenes may also precipitate. Once oil streams are brought to the surface, they are often mixed in the field, in tankers and in pipelines. Blending crudes can also upset the delicate balance and precipitate asphaltenes. It is of great interest to be able to predict the conditions that lead to asphaltene precipitation. Although several models have been proposed in recent years, none of them is capable of predicting precipitation of asphaltene satisfactorily.

The aim of this work is to provide a thermodynamic tool for predicting asphaltene precipitation conditions for light systems such as gas condensate fluids, especially at

reservoir conditions. For this purpose a review is made on asphaltene structure and asphaltene precipitation phenomenon. Then I investigate the existing models in the literature for asphaltene precipitation.

In this study, a thermodynamic model based on a polymer theory is introduced. The main assumption in this model is that the asphaltene precipitation is a reversible process, allowing the use of molecular thermodynamics. It is also assumed that the asphaltene forms a liquid phase. Then results are presented on the effect of different parameters on asphaltene precipitation.

6.2. ASPHALTENE STRUCTURE

The molecular nature of asphaltenes has been the target of many studies over the past decades. One of the conclusions is that asphaltenes do not have a unique structural formula and their structure depends on the way they are formed, i.e. depending on the geo-chemistry of the oil. These studies show that asphaltenes are composed of condensed polynuclear aromatic hydrocarbons with aliphatic side chains and heteroatoms such as *N*, *O* and *S*[1] found in both aromatic and non-aromatic portions (1). Polar molecules of asphaltenes also consist of metal (*Ni, V, Fe*) content of heavy oils, in addition to heteroatoms. The ratio of hydrogen/ carbon atoms is approximately around 0.8-1.4 and their molecular weights are typically in the 500-50,000 ranges.

The asphaltenes and resins (compounds soluble in n-pentane but insoluble in propane) may associate to form large aggregates of high molecular weight. As early as 1938, it

[1] Heteroatoms acting as polar functional group and the followings are the typical range of heteroatoms in asphaltenes: *S=0.5-10 wt% ; N=0.6-2.6 wt% ; O=0.3-4.8 wt%*

was recognised that asphaltenes and resins form micelle particles (2). The asphaltene micelle particle has a core, which is formed by several aggregated asphaltene molecules; bipolar resin molecules are adhered on the surface of the core. For the residue from heavy oil, a micelle is composed of 100 asphaltene molecules with a core diameter of 66 Å (1). If not for the resins, most of the asphaltene material would immediately precipitate from the oil due to a low solubility of asphaltene monomeric molecules in the bulk of the petroleum fluid. Figures 2.2 and 2.3 show micellar structure of asphaltenes (3).

Based on comprehensive studies of the structure of asphaltene aggregates in oil, it has been concluded that micellar shape is approximately spherical, and a solvated shell surrounds the asphaltene micellar core (3). Recently, it has been proposed that the aggregate of asphaltenes forms the core and a layer of resin molecules surrounds it (3). Another layer of aromatic materials may surround the outside resin layer. The state of asphaltenes in the core has been reported liquid-like (3).

6.3. ASPHALTENE IDENTIFICATION

Oils are complex mixtures of hydrocarbons and other compounds. Often these components are divided, somewhat arbitrarily, into saturates, aromatics, resins and asphaltenes (*SARA*). The amorphous compounds that are toluene/ benzene soluble but n-heptane/ n-pentane insoluble, called asphaltenes[1], which are the most aromatic and highest molecular weight fraction of petroleum. This fraction alone contains at least 100,000 different molecules and yet not one has ever been positively identified. The

[1] The portion which is soluble in n-alkane (usually n-pentane or n-heptane) is termed as "maltenes" and the insoluble portion is called "asphaltenes". Sometimes the remaining oil after separating asphaltenes and resins is called "maltenes".

yield and quality of this fraction depends on how it was separated: the ratio of n-heptane/ n-pentane to oil, the time before filteration, the pore size and material of the filter, etc. However, by keeping these variables constant, the yield and quality are reproducible. This is also the case for the resins, separated from n-heptane/ n-pentane solution by adsorption on Attapulagus clay and desorbed by a mixture of toluene and acetone (Resins have some polynuclear aromatics with some tendency to associate, but much less than for the asphaltenes). Saturates are the compounds that crystallise out of the remaining oil after evaporating the n-heptane/ n-pentane and cooling a methyl ethyl ketone (*MEK*) solution of the oil to 195 K with dry ice. The remaining oil is called aromatics.

Asphaltene precipitation from crudes is different from other types of precipitation such as wax precipitation. For example, an increase in pressure increases the wax appearance temperature (*WAT* or cloud point) in crudes (i.e., enhances wax precipitation), while pressure increase may inhibit asphaltene precipitation. Wax precipitation is strongly dependent on temperature, whereas asphaltene precipitation may not be affected by temperature. Temperature may weakly enhance/ inhibit asphaltene precipitation. At high temperatures, an increase in concentration of light hydrocarbons such propane and butanes and non-hydrocarbons such as CO_2 decreases the *WAT*; on the other hand, an increase in the amount of these components can significantly enhance asphaltene precipitation.

Another distinct feature of wax and asphaltene precipitation is the state of the precipitated phase. The precipitated wax phase is in the solid state while at high reservoir temperatures, the precipitated asphaltene phase may be in the liquid- like state.

6.4. ASPHALTENE FLOCCULATION, PRECIPITATION AND SOLUBILITY

As mentioned before, asphaltenes are, by definition, a solubility class that precipitate from petroleum by the addition of an excess of the hydrocarbon precipitant. When a precipitant is mixed with petroleum, a certain amount can be blended before asphaltenes begin to precipitate. Flocculation is a thermodynamic transition of asphaltenes from a first liquid phase (the oil) to the asphaltenic deposit. The quantity of asphaltenes precipitated from a crude oil sample is obtained as a function of the quantity of flocculent (an alkane) added to the oil by standard methods like *IP-143* (4) method.

It has been shown, as more alkane is added to the crude the amount of phase that is precipitated increases but approaches an asymptotic value at high ratios of alkane to oil (Figure 6.1, ref. 5). According to Figure 6.2 (5), as the number of carbons in the normal alkane is increased, the asymptotic quantity of heavy precipitated phase decreases. However, as the number of carbons in the normal alkane is increased, the volume of normal alkane at the flocculation point first increases goes through a maximum (about C_9) and then decreases (5). The solubility phenomenon of asphaltenes may consist of a number of different equilibrium conditions, which can be generalised into three categories (5):

1. Solubility or distribution between liquid (L) and precipitated phases (P):

$$\text{Asphaltene(L)}=\text{Asphaltene(P)} \qquad (6.1)$$

2. Aggregation or association of asphaltene molecules:

$$A_1+A_{i-1}=A_i \qquad (6.2)$$

3. Interaction / solubilisation by resins:

$$A+R=A-R \tag{6.3}$$

The solubilisation or peptisation (or coating) of the asphaltenes by resins is assumed to keep the asphaltene molecules in solution. It is obvious that the degree of solubilisation decreases if resins are preferentially dissolved in the oil or added solvent.

It should be noted that if the oil includes components that are near or above their critical temperature, such as in live oil, then volume expansion effects are important. In these cases increasing the temperature can lower asphaltene solubility. However, in dead oils (without components that are near or above their critical temperature) increasing temperature always increases asphaltene solubility.

6.5. REVERSIBILITY AND STATE OF THE PRECIPITATED PHASE

Reversibility of asphaltene precipitation is often an issue. Observations show reversibility of asphaltene precipitation with pressure at high temperatures (6). Reversibility with respect to composition at low temperatures is still unresolved (7, 8, 9), although Ramos et al. (10), Cimino et al. (11) and Hirschberg et al. (6) comment that the titration experiments are reversible. It seems that the dissolution of the precipitated asphaltene at low temperature is a kinetically slow process and therefore the reversibility may require a very long time (12). In addition, the reversibility of asphaltene precipitation at high temperatures (reservoir temperatures) with respect to pressure or composition has been confirmed by experimental observations (13, 14, 15).

The precipitated phase from oil may have two different states. It may have a solid-like or a liquid-like state. Precipitation as a solid-like state would apply mainly to precipitation from crude at room temperature (8, 15). However, liquid state is valid at high temperatures (6, 14 -16).

As mentioned before, the precipitated solid phase may be very slow to re-dissolve in the oil due to a large kinetic barrier to dissolution. Contrary to the solid state, the equilibrium between the precipitated liquid phase and the oil phase is achieved at a faster rate at high temperatures (12).

A detailed composition for the precipitated liquid phase has not yet been reported in the literature. It is likely that the precipitated phase, in addition to asphaltene and resin, may contain components as light as methane. However, the bulk of the precipitated phase consists of asphaltene and in certain cases resin may be present.

6.6. PRECIPITATION MODELS

Asphaltene precipitation has been the subject of several theoretical investigations (e.g., 6, 19-29). One of the fundamental difficulties encountered in describing the phase behaviour of asphaltene-containing systems is the lack of suitable characterisation parameters. It is hard to model asphaltene precipitation because of the tendency of asphaltenes to aggregate, which makes their characterisation difficult. This aggregation tendency is caused by the polar nature of asphaltenes components, which has not been well understood yet. In fact, asphaltenes are not well-identified components/ mixtures. They consist of several polar components of aromatic nature with high molecular weights.

For multi-component systems, such as petroleum, the first step in thermodynamic modelling is the lumping of similar components into pseudo-components in order to simplify the calculations. In general, components that are higher boiling than heptane are grouped in several pseudo components; this is also the case for the models concerned with asphaltenes.

In the majority of the cases, the complexity of the asphaltene fraction leads to the assumption that the asphaltenes can be regarded as one single pseudo-component (monodisperse). The main drawback of the monodisperse models is that they do not take into account the aggregation phenomenon of asphaltenes. This assumption can explain why these models can be correct in some cases and not in others, depending on asphaltene dispersion, which in turn depends on the asphaltene and solvent nature. In fact, the aggregation process produces a molecular weight distribution of aggregates, which also causes a polydispersity in asphaltene properties. A few models use a polydisperse concept in terms of asphaltene properties, especially molecular weight and size. Both concepts are still questionable because of the diversity of the asphaltene fraction.

Most of the models in the literature are based on polymer solutions theories (Scatchard-Hildebrand (17), Flory-Huggins (17), and Scott-Magat (18)) to model the phase behaviour of asphaltene-containing fluids (e.g. Hirschberg et al. (6), Burke et al. (19), Kawanaka et al. (20), Park (21)). In addition to these models, there are also a few models, which are based on equations of state (*EoS*) (e.g. Nghiem et al. (22)). The main assumption in these models is that the precipitation process is reversible. While these models are simple and can explain some experimental results and have some use in describing some selected asphaltene precipitation phenomena in petroleum fluids,

they are inadequate for explaining other experimental results. The two factors that determine the precipitation of asphaltenes from oil are not addressed in these classical models: one is the chemical association between asphaltene molecules and the second one is the peptising effect of resin molecules. In other word, the micellar nature of asphaltenes is neglected in these models.

In colloidal models (e.g. Leontaritis and Mansoori (23)), the precipitation process is taken as being irreversible and asphaltenes are considered as particles maintained in suspension due to the peptising action of the resins. According to this view, adsorbed resin molecules stabilise asphaltene particles and are removed by dissolution when a precipitating agent is added to the oil. The flocculation threshold corresponds to a situation where only a monolayer of resins remains around the asphaltene particle. After this point, any addition of precipitating agent will produce asphaltene flocculation and precipitation. This model is good for determining flocculation threshold, but it has a poor predictability for the quantity of precipitated asphaltenes. The model of Leontaritis and Mansoori (23) was unable to correctly quantify the amount of precipitated asphaltene in titration experiments.

An alternative method for describing precipitation is provided by the micellisation theory. Some researchers (e.g. Victorov and Firoozabadi (24), Pan and Firoozabadi (25), Pan and Firoozabadi (26, 27)) consider asphaltenes to be particles that are suspended in the crude oil, stabilised by resin molecules. Thermodynamic micellisation models, based on the micellisation process, have been established to describe asphaltene aggregation and precipitation in crudes. The precipitation process is assumed reversible for these models because the models are based on the

equilibrium thermodynamic concept. A thermodynamic micellisation model assumes that micelles of asphaltene and resin molecules are always soluble in oil; asphaltene precipitation is due to the concentration of asphaltene monomers becoming higher than the solubility of asphaltenes in the oil without forming micelles. These micelle-based models are helpful for understanding the effect of resin on asphaltene precipitation and the mechanism of asphaltene precipitation from oil. Most of these models cannot readily explain the observed effects of oil composition on asphaltene-precipitation phenomena. Almost all thermodynamic micellisation models assume that all the micelles are monodispersed. This assumption is made for the sake of computational simplicity.

Another approach considers asphaltenes and resins as pseudo components and all other components in oil are presented by a continuous medium that affects van der Waals attractions among asphaltene and resin molecules (e.g. Wu et al. (28), Wu et al. (29)). In this model it is also assumed that asphaltene precipitation is reversible. Model parameters are evaluated systematically from average properties of asphaltenes and resins in crude oils and from dispersion-force properties of the oil medium. In this approach, asphaltenes are represented by attractive hard spheres that can associate with themselves and resins are represented by attractive hard sphere chains that can associate with asphaltenes but not with themselves. It should be noted that association between asphaltene and resin is usually stronger than that between asphaltene and asphaltene. In this approach, asphaltene molecules and resin chains are dissolved in a continuous medium that affects dispersion-force interactions among asphaltenes and resin chains. The Helmholtz energy of the system is given by an expression based on

statistical associated fluid theory (*SAFT*)[1]. When two phases co-exist at equilibrium, the chemical potential for each component is the same in both phases. Chemical potentials are obtained from Helmholtz energy. For phase equilibrium calculations, this approach uses average properties for pure asphaltenes and resins.

6.7. ASPHALTENE FLOCCULATION/ PRECIPITATION IN GAS CONDENSATE SYSTEMS

Asphaltene precipitation is generally not expected in gas condensate systems, however, problems affecting production in some gas condensate reservoirs have recently been reported (30, 31). It is believed that there is an oil rim in the reservoir, which is thought to be one of the possible regions of the asphaltenes. In this case, the gas condensate could have migrated through these layers in the reservoir and CO_2 could have extracted the asphaltenes (30, 31). Some gas condensates contain as low as *0.001 wt%* asphaltenes but form deposits in the flow-lines and production facilities (30). The existence of significant amount of paraffins within the asphaltene powder has also been confirmed (31). *It seems this typical wt% asphaltenes is lower than typical values reported in the literature for critical micelle concentrations (CMC) of asphaltenes, at which a micelle starts forming*. Furthermore, *there is no evidence of presenting a micelle in paraffinic reservoir fluids*. Andersen and Potsch (30) performed the flocculation tests on the various samples containing asphaltenes to understand the stability of the samples. The examination of samples was hampered by the very low content of asphaltenes, which made detection of the onset of flocculation impossible, even for an undiluted sample. Various detection principles (microscopy and spot test) were tested without success.

---

[1] Strong associations between asphaltene molecules and between asphaltene and resin molecules are taken into account using the SAFT theory.

They also indicated that the deposit from drying the liquid sludge from separator (Black viscous oil, solubility parameter equal to 15.70 $MPa^{0.5}$) is more unstable compared to the liquid sludge (solubility parameter equal to 15.84 $MPa^{0.5}$) and the asphaltenes (solubility parameter equal to 15.93 $MPa^{0.5}$) derived from this. The condensate was used to precipitate an oil sample of known flocculation onset, in order to estimate the solubility parameter. The solubility parameter of the condensate was reported to be 15.84 $MPa^{0.5}$ at room temperature. This is close to the critical solubility parameter of the sludge. Hence, the deposition is likely to occur due to mixing of large quantities of condensate with an oil carrying the asphaltenes. Hence the problem can be related to *incompatibility of fluids* (30) and the deposit has a low solubility even in toluene.

Based on the work of Andersen and Potsch (30), it seems that the mechanism of asphaltene flocculation/precipitation in gas condensate systems is based on the solubility concept of asphaltenes and the micellar/ colloidal based models may not be helpful for understanding the mechanism of asphaltene precipitation from these systems. In fact, this is the case for the studied systems and observations reported by Cimino et al. (11) that the precipitated asphaltenes do dissolve in a proper solvent, in the absence of resins. It clearly makes no sense to study colloidal/micellar approaches on asphaltene precipitation in gas condensate systems, as according to the mathematical description underlying the colloidal/micellar approaches, resins must be present in the system in order to stabilise the asphaltenes.

Phase behaviour data reported by Cimino et al. (11) on several asphaltene-solvent-antisolvent mixtures showed that the existing approaches based on activity coefficient and colloidal models for asphaltene stability modelling do not satisfactorily re-

produce behaviour of the system, especially at flocculation point. They employed the Flory-Huggins theory to represent asphaltene stability. Despite the previously reported activity coefficient based models, which assume *the precipitated phase forms pure asphaltenes*. They assumed that the precipitated phase is *concentrated in asphaltenes but contains a fraction of solvent*.

In the Cimino et al.'s model (11), it is assumed that asphaltenes have a single molecular weight as the Flory-Huggins theory (17) is employed. A more correct approach for estimating asphaltene precipitation in oil systems can be developed using the Scott-Magat theory (18), in which it is assumed that asphaltenes have a distribution of molecular weight. A summary of the Scott-Magat theory (18) and Cimino et al.'s model (11) is given in Appendix A.3. To determine the solubility/ precipitation at any other point than at the critical point, one must utilise the equilibrium conditions between the two-phases:

$$\overline{\Delta G_m} = \overline{\Delta G_m'} \tag{2.44}$$

$$\overline{\Delta G_i} = \overline{\Delta G_i'} \tag{2.45}$$

where $\overline{\Delta G_m}$ and $\overline{\Delta G_i}$ are partial molar Gibbs free energies of mixing of the maltene (asphaltene free oil) and of the *i*th fraction of the asphaltene and the *prime* represents the asphalt phase. There are, of course, *i* simultaneous equations of the type of equation (2.44), one for each distinct fraction of asphaltene:

$$ln\Phi_m+(1-\Phi_m)\left(1-\frac{1}{\overline{M}_N}\right)+\chi(1-\Phi_m)^2=ln\Phi_m'+(1-\Phi_m')\left(1-\frac{1}{\overline{M}_N'}\right)+\chi(1-\Phi_m')^2 \tag{2.46}$$

$$ln\Phi_i+1-\frac{M_i}{\overline{M}_N}(1-\Phi_m)-M_i\Phi_m+\chi M_i\Phi_m^2=ln\Phi_i'+1-\frac{M_i}{\overline{M}_N'}(1-\Phi_m')-M_i\Phi_m'+\chi M_i\Phi_m'^2 \tag{2.47}$$

where Φ_m and Φ_i are the volume fractions of maltene and the *i*th fraction of asphaltenes, respectively. M_i is the molecular weight of the *i*th fraction of asphaltene and $\overline{M_N}$ is the average M. χ stands for the interaction parameter between asphaltenes and maltene.

Note that the distribution functions in the two-phases are presumed to be different; hence $\overline{M_N'}$ is not the same as $\overline{M_N}$. Solving equation (2.47) for $ln\frac{\Phi_i'}{\Phi_i}$ and substituting from equation (2.46), one obtains:

$$ln\frac{\Phi_i'}{\Phi_i} = M_i[2\chi(\Phi_m - \Phi_m') - \ln\frac{\Phi_m}{\Phi_m'}] \tag{6.4}$$

or

$$\frac{\Phi_i'}{\Phi_i} = exp(AM_i) \tag{6.5}$$

where

$$A = 2\chi(\Phi_m - \Phi_m') - ln\frac{\Phi_m}{\Phi_m'} \tag{6.6}$$

Equation (6.5) represents the fundamental basis of precipitation in this model. This equation, while correct, is not very helpful when it comes to the actual calculation. That is, the computation may be exceedingly long and tedious. The exact calculation of A is extremely difficult, since both Φ_m and Φ_m' are functions of not only $\overline{M_N}$ and $\overline{M_N'}$ but also the distribution function itself. It should be noted, however, the values of Φ_a' (i.e., 1-Φ_m'), calculated for various M's, approach the limiting curve for M=∞ asymptotically as χ increases. Hence, for values of χ sufficiently above the critical point, one may take for A, the value A_∞ calculated for M=∞. For M=∞, Φ_m =1, so that:

$$A_{\infty}=2\chi(\Phi_a^{'})_{M=\infty}+ln[1-(\Phi_a^{'})_{M=\infty}] \quad (2.50)$$

where $\Phi_a^{'}$ represents volume fraction of total asphaltenes. Since, when $M=\infty$, $(\Phi_a^{'})_{M=\infty}$ is a function of χ alone:

$$ln[1-(\Phi_a^{'})_{M=\infty}]+(\Phi_a^{'})_{M=\infty}+\chi(\Phi_a^{'})^2_{M=\infty}=0 \quad (2.51)$$

Equation (2.51) is similar to that reported by Cimino et al. (11) and allows the determination of asphaltene flocculation in oil systems. According to Cimino et al. (11), experimental flocculation data are regressed to find $(\Phi_a^{'})_{M=\infty}$, the solubility parameter of maltene, δ_m, and the solubility parameter of asphaltene, δ_a, at the temperature of the experiment (In Cimino et al.'s model (11), V_m can be calculated from density and molecular weight). Once δ_a and $(\Phi_a^{'})_{M=\infty}$ at a given temperature have been calculated, it is possible to calculate stability, as equation (2.51) becomes a function of V_m and δ_m, once temperature has been fixed. For this purpose, an independence of δ_a on pressure is assumed. $(\Phi_a)_{M=\infty}$ is assumed not to be very sensitive to the interaction parameter, hence assumed constant and equal to the value obtained from the stock tank oil flocculation measurement.

In order to investigate application of this approach for gas condensate systems, values of $(\Phi_a^{'})_{M=\infty}$ (from equation 2.51) are shown graphically in Figure (6.3). As can be seen, $(\Phi_a^{'})_{M=\infty}$ at high values of χ is not very much sensitive to the solvent. This may be correct for oil systems, but according to the solubility parameters of asphaltene and gas condensate measured by Andersen and Potsch (30), values of χ are close to 0.5. That is, values of $(\Phi_a^{'})_{M=\infty}$ cannot be assumed constant for such systems, indicating this approach and the principal modellistic approaches may not accurately describe asphaltene stability conditions in gas condensate systems. In other word, nearer the critical point, the solubility is considerable and $\Phi_a^{'}$ is less than $(\Phi_a^{'})_{M=\infty}$. By taking

into account the behaviour of polymeric of such systems, the instability conditions can be estimated as described in the next section.

6.8. A NEW MODEL FOR PREDICTING ASPHALTENE PRECIPITATION

6.8.1. Stability analysis

In the Scott-Magat (18) theory, χ represents the maltene solvency power with respect to the asphaltenes. Therefore, there should be a critical value of χ, χ_c, at which the oil phase splits into two phases. Using instability conditions, the following value is obtained for χ_c:

$$\chi_c = \frac{V_m[(\delta_m - \delta_a)^2 + 2l\delta_m\delta_a]}{RT} = \frac{1}{2[1+(\frac{1}{\overline{M}_N})^{0.5}]^2} \qquad (6.7)$$

where δ stands for the solubility parameter and subscripts m and a indicate maltene and asphaltene, respectively, R, T and l represent the universal gas constant, temperature and an interaction parameter, respectively. As can be seen, these critical conditions depend only on $\overline{M}_N$ and not on the precise nature of the distribution function, which may correspond either to a fairly narrow, homogeneous fraction, or to a very broad distribution. The critical point corresponds also to a critical value of Φ_m and of Φ_a:

$$(\Phi_m)_c = \frac{\overline{M}_N}{1+\sqrt{\overline{M}_N}} = \frac{1}{1+\frac{1}{\sqrt{\overline{M}_N}}} \qquad (6.8)$$

$$(\Phi_a)_c = (\Sigma\Phi_i)_c = \frac{1}{1+\sqrt{\overline{M}_N}} \qquad (6.9)$$

Similarly one may consider a critical solution temperature T_c or a critical value of $(\delta_m - \delta_a)_c^2$:

$$T_c = \frac{V_m[(\delta_m - \delta_a)^2 + 2l\delta_a\delta_m]}{\frac{R}{2(1+\frac{1}{\sqrt{\overline{M}_N}})^2}} \tag{6.10}$$

$$(\Delta\delta)_c \approx \frac{\frac{RT}{2(1+\frac{1}{\sqrt{\overline{M}_N}})^2}}{V_m} \tag{6.11}$$

Certain consequences follow immediately from these equations: 1) As pointed out above, the critical point is dependent upon the average molecular weight. Since, for values of χ less than χ_c, no separation of a asphalt phase is possible, it is clear that the presence of low molecular weight materials in the asphaltenes tend to keep the high molecular weight materials in maltene by decreasing the value of $\overline{M}_N$. In short, low molecular weight materials actually make the higher fractions more soluble. This factor is crucial in any consideration of precipitation. 2) Since χ_c is inversely proportional to T, the solubility increases with an increase in temperature. 3) If for a given oil (asphaltene-maltene) system, $(\delta_m - \delta_a)$ is less than the critical $(\delta_m - \delta_a)_c$ in equation 6.11, the asphaltenes and maltene are necessary completely miscible in all proportions.

6.8.2. Phase equilibrium calculations

Equation (6.5) represents the fundamental basis of precipitation presented in this section. For any given system, equation (6.5) may be used as a strictly valid relation, showing the distribution of asphaltenes of different molecular weights between the maltene and the asphalt phases. We may now undertake to express the precipitation.

Let the actual distribution of molecular weights be represented by a distribution function:

$$dw_i = f(M)dM_i \tag{6.12}$$

where dw_i is the *fraction* of the asphaltene of molecular weight M_i and $f(M)$ is a normalised function, such that:

$$\int_{M_m}^{\infty} f(M)dM = 1 \tag{6.13}$$

where M_m is the minimum molecular weight of asphaltenes. Note that, *fraction* could be either weight fraction or volume fraction (Since the density of the asphaltenes is presumed to be *uniform*, independent of molecular weight (5)). This assumption, however, is only an approximate, but is justified for high molecular weights.

The total volume of any given fraction of asphaltene, v_i, is the sum of the volume in the oil phase (superscript s) and that in the asphalt phase (superscript p):

$$v_i = \Phi_i v_s + \Phi_i v_p \tag{6.14}$$

where $v_i = v_a dw_i = v_a f(M)dM_i$; v_s= volume of oil phase; v_p= volume of asphalt phase and v_a= volume of asphaltene. Substituting the condition of equation 6.5:

$$v_i = \Phi_i v_s + \Phi_i v_p exp(AM_i) \tag{6.15}$$

$$\Phi_i = \frac{v_i}{v_s + v_p \exp(AM_i)} = \frac{v_a f(M)dM_i}{v_s + v_p \exp(AM_i)} \tag{6.16}$$

The total solubility in terms of volume fraction of asphaltenes is therefore:

$$\Phi_a = \Sigma\Phi_i = \int_{M_m}^{\infty} \frac{v_a f(M)dM}{v_s + v_p \exp(AM)} \tag{6.17}$$

Equation (6.17), while rigorously correct is not very helpful when it comes to actual calculation. Given the distribution function *f(M)* and the value of χ for the mixture, one can make the calculation, but the computation may be exceedingly long and tedious.

Certain other approximations may also be made: For dilute solutions, where the asphalt phase is small in comparison with the oil, volume of the oil phase, v_s, may be taken as approximately equal to v_o, the volume of feed (reservoir fluid). Furthermore, one may write v_p as a function of the volume of asphaltene in the precipitate, $v_a^{'}$ and the volume fraction of the precipitate, which is asphaltene, $\Phi_a^{'}$.

$$v_p = \frac{v_a^{'}}{\Phi_a^{'}} = \frac{v_a^{'}}{1-\Phi_m^{'}} \tag{6.18}$$

hence

$$\Phi_a = \int_{M_\infty}^{\infty} \frac{v_a f(M)dM}{v_0 + \frac{v_a^{'}}{\Phi_a^{'}}\exp(AM)} \tag{6.19}$$

An approximate limiting value of $\Phi_a^{'}$ is determined by taking the value for $\overline{M_N} = \infty$, which is the asymptote for all finite values of $\overline{M_N}$ as χ increases. The asymptote value $\frac{1}{(\Phi_a^{'})_{M=\infty}}$, which we shall henceforth call β_∞ is a function of χ only, and may be calculated from equation (2.51).

A further approximation may be made in cases where χ is appreciably greater than the χ_c. Then the solubility will be small and nearly all the asphaltenes will be in the asphalt and one may write:

$$v_a^{'} \equiv v_a \tag{6.20}$$

Nearer the critical point, the solubility is considerable and $v_a^{'}$ is appreciably smaller than v_a. However, $\Phi_a^{'}$ is less than $(\Phi_a^{'})_{M=\infty}$ and partially compensates. Since this deviation of $\Phi_a^{'}$ is not usually as marked as that of v_a, one may say as a general rule (It can be shown mathematically that, even at the critical point, $\Phi_a^{'}$ is greater than $\frac{1}{3}(\Phi_a^{'})_{M=\infty}$. Hence $\beta_\infty < \beta < 3\beta_\infty$):

$$\beta v_a^{'} = \frac{v_a^{'}}{\Phi_a^{'}} \leq \frac{v_a}{(\Phi_a^{'})_{M=\infty}} = \beta_\infty v_a \tag{6.21}$$

Therefore one may write as a final approximate form for the solubility:

$$\Phi_a \cong \int_{M_m}^{\infty} \frac{f(M)dM}{\frac{v_0}{v_a} + \frac{1}{(\Phi_a^{'})_{M=\infty}} \exp(A_\infty M)} \tag{6.22}$$

On the other hand,

$$\frac{v_0}{v_a} = (\frac{\rho_a}{\rho_0})(\frac{1-w_a}{w_a}) \tag{6.23}$$

where ρ_a, ρ_0 and w_a are the density of asphaltene (1.28 g/cm^3: ref. 32), density of oil, and weight fraction of asphaltene in the reservoir fluid, respectively. Therefore,

$$\Phi_a \cong \int_{M_m}^{\infty} \frac{f(M)dM}{(\frac{\rho_a}{\rho_0})(\frac{1-w_a}{w_a}) + \frac{1}{(\Phi_a^{'})_{M=\infty}} \exp(A_\infty M)} \tag{6.24}$$

The solubility can be expressed as the fraction of the asphaltene dissolved ($\frac{\Phi_a v_s}{v_a}$). In this case, one may write:

$$\text{Asphaltene fraction dissolved} = \int_{M_m}^{\infty} \frac{f(M)dM}{1 + (\frac{\rho_0}{\rho_a})(\frac{w_a}{1-w_a}) \times \frac{1}{(\Phi_a^{'})_{M=\infty}} \times \exp(A_\infty M)} \tag{2.49}$$

Asphaltene fraction precipitated =*1- Asphaltene fraction dissolved* (6.25)

One further point should be noted. The above relations apply only to asphaltenes, which are fully soluble in maltenes ($\chi<\chi_c$), the so-called *"sol-asphaltenes"*. Some asphaltenes may consist of some materials, which are completely insoluble in all solvents, the so-called *"gel-asphaltenes"*. We may therefore write as the generalised case:

Asphaltene fraction precipitated = *(1- Asphaltene fraction dissolved)*×*(fraction of the asphaltenes, which is "gel")* (6.26)

In addition, for $\chi<\chi_c$, the *sol-asphaltenes* are completely soluble, but the *gel-asphaltenes* are never soluble.

Equation (2.49) can be used along with equations (2.50) and (2.51) in order to model asphaltene solubility/precipitation. For this purpose, a vapour-liquid flash calculation should be performed on reservoir fluid for establishing the liquid phase from which asphaltenes may flocculate/precipitate.

6.9. FLUID CHARACTERISATION

For calculating asphaltene solubility/precipitation, solubility parameter of asphaltenes, solubility parameter of maltene and molecular volume of maltene are necessary. The solubility parameter of asphaltenes δ_a can be calculated using the following relation (6):

$$\delta_a=20.04\ [1-1.07\times 10^{-3}(T-273.15)] \quad (6.27)$$

where T is in *Kelvin* and δ_a is in $MPa^{0.5}$. The solubility parameter of the maltene can be calculated from:

$$\delta_m = \sqrt{\frac{\Delta u_m^V}{V_m}} \tag{6.28}$$

where Δu_m^V is the energy change upon isothermal vaporisation of one mole of the maltene to the ideal gas state and V_m is the molecular volume of the maltene. Figures 6.4 and 6.5 show a comparison between experimental and predicted Δu^V and V, respectively, using the Peng-Robinson (*PR*) (33) and Soave-Redlich-Kwang (*SRK*) (34) equations of states, which are frequently used in petroleum industry. As can be seen, the *PR-EoS* (33) gives better results for predicting V, whereas the results of the *SRK-EoS* (34) for Δu^V are in better agreement with experimental data. Therefore, V_m is calculated using the *PR-EoS* (33). From the *SRK-EoS* (34), the expression of Δu^V is:

$$\Delta u^V = \left(\frac{a}{b} - \frac{T}{b}\frac{da}{dT}\right)\ln\left(1+\frac{b}{V}\right) \tag{6.29}$$

where a, b and V are parameters of the *SRK* equation of state and molar volume, respectively.

In this work, *Twu*'s correlation (35) for critical properties and the *Lee-Kesler* correlation (36) for acentric factor are used for all petroleum fractions, as recommended by Danesh (37). The binary interaction parameters (*BIP*) for the *PR* (33) and *SRK- EoS* (34), which have been used in this work, derived from Knapp and Doring (38). For the *BIP*s between hydrocarbon-hydrocarbon (excluding those reported in Knapp and Doring), the *Chueh-Prausnitz*'s correlation (39) has been used:

$$k_{ij} = \left[1.0 - \left(\frac{2(V_{c,i}V_{c,j})^{1/6}}{V_{c,i}^{1/3} + V_{c,j}^{1/3}}\right)^{\bar{\theta}}\right] \tag{6.30}$$

In this correlation, the power coefficient ($\bar{\theta}$) is tuned by, at least, one experimental bubble point pressure.

A preliminary study showed that the recommended *BIP*s between nitrogen-hydrocarbons and carbon dioxide-hydrocarbons for the *PR-EoS* (33) are well represented by the following equation, as shown in Figures 6.6 and 6.7, in which, δ is the solubility parameter at 298.15 K:

$$k_{ij} = a_1 + b_1\left|\delta_{N_2/CO_2} - \delta_{HC}\right| \tag{6.31}$$

where k_{ij} is the *BIP* and subscripts N_2, CO_2 and HC represent nitrogen, carbon dioxide and hydrocarbon, respectively and a_1 and b_1 are constants, which are reported in Table 6.1.

6.9.1. Molecular Weight Distribution Functions

Kawanaka et al. (20) and Park (21) were the pioneers to employ a distribution function to characterise the asphaltenes. Kawanaka et al. (20) used the Gamma function as the distribution function. Later, Park (21) changed this distribution function by another analytical function based on the aggregation theory, as proposed by Botet and Jullien (40):

$$f(M) = \left(\frac{(1-2\varpi)^{1-2\varpi}}{\Gamma(1-2\varpi)}\right) M^{-2\varpi} \exp[-(1-2\varpi)M] \tag{6.32}$$

where Γ is the Gamma function. Park (21) considered ϖ as a parameter depending on the resin concentration:

$$\varpi = C_1 + C_2\sqrt{C_r} \tag{6.33}$$

where C_r is the resin concentration in the liquid phase, C_1 and C_2 are parameters to be determined by matching some experimental data. Park (21) obtained good results for the quantity of the precipitated asphaltenes, using experimental data for the titration of

a *STO* at low-pressure conditions. However, when the model was used for mixtures of an oil with CO_2 at high-pressures, poor quantitative results were obtained.

Yarranton and Masliyah (41) have employed the following distribution function:

$$f(M) = c\{1+\alpha exp(-\beta M)\} \tag{6.34}$$

where α and β are the distribution function parameters, M is the molecular weight of the asphaltene and c is a normalisation constant. They obtained several asphaltene sub-fractions experimentally by adding asphaltenes to a toluene / hexane mixture and then proposed the above equation. The quantitative results of this function were not satisfactory neither for the alkanes nor for the aromatic solvents (They used the same parameters for the distribution function in all the cases, which means that asphaltenes aggregation is the same in different solvents).

Rassamdana and Sahimi (7) proposed the following equation for asphaltenes molecular weight distribution function:

$$f(M) = c\left(\frac{(M-M_m)^{-2\varpi}}{M}\right)exp[-a(M-M_m)] \tag{6.35}$$

where M is the continuous molecular weight of asphaltenes, M_m the minimum molecular weight of asphaltenes and a and c are parameters to be estimated. The c parameter is a normalisation constant obtained from:

$$\int_M^\infty f(M)\,dM = 1 \tag{6.36}$$

and the average molecular weight of asphaltenes is obtained from:

$$\int_M^\infty M f(M)\,dM = \overline{M}_N \tag{6.37}$$

For a specified value of average molecular weight of asphaltenes $\overline{M}_N$, the value of a can be calculated. They proposed the following values for ϖ:

ϖ= -0.13 *for* CO_2 *titration*

ϖ= -0.50 *for normal-alkanes titration*

M_m=500 *g/gmol*

Monteagudo et al. (42) employed the above equation (6.35) for asphaltenes. However, they tuned ϖ parameter against the experimental data. In addition, their model showed less deviation in comparison with other models.

In the present work, the later distribution function is used, as ϖ parameter is different for CO_2 titration and also normal-alkanes titration.

6.10. MODEL RESULTS

Cimino et al. (11) performed some tests (Table 6.2) in order to find flocculation points of dissolved asphaltenes in different ratios of solvent and precipitant and then indicated that the precipitated asphaltenes do dissolve in appropriate solvents (even in the absence of resins) and at flocculation, the ratio of "solvent mass per asphaltene mass" and "precipitant mass per asphaltene mass" is linear and is independent on the asphaltene concentration. Figures 6.8 – 6.10 show a comparison between the behaviour of *Tradditional activity coefficient* based model (6), *colloidal* model (23), Cimino et al.'s model (11), model developed in this study and some experimental data on a stock tank oil reported by Cimino et al. (11). As can be seen, the capability of *colloidal* model (23) and *Tradditional activity coefficient* based model (6) to re-produce the observed behavior is poor. However, the newly developed model

produces encouraging results. This shows that the use of the solubility concept of asphaltenes may be in better agreement with the mechanism of asphaltene flocculation/precipitation in light systems. In other word, the colloidal/micellar models are helpful for understanding the effect of resin on asphaltene precipitation and the mechanism of asphaltene precipitation from crude oil. That is, according to the mathematical description underlying the colloidal/micellar models, resins must be present in the system in order to stabilise the asphaltenes. However, such models may forecast complete insolubility in light systems.

Furthermore, Figures 6.11 and 6.12 illustrate asphaltene flocculation conditions for different ratios of solvent and precipitant based on the data reported in Table 6.2. As it can be seen, the data presented in these figures are strongly suggestive of the possibility that they may all be collapsed onto scaling lines, since all the points start at the same point. These data are well represented by the following equation, in which c depends on asphaltene nature:

$$\frac{(wt.\ precipitant)^c}{wt.\ asphaltene} = \left(\frac{wt.\ solvent}{wt.\ asphaltene}\right) \tag{6.38}$$

Figures 6.13 and 6.14 show the collapse of the data shown in Figures 6.11 and 6.12 for C_5-Asphaltenes and C_7-Asphaltenes with c = -0.84 and c = -0.65, respectively. As it can be seen, since we have collapsed the data onto a single line, the value for c should be the same for all the precipitants and solvents and is dependent only on the type of the asphaltene.

The collapse of the data onto scaling lines has an important implication: The scaling line can provide predictions for those values of precipitant/solvent, for which no data are available or their measurement may be difficult.

6.11. CONCLUSIONS

Accurate information, including reliable thermodynamic models on light systems are necessary in order to avoid asphaltene flocculation/precipitation problem. In this work, it has been shown that the use of the solubility concept of asphaltenes may be in better agreement with the mechanism of asphaltene flocculation/precipitation in light systems (section 6.7). In order to estimate asphaltene flocculation/precipitation, a polydisperse thermodynamic model based on *Scott-Magat* theory (18) was developed for modelling asphaltene flocculation/precipitation (section 6.8). The results of the model were in good agreement with a previously reported statement that the flocculation point is independent on the asphaltene concentration (11).

A new corresponding state approach for predicting asphaltene precipitation conditions for dissolved asphaltenes in various ratios of solvents and precipitants was developed (equation 6.38). The developed approach showed that the parameter of this method is the same for all the precipitants and solvents and is dependent only on the type of the asphaltene. It was shown that the results of this method are in good agreement with the literature data. Further experimental data, especially on live fluids are required to further evaluate the performance of this approach.

TABLES

Table 6.1. Constants a_1 and b_1 in equation 6.31.

Constant	N_2-HC system	CO_2-HC system
a_1	-0.13987	0.14000
b_1	0.02705	-3.0815×10^{-08}

Table 6.2. Weight fractions at flocculation points at 298.15 K and 0.101325 MPa (11).

Precipitant / Solvent	C_5-Asphaltenes			Precipitant / Solvent	C_7-Asphaltenes		
	Precipitant	Solvent	Asphaltenes		Precipitant	Solvent	Asphaltenes
C_5 / Toluene	0.367	0.621	0.012	C_5 / Toluene	0.293	0.694	0.013
	0.369	0.623	0.008		0.294	0.696	0.010
	0.370	0.624	0.006		0.297	0.696	0.007
	0.403	0.594	0.003		0.294	0.703	0.003
C_5 / Tetraline	0.477	0.513	0.010	C_5 / Tetraline	0.427	0.562	0.011
	0.480	0.513	0.007		0.430	0.562	0.008
	0.480	0.515	0.005		0.445	0.550	0.005
	0.480	0.518	0.002		0.444	0.554	0.002
C_7 / Toluene	0.420	0.569	0.011	C_7 / Toluene	0.352	0.636	0.012
	0.422	0.570	0.008		0.354	0.637	0.009
	0.423	0.571	0.006		0.355	0.639	0.006
	0.422	0.576	0.002		0.389	0.608	0.003
C_7 / Tetraline	0.521	0.470	0.009	C_7 / Tetraline	0.481	0.509	0.010
	0.527	0.466	0.007		0.494	0.499	0.007
	0.524	0.471	0.005		0.501	0.494	0.005
	0.524	0.474	0.002		0.525	0.473	0.002
C_{10} / Toluene	0.437	0.553	0.010	C_{10} / Toluene	0.366	0.622	0.012
	0.440	0.552	0.008		0.407	0.585	0.008
	0.440	0.555	0.005		0.407	0.588	0.005
	0.440	0.558	0.002		0.407	0.591	0.002
C_{10} / Tetraline	0.538	0.453	0.009	C_{10} / Tetraline	0.492	0.498	0.010
					0.496	0.497	0.007
					0.520	0.475	0.005
					0.542	0.456	0.002

FIGURES

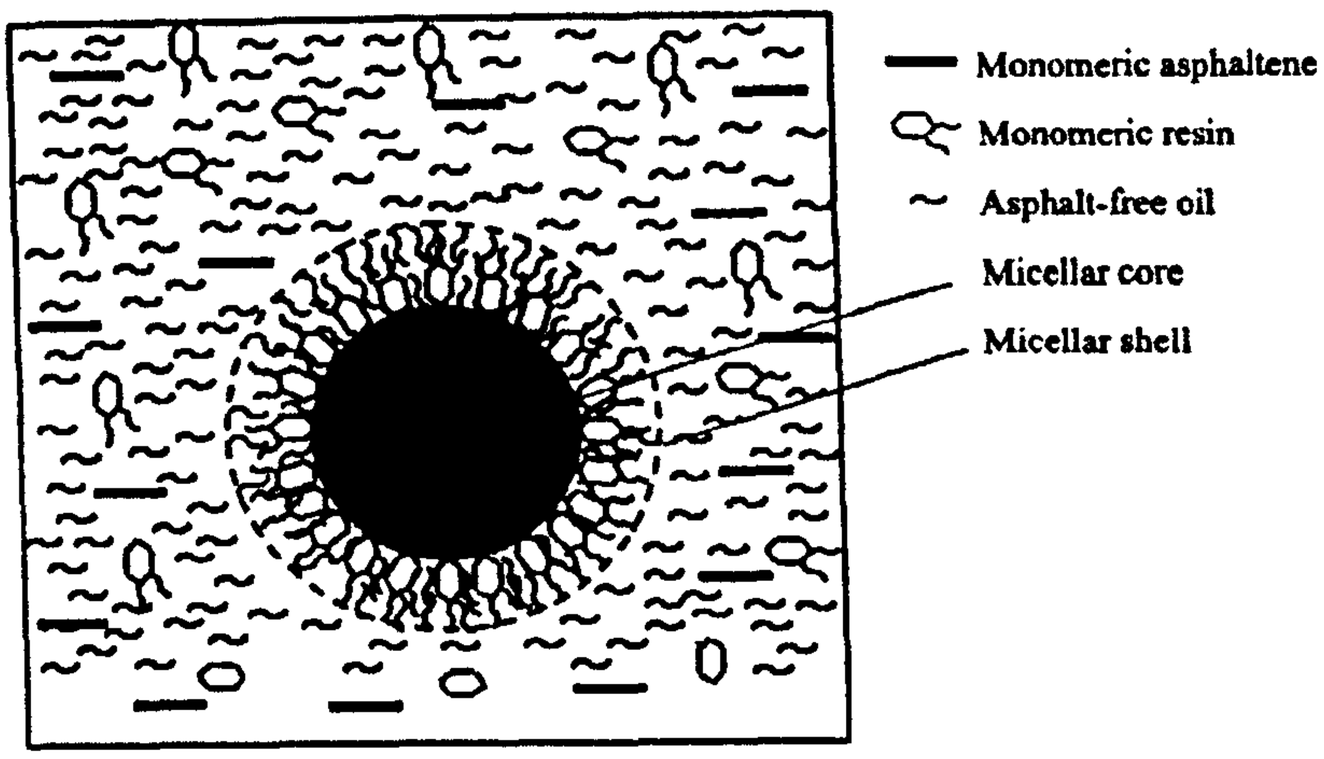

Figure 2.1 - Schematic of a micelle in crude (3).

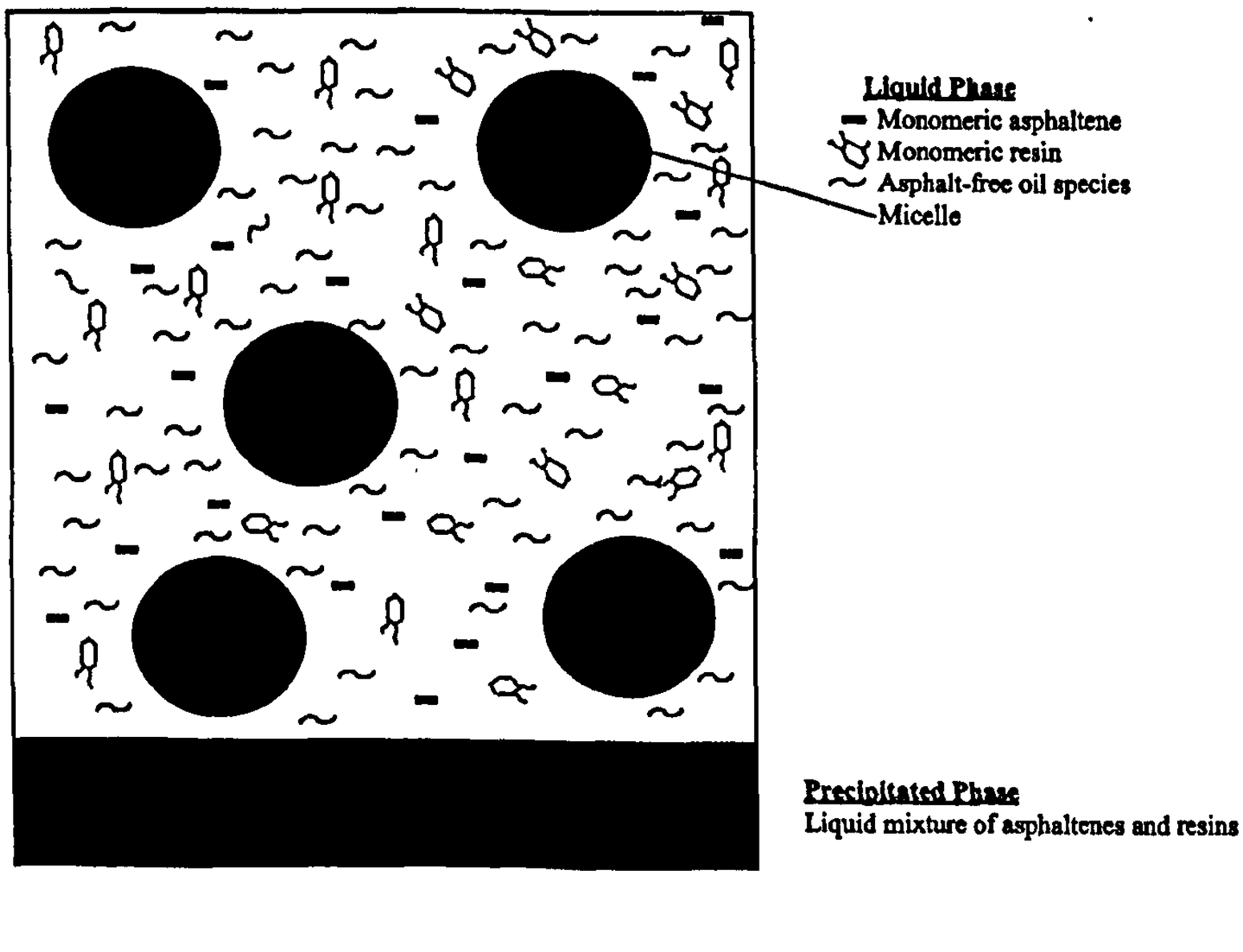

Figure 2.2 - Schematic representation of crude system (3).

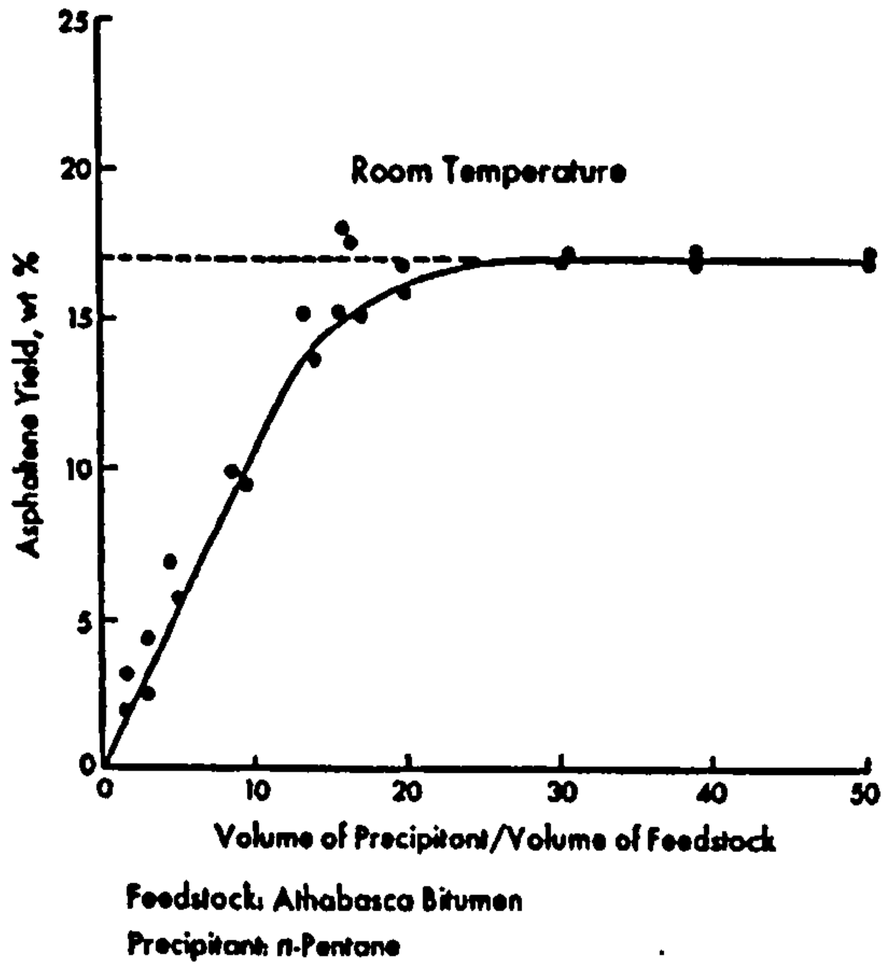

Figure 6.1 – Typical asphaltene yield versus the amount of precipitant (5).

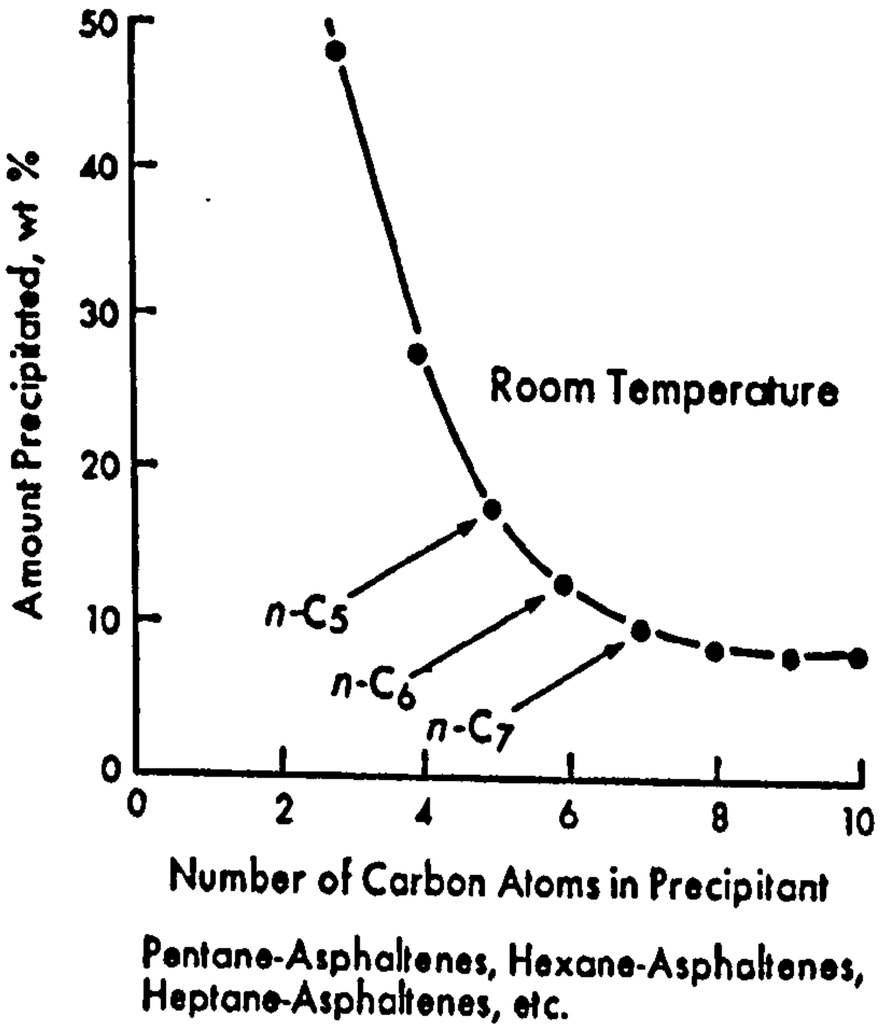

Figure 6.2 – Typical asphaltene precipitated versus number of carbon atoms in precipitant (5).

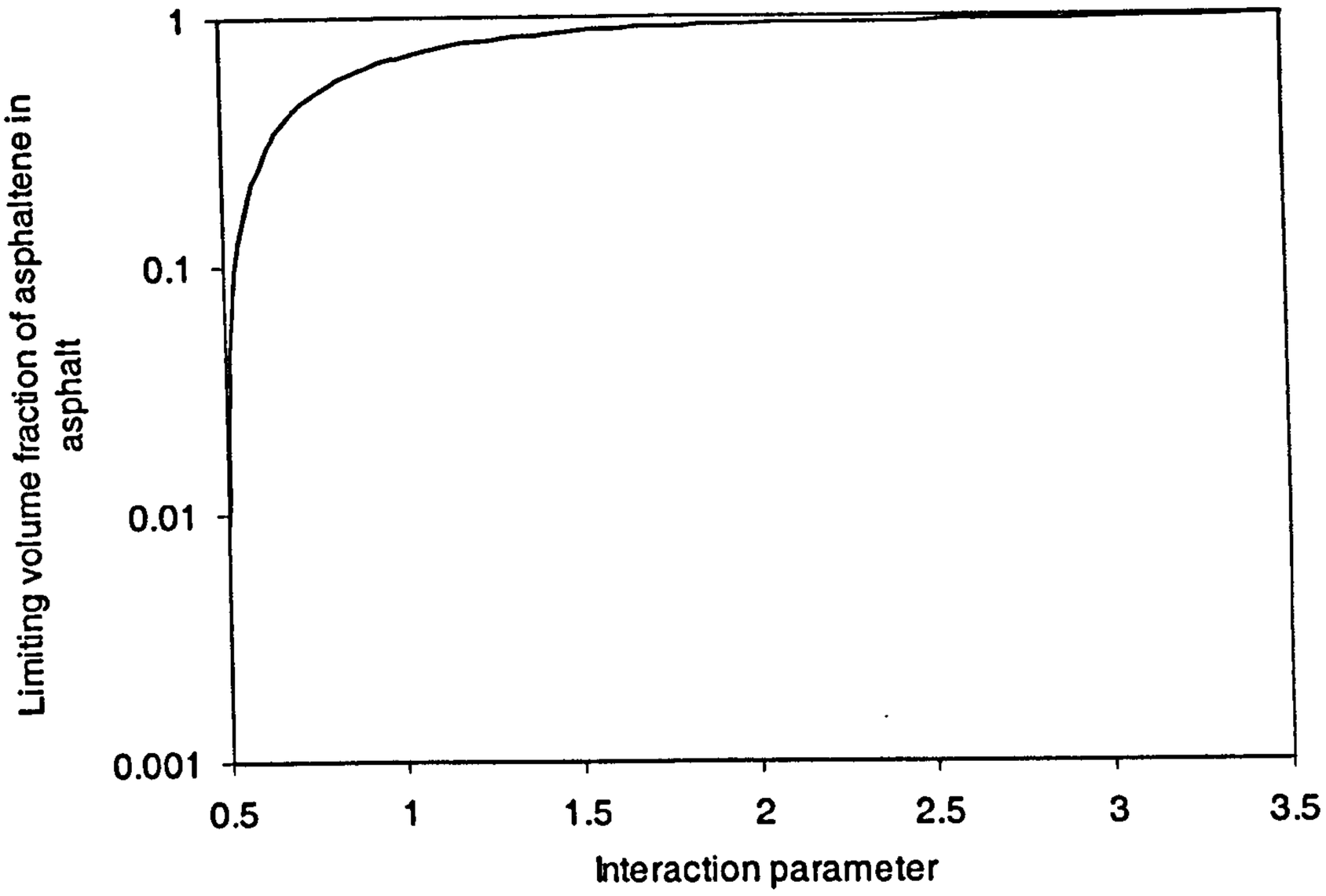

Figure 6.3 – Limiting volume fraction of asphaltene in asphalt versus interaction parameter.

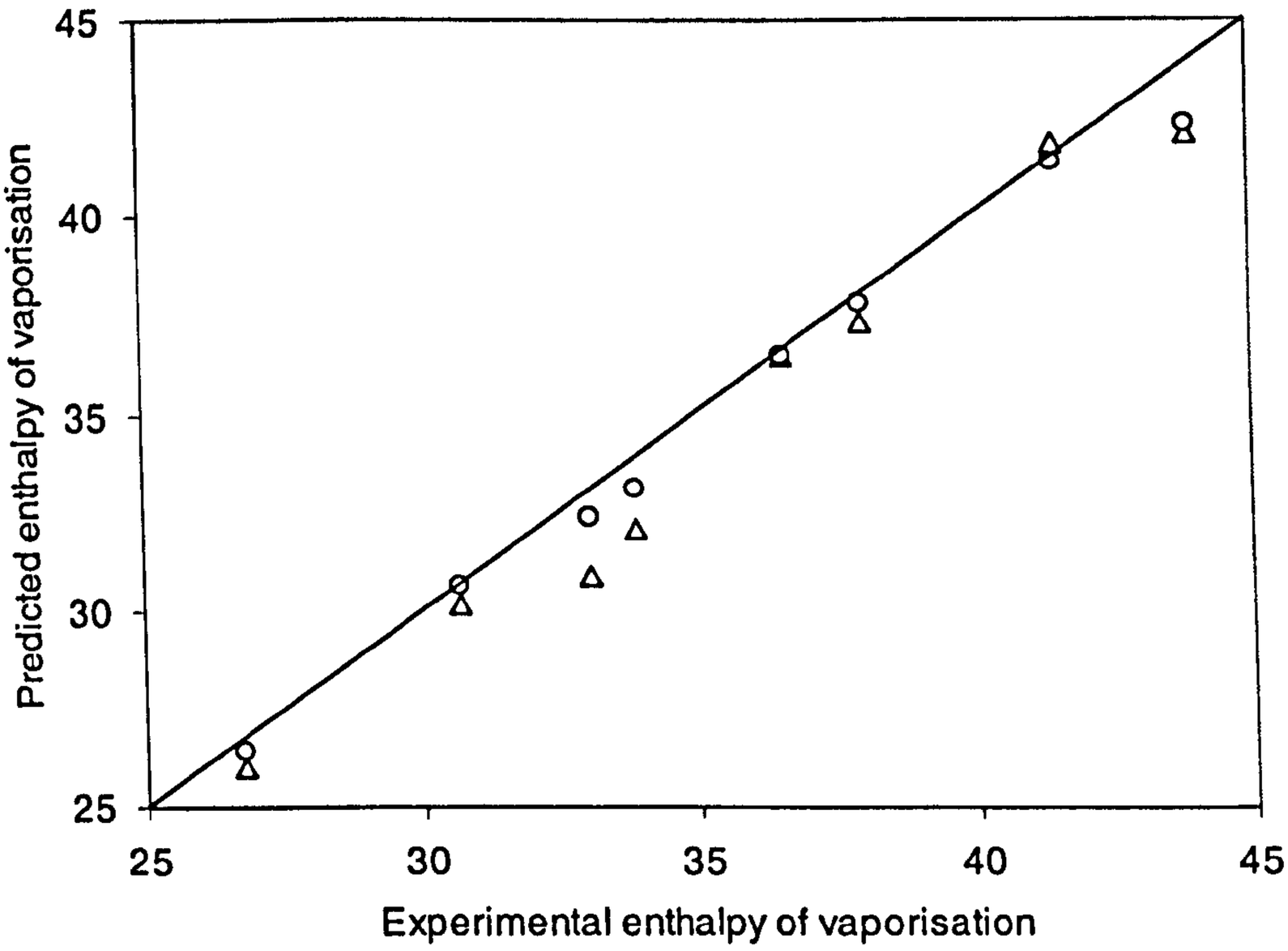

Figure 6.4 – Evaluation of the *PR* (33) (Δ) and *SRK-EoS* (34) (○) for the prediction of pure hydrocarbons (n-Pentane, n-Heptane, n-Octane, Cyclohexane, Benzene, Toluene, Styrene, 1-Hexene) enthalpy of vaporization (kJ/gmol) (Experimental data from 43).

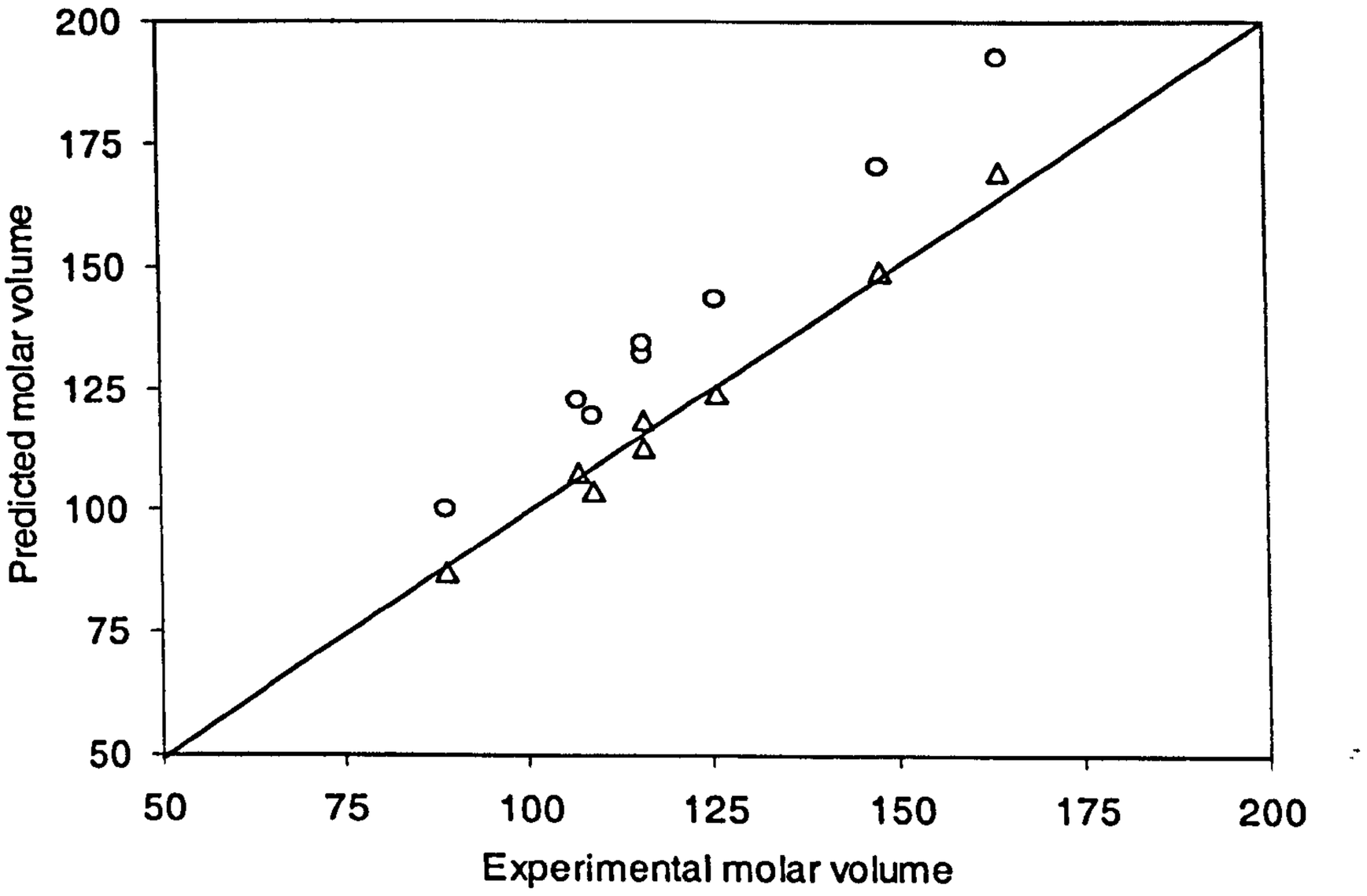

Figure 6.5 – Evaluation of the *PR* (33) (Δ) and *SRK- EoS* (34) (o) for the prediction of pure hydrocarbons (n-Pentane, n-Heptane, n-Octane, Cyclohexane, Benzene, Toluene, Styrene, 1-Hexene) molar volume (cm^3/gmol) (Experimental data from 43).

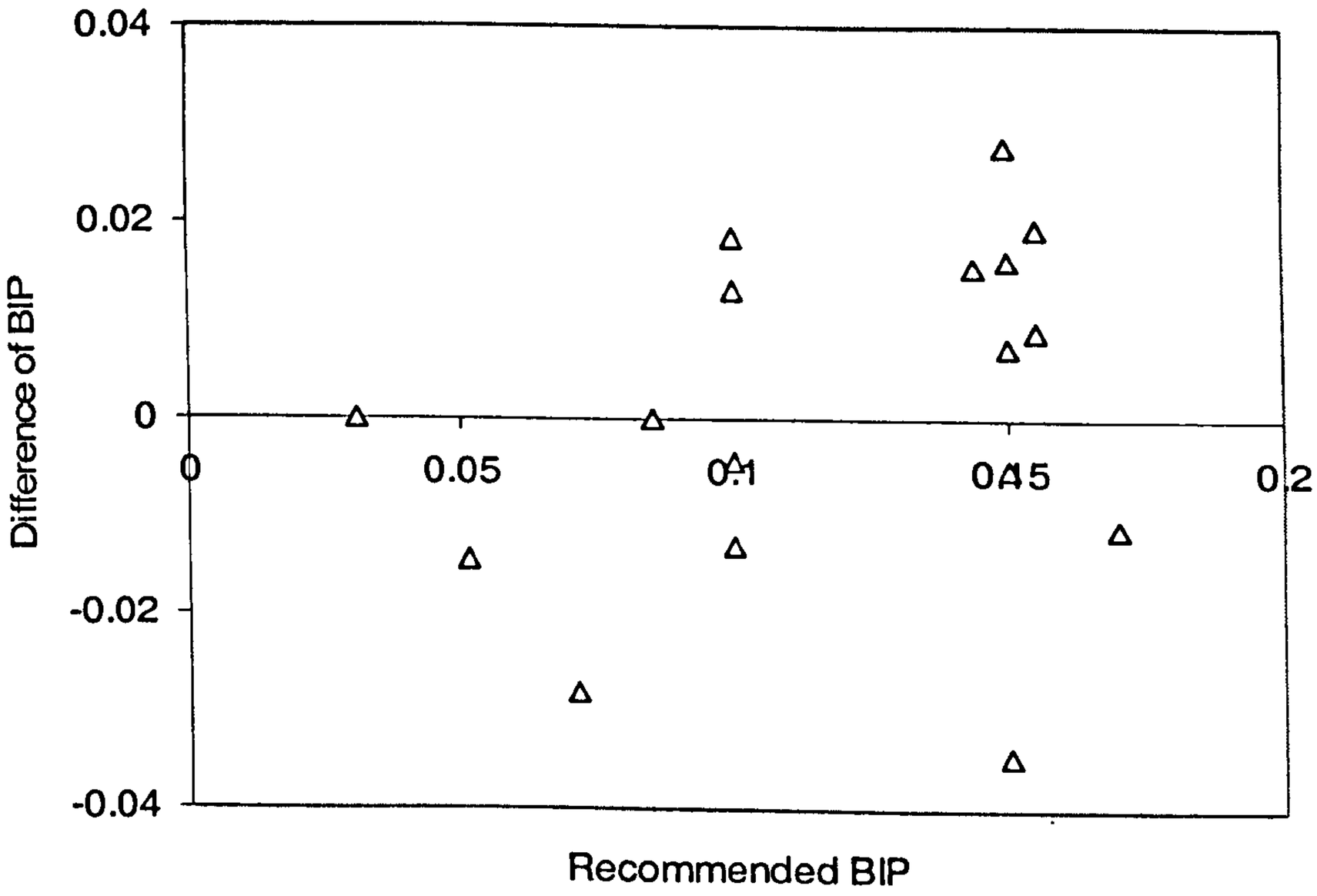

Figure 6.6 - Difference of *BIP*s versus recommended *BIP*s between nitrogen and hydrocarbons for *PR-EoS* (33).

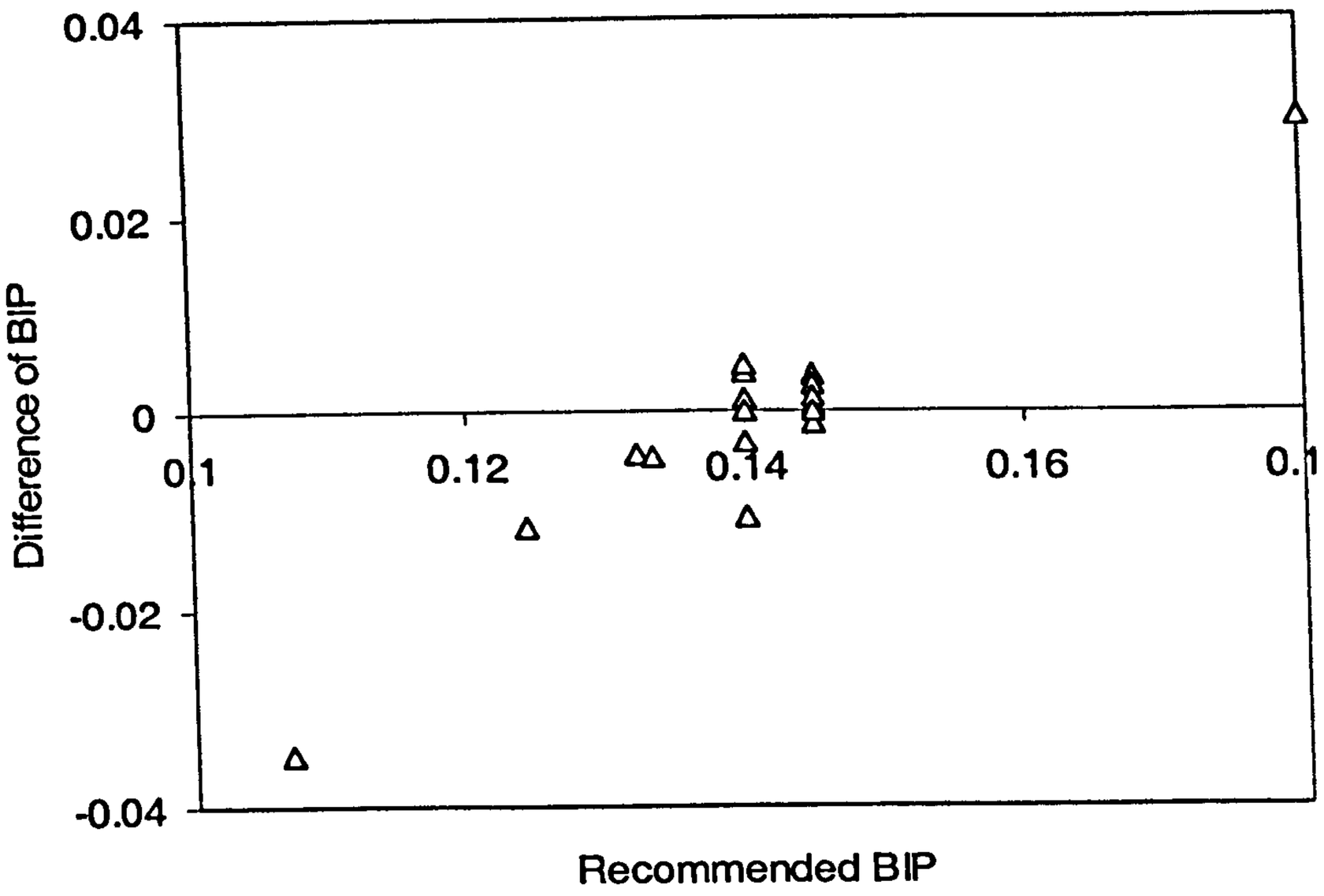

Figure 6.7 - Difference of *BIP*s versus recommended *BIP*s between carbon dioxide and hydrocarbons for *PR-EoS* (33).

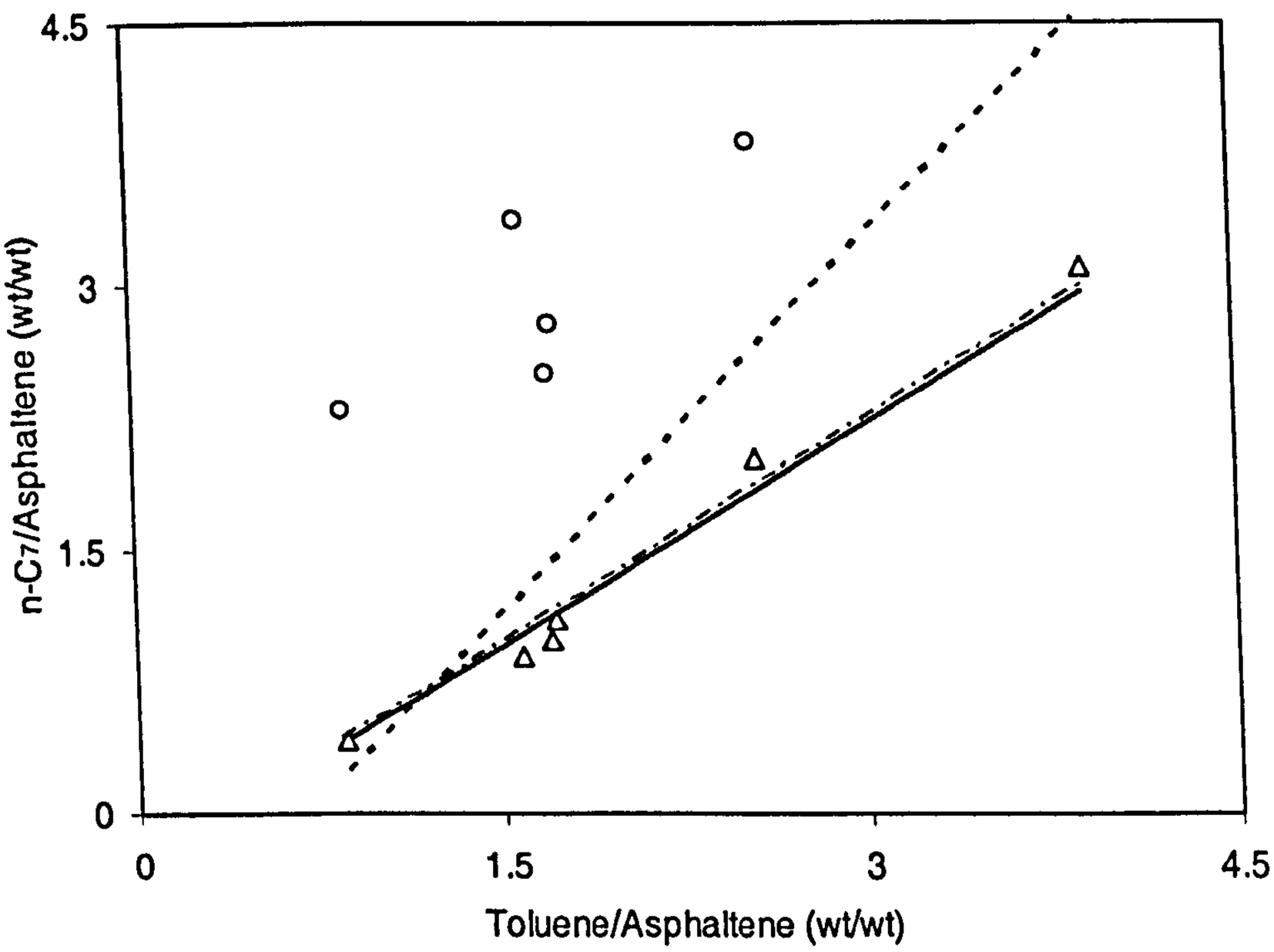

Figure 6.8 - Comparison of predicting asphaltene flocculation by several models (Δ: Experimental data (11); o: Colloidal model; Bold dashed line: Traditional activity coefficient based model; Dashed line: Cimino et al. model (11); Solid line: This model).

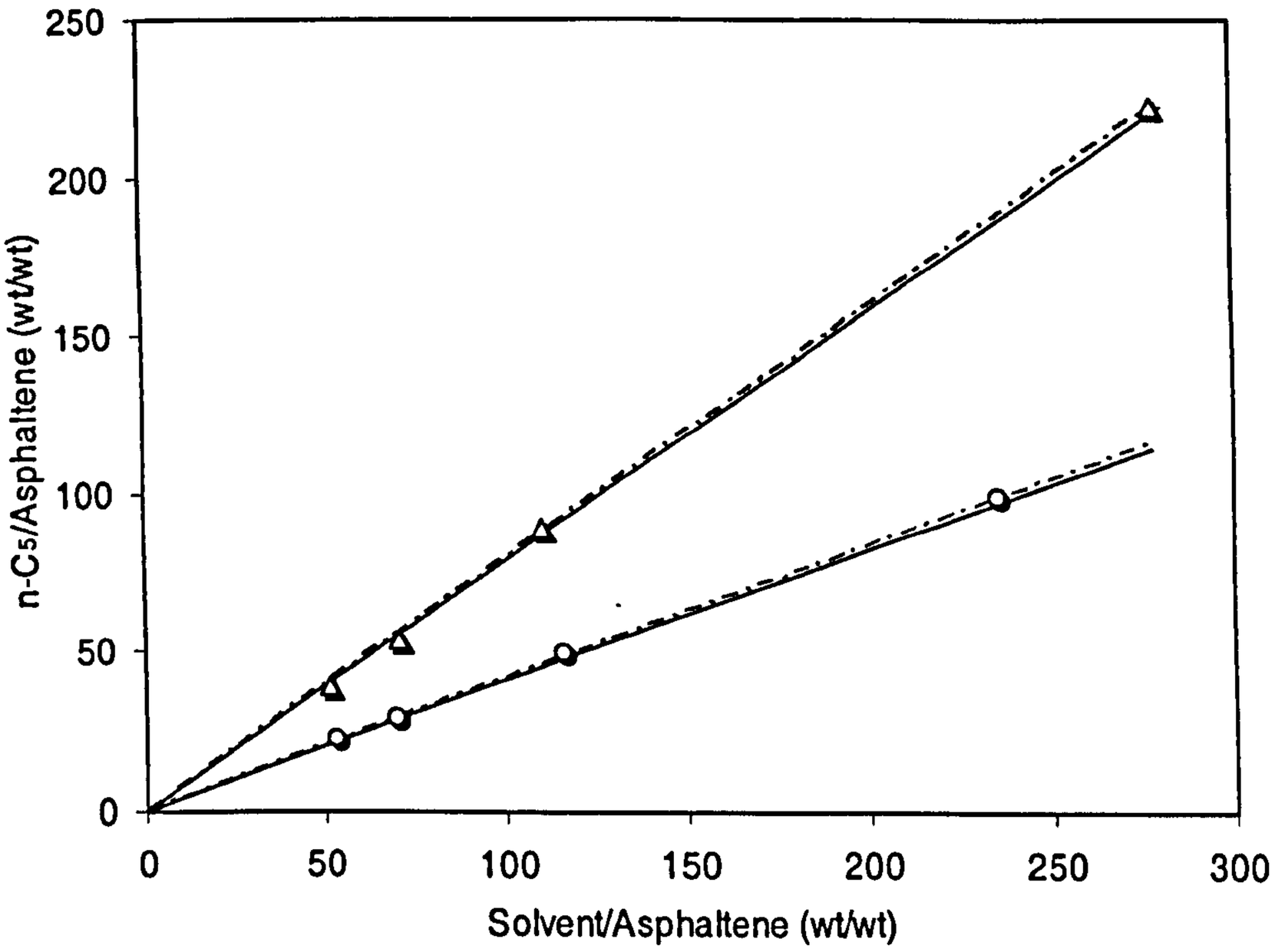

Figure 6.9 - Comparison of predicting C_7-asphaltene flocculation (Δ: Tetraline; ○: Toluene). Dashed line: Cimino et al. model (11); Solid line: This model.

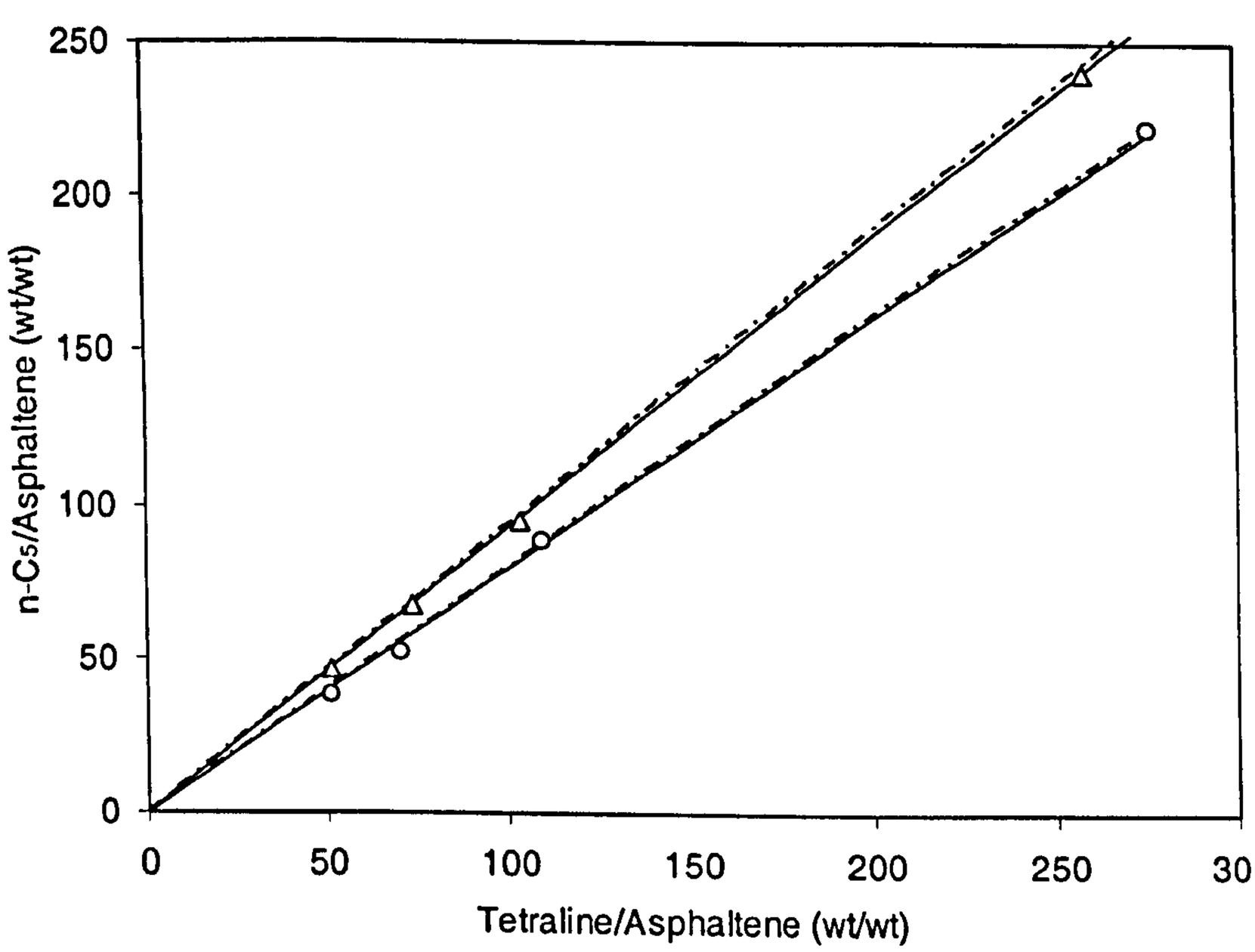

Figure 6.10 - Comparison of predicting asphaltene flocculation (Δ: C_5-asphaltene; ○: C_7-asphaltene). Dashed line: Cimino et al. model (11); Solid line: This model.

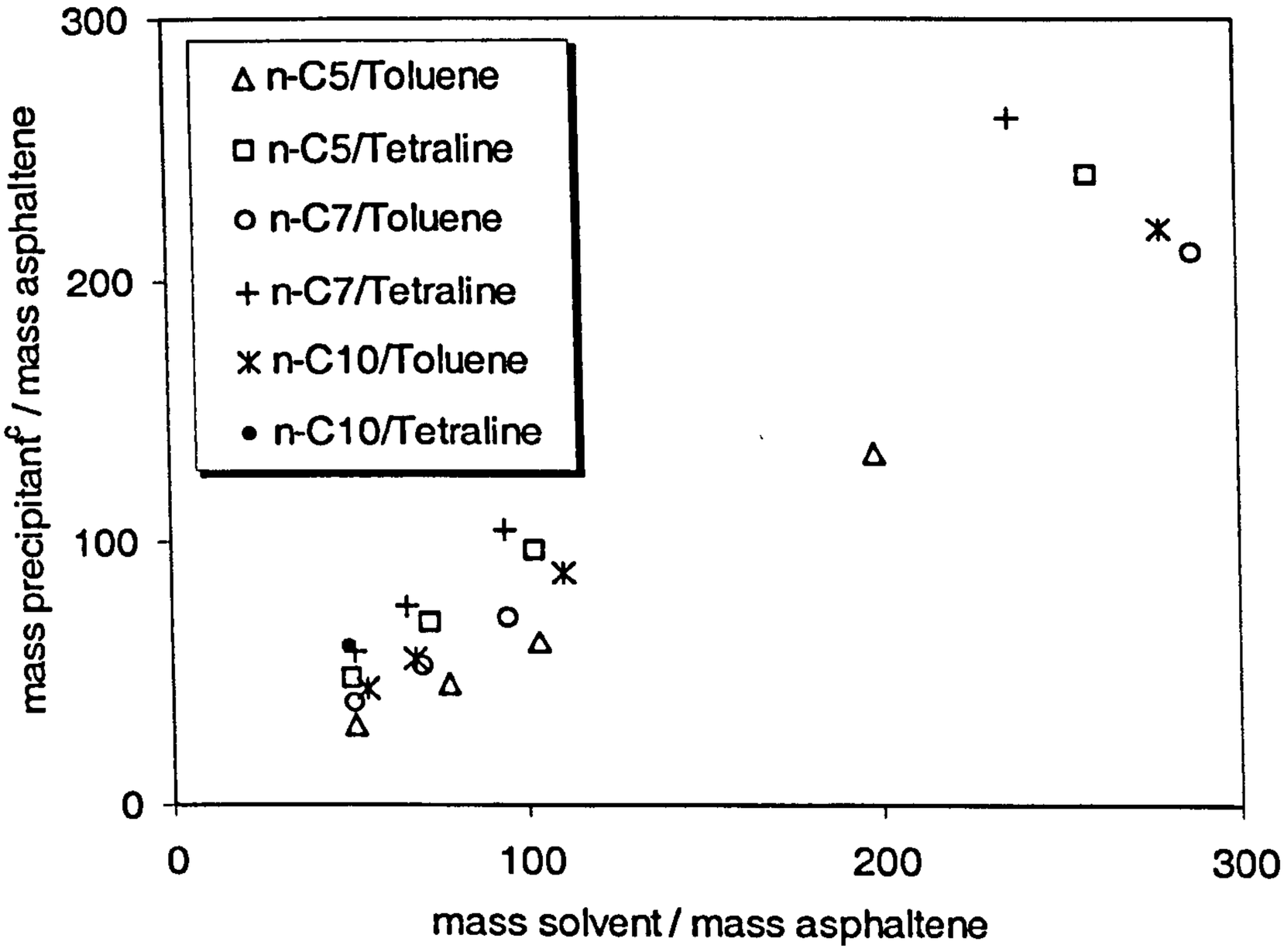

Figure 6.11 - Asphaltene flocculation conditions for C_5-Asphaltenes and different ratios of solvent and precipitant.

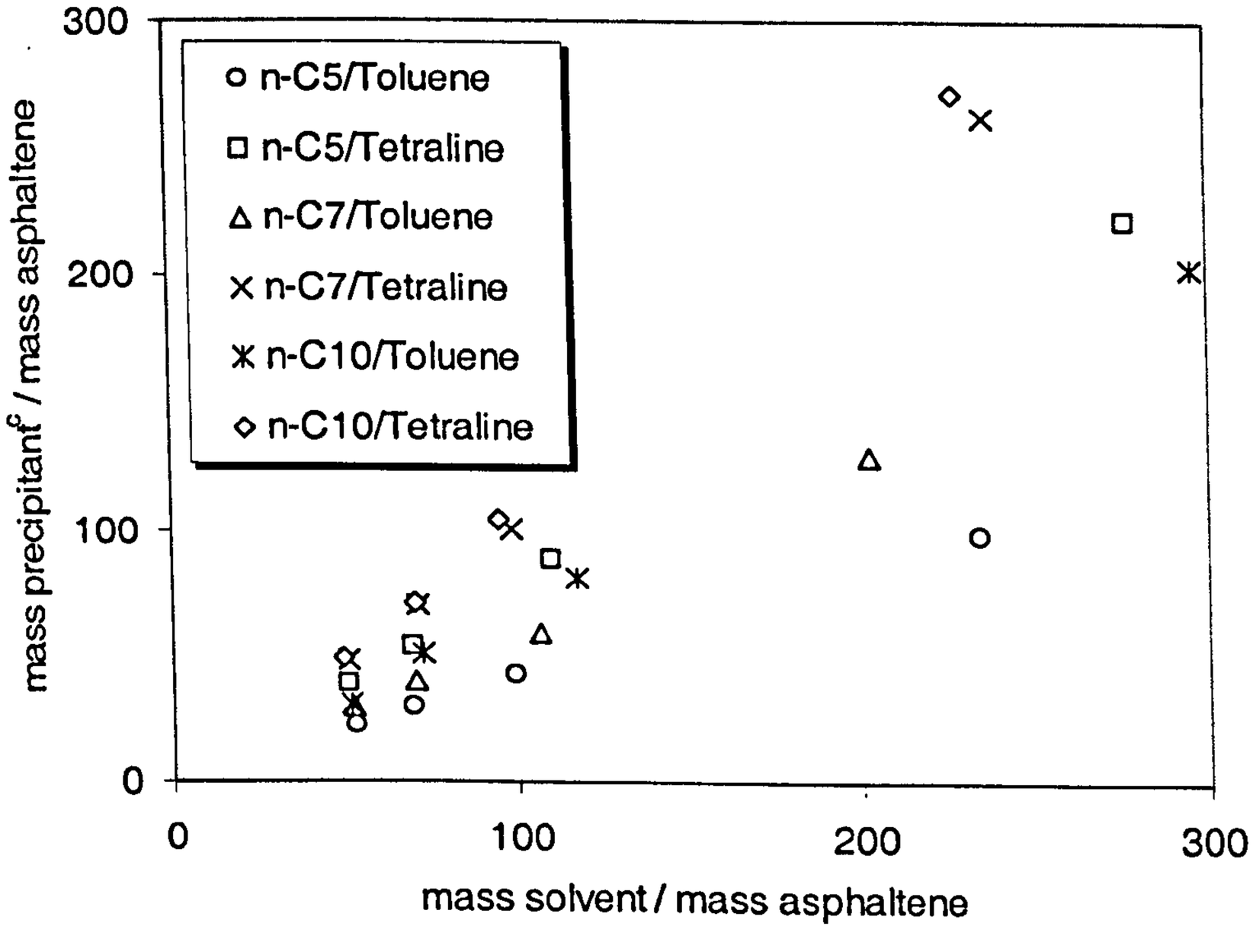

Figure 6.12 - Asphaltene flocculation conditions for C_7-Asphaltenes and different ratios of solvent and precipitant.

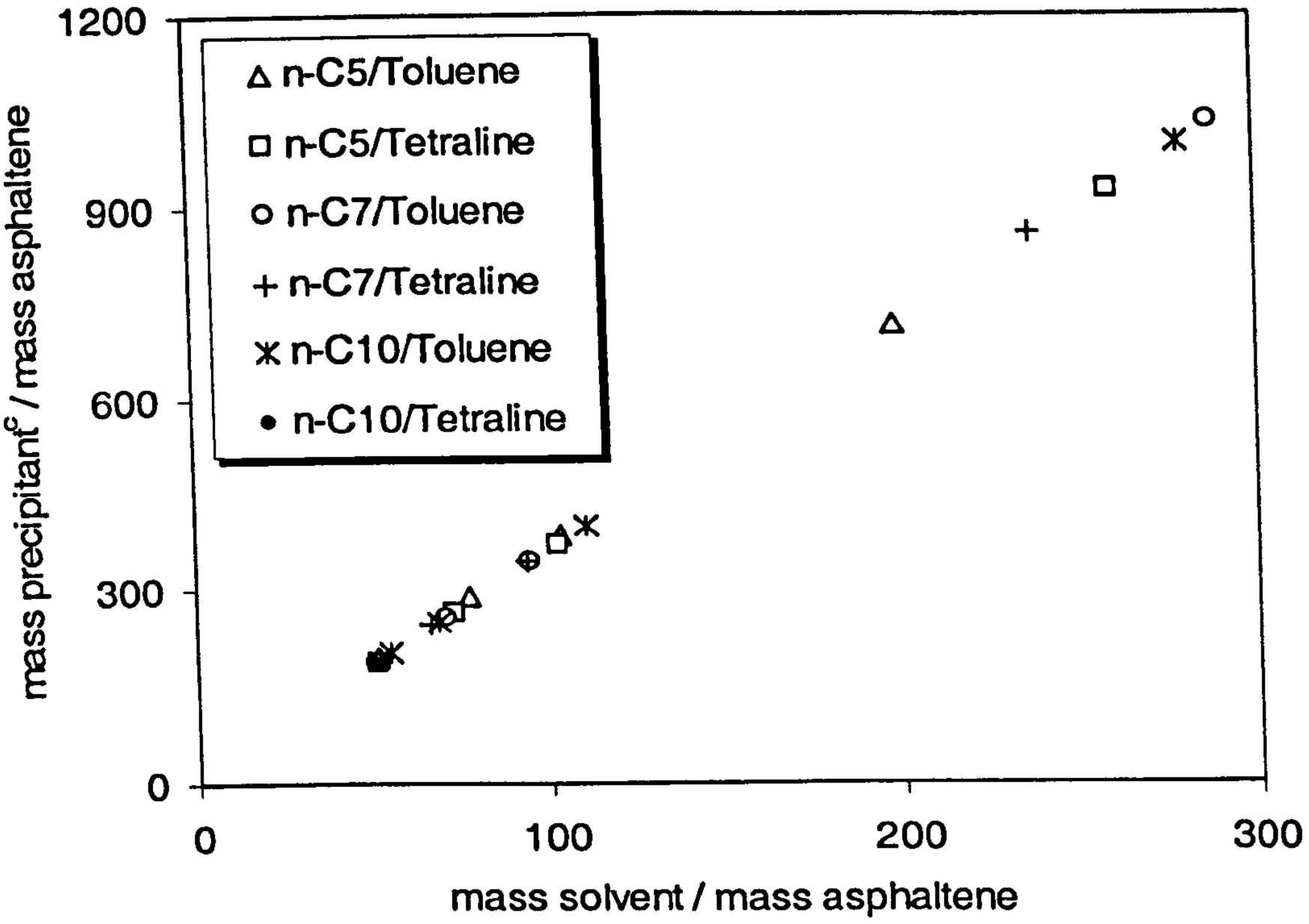

Figure 6.13 - The collapse of the data shown in Figure 6.11 for C_5-Asphaltenes with c = -0.84.

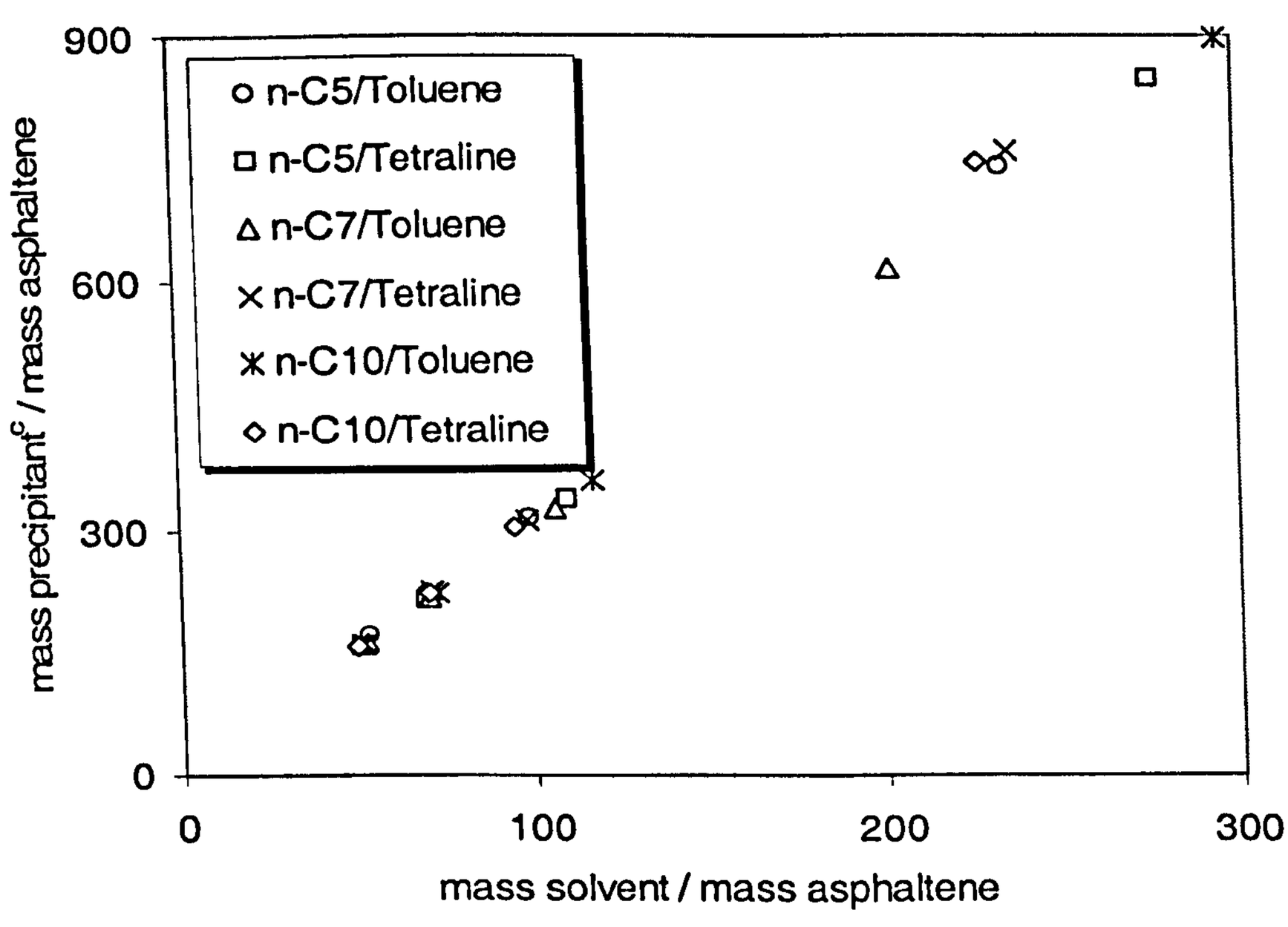

Figure 6.14 - The collapse of the data shown in Figure 6.12 for C_7-Asphaltenes with c = -0.65.

REFERENCES

1. Speight, J. G. The Chemistry and Technology of Petroleum, Marcel Dekker, New York. 1991.

2. Nellensteyn, F. I. The Colloidal Structure of Bitumens. The Science of Petroleum, Oxford University Press, London, 4, 2760, 1938.

3. Firoozabadi, A. Thermodynamics of Hydrocarbon Reservoirs, McGraw-Hill, 1999.

4. IP 143/90 (Standard Number) Asphaltene (heptane insolubles) in Petroleum Products, Standards for Petroleum and its Products, Institute of Petroleum, London, UK, 143.1-143.7, 1985.

5. Andersen, S. I.; Speight, J. G. Thermodynamic models for asphaltene solubility and precipitation. *Journal of Petroleum Science and Engineering* 1999, *22*, 53-66.

6. Hirschberg, A.; DeJong, L. N. J.; Schipper, B. A.; Meijer, J. G. Influence of Temperature and Pressure on Asphaltene Flocculation. *SPE J.* June 1984, *24*, 283-293.

7. Rassamdana, H. et al. Asphalt Flocculation and deposition: I. The onset of Precipitation. *AIChE J.* 1996, *42*, 10 (Also: Rassamdana, H.; Sahimi, M. Asphalt Flocculation and deposition: II. Formation and Growth of Fractal Aggregates. *AIChE J.* 1996, *42(12)*, 3318-3332.

8. Chung, F.; Sarathi, P.; Jones, R. Modeling of Asphaltene and Wax Precipitation, *DOE*, Topical Report No. NIPER-498, January 1991.

9. Leontaritis, K. J. Asphaltene deposition: a comprehensive description of problems manifestations and modelling approaches. *Proceedings of the SPE Production Operations Symposium, Oklahoma City*, March 1989, *13/14*, 599-609.

10. Ramos, A. C. S. et al. Reversibility and Inhibition of Asphaltene Precipitation in Brazilian Crude Oils. *SPE 38967 presented at the 1997 American and Caribbean Petroleum Engineering Conference and Exhibition, Rio de Janeiro,* 30 August - 3 September 1997.

11. Cimino, R.; Correra, S.; Sacomani, P. A.; Carniani, C. Thermodynamic Modelling for Prediction of Asphaltene Deposition in Live Oils. *SPE 28993, Presented at the SPE International Symposium on Oilfield Chemistry held in San Antonio, TX, USA,* 14-17 February 1995.

12. Pan, H.; Firoozabadi, A. Thermodynamic Micellization Model for Asphaltene Precipitation From Reservoir Crudes at High Pressures and Temperatures. *SPE Prod. and Fac.* February 2000a, *15(1)*, 58-65.

13. Pan, H.; Firoozabadi, A.; Fotland, P. Pressure and Composition Effect on Wax Precipitation: Experimental Data and Model Results. *SPE Prod. and Fac.* Nov. 1997, 250.

14. Godbole, S. P.; Thele, K. J.; Reinbold, E.W. EOS Modelling and Experimental Observations of Three- Hydrocarbon-Phase Equilibria. *SPE RE* May 1995, 101.

15. Kokal, S. L. et al., Measurement and Correlation of Asphaltene Precipitation from Heavy Oils by Gas Injection. *J. Can. Pet. Tech.* 1992, *31*, 24.

16. Storm, D. A.; Barresi, R. J.; Sheu, E. Y. Development of Solid Properties and Thermochemistry of Asphalt Binders in the 25-65 °C Temperature Range. *Energy Fuels* 1996, *10*, 855.

17. Flory, P. J. *J. Chem. Phys.* 1941, *9*, 660 (Also: Flory, P. J. *J. Chem. Phys.* 1942, *10*, 51. Flory, P. J.; Rehner, J. *J. Chem. Phys.* 1943, *11*, 521. Flory, P. J. Principles of polymer chemistry, Cornell University Press, New York, 1953).

18. Scott, R. L; Magat, M. The Thermodynamics of High-Polymer Solutions: The Free Energy of Mixing of Solvents and Polymers of Heterogeneous Distribution. *The Journal of Chemical Physics* 1945, *13/5*, 172-177.

19. Burke, N. E.; Hobbs, R. E.; Kashou, S. F. Measurement and Modelling of Asphaltene Precipitation. *Journal of Petroleum Technology* November 1990, 1440.

20. Kawanaka, S.; Park, S. J.; Mansoori, G. A. The role of asphaltene deposition in EOR gas flooding: a predictive technique. *Proceedings of the SPE/DOE Enhanced Oil Recovery Symposium, Tulsa, Oklahoma*, 617-627, 17-20 April 1988.

21. Park, S. J. A thermodynamic polydisperse polymer model: asphaltene flocculation, aggregation and deposition; Ph.D dissertation, University of Illinois, Chicago, USA, 1989.

22. Nghiem, L. X.; Hassam, M. S.; Nutakki, R. Efficient Modelling of Asphaltene Precipitation. SPE 26642 *presented at the 68th Annual Technical Conference and Exhibition of the SPE held in Houston, Texas*, 1993.

23. Leontaritis, K. J.; Mansoori, G. A. Asphaltene Flocculation During Oil Production and Processing: A Thermodynamic Colloidal Model, SPE 16258, *SPE Int. Symp. Oil field Chemistry*, San Antonio, TX, 4-6 February 1987.

24. Victorov, A. I.; Firoozabadi, A. Thermodynamic Micellization Model of Asphaltene Precipitation from Petroleum Fluids. *AIChE J.* June 1996, *42(6)*, 1753-1764.

25. Pan, H.; Firoozabadi, A. Thermodynamic Micellization Model for Asphaltene Aggregation and Precipitation in Petroleum Fluids. *SPE Prod. and Fac.* May 1998, 118-127.

26. Pan, H.; Firoozabadi, A. Thermodynamic Micellization Model for Asphaltene Precipitation From Reservoir Crudes at High Pressures and Temperatures. *SPE Prod. and Fac.* February 2000a, *15(1)*, 58-65 (See also: Pan, H.; Firoozabadi, A. Thermodynamic Micellization Model for Asphaltene Precipitation From Reservoir Crudes at High Pressures and Temperatures. SPE 38857, *Presented at the SPE*

Annual Technical Conference and Exhibition held in San Antonio, Texas October 1997. Also: Pan, H.; Firoozabadi, A. Complex Multiphase Equilibrium Calculations by Direct Minimization of Gibbs Free Energy by Use of Simulated Annealing. *SPE Res. Eval. & Eng.* February 1998, 36-42).

27. Pan, H.; Firoozabadi, A. Thermodynamic Micellization Model for Asphaltene Precipitation Inhibition. *AIChE J.* February 2000b, *46(2)*, 416-426.

28. Wu, J.; Prausnitz, J. M.; Firoozabadi, A. Molecular-Thermodynamic Framework for Asphaltene-Oil Equilibria. *AIChE J.* May 1998, *44(5)*, 1188-1199.

29. Wu, J.; Prausnitz, J. M.; Firoozabadi, A. Molecular Thermodynamics of Asphaltene Precipitation in Reservoir Fluids. *AIChE J.* January 2000, *46(1)*, 197.

30. Andersen, S. I.; Potsch, K. Solid organic deposition from a gas condensate field. *AIChE National Spring Meeting* 14-18 March 1999, 328-334.

31. Thou, S.; Ruthammer, G.; Potsch, K. Detection of Asphaltenes Flocculation Onset in a Gas Condensate System. SPE 78321, *presented at the SPE 13th European Petroleum Conference held in Aberdeen, Scotland, U.K* 29-31 October 2002.

32. Parkash, S.; Moschopedis, S.; Speight, J. G. Fuel 1997, *58*, 877.

33. Peng, D.-Y.; Robinson, D. B. A New Two-Constant Equation of State. *Ind. Eng. Chem. Fundam.* 1976, *15(1)*, 59-64.

34. Soave, G. Equilibrium Constants from a Modified Redlich-Kwong Equation of State. *Chem. Eng. Sci.* 1972, *27*, 1197-1203.

35. Twu, C. H. An Internally Consistent Correlation for Predicting the Critical Properties and Molecular Weights of Petroleum and Coal-Tar Liquids. *Fluid Phase Equilibria* 1984, *16*, 137-150.

36. Kesler, M. G.; Lee, B. I. Improve Predictions of Enthalpy of Fractions. *Hydro. Proc.* March 1976, 153-158 (Also: Lee, B. I.; Kesler, M.G. Improve Vapour Pressure Prediction. *Hydro. Proc.* July 1980, 163-167).

37. Danesh, A. PVT and Phase Behaviour of Petroleum Reservoir Fluids, Elsevier Science B.V., Amsterdam, The Netherlands, 1998.

38. Knapp, H.; Doring, R. Vapour-Liquid Equilibria for Mixtures of Low Boiling Substances' Berhens, D. and Eckerman R., Eds (Dechema Chemistry Data Ser.), Part I-Binary System, 1986.

39. Chueh, P. L.; Prausnitz, J. M. Vapour-Liquid Equilibria at High Pressures. Calculation of Partial Molar Volume in Non-Polar Liquid Mixtures. *AIChE J.* 1967, *13(6)*, 1099-1113.

40. Botet, R.; Jullien, R. Size distribution of clusters in irreversible kinetic aggregation. *Journal of Physics A: Mathematical and general,* 1984, *17*, 2517-2530.

41. Yarranton, H.W.; Masliyah, J. H. *AIChE J.* 1996, *44(5)*, 1188-1199.

42. Monteagudo, J. E. P; Lage, P. L. C.; Rajagopal, K. Towards a polydisperse molecular thermodynamic model for asphaltene precipitation in live oil. *Fluid Phase Equilibria* 2001, *187-188*, 443-47.

43. Barton, A. F. M. Handbook of Solubility Parameters and Other Cohesion Parameters. 2nd Edition, CRC Press, Boca Raton, FL, USA, 1985.

CHAPTER 7

AN $EoS + G^E$ BASED MODEL FOR PREDICTING ASPHALTENE PRECIPITATION

7.1. INTRODUCTION

In chapter 6, a new activity coefficient based model was proposed, which took into account the polydispersity of asphaltenes. It was shown that the results of this model were in a better agreement with experimental data in comparison with leading activity coefficient based models in the literature. The main limitation of activity coefficient models is that they cannot efficiently account for the effect of pressure on condensed phases.

In the present work, a thermodynamic model based on equation of state (*EoS*) is introduced. The main assumption is that the asphaltene precipitation is a reversible process, allowing the use of molecular thermodynamics. It is also assumed that the asphaltenes form a liquid phase free of other components. Asphaltene is defined as the aromatic part of the heavy end (plus fraction). The non-aromatic part of the plus fraction is considered non-precipitating. It is assumed that these two parts in the plus fraction have *different* critical properties, acentric factor and binary interaction parameters (*BIP*). Then, the model is extended by characterising the asphaltene with a continuous distribution of components. The polydispersity is taken into account in critical properties, molecular weight and mole fractions.

In this work appropriate mixing rules for equation of state based on the *Gibbs free energy* are employed to describe the condensate phases. Using such mixing rules, the

precipitation model can distinguish between the compounds of similar characteristics for vapour-liquid equilibrium, such as n-C_7 and benzene that are vastly different as one promotes precipitation the other demotes it.

One of the most commonly used model based on *EoS* is that reported by Nghiem et al. (1), a review is made on this model before discussing the new model.

7.2. LITERATURE MODEL: EoS - BASED

Nghiem et al. (1) developed a model based on *EoS* and *random mixing rules* to quantify asphaltene precipitation in the reservoir fluid system, which is frequently referred in the literature. In this model, the asphaltene component is characterised by dividing the heaviest component (typically C_{30+} or C_{31+}) into two pseudo-components, one precipitating (C_B) and the other non-precipitating (C_A) component. These two pseudo-components have the *same* molecular weight, critical properties and acentric factor but their binary interaction parameters with light components are different. The precipitating component has larger interaction parameters with the light components. An average value is used for the interaction parameter with the light components and interaction parameters between the precipitating component and heavy components are set to zero. The precipitating component forms a pure asphalt phase. Nghiem et al. (1) used experimental data to fit the parameters of their model, however quantitative results were not completely satisfactory. The model was later modified by incorporating the *Péneloux* and *Rauzy* (2) shift volume method (3). They also used a *BIP* correlation based on critical volume of components suggested by *Chueh-Prausnitz* (4), where different values of the exponents were assigned (one for the asphaltene component and the components C_1-N_2 through C_5, the second value for the asphaltene component and the components C_6 through the heavy plus fraction and

the third value for all other pairs of hydrocarbon components) (5). The authors made the modification with an intention to improve the fugacity calculation; however the quantitative results remained almost unchanged.

A preliminary study shows that Nghiem et al. model (1) is not in better agreement with the aromatic nature of asphaltenes. For example, they used the experimental data from Burke et al. (6) for tuning and comparing their model which only describe the heavy end by C_{7+} without addressing the nature of asphaltenes and interaction with aromatics such as benzene and toluene. These data together with the fluid characterisation proposed by Nghiem et al. (3) are presented in Tables 7.1 and 7.2.

In order to calculate specific gravity of the components, the method of *Whitson* (7) is used. In this method, the *Whitson* characterisation factor, *C*, is calculated as below:

$$C = [0.16637\, S_D \sum_{k=1}^{N} z_k M_k^{0.86459} / (z_D M_D)]^{-0.84573} \qquad (7.1)$$

where *D* represents the plus fraction and *z*, *M* and *S* are mole fraction, molecular weight and specific gravity, respectively. Then the specific gravities of components are calculated using the following relation:

$$S_k = 6.0108\, M_k^{0.13541} C^{-1.18241} \qquad (7.2)$$

On the other hand, the *Watson* characterisation factor, K_w, of the components can be calculated using the following relation:

$$K_w = 4.5579\, M^{0.15178} S^{-0.84573} \qquad (7.3)$$

These calculations have been shown in Table 7.3. As can be seen, the *Watson* characterisation factor for C_{31B+}, which represents the asphaltenic component is *11.9*, which is not in good agreement with the aromatic nature of asphaltenes (the *Watson*

characterisation factor for aromatic components is between 8.5 and 11 (8)). This could be due to this fact that equation 7.1 was developed for typical single carbon number groups and not aromatic fractions. Also, it seems that assuming the same critical properties and acentric factor for plus fractions C_A and C_B may not be valid and the properties of precipitating components should be different from those of non-precipitating and should be calculated accordingly. In other words, using two different sets of critical properties and acentric factor for plus fractions C_A and C_B is in better agreement with the aromatic nature of asphaltene. That is, it is assumed that the plus fraction C_A has naphthenic nature and its critical properties and acentric factor are calculated using the correlation reported by Pan et al. (9), however as this component does not strongly affect the results, its critical properties and acentric factor can be calculated like other petroleum fractions in the reservoir fluid. For this plus fraction C_B the required properties are calculated by tuning the phase behaviour model to match some measured data.

7.3. THERMODYNAMIC MODEL

As mentioned earlier, the main assumption in this model is that asphaltene precipitation is considered as a reversible process, and thus, allowing the use of molecular thermodynamics. It is also assumed that the asphaltene forms a liquid phase free of other components, in other word only asphaltene precipitate into a new condensed phase.

A typical asphaltene precipitation problem involves multiphase equilibrium, e.g., vapour/ gas, liquid hydrocarbon, and asphaltene phases. Furthermore, chemical inhibitors, may also be present, leading to relatively complex calculations.

For a chemical system to be at thermodynamic equilibrium, the chemical potential of each component throughout the system must be uniform:

$$\mu_{i1} = \ldots = \mu_{ij} = \ldots = \mu_{i\pi} \quad , \qquad i = 1, 2, \ldots, N \tag{2.1}$$

where μ_{ij} is the chemical potential of component i in phase j, N is the number of components and π is the number of phases. For an isothermal system equation 2.1 reduces to equality of fugacity for each component in different phases:

$$f_{i1} = \ldots = f_{ij} = \ldots = f_{i\pi} \quad , \qquad i = 1, 2, \ldots, N \tag{2.2}$$

In the most general case, i.e., when all components are present in all phases, there will be $N(\pi\text{-}1)$ such equations. In addition, material balances impose another set of $N+\pi$ equations:

$$z_i = \sum_j^{\pi} F_j x_{ij} \qquad i=1,2,\ldots,N \qquad j=1, 2, \ldots, \pi \tag{2.3}$$

$$\sum_i^N x_{ij} = 1 \qquad i=1,2,\ldots,N \qquad j=1, 2, \ldots, \pi \tag{2.4}$$

where z_i is the specified molar composition of component i in the feed, F_j is the molar fraction of phase j, and x_{ij} is the mole fraction of component i in phase j. Totally, equation 2.2 to 2.4 results in $\pi(N+1)$ equations with an equal number of unknowns.

Concerning asphaltene equilibrium calculations, two cases are of interest, asphaltene precipitation envelope calculations where $F_{asphalt} = 0$, and asphaltene precipitation calculations where $F_{asphalt} \neq 0$ for all included phases. In this work a simple multiphase flash routine is adopted to solve the governing equations, explicitly expressing the fugacities of all components of all phases, as functions of temperature, pressure and composition.

An appropriate *EoS* is used to calculate fugacities. As mentioned before, it is also assumed that the asphalt phase is liquid- like containing asphaltene only. The liquid state of asphaltene corresponds with the visual observations, where the precipitated phase is seen as a sticky phase, at reservoir temperatures.

The upper boundary of asphaltene precipitation is a thermodynamic transition of asphaltenes dissolved in a single-phase hydrocarbon above its saturation pressure to the precipitated phase. To calculate the upper boundary of asphaltene precipitation, a two- phase equilibrium calculation is made:

$$f_i^{HC} = f_i^{D} \qquad i = M+1, N \tag{2.52}$$

The lower boundary of asphaltene precipitation is a thermodynamic transition of asphaltenes from the precipitated phase to a two-phase hydrocarbon system. For calculation of the lower boundary of asphaltene precipitation, a vapour-liquid-liquid equilibrium calculation is done.

$$f_i^{V} = f_i^{L} \qquad i=1,M \tag{2.53}$$

$$f_i^{V} = f_i^{L} = f_i^{D} \qquad i= M+1, N$$

In the above equations, f_i is the fugacity of component i, and superscripts *HC, V, L* and *D* represent the hydrocarbon, vapour, liquid and deposit (asphalt) phases, respectively and the subscripts *M* and *N* correspond to the number of non-asphaltenic components and the total number of components in the system, respectively.

After finding these boundaries, the amount of the precipitated asphaltene is estimated by either a two-phase flash calculation (between the upper point and the saturation point) or a vapour-liquid-liquid flash calculation (between the lower point and the saturation point). Otherwise, to find the number of the existing phases in equilibrium,

it is necessary to do a phase stability analysis by using the Gibbs free energy minimisation method. For this purpose, a reasonable maximum number of phases at equilibrium is assumed and then the model searches for the non-existing phases using material balance restrictions, as discussed in the negative flash approach (10).

7.4. FLUID CHARACTERISATION

Fluid characterisation affects properties and concentration of identified asphaltenes. Depending on the asphaltene content, a crude may be originally unstable or reveal no precipitation. Therefore, a detailed characterisation of the crude is indispensable for asphaltene precipitation modelling.

For characterising the heavy end, a linear relationship is normally assumed between the molecular weight of single carbon number (*SCN*) and logarithm of mole fraction. A detail description of this method has been reported by Danesh (8). It should be noted that this assumption is more valid for gas condensate systems than oil systems.

For any model based on *EoS*, it is necessary to know the mole fraction of asphaltenes in the reservoir fluid. Unfortunately, only the asphaltene weight fraction at stock tank oil (*STO*) conditions is generally reported. The measurement of the average molecular weight of asphaltenes is a challenge because they are non-volatile, self-associate to form colloid in solvents and strongly adsorbed to most surfaces. The lack of volatility causes mass spectrometry to measure values that are low; adsorption causes gel permeation chromatography to yield low values and self-association produces high values with measurements in solvents, such as vapour pressure osmometry. The lesser of these appears to be vapour pressure osmometry with o-

dichlorobenzene as the solvent and at a temperature of 403.15 K. Experimental evidences indicate that break-up of the asphaltene self-association at these conditions.

Erickson et al. (11) have shown that the amount of normal paraffins in real reservoir fluids follows an exponential decay with the carbon number using high-temperature gas chromatography; the amount of normal alkanes becomes negligible at very high-molecular weights.

In this work, to estimate the asphaltene mole fraction, it is assumed that the aromatic part of the plus fraction is asphaltene. The non-aromatic part of the plus fraction is assumed to be non-precipitating component, with naphthenic nature. It is first assumed that asphaltenes form a single pseudo-component (This assumption, however, is relaxed later) and these two pseudo components in plus fraction have identical molecular weight but different critical properties, acentric factor and binary interaction parameters.

To determine the boundary between the ordinary aromatics and asphaltenes, the weight percent of asphaltenes precipitated at *STO* conditions is compared with the aromatic part of the heavy end. The aromatic distribution is approximated according to the equations reported by van Nes and Westen (12). They measured paraffin-naphthane-aromatic (*PNA*) distribution of several crude oils taken from the USA reservoirs and reported an expression (*n-d-M* method) based on the refractive index (n), density (d) and average molecular weight (M). Table 7.5 shows equations used in this work.

Van Nes and Westen (12) have mentioned that if, in exceptional cases, no data are available at 293.15 K or 343.15 K but at some other temperature, similar equations are

valid, the numerical constants for which can easily be derived from those of Table 7.5 by linear interpolation. They have given a numerical example of such interpolation and shown that such interpolation will not introduce serious errors. In our calculations, the above equations have been used at 293.15 K. Buckley et al. (13) have reported that the estimated n for asphaltene is about 1.6

Several correlations exist in the literature for calculating the critical properties and the acentric factor of petroleum fractions. In this work, the Twu correlation (14) for critical properties and the Lee-Kesler correlation (15) for the acentric factor are used for all petroleum fractions (except for asphaltene), as recommended by Danesh (8). The values of the acentric factor and the critical properties for the non-precipitating component of the plus fraction are calculated using the Pan et al. correlation (9) for naphtenes. The values of acentric factor and critical properties for asphaltene are used as tuning parameters.

The standard binary interaction parameters, which have been used in this work, derived from Knapp and Doring (16). For the *BIP*s between hydrocarbon-hydrocarbon (excluding those reported in Knapp and Doring), the Chueh-Prausnitz (4) correlation has been used:

$$k_{ij} = \left[1.0 - \left(\frac{2(V_{c,i}V_{c,j})^{1/6}}{V_{c,i}^{1/3} + V_{c,j}^{1/3}}\right)^{\bar{\theta}}\right] \tag{6.30}$$

In this correlation, the power parameter ($\bar{\theta}$) is tuned by, at least, one experimental bubble point pressure.

7.5. COMPARISON OF IMPROVED MONODISPERSE MODEL WITH EXPERIMENTAL DATA

In this work, asphaltene precipitation in a live oil system from the Middle East region is studied, using the data reported by Jamaluddin et al. (17). The reservoir and fluid properties are presented in Tables 7.6 and 7.7. As can be seen, the API gravity for this oil is 39 confirming a typical oil sample. The asphaltene content of this oil is measured at 1.3 %(w/w).

As can be seen in Figures 7.1 and 7.2, the pressure-temperature (*P-T*) region defining the precipitation conditions above the bubble point is defined as the upper boundary of asphaltene precipitation. Above the upper boundary of asphaltene precipitation curve, there is only single-phase oil. When reducing pressure at a given temperature, a new liquid phase with high asphaltenic content starts to form on the upper boundary of asphaltene precipitation. The amount of precipitated asphaltenes increases as the pressure decreases. The amount of precipitation reaches a maximum at the bubble point pressure. Amounts decrease as the pressure decreases farther below the bubble point pressure. The *P-T* region below the bubble point is defined as the lower boundary of asphaltene precipitation. Below the lower boundary, there is no asphaltene.

Table 7.8 shows the experimental data for upper and lower boundaries of asphaltene precipitation as well as bubble point pressures for this oil, which have been measured using *ART* (Acoustic resonance technique), *LST* (Light-scattering technique) and gravimetric methods (17).

Figure 7.1 shows the upper and lower boundaries of asphaltene precipitation as well as bubble point pressures for this oil. Asphaltene content of the reservoir fluid as a

function of pressure at reservoir temperature (389.15 K) has been shown in Figure 7.2.

In Figure 7.1, only the experimental data at 389.15 K have been used for tuning. As mentioned earlier, first the hydrocarbon-hydrocarbon *BIP*s were simultaneously adjusted (using $\bar{\theta}$ in equation 6.30) to match the measured bubble point pressure at 389.15 K. Then, the measured upper boundary of asphaltene precipitation at 389.15 K was used to tune the critical properties and acentric factor of asphaltenes, assuming asphaltenes as a pseudo-component. Obviously the more data for tuning, the better the model predictions. The power parameter ($\bar{\theta}$) tuned to be 0.367, using the *SRK-EoS* and the critical properties and the acentric factor of asphaltene are given in Table 7.9.

Figure 7.1 shows that the predicted phase boundaries are in a good agreement with the experimental data. However it cannot predict the amount of the precipitated phase reliably nor the effect of changes in compositions on the asphaltene phase. To solve these shortcomings, we introduce property distribution functions for asphaltenes, as explained in the following section.

7.6. ASPHALTENE CHARACTERISATION

In the previous monodisperse model, asphaltenes were assumed as one pseudo-component. The critical properties and acentric factor of asphaltene as well as the binary interaction parameters were generally determined by tuning of phase behaviour model against the experimental data. As mentioned before, such models, which consider asphaltenes as one pseudo-component (monodisperse) cannot predict the effect of changes in compositions. Andersen and Speight (18) reviewed this approach

and concluded that none of monodisperse models were able to quantitatively describe asphaltene precipitation. The main drawback is that they do not take into account the aggregation phenomenon of asphaltenes. This phenomenon leads to a molecular weight distribution of asphaltenes, which causes a polydispersity in asphaltene properties. This would explain the existence of a group of asphaltenes that will precipitate and a group that will remain in the oil. In addition, the experimental evidence that asphaltenes have different molecular weights leads to the use of concepts of thermodynamics of semi-continuous mixtures for modelling phase equilibrium.

In the present work, the effect of taking into account the polydispersity of asphaltenes in the model is studied by introducing distribution functions:

7.6.1. Molecular weight distribution function

As mentioned in chapter-6, the following equations proposed by Rassamdana and Sahimi (19) are used for asphaltenes molecular weight distribution function:

$$f(M_a)=c\left(\frac{(M_a-M_m)^{-2\varpi}}{M_a}\right)exp[-a(M_a-M_m)] \qquad (6.35)$$

where M_a is the continuous molecular weight of asphaltenes, M_m the minimum molecular weight of asphaltenes and a and c are parameters to be estimated. The c parameter is a normalisation constant obtained from:

$$\int_{M_m}^{\infty} f(M_a)\,dM_a=1 \qquad (6.36)$$

and the average molecular weight of asphaltenes is obtained from:

$$\int_{M_-}^{\infty} M f(M_a) \mathrm{d}M_a = \overline{M}_a \tag{6.37}$$

For a specified value of average molecular weight of asphaltenes $\overline{M}_a$, the value of a can be calculated. They proposed the following values for ϖ:

ϖ= -0.13 *for CO_2 titration*

ϖ= -0.50 *for normal-alkanes titration*

M_m=500 g/gmol

The above integrals are solved using a *quadrature* method as explained by Danesh (8).

7.6.2 Critical properties and acentric factor

The use of generalised single carbon number correlations, such as these of Twu (14) and Cavet (20), for calculating critical properties of asphaltenes with a *Watson* characterisation factor between 8.5 and 11 failed to produce physically meaningful results. For example, in *Cavet* correlation (20), negative *API* gravity is obtained as asphaltenes have specific gravities more than unity. Therefore correlations accounting for use of *PNA* fractions were considered:

Riazi and Al-Sahhaf (21) used the following equation to estimate the properties of paraffin, naphthene and aromatic (*PNA*) groups:

$$\theta = \theta_\infty - exp(a - bM^c) \tag{7.4}$$

where θ is a physical property such as the critical properties, acentric factor, normal boiling point, density and specific gravity, refractive index parameter, and surface tension and θ_∞ is the limiting value for that property as $M \rightarrow \infty$. Later, Pan et al. (9)

modified the correlation of Riazi and Al-Sahhaf (21) for the critical pressure (P_C) of *PNA* species with a molecular weight of more than 300 g/gmol:

$$P_C = A - B\exp(-CM) \tag{7.5}$$

where M is the molecular weight, $A = 4.85$, $B = 42.9311$ and $C = -0.00561927$.

They also proposed the following expression for estimating the acentric factor (ω) of aromatics:

$$\ln \omega = -36.1544 + 30.94\, M^{0.026261} \quad M \leq 800 \tag{7.6}$$

$$\omega = 2.0 \quad M > 800$$

Pan et al. (9) suggested that the critical properties and acentric factors for heavy aromatics should be only a function of the molecular weight. However they accepted the correlation of Riazi and Al-Sahhaf (21) for the critical temperature, which is a function of the boiling point and the molecular weight.

Almost all available correlations are based on data of compounds much lighter than asphaltenes. Hence extrapolation of these relations to asphaltene components may not be accurate. Considering the above relations and the average values reported in the literature for asphaltene, the following relations are suggested for the critical properties and the acentric factor of asphaltenes:

$$T_c = a\, M^b \tag{7.7}$$

$$P_C = c - 42.9311\, \exp(-0.00561927M) \tag{7.8}$$

$$\omega = d \tag{7.9}$$

$$Vc = 2500.0 \tag{7.10}$$

In the above relations, these values are proposed for the above parameters: $a = 880$, $b = 0.06$, $c = 8.5$ and $d = 2.0$, where the critical temperature, critical pressure and

critical volume are in *Kelvin*, *atm* and $cm^3/gmol$, respectively. However, these parameters can be tuned using experimental asphaltene flocculation / precipitation data.

7.6.3. K-values for asphaltene components

Considering asphaltene to be polydisperse, i.e. asphaltene is a mixture of components, the precipitation can be calculated in a manner analogous to a multiphase multi-component equilibrium. In this case, a liquid-liquid equilibrium (*LLE*) or vapour – liquid – liquid equilibrium (*VLLE*) should be performed, which requires appropriate equilibrium ratios for components involved to be estimated as the initial values to setup equations of state based models. The following method proposes a simple equation for estimating *K*-values of asphaltene components, which will be used as an initial guess in phase equilibrium calculations:

The equilibrium ratio can be determined by equating the fugacity of each asphaltene component in all phases:

$$x_i^{L2}\gamma_i^{L2}f_i^{oL2} = x_i^{L1}\gamma_i^{L1}f_i^{oL1} \tag{7.11}$$

$$K_i = \frac{x_i^{L2}}{x_i^{L1}} = \frac{\gamma_i^{L1}}{\gamma_i^{L2}} \tag{7.12}$$

where x_i, γi, f_i^o and K_i are the mole fraction , activity coefficient, standard state fugacity and equilibrium ratio of component *i* in both liquid phases, respectively. Superscripts *L1* and *L2* represent the oil-rich phase and the asphalte phase, respectively. Neglecting the pressure effect, the activity coefficients are estimated using the *Flory – Huggins* model (22). This model describes the equilibrium between a polymer and a solvent and predicts the solubility of the polymer in the solvent.

Using the above model for calculating the activity coefficients of asphaltenes in the liquid phase and assuming the activity coefficients of asphaltenes are unity in the precipitated phase, the following relation can be obtained:

$$K_i = exp\{1 - \frac{v_i^{L2}}{v_m} + \ln(\frac{v_i^{L2}}{v_m}) + \frac{v_i^{L2}}{RT}(\delta_m - \delta_i^{L2})^2\} \quad (7.13)$$

In the above relations, δ, v, R and T refer to the solubility parameter, molar volume, universal gas constant and temperature, respectively and subscripts i and m represent the *ith* asphaltene component and the oil, respectively.

Yarranton and Masliyah (23) obtained several asphaltene sub-fractions experimentally by adding previously precipitated asphaltene in a toluene (solvent) / hexane (precipitant) mixture with various solvent / precipitant ratios. Finally, they proposed the following relations for solubility parameter, density and molar volume of asphaltenes:

$$\delta_i = (0.367\,\rho_i)^{0.5} \quad (7.14)$$

$$\rho_i = 0.017\,M_i + 1080 \quad (7.15)$$

$$v_i = \frac{M_i}{\rho_i} \quad (7.16)$$

were ρ_i is density of the i^{th} asphaltene component in kg /m^3.

A preliminary study showed that contrary to the molecular weight and molar volume of asphaltenes, the density and solubility parameter of asphaltenes change in a small range. In other word, by assuming the polydispersity only in molecular weight of asphaltene sub-fractions, a simple relation can be obtained for estimating the K-values for asphaltene sub-fractions.

The solubility parameter of asphaltene has been reported to be in the range 20-22 $MPa^{0.5}$ (18, 24) and the density of the asphaltene is taken as 1280 kg / m^3 (25). The solubility parameter of oil is typically in the range 16-21 $MPa^{0.5}$. Therefore, assuming $\rho_i = 1200\ kg / m^3$ and $\delta_i = 20.5\ MPa^{0.5}$ for asphaltene components and $\rho_m =$ $850\ kg / kgmol$ and $\delta_m = 18.5\ MPa^{0.5}$ for the oil, the following equation can be obtained for estimating *K*-values of asphaltene sub-fractions at low-pressure conditions:

$$K_i = exp\{1 - \frac{17M_i}{24M_m} + \ln(\frac{17M_i}{24M_m}) + \frac{10M_i}{3RT}\} \qquad (7.17)$$

where $R = 8.314\ J/gmol\ K$ and T is in *Kelvin*. The above relation can be used as an initial guess for *K*-values, when a *LLE /VLLE* is made for calculating asphaltene flocculation / precipitation using an *EoS* method.

7.6.4. Mixing rules

Among the modern approaches presented in the literature to describe phase equilibria in mixtures, methods of the type "*EoS + Gibbs free energy*" seem to be the most appropriate for modelling mixtures with asymmetric components. Since the first proposals of *Huron* and *Vidal* (26), these models have been extensively used and applied to low and high pressure vapour-liquid, liquid-liquid and gas-solid equilibria. Knudsen et al. (27) evaluated the capability of different leading mixing rules to describe the phase behaviour of mixtures containing asymmetric compounds by comparing prediction with experimental data. The *Huron* and *Vidal* approach (26), based on the principle of excess Gibbs energy, overally performed more reliably than others. In this work, a modified version of the *Huron* and *Vidal* approach (28) is used to calculate attractive term. A detail description of fugacity calculations is given in

Appendix A.4. The *Gibbs free energy* term is calculated based on *Scott-Magat* theory (29) (The detail of the work is presented in Chapter-6):

$$\frac{a}{bRT}=\sum_i x_i\frac{a_i}{b_iRT}+\frac{1}{A}\left(\frac{G^E}{RT}+\sum_i x_i\ln\frac{b}{b_i}\right) \tag{7.18}$$

$$b=\sum_i x_i b_i \tag{7.19}$$

In the above mixing rules, the solubility parameter of asphaltenes, the solubility parameter of maltene and the molecular volume of maltene are necessary. The solubility parameter of asphaltenes δ_a can be calculated using the following relation (6):

$$\delta_a=20.04\,[1-1.07\times 10^{-3}(T-273.15)] \tag{6.27}$$

where T is in *Kelvin* and δ_a is in $MPa^{0.5}$. The solubility parameter of the maltene can be calculated from:

$$\delta_m=\sqrt{\frac{\Delta u_m^{\,v}}{V_m}} \tag{6.28}$$

where $\Delta u_m{}^v$ is the energy change upon isothermal vaporisation of one mole of the maltene to the ideal gas state and V_m is the molecular volume of the maltene, which is the average value of molecular volume of each component in the maltene. $\Delta U_m{}^v$ is calculated using the following method.

7.6.4.1. Prediction of vaporisation enthalpy of hydrocarbons at the normal boiling temperature

The enthalpy of vaporisation data is important in many applications. They can be involved in heat flux calculations of many production and processing facilities. Further, as ingredients of the *solubility parameter*, they are an indirect essential tool

for the correlation and prediction of many physical phenomena. The enthalpy of vaporisation data are usually calculated at the normal boiling point temperature through an appropriate correlation and then are extended to the required temperature by using the well-known relation of *Watson* (29) ($\Delta H^{vap}=K[1-T_r]^{0.38}$).

The correlations for predicting the enthalpy of vaporisation are grouped into two classes: The first comprises equations relating the enthalpy of vaporisation at the normal boiling point temperature to the critical values and the normal boiling point (For review, see Reid et al. (31)). The second class consists of empirical correlations, which relate the enthalpy of vaporisation at the normal boiling temperature to a few easily obtainable parameters such as the normal boiling point, the molecular weight and specific gravity. Since the critical constants of petroleum fractions may be unknown or inaccurately evaluated with empirical methods, the first class of correlations can suffer a significant loss of accuracy for petroleum fractions. The second class of correlations with the required input parameters, which are known characterisation properties of petroleum fractions, are practical in petroleum industry (32, 33).

Table 7.10 summarises the second class of correlations with the required input parameters. As can be seen a few equations have been reported for the second class. The majority of these correlations were developed based on experimental data of vaporisation enthalpy for pure hydrocarbons, where direct calorimetric data of vaporisation enthalpy for petroleum fractions were not available at that time. Fang et al. (33) have recently reported these experimental data for 58 petroleum fluids and have developed a new correlation and showed that their correlation gives more accurate results, particularly for heavy hydrocarbons.

The following equation has been developed in this study for predicting enthalpy of vaporisation of hydrocarbons:

$$\Delta H^{vap} = 10.69884 + 0.0005091 T_b^{0.800796} S^{0.1519889} (lnT_b + T_b) \quad (7.20)$$

where ΔH^{vap} is in *kJ/gmol*. As can be seen, the new correlation has a similar form as the correlation of Gopinathan and Saraf (34) and Riazi and Daubert (35), in which *the normal boiling point temperature, and specific gravity are used as input variables.* The parameters of this equation were tuned using experimental enthalpy of vaporisation data for 58 petroleum fractions in a wide boiling point range from 231.1 to 722.8 K obtained from four different crude oils (One from Russia, one from Iran and two from China) and 64 pure hydrocarbons (C_3-C_{30}) reported in Tables 7.11 and 7.12, respectively. These tables also show comparisons of enthalpy of vaporisation calculated by various correlations. As it can be observed, the newly developed correlation yields good results, especially for heavy hydrocarbons and petroleum fractions. It can be seen from Table 7.11 that the average absolute deviation (*AAD%*) for Fang et al. (33) correlation and this work are the lowest of the seven correlations. *The new correlation has four universal parameters and only two variables (normal boiling point temperature and specific gravity) are used as inputs.* It should be noted that other correlations gave reasonable results for the lower and middle petroleum fractions but unacceptable values for the heavier fractions. This may be due to the fact that these methods were essentially developed for pure hydrocarbons, that covered only a limited boiling point range.

In addition, the new correlation can be used in a wide boiling point range and has a satisfactory accuracy. Independent data can be used to further investigate the reliability of the correlation.

7.7 MODEL RESULTS

As mentioned in Chapter-6, Cimino et al. (37) performed some tests in order to find flocculation points of dissolved asphaltenes in different ratios of solvent and precipitant and then indicated that the precipitated asphaltenes do dissolve in appropriate solvents and at flocculation, the ratio of "solvent mass per asphaltene mass" and "precipitant mass per asphaltene mass" is linear. Figures 7.3 – 7.5 show a comparison between the behaviour of *Tradditional activity coefficient* based model (38), *colloidal* model (39), Cimino et al. model (37) and model developed in this study and some experimental data on a stock tank oil reported by Cimino et al. (37). As can be seen, the capability of *colloidal* model (39) and *Tradditional activity coefficient* based model (38) to re-produce the observed bahaviour is poor. However, the developed model produces encouraging results.

Figure 7.1 shows experimental and predicted upper and lower boundaries of asphaltene precipitation as well as bubble point pressures for the live oil system reported by Jamaluddin et al. (17). As mentioned earlier, the reservoir and fluid properties are presented in Tables 7.6 and 7.7. Experimental and predicted asphaltene content of the reservoir fluid as a function of pressure at reservoir temperature (389.15 K) has also been shown in Figure 7.2. In Figure 7.1, all experimental data have been used for tuning the polydispers model. The model is then used to predict asphaltene content of the reservoir fluid as a function of pressure. Figure 7.2 shows improvements in prediction of the amount of the precipitated phase using the polydisper thermodynamic model.

To further evaluate the developed model for prediction of asphaltene precipitation, the live oil given in Table 7.13 was used along with the fluid characterisation indicated in

Table 7.14. The molecular weights and mole fractions of asphaltene components were calculated using equation 6.35 (assuming $\varpi = -0.13$) and a quadrature method (8). As mentioned earlier, the *Twu* correlation (14) for critical properties and the *Lee-Kesler* correlation (15) for acentric factor are used for all petroleum fractions except for asphaltenes. Equations 7.7 to 7.10 were used for calculating the critical properties and acentric factor of asphaltene components. The power coefficient in the *Chueh - Prausnitz* correlation (4) was adjusted to match the bubble point pressure of the mixture. The Peng-Robinson (*PR*) *EoS* (36) was used to perform phase equilibrium calculation. The acentric factor of asphaltene was adjusted using the dependent data illustrated in Figure 7.6. As can be seen, this model shows a good trend. On the other hand, some inconsistency is observed among the experimental data. Experimental data at 50 and 85 mole% of solvent show unusual values. It seems these values should be lower than those showed in Figure 7.6. That means the precipitation data at 50 and 85 mole% of solvent may not be correct.

The dead oil given in Table 7.16 is then used along with the fluid characterisation indicated in Table 7.17. Table 7.18 shows mole% of diluent in diluent + tank oil (or cm^3 of diluent /g of oil). The *Twu*'s (14) correlation for critical properties and the *Lee-Kesler* (15) correlation for acentric factor are used for all petroleum fractions except for asphaltenes. The previously suggested equations were used for calculating the critical properties and acentric factor of asphaltene components. The Peng-Robinson (*PR*) *EoS* (36) was used to perform phase equilibrium calculation.

Table 7.19 shows experimental and predicted asphaltene precipitation from the tank oil using the *EoS* + G^E model. The molecular weight of asphaltene was adjusted using the dependent data illustrated in Table 7.19. The trend of the model is in good

agreement with that reported by Pan and Firoozabadi (9) that the amount of the precipitated asphaltene slighty decreases at very high-concentrations of n-alkanes. Obviously, the predictions of the model can improve using more data for tuning.

7.8 CONCLUSIONS

In this work a monodisperse thermodynamic approach based on *EoS* was first developed for predicting asphaltene precipitation (Page 225). This model could predict the effect of temperature and pressure on asphaltene phase boundaries. However, it could not reliably predict the amount of the precipitated phase nor the effect of changes in compositions (i.e. solvent/ gas injection) (section 7.5). To solve this shortcoming, the polydispersity of asphaltenes was taken into account in molecular weight, mole fraction and critical properties (section 7.6). An appropriate mixing rule based on "*EoS + Gibbs free energy*" method was employed in order to obtain the attractive term (equation 7.18). Using this mixing rule, the precipitation model can distinguish the vast differences between compounds of similar characteristics for vapour-liquid equilibrium, such as n-C_7 and benzene, where one promotes precipitation the other demotes it.

Furthermore, a new correlation was developed to relate the enthalpy of vaporisation at the normal boiling temperature to the normal boiling point, and the specific gravity of hydrocarbons and petroleum fractions (equation 7.20). This correlation worked well for a wide range of pure hydrocarbons and petroleum fractions and gave reasonable improvement to the existing methods, particularly for the heavy petroleum fractions and hydrocarbons.

TABLES

Table 7.1 - Composition (mole%) and properties of investigated oil (6).

Component	mole %
N_2	0.57
CO_2	2.46
C_1	36.37
C_2	3.47
C_3	4.05
$_i$-C_4	0.59
$_n$-C_4	1.34
$_i$-C_5	0.74
$_n$-C_5	0.83
C_6	1.62
C_{7+}	47.96
Total	100
C_{7+} molecular weight	329
C_{7+} sp.gr	0.9594
Live-oil molecular weight	171.4
API gravity of stock tank oil	19
Reservoir temperature/ K	373.15
Saturation pressure/ MPa	20.33

Table 7.2 - Modelled fluid composition (3).

Component	mole%	M
CO_2	2.46	44.01
N_2 & C_1	36.94	16.23
C_2	3.47	30.07
C_3	4.05	44.09
C_4	1.93	58.12
C_5	1.57	72.15
C_6 -C_7	4.35	92.67
C_8 -C_{13}	13.409	143.32
C_{14} -C_{19}	9.434	227.48
C_{20} -C_{24}	5.686	305.37
C_{25} -C_{30}	4.951	381.76
C_{31A+}	7.681	665.62
C_{31B+}	4.068	665.62
Total	100.0	

M: Molecular weight

Table 7.3 - *Watson* characterisation factor for C_{7+} fractions.

Component	mole%	M	S	K_w	z	zM	$zM^{0.86459}$	C
CO_2	2.46							
N_2	0.57							
C_1	36.37							
C_2	3.47							
C_3	4.05							
i-C_4	0.59							
n-C_4	1.34							
i-C_5	0.74							
n-C_5	0.83							
C_6	1.62							
C_7	2.73	96	0.7943	11.1	0.0569	5.4646	2.945	
C_8-C_{13}	13.4	143.32	0.8385	11.2	0.2796	40.072	20.46	
C_{14}-C_{19}	9.43	227.48	0.8927	11.4	0.1967	44.745	21.46	
C_{20}-C_{24}	5.69	305.37	0.929	11.6	0.1186	36.206	16.68	
C_{25}-C_{30}	4.95	381.76	0.9575	11.7	0.1032	39.412	17.62	
C_{31A+}	7.68	665.62	1.0324	11.9	0.1602	106.61	44.21	
C_{31B+}	4.07	665.62	1.0324	**11.9**	0.0848	56.46	23.41	
Total					1.0	328.96	146.8	9.341

M: Molecular weight of component *i* in C_{7+} fraction
S: Specific gravity of component *i* in C_{7+} fraction
K_w: Watson characterisation factor of component *i* in C_{7+} fraction
z: Specific gravity of component *i* in C_{7+} fraction
C: Whitson characterisation factor

Table 7.4 – Physical properties of studied reservoir fluid.

Component	mole%	M	S	T_b /K	T_C/K	P_C / MPa	V_C/ m^3/kgmol	ω
CO_2	2.46							
N_2	0.57							
C_1	36.37							
C_2	3.47							
C_3	4.05							
i-C_4	0.59							
n-C_4	1.34							
i-C_5	0.74							
n-C_5	0.83							
C_6	1.62							
C_7	2.73	96	0.7943	377.9	574.6	3.486	0.368	0.2564
C_8-C_{13}	13.409	143.32	0.8385	465.0	666.5	2.618	0.534	0.3963
C_{14}-C_{19}	9.434	227.48	0.8927	590.8	787.1	1.824	0.839	0.6418
C_{20}-C_{24}	5.686	305.37	0.929	688.1	873.6	1.410	1.120	0.8683
C_{25}-C_{30}	4.951	381.76	0.9575	772.5	945.9	1.142	1.384	1.0563
C_{31A+}	7.681	665.62	1.0324	1030.3	1163.9	0.603	2.250	1.4947
$C_{31B+,1}$	2.389	553.13	1.0039	934.8	1285.4	1.042	2.500	2
$C_{31B+,2}$	1.542	787.51	1.053	1122.5	1313.0	0.901	2.500	2
$C_{31B+,3}$	0.136	1247.11	1.1207	1424.3	1349.7	0.854	2.500	2
$C_{31B+,4}$	0.001	2047.24	1.1985	1841.3	1390.4	0.850	2.500	2

M: Molecular weight of component *i* in C_{7+} fraction
S: Specific gravity of component *i* in C_{7+} fraction
T_b: Boiling point of component *i* in C_{7+} fraction
T_c: Critical temperature of component *i* in C_{7+} fraction
P_c: Critical pressure of component *i* in C_{7+} fraction
V_c: Critical volume of component *i* in C_{7+} fraction
ω : Acentric factor of component *i* in C_{7+} fraction

Table 7.5 - Formulate of the n-d-M method (12)[1].

Measurements at 293.15 K	Measurements at 343.15 K
Calculate: v=2.51(n-1.4750)-(d-0.8510)	Calculate: x = 2.42(n-1.4600)-(d-0.8280)
% C_A: if v is positive: % C_A=430v + 3660/M if v is negative: % C_A =670v + 3660/M	% C_A: if x is positive: % C_A =410x + 3660/M if x is negative: % C_A =720x + 3660/M

[1] M, d, n and % C_A are molecular weight, density, refractive index and the percentage carbon in aromatic structure of plus fraction, respectively.

Table 7.6 - Characteristics of a live oil system (17).

Parameters	Reservoir Fluid
Region	Middle East
Reservoir Temperature /K	389.15
Reservoir Pressure / MPa	62.05
Bubble Point Pressure at Reservoir Temperature / MPa	22.68
Gas / Oil Ratio (GOR) (m^3/ m^3)	195.9
API	39
Saturates (wt% of STO)	68.3
Aromatics (wt% of STO)	11.6
Resins (wt% of STO)	18.8
Asphaltenes (n-pentane insoluble) / wt%	1.3

Table 7.7- Compositions of oil system (17).

Components	Monophasic fluid composition (mole%)
N_2	0.48
CO_2	0.92
C_1	43.43
C_2	11.02
C_3	6.55
i-C_4	0.79
n-C_4	3.7
i-C_5	1.28
n- C_5	2.25
C_6	2.7
C_{7+}	26.88
Total	100.0
MW	82.49
C_{7+} MW	228.07
C_{7+} density	0.865

Table 7.8 - Measured upper and lower boundaries of asphaltene precipitation pressures as well as bubble point pressures, using ART (Acoustic resonance technique) and LST (Light-scattering technique) methods (17).

T/K	P_{upper} / MPa	P_{bubble} / MPa	P_{lower} / MPa
372.2	47.26	22.21	-
377.2	45.42	22.64	-
383.2	44.26	22.59	-
389.2	42.92	22.68	13.51

Table 7.9 – Characterisation of C_{7+} fractions of studied live oil (17).

Component	MW / g/gmol	T_C / K	P_C / MPa	V_C / cm^3/gmol	ω
C_7	96	546.57	3.07	392	0.2804
C_8	107	574.35	2.88	433	0.3130
C_9	121	602.90	2.66	484	0.3515
C_{10}	134	627.06	2.48	532	0.3901
C_{11}	147	649.16	2.31	584	0.4293
C_{12}	161	670.12	2.17	635	0.4670
C_{13}- C_{20}	219	737.87	1.79	819	0.6022
C_{21}- C_{30}	334	840.60	1.29	1177	0.8686
C_{31}- C_{40}	444	918.70	1.00	1498	1.0926
C_{41}- C_{50}	557	969.10	0.85	1726	1.2201
C_{51}- C_{57}	746	1007.88	0.75	1907	1.3125
C_{58A+} [1]	905	937.05	0.31	2066	2.2809
C_{58B+} [2]	905	1400.0	0.86	2500	1.9336

[1] non precipitating component
[2] precipitating component

Table 7.10 - The second class of correlations with the required input variables for predicting enthalpy of vaporisation at the normal boiling temperature of hydrocarbons.

Equation	Reference
$\Delta H^{vap}=88T_b$	Trouton's rule (33)
$\Delta H^{vap}=T_b(36.6+8.314\ln T_b)$	Kistiakowsky (33)
$\Delta H^{vap}=\frac{T_b(58.20+5.94\ln M-[6.485\{T_b-(263M)^{0.581}\}^{1.037}])}{M}$	Vetere (40)
$\Delta H^{vap}=19.73809(1.8T_b)^{1.1347}S^{0.0214}$	Riazi and Daubert (35)
$\Delta H^{vap}=4.1868\,T_b(9.08+4.36\ln T_b+0.0068\frac{T_b}{M}+0.0009\frac{T_b^2}{M})$	Vetere (32)
$\Delta H^{vap}=1081+(S^{-0.01418}T_b)(31.98\ln T_b+\frac{22.12T_b^{-1.573}}{M})$	Gopinathan and Saraf (34)
$\Delta H^{vap}=T_b(9.549+14.811\ln T_b+12.346\frac{T_b}{M}-0.06662\frac{T_b^2}{M}+7.833\times10^{-5}\frac{T_b^3}{M}+19.334\ln S)$	Fang et al. (33)

ΔH^{vap}: Enthalpy of vaporisation at the normal boiling temperature (J/gmol); M: Molecular weight; S: Specific gravity at 288.8 / 288.8 K; T_b: Normal boiling point temperature (K)

Table 7.11 - Comparison (AD%) of enthalpy of vaporisation calculated by various correlations for petroleum fractions (Experimental data from Fang et al. (33)).

Fraction	ΔH^{vap}/ kJ gmol^{-1}	Trouton (33)	Kistiakowsky (33)	R–D (35)	Vetere (40)	Vetere (32)	G–S (34)	Fang et al. (33) (Dependent)	This work (Dependent)
1	30.8	1.6	1.3	2.9	1.3	3.5	1.9	2.5	2.7
2	32.02	1.8	4.6	6	4.8	0.2	5.1	5.2	5.7
3	33.83	1.9	4.1	5.3	3.5	0.5	4.5	4.3	4.7
4	32.89	1	1.3	2.6	0.7	3.4	1.7	1.5	1.9
5	33.95	1.4	3.5	4.8	3.4	1.2	3.9	4.1	4.1
6	33.24	0.9	1.3	2.5	1.2	3.6	1.7	1.4	1.7
7	36.21	6.3	8.3	9.3	6.3	4.2	8.6	7.5	8.4
8	35.46	0.1	1.7	2.7	1.1	3.1	2	1.1	1.3
9	35.29	1.4	0.2	1.1	0.1	4.8	0.4	0.5	0.5
10	37.27	3.7	5.2	6.1	5.2	0.4	5.4	4.8	4.6
11	37.09	2.5	3.9	4.7	1.8	0.4	4.1	2.2	2.9
12	38.74	2.9	4	4.6	3.2	0.7	4	2.4	2.3
13	38.99	3.2	4.2	4.8	4	0.7	4.2	2.7	2.4
14	39.46	3.9	4.9	5.5	4.7	0	4.9	3.3	3.0
15	39.16	3.1	4	4.7	3.6	0.8	4.1	2.2	2.1
16	39.69	3.9	4.8	5.5	4.9	0.1	4.9	3.6	3.1
17	39.39	3.1	4.1	4.7	4	0.8	4.1	2.4	2.1
18	39.9	4.1	5	5.6	4.8	0.1	5	3.2	2.9
19	39.14	1.7	2.6	3.2	1.7	2.2	2.6	0.4	0.4
20	40.51	5	5.8	6.4	5.7	1	5.8	4	3.7
21	40.44	4.3	5.1	5.6	4.9	0.3	5.1	3.1	2.8
22	39.66	1.7	2.4	3	2.3	2.6	2.4	0.3	0.1
23	41.09	4.5	5.2	5.7	5	0.4	5.2	2.9	2.6
24	40.94	4.1	4.8	5.2	3.5	0.2	4.7	2	2.1
25	41.4	3.9	4.5	4.9	3.6	0.2	4.4	1.7	1.5
26	39.88	0.5	0	0.4	1.7	4.7	0.1	3.6	3.4
27	42.74	5.9	6.3	6.7	5.9	1.5	6.2	3.5	3.2
28	42.45	5.2	5.6	6	5.1	0.9	5.5	2.5	2.3
29	41.05	1.2	1.5	1.8	0.3	3.1	1.4	2.8	2.4
30	41.39	0.6	0.8	1.1	1.9	3.5	0.6	3.9	3.4
31	45.13	6.9	6.9	7.1	5.9	2.3	6.6	2.7	2.5
32	45.38	7.2	7.3	7.4	6.2	2.7	7	2.9	2.8
33	45.44	6.8	6.7	6.8	6	2	6.5	2	1.9
34	44.78	3.6	3.4	3.4	2.2	1.4	3	2	2.1
35	51.27	13.8	13.4	13.2	10.4	9.7	13.1	6.6	7.3
36	48.03	7.7	7.3	7.2	6	2.7	6.9	1.3	1.2
37	47.82	6.7	6.3	6.2	5.1	1.6	5.8	0.1	0.0
38	48.21	7	6.5	6.4	4.9	2.1	6.1	0.2	0.0
39	49.79	6.9	6.1	5.8	4.3	1.6	5.5	1.7	1.6
40	51.16	8.8	8	7.7	6.4	3.5	7.4	0.2	0.2
41	51.63	9.5	8.6	8.3	6.7	4.4	8.1	0.5	0.8
42	52.14	10.3	9.4	9.1	7.9	5	8.8	1.5	1.6
43	52.56	9.2	8.1	7.7	6.3	3.7	7.5	0.7	0.5
44	55.5	11.7	10.5	10	8.6	6.2	9.8	1	1.2
45	54.97	10.9	9.6	9.1	7.4	5.4	8.9	0.2	0.1
46	55.36	11.4	10.1	9.6	8.3	5.8	9.4	0.5	0.7
47	53.07	7.3	5.9	5.4	3.3	1.7	5.2	4.5	4.2
48	58.17	12.6	11.1	10.4	8.7	7	10.3	0.3	0.2
49	58.45	12.4	10.8	10.1	8.2	6.7	9.9	0.8	0.3
50	58.69	12.5	10.9	10.2	8.7	6.7	10	0.6	0.2
51	59.71	12.3	10.5	9.7	8.1	6.4	9.6	2	1.5
52	61.37	13.8	12	11.1	9.2	8	11	1.1	0.5
53	62.34	14.3	12.4	11.5	9.7	8.5	11.4	0.8	0.3
54	62.86	14.5	12.6	11.7	10.2	8.5	11.6	0.9	0.3
55	66.37	17.2	15.2	14.2	12	11.5	14.1	1	1.6
56	68.15	18.7	16.6	15.6	13.6	13	15.6	2.4	3.0
57	69.65	19.9	17.7	16.7	15	14.1	16.7	3.3	4.0
58	73.03	22.1	19.9	18.8	16.5	16.5	18.8	4.9	5.5
AAD%		**6.9**	**6.8**	**7.0**	**5.6**	**3.8**	**6.5**	**2.3**	**2.2**

Table 7.12 - Comparison of enthalpy of vaporisation calculated (Dependent data) by Fang et al.'s (33) correlation and this work for pure hydrocarbons.

Hydrocarbon	T_b/ K	S	M	Exp.	Fang et al. (33)	AD%	This work	AD%	Ref. for experimental data
Propane	231.1	0.5081	44.094	19.04	19.18	0.8	19.19	0.8	Gopinathan and Saraf (34)
n-Butane	272.7	0.5852	58.124	22.44	22.44	0	22.35	0.4	Gopinathan and Saraf (34)
iso-Butane	261.3	0.5638	58.124	21.3	21.48	0.8	21.44	0.6	Gopinathan and Saraf (34)
n-Pentane	309.2	0.6314	72.151	25.79	25.45	1.3	25.45	1.3	Gopinathan and Saraf (34)
iso-Pentane	301	0.6252	72.151	24.69	24.82	0.5	24.74	0.2	Gopinathan and Saraf (34)
2,2-Dimethylpropane	282.7	0.5972	72.151	22.74	23.26	2.3	23.16	1.9	Gopinathan and Saraf (34)
n-Hexane	341.9	0.6644	86.178	28.85	28.38	1.6	28.49	1.2	Gopinathan and Saraf (34)
iso-Hexane	333.4	0.6583	86.178	27.79	27.68	0.4	27.68	0.4	Gopinathan and Saraf (34)
3-Methyl pentane	336.4	0.6694	86.178	28.06	28.01	0.2	28.00	0.2	Gopinathan and Saraf (34)
2,2-Dimethyl butane	322.9	0.6545	86.178	26.31	26.86	2.1	26.73	1.6	Gopinathan and Saraf (34)
2,3-Dimethyl butane	321.1	0.6668	86.178	27.38	26.84	2	26.61	2.8	Gopinathan and Saraf (34)
n-Heptane	371.6	0.6886	100.21	31.77	31.24	1.7	31.46	1.0	Gopinathan and Saraf (34)
2-Methyl hexane	363.2	0.6835	100.21	30.62	30.51	0.4	30.60	0.0	Gopinathan and Saraf (34)
3-Methyl hexane	365	0.6921	100.21	30.89	30.74	0.5	30.82	0.2	Gopinathan and Saraf (34)
3-Ethyl pentane	366.6	0.7032	100.21	31.12	30.98	0.4	31.03	0.3	Gopinathan and Saraf (34)
2,2-Dimethyl pentane	352.4	0.6787	100.21	29.23	29.6	1.3	29.54	1.1	Gopinathan and Saraf (34)
2,3-Dimethyl pentane	362.9	0.7	100.21	30.46	30.65	0.6	30.65	0.6	Gopinathan and Saraf (34)
2,4-Dimethyl pentane	352.4	0.6777	100.21	29.55	29.59	0.1	29.53	0.1	Gopinathan and Saraf (34)
3,3-Dimethyl pentane	352.4	0.698	100.21	29.62	29.79	0.6	29.62	0.0	Gopinathan and Saraf (34)
2,2,3-Trimethyl	352.4	0.695	100.21	28.9	29.76	3	29.61	2.4	Gopinathan and Saraf (34)
n-Octane	398.8	0.7072	114.23	34.41	34.05	1	34.35	0.2	Gopinathan and Saraf (34)
2-Methyl heptane	390.8	0.7025	114.23	33.26	33.3	0.1	33.48	0.7	Gopinathan and Saraf (34)
3-Methyl heptane	392.1	0.7105	114.23	33.66	33.5	0.5	33.66	0.0	Gopinathan and Saraf (34)
4-Methyl heptane	390.9	0.7094	114.23	33.35	33.38	0.1	33.53	0.5	Gopinathan and Saraf (34)
3-Ethylhexane	391.7	0.7182	114.23	33.59	33.55	0.1	33.66	0.2	Gopinathan and Saraf (34)
2,2-Dimethyl	382	0.7001	114.23	32.07	32.52	1.4	32.56	1.5	Gopinathan and Saraf (34)
2,3-Dimethyl hexane	388.8	0.717	114.23	33.17	33.28	0.3	33.35	0.5	Gopinathan and Saraf (34)
2,4-Dimethyl hexane	382.6	0.7051	114.23	32.51	32.62	0.3	32.65	0.4	Gopinathan and Saraf (34)
2,5-Dimethyl hexane	382.3	0.6984	114.23	32.54	32.52	0.1	32.59	0.1	Gopinathan and Saraf (34)
3,3-Dimethyl hexane	385.1	0.7147	114.23	32.31	32.94	1.9	32.95	2.0	Gopinathan and Saraf (34)
3,4-Dimethyl hexane	390.9	0.724	114.23	33.24	33.54	0.9	33.60	1.1	Gopinathan and Saraf (34)
3-Ethyl-2-methyl pentane	388.8	0.724	114.23	32.93	33.35	1.3	33.38	1.4	Gopinathan and Saraf (34)
3-Ethyl-3-methyl pentane	391.4	0.7319	114.23	32.78	33.66	2.7	33.69	2.8	Gopinathan and Saraf (34)
2,2,3-Trimethyl pentane	383	0.7206	114.23	31.94	32.82	2.7	32.76	2.6	Gopinathan and Saraf (34)
2,2,4-Trimethyl pentane	372.4	0.6966	114.23	30.79	31.66	2.8	31.58	2.6	Gopinathan and Saraf (34)
2,3,3-Trimethyl pentane	387.9	0.7307	114.23	32.12	33.34	3.8	33.32	3.7	Gopinathan and Saraf (34)
2,3,4-Trimethyl pentane	386.6	0.7237	114.23	32.36	33.16	2.5	33.15	2.4	Gopinathan and Saraf (34)
n-Nonane	426.5	0.7221	128.26	36.39	37.06	1.9	37.45	2.9	Gopinathan and Saraf (34)
n-Decane	447	0.7345	142.29	38.95	39.5	1.4	39.87	2.4	Gopinathan and Saraf (34)
n-Dodecane	487.5	0.7526	170.34	43.31	44.55	2.9	44.90	3.7	Gopinathan and Saraf (34)
n-Octadecane	590	0.7856	254.5	54.37	59.05	8.6	59.15	8.8	Gopinathan and Saraf (34)
n-Nonadecane	603	0.7892	268.53	56.03	61.06	9	61.11	9.1	Gopinathan and Saraf (34)
Benzene	353.1	0.8849	78.114	30.49	30.97	1.6	30.38	0.3	Gopinathan and Saraf (34)
Toluene	383.8	0.8722	92.141	33.17	33.78	1.8	33.50	1.0	Gopinathan and Saraf (34)
o-Xylene	417	0.8852	106.17	36.51	37.29	2.1	37.20	1.9	Gopinathan and Saraf (34)
m-Xylene	412.3	0.8691	106.17	36.11	36.7	1.6	36.60	1.4	Gopinathan and Saraf (34)
p-Xylene	411.5	0.8661	106.17	35.76	36.6	2.3	36.50	2.1	Gopinathan and Saraf (34)
Cyclohexane	353	0.7838	84.162	29.81	30.29	1.6	30.01	0.7	Gopinathan and Saraf (34)
Methyl cyclohexane	374	0.7744	98.189	31.44	32.24	2.5	32.08	2.0	Gopinathan and Saraf (34)
Cyclopentane	322.4	0.7508	70.135	27.3	27.4	0.4	27.02	1.0	Vetere (32)
Methyl cyclopentane	345	0.7541	84.162	29.08	29.41	1.1	29.13	0.2	Vetere (32)
Ethyl cyclohexane	404.9	0.7926	112.22	31.96	35.44	10.9	35.43	10.8	Vetere (32)
cis-Butene-2	276.9	0.6277	56.108	23.34	23.08	1.1	22.80	2.3	Vetere (32)
Ethyl benzene	409.3	0.8722	106.17	35.57	36.45	2.5	36.28	2.0	Vetere (32)
n-Heneicosane	629.7	0.7953	296.58	66.08	65.28	1.2	65.25	1.3	Kudchadker & Zwolinski (41)
n-Docosane	641.8	0.7981	310.61	67.82	67.24	0.9	67.17	1.0	Kudchadker & Zwolinski (41)
n-Tricosane	653.3	0.8006	324.63	69.51	69.11	0.6	69.02	0.7	Kudchadker & Zwolinski (41)
n-Tetracosane	664.5	0.8029	338.66	71.16	70.96	0.3	70.86	0.4	Kudchadker & Zwolinski (41)
n-Pentacosane	675.1	0.805	352.69	72.74	72.72	0	72.61	0.2	Kudchadker & Zwolinski (41)
n-Hexacosane	685.4	0.8069	366.71	74.31	74.45	0.2	74.34	0.0	Kudchadker & Zwolinski (41)
n-Heptacosane	695.4	0.8088	380.74	75.8	76.14	0.5	76.04	0.3	Kudchadker & Zwolinski (41)
n-Octacosane	704.8	0.8104	394.77	77.3	77.74	0.6	77.65	0.4	Kudchadker & Zwolinski (41)
n-Nonacosane	714	0.8119	408.79	78.73	79.3	0.7	79.24	0.6	Kudchadker & Zwolinski (41)
n-Triacontane	722.8	0.8134	422.82	80.12	80.81	0.9	80.78	0.8	Kudchadker & Zwolinski (41)
AAD%						**1.6**		**1.5**	

(Experimental data for vaporisation enthalpy of pure hydrocarbons reported in *Gopinathan and Saraf* ref. 34, have been taken from *Reid et al.* (31), *Majer and Svoboda* (42) and *Perry and Chilton* (43)).

Table 7.13 - Composition (mole%) and properties of investigated oil (6).

Component	mole %
N_2	0.51
CO_2	1.42
C_1	6.04
C_2	7.00
C_3	6.86
$_i$-C_4	0.83
$_n$-C_4	3.35
$_i$-C_5	0.70
$_n$-C_5	3.46
C_6	3.16
C_{7+}	66.68
Total	100
C_{7+} molecular weight	281
C_{7+} sp.gr	0.9020
Live-oil molecular weight	202.4
API gravity of stock tank oil	24.0
Reservoir temperature/ K	379.65
Saturation pressure/ MPa	4.14

Table 7.14 - Modelled fluid composition.

Component	mole%	M
CO_2	1.42	44.01
N_2 & C_1	6.55	17.17
C_2	7.00	30.07
C_3	6.86	44.097
C_4 –C_9	24.66	91.72
C_{10} -C_{16}	22.40	179.16
C_{17} –C_{30}	19.62	315.12
C_{31A+}	8.92	617.55
C_{31B+}	2.55	617.55
Total	100.0	

M: Molecular weight

Table 7.15 – Composition of solvent.

Component	mole%
N_2	3.17
CO_2	17.76
C_1	30.33
C_2	26.92
C_3	13.09
i-C_4	1.26
n-C_4	4.66
i-C_5	0.77
n-C_5	1.26
C_6	0.78

Table 7.16 – Composition (mole%) and molecular weight of investigated oil (38).

Comp	mole%	Mw
C_1	0.1	16.043
C_2	0.48	30.07
C_3	2.05	44.096
n-C_4	3.16	58.123
i-C_4	0.88	58.123
n-C_5	2.58	72.15
i-C_5	1.93	72.15
C_6	4.32	84
C_{7+}	84.50	151.7

Table 7.17 – Modelled fluid composition (9).

Comp.	mole%	Mw
C_1	0.1	16.043
C_2	0.48	30.07
C_3	2.05	44.096
n-C_4	3.16	58.123
i-C_4	0.88	58.123
n-C_5	2.58	72.15
i-C_5	1.93	72.15
C_6	4.32	84
P-C1	47.45	151.7
P-C2	24.841	239.3
P-C3	6.973	523.5
P-C4	4.319	800
P-C5	0.492	900
Asph-1	0.093	950
Asph-2	0.332	1000

Table 7.18 – Mole% of diluent in diluent + stock tank oil.

cm^3/g	n-C_5	n-C_7	n-C_{10}
5	91	88	85
10	95	94	92
20	97	97	96
50	99	99	98

Table 7.19 – Experimental and predicted asphaltene precipitation from STO.

n-C_{10}		
cm^3/g	Model	Experimental
5	1.92	1.34
10	1.89	1.45
20	1.81	1.5

n-C_7		
cm^3/g	Model	Experimental
5	1.96	1.53
10*	**1.85**	**1.82**
20	1.79	1.89
50	0.71	*1.87*

*Dependent data

n-C_5		
cm^3/g	Model	Experimental
10	1.93	3.61
20	2.25	3.79
50	0.90	3.87

FIGURES

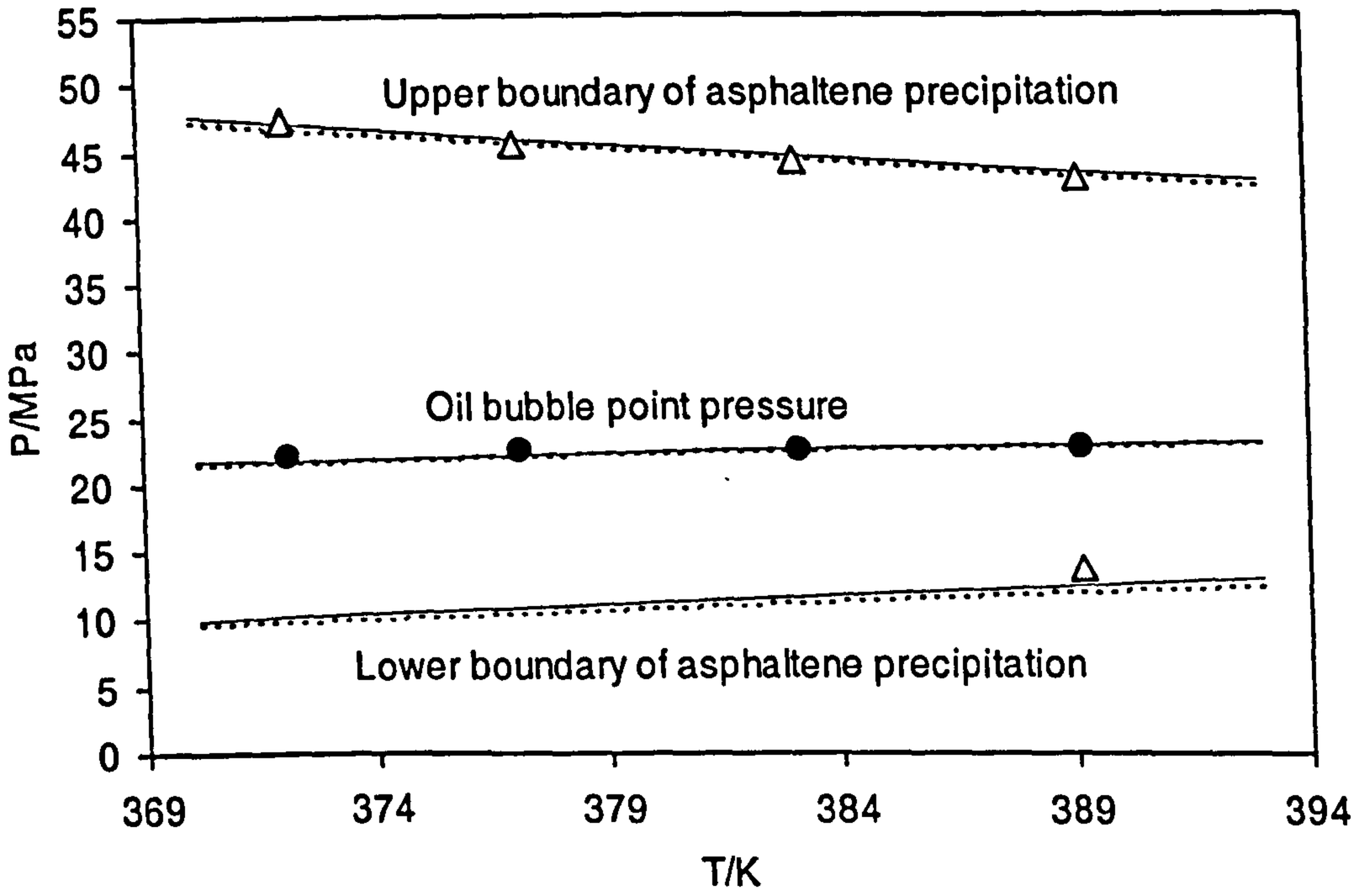

Figure 7.1 - Upper and lower boundaries of asphaltene precipitation as well as bubble point pressures for a live oil (Dashed curve: Predictions of monodispers model, Solid curve: Predictions of polydispers model, Points: Experimental Data (17)).

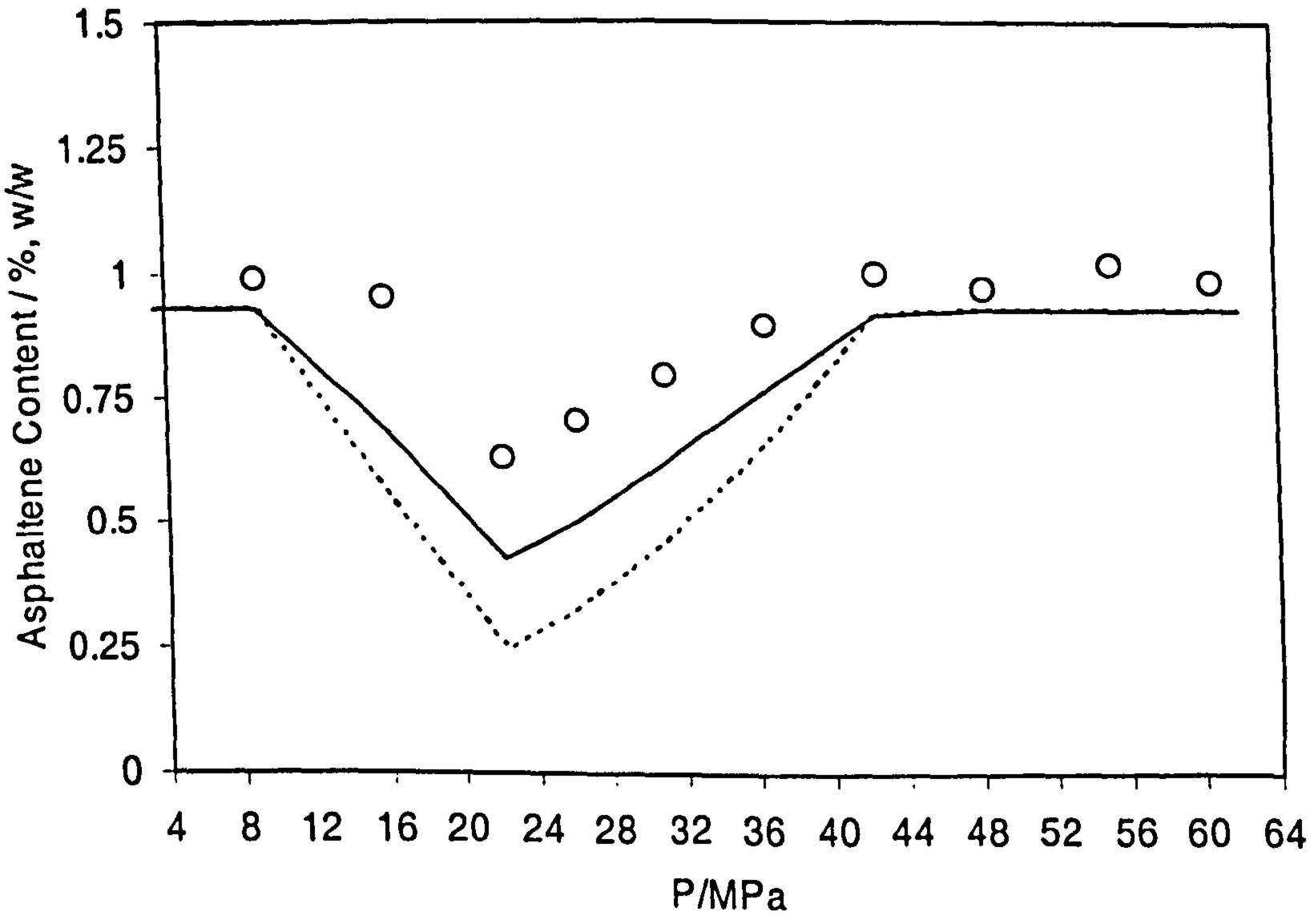

Figure 7.2 – Asphaltene content of reservoir fluid as a function of pressure at reservoir temperature, 389.15 K (Dashed curve: Predictions of monodispers model, Solid curve: Predictions of polydispers model, Points: Experimental data (17) measured data using gravimetric method).

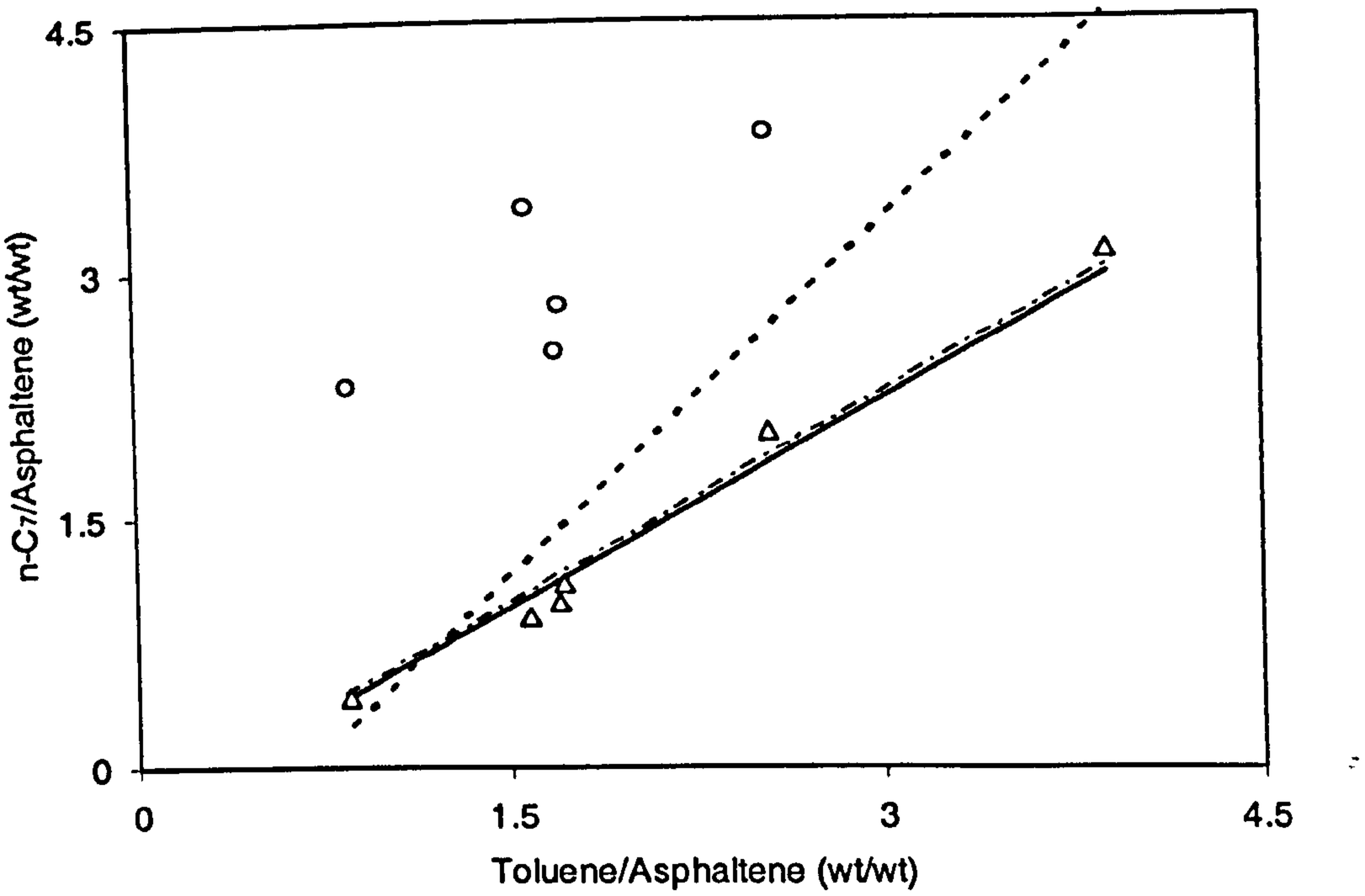

Figure 7.3 - Comparison of predicting asphaltene flocculation by several models (Δ: Experimental data (37); o: Colloidal model (39); Bold dashed line: Traditional activity coefficient based model (38); Dashed line: Cimino et al. model (37); Solid line: This model).

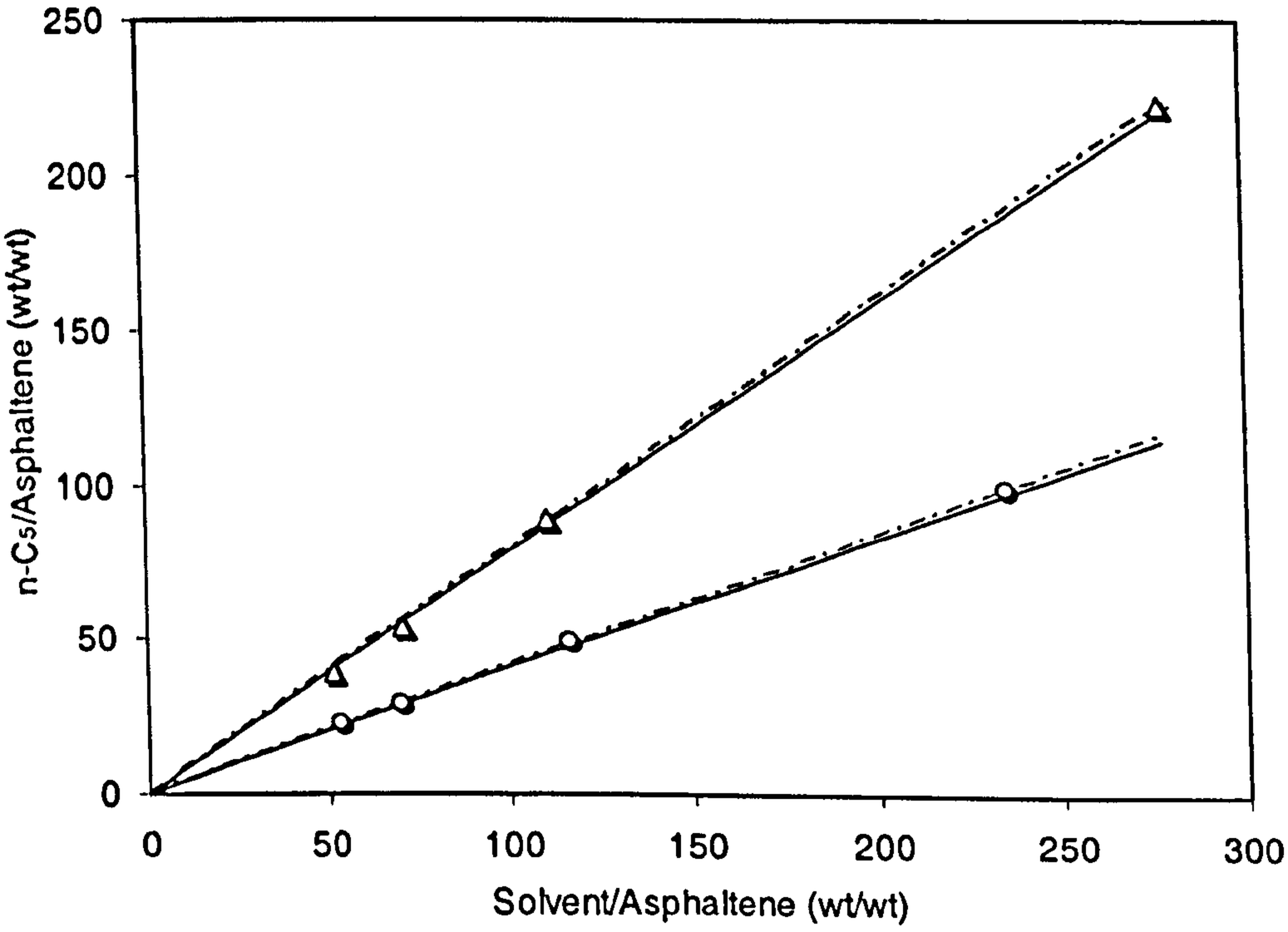

Figure 7.4 - Comparison of predicting C_7-asphaltene flocculation (Δ: Tetraline; o: Toluene). Dashed line: Cimino et al. model (37); Solid line: This model.

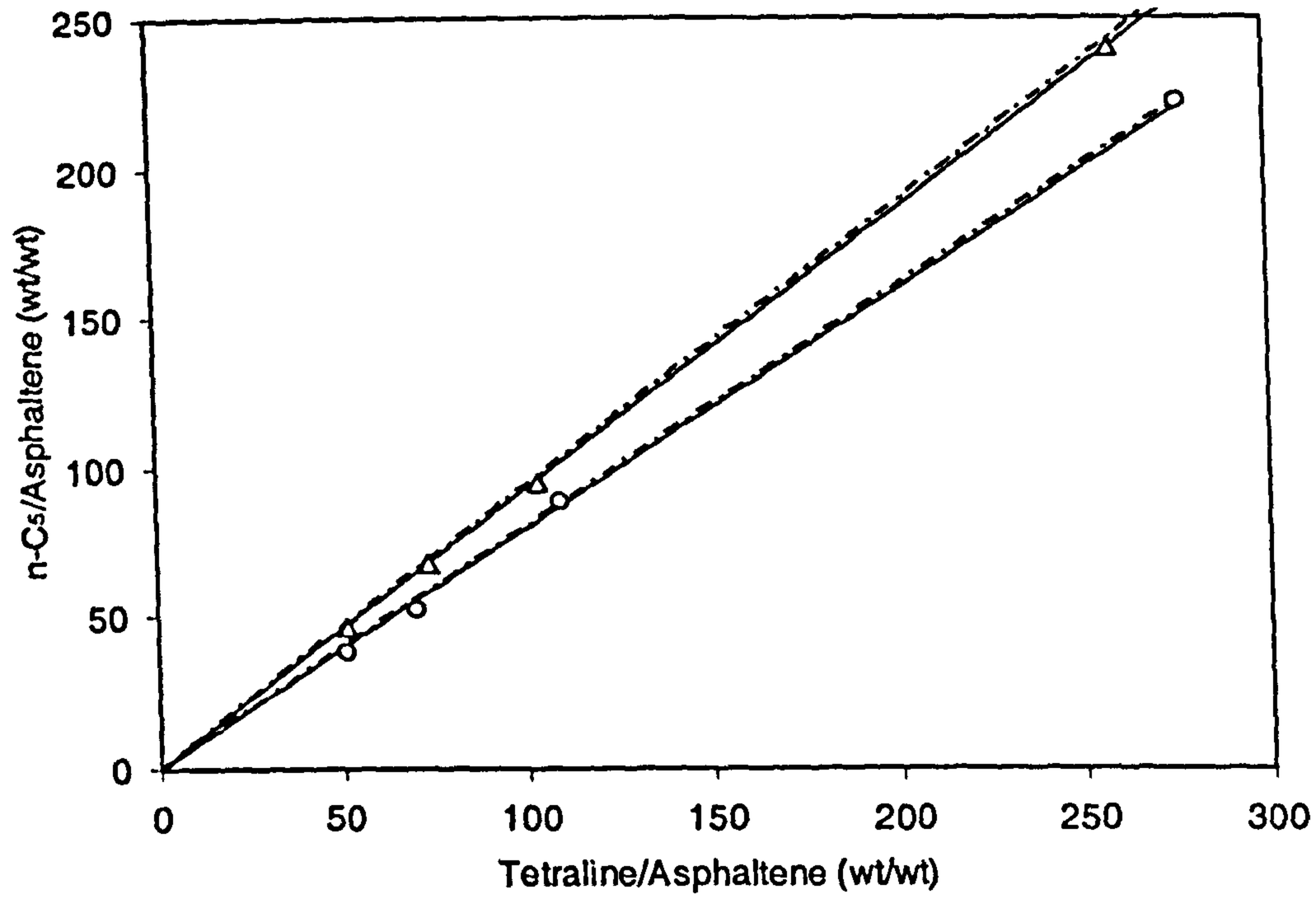

Figure 7.5 - Comparison of predicting asphaltene flocculation (Δ: C_5-asphaltene; ○: C_7-asphaltene). Dashed line: Cimino et al. model (37); Solid line: This model.

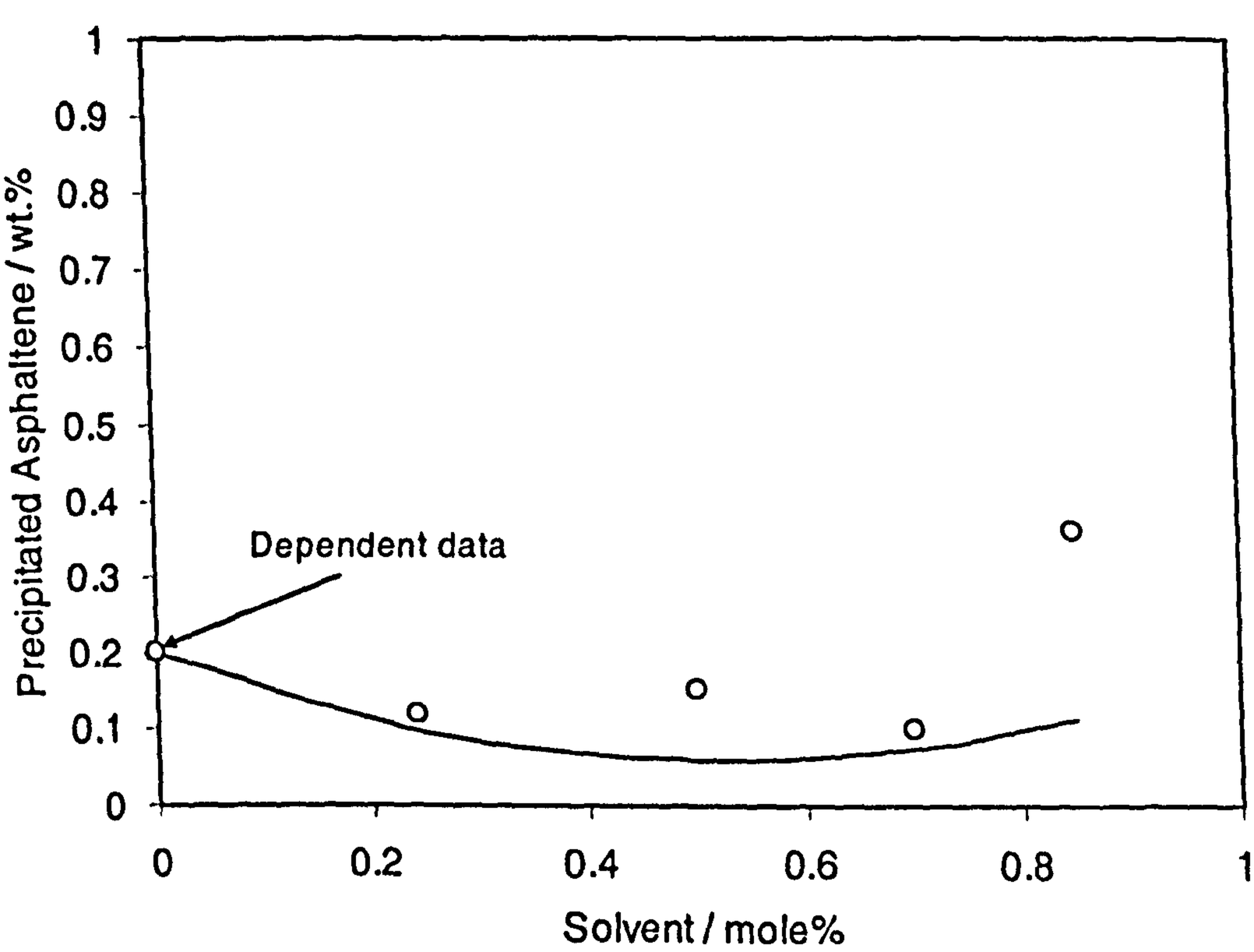

Figure 7.6 - A Comparison between the predictions and experimental data at 379.65 K and 3.55 MPa (Curves: Predictions, Points: Experimental Data (6)).

REFERENCES

1. Nghiem, L. X.; Hassam, M. S.; Nutakki, R. Efficient Modelling of Asphaltene Precipitation. SPE 26642, *presented at the 68th Annual Technical Conference and Exhibition of the SPE held in Houston, Texas* 1993.

2. Péneloux, A.; Rauzy, E.; Freze, R. A Consistent Correlation for Redlich-Kwong-Soave Volumes. *Fluid Phase Equilibria* 1982, *8*, 7-23.

3. Nghiem, L. X.; Coombe, D. A. Modelling of Asphaltene Precipitation during Primary Depletion. SPE 36106, *presented at the IV Latin American/Caribbean Petroleum Engineering Conference held in Trinidad and Tobago,* 1996.

4. Chueh, P. L.; Prausnitz, J. M. Vapour-Liquid Equilibria at High Pressures. Calculation of Partial Molar Volume in Non-Polar Liquid Mixtures. *AIChE J.* 1967, *13 (6)*, 1099-1113.

5. Kohse, B. F.; Nghiem, L. X.; Maeda, H.; Ohno, K. Modelling Phase Behaviour Including the Effect of Pressure and Temperature on Asphaltene Precipitation. SPE 64465, *presented at the SPE Asia Pacific Oil and Gas Conference and Exhibition held in Brisbane, Australia* 2000.

6. Burke, N. E.; Hobbs, R. E.; Kashou, S. F. Measurement and Modelling of Asphaltene Precipitation. *Journal of Petroleum Technology* November 1990, 1440.

7. Whitson, C. H.; Anderson, T. F.; Soreide, I. C_{7+} Characterisation of Related Equilibrium Fluids Using Gamma Distribution, in: C_{7+} Characterisation. Ed.: Chorn, L. G.; Mansoori, G. A., Taylor & Francis, 35-56, 1989.

8. Danesh, A. PVT and Phase Behaviour of Petroleum Reservoir Fluids, Elsevier Science B.V., Amsterdam, The Netherlands, 1998.

9. Pan, H.; Firoozabadi, A.; Fotland, P. Pressure and Composition Effect on Wax Precipitation: Experimental Data and Model Results. *SPE Prod. and Fac.* Nov.1997, 250 (Also: Pan, H.; Firoozabadi, A. Thermodynamic Micellization Model for Asphaltene Aggregation and Precipitation in Petroleum Fluids. *SPE Prod. and Fac.* May 1998, 118-127).

10. Avlonotis, D. A. Thermodynamics of Hydrate Equilibria; Ph.D Thesis, Department of Petroleum Engineering, Heriot-Watt University, Edinburgh, 1992.

11. Erickson, D. D.; Niesen, V. G.; Brown, T. S. Thermodynamic Measurement and Prediction of Paraffin Precipitation in Crude Oil. SPE 26604, *presented at the SPE Annual Technical Conference and Exhibition, Houston, TX*, 1993.

12. van Nes, K.; van Westen, H. A. Aspects of the Constitution of Mineral Oils, Elsevier, 1951.

13. Buckley, J. S.; Hirasaki, G. J.; Liu, Y.; Von Drasek, S.; Wang, J-X.; Gill, B. S.; Asphaltene precipitation and solvent properties of crude oils. *Petroleum Science and Technology* 1998, *16(3-4)*, 251-285.

14. Twu, C. H. An Internally Consistent Correlation for Predicting the Critical Properties and Molecular Weights of Petroleum and Coal-Tar Liquids. *Fluid Phase Equilibria* 1984, *16*, 137-150.

15. Lee, B. I.; Kesler, M. G. Improve Vapour Pressure Prediction. *Hydro. Proc.* July 1980, 163-167 (Also: Kesler, M. G.; Lee, B. I. Improve Predictions of Enthalpy of Fractions. *Hydro. Proc.* March 1976, 153-158)

16. Knapp, H.; Doring, R. Vapour-Liquid Equilibria for Mixtures of Low Boiling Substances. 1986. Berhens, D.; Eckerman, R. Eds (Dechema Chemistry Data Ser.), Part I-Binary System.

17. Jamaluddin, A. K. M.; Creek, J.; Kabir, C. S.; McFadden, J. D.; Cruz, D. D.; Joshi, N.; Ross, B. A Comparison of Various Laboratory Techniques to Measure Thermodynamic Asphaltene Instability. SPE 72154, *presented at the SPE Asia Pacific Improved Oil Recovery Conference held in Kuala Lumpur, Malaysia* 2001.

18. Andersen, S. I.; Speight, J. G. Thermodynamic models for asphaltene solubility and precipitation. *Journal of Petroleum Science and Engineering*. 1999, 22, 53-66 (Also: Andersen, S. I. *Fuel Sci. Technol. Int.* 1992, *10*, 1743.

19. Rassamdana, H.; Sahimi, M. Asphalt Flocculation and deposition: II. Formation and Growth of Fractal Aggregates. *AIChE J.* 1996, *42(12)*, 3318-3332.

20. Cavett, R. H. Physical Data for Distillation Calcuations, Vapour–Liquid Equilibria. *Proc. of 27th API Meeting, San Francisco* 1962, 351-366.

21. Riazi, M. R.; Al-Sahhaf, T. A. Physical Properties of heavy petroleum fractions and crude oils. *Fluid Phase Equilibria* 1996, *117*, 217-224.

22. Flory, P. J. Principles of polymer chemistry, Cornell University Press, New York, 1953.

23. Yarranton, H. W.; Masliyah, J. H. Molar Mass Distribution and Solubility Modeling of Asphaltenes. *AIChE J.* 1996, *42(12)*, 3533-3543.

24. Andersen, S. I. PhD Thesis, Tech. Univ. Denmark, 1990.

25. Parkash, S.; Moschopedis, S.; Speight, J. G. *Fuel* 1997, *58*, 877.

26. Huron, M.-J.; Vidal, J. New mixing rules in simple equations of state for strongly non-ideal mixtures. *Fluid Phase Equilibria* 1979, *3*, 255-271.

27. Knudsen, K.; Stenby, E. H.; Fredenslund, A. A. A Comprehensive Comparison of Mixing Rules for Calculation of Phase Equilibria in Complex Systems. *Fluid Phase Equilibria* 1993, *82*, 361-369.

28. Louli, V.; Dimitrios Tassios, D. Vapor–liquid equilibrium in polymer–solvent systems with a cubic equation of state. *Fluid Phase Equilibria* 2000, *168*, 165–182.

29. Scott, R. L.; Magat, M. The Thermodynamics of High-Polymer Solutions: The Free Energy of Mixing of Solvents and Polymers of Heterogeneous Distribution. *The Journal of Chemical Physics* 1945, *13/5*, 172-177.

30. McCain, W. D. Jr. The Properties of Petroleum Fluids; second edition, Pennwell Publishing Company, Tulsa, OK, 1990 (Also, see ref. 8)

31. Reid, R. C.; Prausnitz, J. M.; Poling, B. E. The Properties of Gases and Liquids, 4th ed., McGraw-Hill, New York, 1987.

32. Vetere, A. Methods to predict the vaporization enthalpies at the normal boiling temperature of pure compounds revisited. *Fluid Phase Equilibria* 1995, *106*, 1-10.

33. Fang, W.; Lei, Q.; Lin, R. Enthalpies of vaporization of petroleum fractions from vapor pressure measurements and their correlation along with pure hydrocarbons. *Fluid Phase Equilibria* 2003, *205*, 149–161.

34. Gopinathan, N.; Saraf, D. N. Predict heat of vaporization of crudes and pure components: Revised II. *Fluid Phase Equilibria* 2001, *179*, 277–284.

35. Riazi, M. R.; Daubert, T. E. Simplify Property Predictions. *Hydrocarbon Process.* 1980, *59*, 115–116.

36. Peng, D.-Y.; Robinson, D. B. A New Two-Constant Equation of State. *Ind. Eng. Chem. Fundam.* 1976, *15(1)*, 59-64.

37. Cimino, R.; Correra, S.; Sacomani, P. A.; Carniani, C. Thermodynamic Modelling for Prediction of Asphaltene Deposition in Live Oils. SPE 28993, *Presented at the SPE International Symposium on Oilfield Chemistry held in San Antonio, TX, USA* 14-17 February 1995.

38. Hirschberg, A.; DeJong, L. N. J.; Schipper, B. A.; Meijer, J. G. Influence of Temperature and Pressure on Asphaltene Flocculation. *SPE J.* June 1984, *24*, 283-293.

39. Leontaritis, K. J.; Mansoori, G. A. Asphaltene Flocculation During Oil Production and Processing: A Thermodynamic Colloidal Model. SPE 16258, *SPE Int. Symp. Oil field Chemistry, San Antonio, TX* 4-6 February 1987.

40. Vetere, A.; *Chem. Eng. J.* 1979, *17*, 157–162.

41. Kudchadker, A. P.; Zwolinski, B. J. *J. Chem. Eng. Data* 1966, *11*, 253–255.

42. Majer, V.; Svoboda, M. R. Enthalpies of Vaporization of Organic Compounds, IUPACData Series No. 32, Blackwell Scientific Publications, Oxford, 1985.

43. Perry, R. H.; Chilton, C. H. Chemical Engineers Handbook, 5th Edition, McGraw Hill, Tokyo, 1993.

CHAPTER 8

CONCLUSIONS AND RECOMMENDATIONS

8.1. INTRODUCTION

Natural gas hydrate formation and asphaltene precipitation problems in petroleum production and transportation were investigated in this thesis. The study involved: (1) Estimation of water content of natural gases in equilibrium with liquid water, ice and gas hydrates (Chapters 3 and 4), (2) Modelling hydrate inhibition effects of salts and chemical inhibitors associated with deepwater production and transportation of oil and gas (Chapter 5), (3) modelling asphaltene precipitation from petroleum fluids (Chapters 6 and 7). The main conclusions and recommendations for future work are as follows:

8.2. CONCLUSIONS

The focus for the research on this thesis has been on the issue of thermodynamic modeling as related to the flow assurance issues associated with gas hydrates and asphaltene. Models have been modified and new models generated in the various specific areas of application as outlined below:

8.2.1. Water content of natural gases

Water content estimation of natural gases was studied in Chapters 3 and 4, through a combined literature review and theoretical study. The study was divided into two parts:

1) Water content estimation of natural gases in equilibrium with liquid water and ice (Chapter 3): A review was conducted on the existing methods for

predicting water content / water dew point of gases (pages 39-48). The investigation showed that most of the existing predictive methods have been developed at high temperature conditions. A thermodynamic model based on the Valderrama modification of the Patel-Teja equation of state (*EoS*) and non-density mixing rules was extended to estimate the water content/ water dew point of gases (Section 3.3; pages 48-49). The binary interaction parameters of the model were tuned using vapour-liquid equilibrium data for natural gas main components and water (Table 3.1; page 61) from near hydrate forming conditions up to high temperatures. The study showed that using only gas solubility data in tuning binary interaction parameters can lead to accurate predictions of water content data (pages 52-53). Furthermore, a semi-empirical approach based on equality of water fugacities in the existing phases along with analytical correction factors for taking into account the effects of acid gases and heavy hydrocarbons were developed (Sections 3.4 and 3.5). The results showed the superiority of the method developed in this work to the existing methods in the literature, especially for estimating water content of gases at near hydrate forming conditions.

2) Estimation of water content of natural gases in equilibrium with gas hydrates (Chapter 4):

A literature survey showed that limited experimental data and predictive methods have been reported for hydrate-vapour equilibrium (Section 4.2; pages 107-111). The study showed a need for generating new analytical methods for predicting the water content of natural gases in equilibrium with gas hydrates. The newly developed semi-empirical method (Section 4.3; pages 111-116) showed encouraging results.

8.2.2. Thermodynamic modelling of mixed salt and chemical inhibitor

Modelling hydrate inhibition effects of mixed salt and chemical inhibitor was studied in Chapter 5. Three aspects were considered:

1) A combined equation of state and activity coefficient based model (Equation 2.24; page 128) was extended to salts and chemical inhibitors commonly used in deepwater operations by taking into account the interaction of all species in the aqueous solution (Equation 2.25) and correcting the properties of the aqueous phase (i.e., dielectric constant, molecular weight and density) (Equations 5.2 – 5.4). The binary interaction parameters between salts and organic inhibitors (Equation 2.25; page 129) were adjusted using water vapour pressure data in the presence of salts and organic inhibitors. It was found that the dielectric constant mixing rule of salt-free mixture has very important effect on the results. A linear mixing rule was used for determination of dielectric constant of salt-free mixture by introducing an interaction parameter, which is tuned using water freezing point depression data in the presence of salts and organic inhibitors (Equation 5.2). The predictions of the thermodynamic model were compared with experimental hydrate dissociation data for gases in the presence of various concentrations of salts and organic inhibitors for deepwater operations. The thermodynamic model proved reliable in predicting the experimental data. The comparison demonstrated the reliability of the thermodynamic approach.

2) A literature review was then made on the existing correlations for estimating hydrate characteristics of thermodynamic inhibitors (Pages 132-139). The review indicated a need for developing a new method. The extended model

was used to develop a correlation for predicting the hydrate inhibition/freezing point depression effects of various salts, organic inhibitors and combinations of salts and organic inhibitors (Equation 5.44; page 143). For this purpose, the methane hydrate suppression temperatures due to the presence of various thermodynamic inhibitors (Tables 5.2 and 5.18) were generated by the model and were used for developing the correlation, The correlation was validated against the experimental data and the thermodynamic model predictions for various concentrations of salts and organic inhibitors. The developed correlation can be used in spreadsheets as a tool for estimating hydrate stability zone for petroleum fluids in the presence of thermodynamic inhibitors, as well as providing an initial guess for more sophisticated computer programs.

3) The possibility of predicting hydrate inhibition effects of thermodynamic inhibitors from freezing point depression of the aqueous phase due to the presence of salt and/or organic inhibitor could have a real practical use, as measuring freezing point depression of aqueous phase is easier than hydrate suppression temperature, which could have a real benefit since experimental data on gas hydrate formation in some cases such as drilling and completion fluids and combination of salt and organic inhibitor are limited and in many cases inconsistent. For this purpose, hydrate suppression temperatures of methane and freezing point depression points of aqueous phase due to the presence of thermodynamic inhibitors generated by the model for various systems (Table 5.18, page 162) were used for developing an equation, which relates hydrate inhibition effects of thermodynamic inhibitors to freezing point depression of aqueous phase. A linear relationship between hydrate

suppression temperatures and freezing point depressions with a slope of 0.683 (i.e., $\Delta T_{hydrate}=0.683\times\Delta T_{ice}$) was obtained. The expression with only one parameter produced encouraging results. The results of this approach were in acceptable agreement with the experimental data in the literature, demonstrating its reliability for estimating hydrate characteristics of salt(s) and/or organic inhibitor(s).

8.2.3. Asphaltene precipitation modelling

In Chapters 6 and 7, theoretical studies were conducted to model asphaltene precipitation conditions from petroleum fluids. The study was divided into two parts:

1) A review was made on the asphaltene structure (Page 182), the asphaltene precipitation phenomenon (Pages 183-187) and existing models in the literature (Page 187) for predicting asphaltene precipitation. It was shown that the use of the solubility concept of asphaltenes may be in better agreement with the mechanism of asphaltene flocculation/precipitation in light systems (Section 6.7). A new approach based on a polymer theory, in which it is assumed that asphaltenes have a distribution of molecular weight, was then employed for estimating asphaltene precipitation/solubility (Section 6.8). To allow the use of molecular thermodynamics, the asphaltene precipitation was assumed as a reversible process. The reliability of this approach was tested against some experimental data reported in the literature. The model could reliably predict the flocculation behaviour of dissolved asphaltenes in different ratios of solvents and precipitants. That is, it predicted a linear relation between "solvent mass per asphaltene mass" and "precipitant mass per asphaltene mass", as reported experimentally, particularly for light systems

(Figures 6.8 – 6.10). The study showed that the capability of colloidal model and Traditional activity coefficient based models to re-produce the observed behaviour was poor (Figure 6.8). However, the newly developed model produced encouraging results, indicating that the solubility concept of asphaltenes was in better agreement with the mechanism of asphaltene flocculation/precipitation in light systems. However, the main limitation of activity coefficient models is that they cannot efficiently account for the effect of pressure on condensed phases. A new corresponding state approach for predicting asphaltene precipitation conditions for dissolved asphaltenes in various ratios of solvents and precipitants was developed (Equation 6.38). The developed approach showed that the parameter of this method is the same for all the precipitants and solvents and is dependent only on the type of the asphaltene. It was shown that the results of this method are in good agreement with the literature data.

2) A monodisperse thermodynamic model based on an equation of state was then introduced (Pages 225-228). The main assumption in this model is that the asphaltene precipitation is a reversible process, allowing the use of molecular thermodynamics. Asphaltene was defined as the aromatic part of the heavy end (plus fraction). The non-aromatic part of the plus fraction was considered non-precipitating (Page 229). It was assumed that these two parts in the plus fraction had *different* critical properties, acentric factor and binary interaction parameters. This model could predict the effect of temperature and pressure on asphaltene phase boundaries. However, it could not reliably predict the amount of the precipitated phase nor the effect of changes in compositions (i.e. solvent/ gas injection). To solve this shortcoming, the model was extended by

characterising the asphaltene with a continuous distribution of components (Section 7.6; page 232). The polydispersity was taken into account in critical properties, molecular weight and mole fractions. An appropriate mixing rule based on "*Equation of state + Gibbs free energy*" method was then employed to model the condensed phases (Equation 7.18; page 239). Using this mixing rule, the precipitation model could distinguish the difference between compounds of similar characteristics for vapour-liquid equilibrium, such as n-C_7 and benzene, but one encourages and the other discourages asphaltene precipitation. Furthermore, a new correlation was developed to relate the enthalpy of vaporisation at the normal boiling temperature to the normal boiling point and the specific gravity of hydrocarbons and petroleum fractions (Equation 7.20; page 241). This correlation worked well for a wide range of pure hydrocarbons and petroleum fractions and gave reasonable improvement to the existing methods, particularly for the heavy petroleum fractions and hydrocarbons.

8.3. RECOMMENDATIONS FOR FUTURE WORK

Throughout the thesis the issue of good quality data for validating models has been identified. Developing new experimental set-ups and generating new experimental data for validation and/or improving the accuracy of the developed predictive methods are therefore the main recommendations for future work, which are detailed below:

8.3.1. Water content of natural gases

Most of the existing experimental data on water-natural gas equilibria are at high temperature conditions and away from hydrate formation conditions. In this work we have used some recent experimental data which had significant impact on improving the accuracy of the predictions of water content of natural gases. It is recommended to develop new experimental set-ups and generate new experimental data close and inside the hydrate region for validation and/or improving the accuracy of the existing predictive methods.

8.3.2. Thermodynamic modelling of mixed salt and chemical inhibitor

Mixed salts and chemical inhibitors, used in deepwater operations, were modelled in this work. It became clear that for modelling these compounds, limited experimental data were available. In order to achieve better predictions, more experimental data on model systems should be generated, e.g., water freezing point depression data, hydrate suppression data etc. There is also a need for more ternary water/chemical inhibitor/gas subzero VLE data to optimise the model to predict the distribution of chemical inhibitors (e.g., methanol) for gas hydrate applications. It is also recommended to further investigate very high concentrations of salts and/or chemical inhibitor systems, both experimentally and from a modelling point of view.

In this thesis, a correlation was developed to predict the hydrate free zone of reservoir fluids in the presence of thermodynamic inhibitors (Equation 5.44; page 143). The correlation includes various salts and organic inhibitors and few combinations of salt and organic inhibitor. The effects of pressure and compositions were not taken into account. It is recommended to study the effects of pressure and compositions in order

to expand on high concentrations of salts and chemical inhibitors, which the correlation can be applied to.

8.3.3. Asphaltene precipitation modelling

One of the objectives of this work was to study asphaltene precipitation conditions in petroleum fluids. It was obvious that further investigation requires developing novel techniques for generating reliable data, especially for onset of asphaltene precipitation in live fluids and light systems.

The micellar/ colloidal based models are especially helpful for understanding the effect of resin on asphaltene stabilisation/precipitation and the mechanism of asphaltene precipitation from crude oil. As the concentration of asphaltene in light systems seems to be less than the critical micelle concentration (*CMC*) of asphaltene, the above approaches may not be suitable for such systems. A preliminary study on asphaltene precipitation in synthetic light systems showed that the use of solubility concept of asphaltenes may be in better agreement with the mechanism of asphaltene flocculation/precipitation (Section 6.7; page 191). However, a final proof for this statement requires direct measurements by suitable techniques (e.g., interfacial tension (*IFT*) and viscosity measurements) reported in the literature.

A corresponding state approach for predicting onset of asphaltene precipitation for dissolved asphaltenes in various ratios of solvents and precipitants was developed (Equation 6.38; page 206). The method can also be employed to study inhibition effects of asphaltenes solvents.

The effect of wax deposition on asphaltenes precipitation and vice versa was not investigated in this work, which seems to be of interest in some reservoir fluids. For

this purpose, a reliable wax model can be coupled with an asphaltene model. Obviously, generating reliable data on such systems can help in better understanding these phenomena. Furthermore, the developed asphaltene model can be coupled with a reservoir simulator to investigate the effect of asphaltenes precipitation on fluid flow in porous media.

The model can be employed for generating pseudo-experimental data for onset of asphaltene precipitation and relating them to some properties of reservoir fluids such as viscosity, interfacial tension, conductivity, refractive index etc to provide simple tools for predicting onset of asphaltene precipitation. Obviously generating experimental data can help in developing and examining such methods.

APPENDIX

A.1. CALCULATION OF FUGACITY COEFFICIENT

A.1.1. GENERAL CUBIC EQUATION OF STATE

Given is a cubic equation of state (*EoS*) on the general form:

$$P = \frac{RT}{v-b} - \frac{a}{v^2+uv-w^2} \qquad \text{(A.1.1)}$$

with the corresponding fugacity coefficient equation for mixtures (1):

$$\ln\phi_i = -\ln(Z-B) + \frac{B_i'B}{Z-B} + \frac{A}{\sqrt{U^2+4W^2}}\left[A_i' - \frac{U_i'U^2+4W_i'W^2}{U^2+4W^2}\right]\times$$

$$\ln\left[\frac{2Z+U-\sqrt{U^2+4W^2}}{2Z+U+\sqrt{U^2+4W^2}}\right] - A\left[\frac{2(2Z+U)W_i'W^2+(UZ-2W^2)U_i'U}{(Z^2+UZ-W^2)(U^2+4W^2)}\right] \qquad \text{(A.1.2)}$$

where:

$$A = \frac{Pa}{(RT)^2}, \qquad B = \frac{Pb}{RT} \qquad \text{(A.1.3, A.1.4)}$$

$$U = \frac{Pu}{RT}, \qquad W = \frac{Pw}{RT} \qquad \text{(A.1.5, A.1.6)}$$

$$Z = \frac{Pv}{RT} \qquad \text{(A.1.7)}$$

and:

$$A_i' = \frac{1}{na}\left[\frac{\partial(n^2a)}{\partial n_i}\right]_{T,n_{j\neq i}}, \qquad B_i' = \frac{1}{b}\left[\frac{\partial(nb)}{\partial n_i}\right]_{T,n_{j\neq i}} \qquad \text{(A.1.8, A.1.9)}$$

$$U_i' = \frac{1}{u}\left[\frac{\partial(nu)}{\partial n_i}\right]_{T,n_{j\neq i}}, \qquad W_i' = \frac{1}{w}\left[\frac{\partial(nw)}{\partial n_i}\right]_{T,n_{j\neq i}} \qquad \text{(A.1.10, A.1.11)}$$

A.1.2. NON-DENSITY DEPENDENT MIXING RULES

Avlonitis *et al.* (2) developed non-density dependent (*NDD*) mixing rules in the a-term for prediction of *VLE* and *VLLE* in mixtures containing petroleum fluids and methanol:

$$a = a^C + a^A \qquad \text{(A.1.12)}$$

where a^C is given by the classic quadratic mixing rules:

$$a^C = \sum_i \sum_j x_i x_j a_{ij} \qquad \text{(A.1.13)}$$

$$a_{ij} = (1 - k_{ij})\sqrt{a_i a_j} \qquad \text{(A.1.14)}$$

The asymmetric term a^A is given by:

$$a^A = \sum_p x_p^2 \sum_i x_i a_{pi} l_{pi} \qquad \text{(A.1.15)}$$

$$a_{pi} = \sqrt{a_p a_i} \qquad \text{(A.1.16)}$$

$$l_{pi} = l_{pi}^0 - l_{pi}^1 (T - T_0) \qquad \text{(A.1.17)}$$

where p is the index of polar components.

The 1st order derivative of a with respect to n_i is calculated at constant T and $n_{j\neq i}$ as:

$$\frac{\partial(n^2 a)}{\partial n_i} = \frac{\partial(n^2(a^C + a^A))}{\partial n_i} = \frac{\partial(n^2 a^C)}{\partial n_i} + \frac{\partial(n^2 a^A)}{\partial n_i} \qquad \text{(A.1.18)}$$

The derivative of the classical part is given by:

$$\frac{\partial(n^2 a^C)}{\partial n_i} = \frac{\partial\left(n^2 \sum_i \sum_j x_i x_j a_{ij}\right)}{\partial n_i} = \frac{\partial\left(\sum_i \sum_j n_i n_j a_{ij}\right)}{\partial n_i} = 2\sum_j n_j a_{ij} \qquad \text{(A.1.19)}$$

The derivative of the asymmetric part is given by:

$$\frac{\partial(n^2 a^A)}{\partial n_i} = \frac{\partial\left(\frac{1}{n}(n^3 a^A)\right)}{\partial n_i} = \frac{\partial\left(\frac{1}{n}\right)}{\partial n_i} n^3 a^A + \frac{1}{n}\frac{\partial(n^3 a^A)}{\partial n_i} \qquad \text{(A.1.20)}$$

$$\frac{\partial\left(\frac{1}{n}\right)}{\partial n_i} = -\frac{1}{n^2} \qquad \text{(A.1.21)}$$

$$\frac{\partial(n^3 a^A)}{\partial n_i} = \frac{\partial\left(n^3 \sum_p x_p^2 \sum_i x_i a_{pi} l_{pi}\right)}{\partial n_i} = \frac{\partial\left(\sum_p n_p^2 \sum_i n_i a_{pi} l_{pi}\right)}{\partial n_i} \qquad \text{(A.1.22)}$$

$$= 2n_i \sum_j n_j a_{ij} l_{ij} + \sum_p n_p^2 a_{pi} l_{pi}$$

$$\frac{\partial(n^2 a^A)}{\partial n_i} = -\frac{1}{n^2}\sum_p n_p^2 \sum_j n_j a_{pj} l_{pj} + \frac{1}{n}\left(2n_i \sum_j n_j a_{ij} l_{ij} + \sum_p n_p^2 a_{pi} l_{pi}\right) \qquad \text{(A.1.23)}$$

The term $2n_i \sum_j n_j a_{ij} l_{ij}$ vanishes if $i \neq p$ as l_{ij} becomes zero. Likewise, a_{ij} in this term is actually a_{pj}, i.e., $\sqrt{a_i a_j}$ and NOT $\sqrt{a_i a_j}(1 - k_{ij})$ as for classical mixing.

The dimensionless A_i' for the *NDD* mixing rules then becomes:

$$A_i' = \frac{1}{na}\left[2\sum_j n_j a_{ij} + \frac{1}{n}\left(2n_i \sum_j n_j a_{ij} l_{ij} + \sum_p n_p^2 a_{pi} l_{pi}\right) - \frac{1}{n^2}\sum_p n_p^2 \sum_j n_j a_{pj} l_{pj}\right]$$

$$= \frac{1}{a}\left[2\sum_j x_j a_{ij} + 2x_i \sum_j x_j a_{ij} l_{ij} + \sum_p x_p^2 a_{pi} l_{pi} - \sum_p x_p^2 \sum_j x_j a_{pj} l_{pj}\right]$$

$$= \frac{P}{A(RT)^2}\left[2\sum_j x_j A_{ij}(1-k_{ij})\frac{(RT)^2}{P} + 2x_i \sum_j x_j A_{ij} \frac{(RT)^2}{P} l_{ij}\right. \qquad \text{(A.1.24)}$$

$$\left. + \sum_p x_p^2 A_{pi} \frac{(RT)^2}{P} l_{pi} - \sum_p x_p^2 \sum_j x_j A_{pj} \frac{(RT)^2}{P} l_{pj}\right]$$

$$= \frac{1}{A}\left[2\sum_j x_j A_{ij}(1-k_{ij}) + 2x_i \sum_j x_j A_{ij} l_{ij} + \sum_p x_p^2 A_{pi} l_{pi} - \sum_p x_p^2 \sum_j x_j A_{pj} l_{pj}\right]$$

A.1.3. VPT EOS WITH NDD MIXING RULES

The Valderrama-Patel-Teja (*VPT*) *EoS* is given as (3):

$$P = \frac{RT}{v-b} - \frac{a}{v(v+b)+c(v-b)} \qquad \text{(A.1.25)}$$

Applying the general form of the cubic EoS (Equation A.1.1) on Equation A.1.25 then u and w become:

$$u = b + c \qquad \text{(A.1.26)}$$

$$w = \pm\sqrt{bc} \qquad \text{(A.1.27)}$$

For further use w is defined as:

$$w = \sqrt{bc} \qquad \text{(A.1.28)}$$

Written on a dimensionless form, u and w become:

$$U = B + C \tag{A.1.29}$$

$$W = \sqrt{BC} \tag{A.1.30}$$

If classical mixing rules are applied to b and c:

$$b = \sum_i x_i b_i \tag{A.1.31}$$

$$c = \sum_i x_i c_i \tag{A.1.32}$$

then the derivatives of b, c, u, and w with respect to n_i are calculated at constant T and $n_{j\neq i}$ as:

$$\frac{\partial(nb)}{\partial n_i} = \frac{\partial\left(n\sum_i x_i b_i\right)}{\partial n_i} = \frac{\partial\left(\sum_i n_i b_i\right)}{\partial n_i} = b_i \tag{A.1.33}$$

$$\frac{\partial(nc)}{\partial n_i} = \frac{\partial\left(n\sum_i x_i c_i\right)}{\partial n_i} = \frac{\partial\left(\sum_i n_i c_i\right)}{\partial n_i} = c_i \tag{A.1.34}$$

$$\frac{\partial(nu)}{\partial n_i} = \frac{\partial(n(b+c))}{\partial n_i} = \frac{\partial(nb)}{\partial n_i} + \frac{\partial(nc)}{\partial n_i} = b_i + c_i \tag{A.1.35}$$

$$\begin{aligned}\frac{\partial(nw)}{\partial n_i} &= \frac{\partial\left(n\sqrt{bc}\right)}{\partial n_i} = \frac{\partial\left(\sqrt{n^2 bc}\right)}{\partial n_i} = \frac{1}{2\sqrt{n^2 bc}}\frac{\partial\left(n^2 bc\right)}{\partial n_i} \\ &= \frac{1}{2n\sqrt{bc}}\left[nb\frac{\partial(nc)}{\partial n_i} + nc\frac{\partial(nb)}{\partial n_i}\right] = \frac{1}{2n\sqrt{bc}}\left[ncb_i + nbc_i\right] = \frac{cb_i + bc_i}{2\sqrt{bc}}\end{aligned} \tag{A.1.36}$$

The dimensionless derivatives of b, u, and w become:

$$B_i' = \frac{1}{b} b_i = \frac{B_i RT/P}{BRT/P} = \frac{B_i}{B} \tag{A.1.37}$$

$$U_i' = \frac{1}{b+c}(b_i + c_i) = \frac{B_i + C_i}{B+C} \tag{A.1.38}$$

$$W_i' = \frac{1}{\sqrt{bc}}\left(\frac{cb_i + bc_i}{2\sqrt{bc}}\right) = \frac{CB_i + BC_i}{2BC} \tag{A.1.39}$$

The above relations are inserted into Equation A.1.2:

$$\begin{aligned}\ln \phi_i = {} & -\ln(Z-B) + \frac{\frac{B_i}{B}B}{Z-B} \\ & + \frac{A}{\sqrt{(B+C)^2+4BC}}\left[A_i' - \frac{\frac{B_i+C_i}{B+C}(B+C)^2 + 4\frac{CB_i+BC_i}{2BC}BC}{(B+C)^2+4BC}\right]\times \\ & \ln\left[\frac{2Z+B+C-\sqrt{(B+C)^2+4BC}}{2Z+B+C+\sqrt{(B+C)^2+4BC}}\right] \\ & - A\left[\frac{2(2Z+B+C)\frac{CB_i+BC_i}{2BC}BC + ((B+C)Z-2BC)\frac{B_i+C_i}{B+C}(B+C)}{(Z^2(B+C)Z-BC)((B+C)^2+4BC)}\right]\end{aligned} \tag{A.1.40}$$

If D and Q are defined as:

$$D = \sqrt{BC + \frac{(B+C)^2}{4}} \tag{A.1.41}$$

$$Q = Z + \frac{B+C}{2} \tag{A.1.42}$$

then Equation A.1.40 becomes:

$$\ln\phi_i = -\ln(Z-B)+\frac{B_i}{Z-B}+\frac{A}{2D}\left[A_i'-\frac{(B_i+C_i)(B+C)+2(CB_i+BC_i)}{4D^2}\right]\times$$
$$\ln\left[\frac{2Q-2D}{2Q+2D}\right]-A\left[\frac{2Q(CB_i+BC_i)+((B+C)Z-2BC)(B_i+C_i)}{(Z^2(B+C)Z-BC)4D^2}\right]$$

$$=-\ln(Z-B)+\frac{B_i}{Z-B}+\frac{A}{2D}\left[\frac{C_i(3B+C)+B_i(3C+B)}{4D^2}-A_i'\right]\times\ln\left(\frac{Q+D}{Q-D}\right)$$
$$-A\left[\frac{2Q(CB_i+BC_i)+\left((B+C)\left(Q-\frac{B+C}{2}\right)-2\left(D^2-\frac{(B+C)^2}{4}\right)\right)(B_i+C_i)}{(Q^2-D^2)4D^2}\right]$$

$$=-\ln(Z-B)+\frac{B_i}{Z-B}+\frac{A}{2D}\left[\frac{C_i(3B+C)+B_i(3C+B)}{4D^2}-A_i'\right]\times\ln\left(\frac{Q+D}{Q-D}\right)$$
$$-A\left[\frac{Q(2CB_i+2BC_i)+((B+C)Q-2D^2)(B_i+C_i)}{(Q^2-D^2)4D^2}\right]$$

$$=-\ln(Z-B)+\frac{B_i}{Z-B}+\frac{A}{2D}\left[\frac{C_i(3B+C)+B_i(3C+B)}{4D^2}-A_i'\right]\times\ln\left(\frac{Q+D}{Q-D}\right) \qquad \text{(A.1.43)}$$
$$-A\left[\frac{Q(C_i(3B+C)+B_i(3C+B))-2D^2(B_i+C_i)}{(Q^2-D^2)4D^2}\right]$$

Equation A.1.43 is arranged into a form similar to:

$$\ln\phi_i=-\ln(Z-B)+\frac{B_i}{Z-B}+\frac{A(B_i+C_i)}{2(Q^2-D^2)}-\frac{\ln\left(\frac{Q+D}{Q-D}\right)}{D}\frac{A_i'A}{2} \qquad \text{(A.1.44)}$$
$$+\frac{A}{8D^3}\left[\ln\left(\frac{Q+D}{Q-D}\right)-\left(\frac{2QD}{Q^2-D^2}\right)\right]\times[C_i(3B+C)+B_i(3C+B)]$$

Finally, Equation A.1.24 is inserted into Equation A.1.44 to obtain the fugacity coefficient equation for component *i* in the *VPT EoS* with the *NDD* mixing rules:

$$\ln\phi_i = -\ln(Z-B)+\frac{B_i}{Z-B}-\frac{\ln\left(\frac{Q+D}{Q-D}\right)}{D}\sum_j x_j A_{ij}\left(1-k_{ij}\right)+\frac{A(B_i+C_i)}{2\left(Q^2-D^2\right)}$$
$$+\frac{A}{8D^3}\left[\ln\left(\frac{Q+D}{Q-D}\right)-\left(\frac{2QD}{Q^2-D^2}\right)\right]\times\left[C_i(3B+C)+B_i(3C+B)\right] \qquad \text{(A.1.45)}$$
$$-\frac{\ln\left(\frac{Q+D}{Q-D}\right)}{D}\left(x_i\sum_j x_j A_{ij}l_{ij}+\frac{1}{2}\sum_p x_p^2 A_{pi}l_{pi}-\frac{1}{2}\sum_p x_p^2\sum_i x_i A_{pi}l_{pi}\right)$$

A.2. CALCULATION OF TEMPERATURE PROFILE ALONG A PIPELINE

The energy balance for the gas flow in a pipeline can be calculated using the following equation (4), assuming the work term is ignorable along the pipeline:

$$dh/dx - dq/dx + \bar{V}\,(d\bar{V}/dx) + g\,(dz/dx) = 0 \qquad \text{(A.2.1)}$$

where h, q, $\bar{V}$, g, z and x are molar enthalpy of natural gas. heat transfer flux, velocity of natural gas, gravitational acceleration, pipeline elevation. and distance along the pipe, respectively. The above energy balance can be summarized in order to develop a more simple equation, using appropriate assumptions. Assuming the velocity-change and pipeline elevation terms to be negligible (4), the following equation can be achieved:

$$dh/dx - dq/dx = 0 \qquad \text{(A.2.2)}$$

The following equation can be used to estimate the heat loss from the pipe to the environment (5):

$$dq/dx = [2\pi RU\,(T_E - T)] / \dot{m}_g \qquad \text{(A.2.3)}$$

where $\dot{m}_g$ is mass flow-rate of natural gas, R is the pipe radius, U is the overall-heat transfer coefficient, and T_E is the environment (i.e., surrounding where $\dot{m}_g$ is mass flow-rate of natural gas, R is the pipe radius, U is the overall-heat transfer coefficient, and T_E is the environment (i.e., surrounding ambient) temperature.

In the above equation the enthalpy gradient can be calculated by ignoring the Joule-Thompson expansion effects for long gas pipeline with moderate to small pressure drop:

$$dh/dx = C_p dT/dx \qquad \text{(A.2.4)}$$

where C_p is the heat capacity at constant pressure.

By combining Equations A.2.2 through A.2.4, the following differential equation is obtained for the prediction of temperature profile along a pipeline:

$$C_p dT/dx - 2\pi RU(T_E - T)/\dot{m}_g = 0 \qquad \text{(A.2.5)}$$

Equation A.2.5 can be solved analytically, assuming an average value for C_p of natural gas along the pipeline and using an appropriate initial condition $T = T_I$ at $x = 0$:

$$T = (T_I - T_E)\, exp\,(-A.x) + T_E \qquad \text{(A.2.6)}$$

where

$$A = \frac{2\pi RU}{\dot{m}_s C_P} \qquad \text{(A.2.7)}$$

Equation A.2.6 can be re-arranged in order to find the following equation:

$$x = -\frac{\dot{m}_s C_P}{2\pi RU} ln\left(\frac{T - T_E}{T_I - T_E}\right) \qquad \text{(A.2.8)}$$

A.3. POLYMER BASED MODELS

A.3.1. CIMINO ET AL. MODEL

According to this model (6), thermodynamic equilibrium is described by means of the equality of chemical potentials relative to the two species (asphaltene and maltene) in the two phases, on phase splitting. Some simplification can be done by considering the physics of phase splitting. Considering typical asphaltene volume fraction Φ_a in oils, it can be estimated in the range of 10^{-2} to 10^{-3} for oils with asphaltene weight percent from 1 to 10. It can safely be assumed to be pure solvent, that is Φ_a=0. Such an assumption leads to the final equation, using Flory-Huggins theory (7):

$$ln[1-(\Phi_a')_{M=\infty}] + \left(1 - \frac{V_m}{V_a}\right)(\Phi_a')_{M=\infty} + \chi(\Phi_a')^2_{M=\infty} = 0 \qquad \text{(A.3.1)}$$

where the *prime* represents the asphalt phase, $(\Phi_a')_{M=\infty}$ is the volume fraction of asphaltenes in asphalt phase, χ stands for interaction parameter between asphaltenes and maltene (asphaltene free oil), V_m and V_a are molecular volume of maltene and asphaltene, respectively. By solving the above equation, it is possible to see that $(\Phi_a')_{M=\infty}$ is not very sensitive for oil systems and it generally can be assumed constant.

A.3.2. SCOTT-MAGAT THEORY

Flory and Huggins (7) first developed theories of the mixing entropy of polymers of uniform molecular weight with solvents and then they extended their treatment to include the solubility of *homogeneous* polymers. Later, Scott and Magat (8) presented a new theory for polymers consisting of a *heterogeneous* distribution of chain lengths. Such distributions are to be found in both natural and synthetic rubbers and in all similar chain polymers.

In Scott-Magat theory (8), the partial molar Gibbs free energies of mixing of the solvent, $\overline{\Delta G_m}$, and of the *i*th fraction of the polymer, $\overline{\Delta G_i}$, is presented as:

$$\overline{\Delta G_m} = RT[ln\Phi_m + (1-\Phi_m)(1-\frac{1}{\overline{M}_N}) + \chi(1-\Phi_m)^2] \qquad (A.3.2)$$

$$\overline{\Delta G_i} = RT[ln\Phi_i + (1-\Phi_m)(1-\frac{M_i}{\overline{M}_N}) - M_i\Phi_m + \chi M_i \Phi_m^2] \qquad (A.3.3)$$

where R, T, Φ_m and Φ_i are universal gas constant, temperature, the volume fractions of solvent and the *i*th fraction, respectively. M_i is the molecular weight of the *i*th fraction

and, assuming that the density of the polymers, ρ_r, is independent of the chain length, a direct measure of the molecular weight, M_i.

$$M_i = \frac{V_i}{V_m} = \frac{M_i}{\rho_r V_m} \tag{A.3.4}$$

$\overline{M_N}$ is the number average M, defined as:

$$\overline{M_N} = \frac{\sum_i n_i M_i}{\sum_i n_i} = \frac{\sum_i M_i}{\sum_i \frac{M_i}{\Phi_i}} \tag{A.3.5}$$

and related to the number average molecular weight. χ is a constant for any given system:

$$\chi = \frac{V_m[(\delta_m - \delta_r)^2 + 2l\delta_m\delta_r]}{RT} \tag{A.3.6}$$

where δ_m and δ_r are constants for the polymer and the solvent (the square root of the internal energy of vaporisation per molecular volume).

Equation (A.3.2) is identical with that for the Gibbs free energy of the solvent in a binary system as derived by Huggins, with the exception that $\overline{M_N}$ replaces M. Equation (A.3.3), however is not identical with that of the polymer in the homogeneous system.

A.3.3. HIRSCHBERG ET AL. MODEL

In this model (9), once the liquid/vapour split has been calculated, asphaltene precipitation is calculated with a modified Flory-Huggins theory (8). The conditions for chemical equilibrium between an asphalt-rich phase A and a solvent-rich phase B are:

$$\mu_i^A = \mu_i^B \tag{A.3.7}$$

Following the Flory-Huggins theory (8), the chemical potential μ_i of component i is given by:

$$\frac{\mu_i - (\mu_i)_{ref}}{RT} = ln(\Phi_i) + 1 - \frac{V_i}{V} + \chi_i \tag{A.3.8}$$

where $(\mu_i)_{ref}$ is the chemical potential at the reference state of pure liquid i. Φ_i is the volume fraction of component i. Hence,

$$\Phi_i = \frac{x_i V_i}{V} \tag{A.3.9}$$

The molar volume V, of the mixture and the interaction parameter, χ_i are calculated by using Hildebrand's approximation:

$$V = \sum x_i V_i \tag{A.3.10}$$

and

$$\chi_i = \frac{V_i}{RT}(\delta - \delta_i)^2 \tag{A.3.11}$$

where x_i is the mole fraction of component i and δ is given by:

$$\delta = \sum \Phi_i \delta_i \tag{A.3.12}$$

and T is the absolute temperature and R is the universal gas constant. Assuming that the precipitated phase is pure asphaltene, $\mu_a^A = (\mu_a)_{ref}$ which in combination of above equations, yields:

$$\Phi_a = exp[\frac{V_a}{V_m} - 1 - \frac{V_a}{RT}(\delta_a - \delta_m)^2] \qquad \text{(A.3.13)}$$

A.4. CALCULATION OF FUGACITY USING THE HURON-VIDAL MIXING RULES

The Soave-Redlich-Kwong (*SRK*) (10) and the Peng-Robinson (*PR*) (11) equations of state are the most widely used equations in the petroleum industry. It is common to express these equations by the following general form (1):

$$P = \frac{RT}{v-b} - \frac{a}{(v-\eta_1 b)(v-\eta_2 b)} \qquad \text{(A.4.1)}$$

where η_1 and η_2 are constants equal to 1 and 0 in *SRK* (10) and $1+\sqrt{2}$ and $1-\sqrt{2}$ in *PR* (11), respectively.

Using the *EoS* and appropriate mixing rules, the fugacity of each component in all fluid phases is calculated from:

$$ln\,\phi_i = \frac{1}{RT}\int_V^\infty \left[\left(\frac{\partial P}{\partial n_i}\right)_{T,V,n_{j\neq i}} - RT/V\right] dV - ln\,Z \quad \text{for } i = 1, 2, ..., M \qquad \text{(A.4.2)}$$

$$\text{or} \quad ln\,\phi_i = \int_v^\infty \left[\frac{1}{RT}\left(\frac{\partial P}{\partial n_i}\right)_{T,V,n_{j\neq i}} - \frac{1}{v}\right] dv - ln(\frac{Pv}{RT}) \quad \text{for } i = 1, 2, ..., M \qquad \text{(A.4.3)}$$

$$f_i = x_i \phi_i P \qquad \text{(A.4.4)}$$

where ϕ_i , V, M, n_i, Z and f_i are the fugacity coefficient of component i in the fluid phases, total volume, number of components, number of moles of component i, compressibility factor of the system and fugacity of component i in the fluid phases, respectively.

Hence, the equation of state is written in terms of total volume by substituting $v=V/n$, where n is the total number of moles,

$$n=\sum_{i=1}^{n} n_i \tag{A.4.5}$$

$$P=\frac{nRT}{V-nb}-\frac{n^2a}{(V-\eta_1 nb)(V-\eta_2 nb)} \tag{A.4.6}$$

The derivative of pressure at constant total volume, pressure and all mol numbers, except n, is calculated as,

$$\left(\frac{\partial P}{\partial n_i}\right)_{T,V,n_{j\neq i}}=\frac{RT}{V-nb}+\frac{nRT\left[\frac{\partial(nb)}{\partial n_i}\right]}{(V-nb)^2}-\frac{\frac{\partial(n^2a)}{\partial n_i}}{(V+\eta_1 nb)(V+\eta_2 nb)}+ \tag{A.4.7}$$

$$\frac{\{\eta_1\eta_2[\frac{\partial(nb)^2}{\partial n_i}]+(\eta_1+\eta_2)V[\frac{\partial(nb)}{\partial n_i}]\}(n^2a)}{[(V+\eta_1 nb)(V+\eta_2 nb)]^2}$$

Applying a modified version of the *Huron-Vidal* (12) mixing rules to calculate a and b,

$$\frac{a}{bRT}=\sum_i x_i\frac{a_i}{b_iRT}+\frac{1}{A_1}\left(\frac{G^E}{RT}+\sum_i x_i\ln\frac{b}{b_i}\right) \tag{A.4.8}$$

or

$$a=bRT\left[\sum_i x_i\frac{a_i}{b_iRT}+\frac{1}{A_1}\left(\frac{G^E}{RT}+\sum_i x_i\ln\frac{b}{b_i}\right)\right] \tag{A.4.9}$$

$$b = \sum_i x_i b_i \tag{A.4.10}$$

Therefore,

$$n^2 a = nbRT[\sum_i n_i \frac{a_i}{b_i RT} + \frac{1}{A_1}(n\frac{G^E}{RT} + \sum_i n_i \ln\frac{b}{b_i})] \tag{A.4.11}$$

$$nb = \sum_i nx_i b_i = \sum_i n_i b_i \tag{A.4.12}$$

the derivatives of the two parameters are obtained as,

$$[\frac{\partial(nb)}{\partial n_i}]_{T,V,n_{j\neq i}} = b_i \tag{A.4.13}$$

$$[\frac{\partial(n^2 a)}{\partial n_i}]_{T,V,n_{j\neq i}} = b_i RT[\sum_i n_i \frac{a_i}{b_i RT} + \frac{1}{A_1}(\frac{nG^E}{RT} + \sum_i n_i \ln\frac{b}{b_i})] + nbRT[\frac{a_i}{b_i RT} + \frac{1}{A_1}[\frac{\partial(\frac{nG^E}{RT})}{\partial n_i}]_{T,V,n_{j\neq i}}$$
$$+ \frac{1}{A_1}[\frac{\partial(\sum_i n_i \ln\frac{b}{b_i}))}{\partial n_i}]_{T,V,n_{j\neq i}}]$$

(A.4.14)

or

$$[\frac{\partial(n^2 a)}{\partial n_i}]_{T,V,n_{j\neq i}} = nb_i RT[\sum_i x_i \frac{a_i}{b_i RT} + \frac{1}{A_1}(\frac{G^E}{RT} + \sum_i x_i \ln\frac{b}{b_i})] + nbRT[\frac{a_i}{b_i RT} + \frac{1}{A_1}[\frac{\partial(\frac{nG^E}{RT})}{\partial n_i}]_{T,V,n_{j\neq i}}$$
$$+ \frac{1}{A_1}[\frac{\partial(\sum_i n_i \ln\frac{b}{b_i}))}{\partial n_i}]_{T,V,n_{j\neq i}}]$$

(A.4.15)

According to *Scott-Magat* theory (8),

$$\overline{\Delta G_m} = RT[\ln \Phi_m + (1-\Phi_m)(1-\frac{1}{\overline{M}_N}) + \chi(1-\Phi_m)^2] \qquad \text{(For maltene)} \qquad \text{(A.4.16)}$$

$$\overline{\Delta G_i} = RT[\ln \Phi_i + (1-\Phi_m)(1-\frac{M_i}{\overline{M}_N}) - M_i\Phi_m + \chi M_i \Phi_m^2] \quad \text{(For asphaltenes)}$$

$$\overline{\Delta G} = \sum_i x_i \overline{\Delta G_i} \qquad \text{(A.4.17)}$$

$$\frac{G^E}{RT} = \frac{\Delta G}{RT} - \sum_i (x_i \ln x_i) \qquad \text{(A.4.18)}$$

therefore,

$$\frac{G^E}{RT} = \sum_{i=1}^{n-n_{Asph}} x_i[\ln \Phi_m + (1-\Phi_m)(1-\frac{1}{\overline{M}_N}) + \chi(1-\Phi_m)^2] + \sum_{i=n_{Asph}}^{n} x_i[\ln \Phi_i + (1-\Phi_m)$$

$$(1-\frac{M_i}{\overline{M}_N}) - M_i\Phi_m + \chi M_i \Phi_m^2] - \sum_i (x_i \ln x_i)$$

in which,

$$\Phi_i = \frac{x_i v_i}{\sum_{i=1}^{n} x_i v_i} \qquad \text{(A.4.20)}$$

$$\overline{M_N} = \sum_{i=n_{Asph}}^{n} \frac{x_i}{\sum_{i=n_{Asph}}^{n} x_i} M_i = \sum_{i=n_{Asph}}^{n} \frac{n_i}{\sum_{i=n_{Asph}}^{n} n_i} M_i \qquad \text{(A.4.21)}$$

$$\chi = \frac{v_m[(\delta_m - \delta_a)^2 + 2l\delta_m\delta_a]}{RT} \qquad \text{(A.4.22)}$$

$$v_m = \sum_{i=1}^{n-n_{Asph}} \frac{x_i}{\sum_{i=1}^{n-n_{Asph}} x_i} v_i \qquad \text{(A.4.23)}$$

$$\delta_m = \sum_{i=1}^{n-n_{Asph}} \frac{\Phi_i}{\sum_{i=1}^{n-n_{Asph}} \Phi_i} \delta_i \text{ or } \delta_m = \sum_{i=1}^{n-n_{Asph}} \frac{\sum_i x_i v_i}{\sum_{i=1}^{n-n_{Asph}} \frac{x_i v_i}{\sum_i x_i v_i}} \delta_i \qquad \text{(A.4.24)}$$

where Φ_m and Φ_i are the volume fractions of maltene (Asphaltene free solution) and the ith fraction of asphaltenes, respectively. M_i is the ratio of the molecular weight of the ith fraction of asphaltene and $\overline{M_N}$ is the average M. χ stands for interaction parameter between asphaltenes and maltene and δ_m and δ_a represent solubility parameters of maltene and asphaltene, respectively.

On the other hand,

$$\frac{\partial \Phi_i}{\partial x_i} = \frac{1}{x_i}\Phi_i[1-\Phi_i] \quad \text{and} \quad \frac{\partial \Phi_i}{\partial n_i} = \frac{1}{n}\frac{\partial \Phi_i}{\partial x_i} = \frac{1}{n_i}\Phi_i[1-\Phi_i] \qquad \text{(A.4.25)}$$

$$\frac{\partial \overline{M_N}}{\partial x_i} = \frac{1}{(1-x_m)}[M_i - \overline{M_N}] \text{ and } \frac{\partial \overline{M_N}}{\partial n_i} = \frac{1}{n}\frac{\partial \overline{M_N}}{\partial x_i} = \frac{1}{(1-x_m)n}[M_i - \overline{M_N}] \qquad \text{(A.4.26)}$$

$$\frac{\partial}{\partial n_i}\left(\frac{1}{\overline{M_N}}\right) = -\frac{1}{\overline{M_N}^2}\frac{\partial}{\partial n_i}(\overline{M_N}) \qquad \text{(A.4.27)}$$

$$\frac{\partial v_m}{\partial x_i} = \frac{1}{x_m}[v_i - v_m] = \frac{v_m}{x_m^2}[\Phi_i - \Phi_m] \quad \text{and} \quad \frac{\partial v_m}{\partial n_i} = \frac{1}{x_m n}[v_i - v_m] = \frac{v_m}{x_m^2 n}[\Phi_i - \Phi_m]$$

$$\frac{\partial \delta_m}{\partial x_i} = \frac{1}{x_i}\frac{\Phi_i}{\Phi_m}[\delta_i - \delta_m] \quad \text{and} \quad \frac{\partial \delta_m}{\partial n_i} = \frac{1}{n_i}\frac{\Phi_i}{\Phi_m}[\delta_i - \delta_m] \tag{A.4.29}$$

$$\frac{\partial}{\partial n_i}(\delta_m - \delta_a)^2 = 2(\delta_m - \delta_a) \times \frac{\partial(\delta_m)}{\partial n_i} \tag{A.4.30}$$

$$\frac{\partial \chi}{\partial x_i} = \frac{1}{v_m}\frac{\partial v_m}{\partial x_i}\chi + \frac{2v_m}{RT}\{\delta_m + (l-1)\delta_a\}\frac{\partial \delta_m}{\partial x_i}$$

$$= \frac{1}{x_m^2}[\Phi_i - \Phi_m]\chi + \frac{1}{x_i}\frac{2v_m}{RT}\{\delta_m + (l-1)\delta_a\}\frac{\Phi_i}{\Phi_m}[\delta_i - \delta_m] \tag{A.4.31}$$

$$\text{and} \quad \frac{\partial \chi}{\partial n_i} = \frac{1}{n}\frac{\partial \chi}{\partial x_i} \tag{A.4.32}$$

$$\frac{\partial}{\partial n_i}(n\sum_{i=1}^{n} x_i \ln x_i) = \ln x_i + \sum_{i=1}^{n}(1 - x_i) \tag{A.4.33}$$

$$\frac{\partial}{\partial n_i}(\sum_{i=1}^{n} n_i \ln \frac{b}{b_i}) = \ln \frac{b}{b_i} + \sum_{i=1}^{n} x_i(\frac{b_i}{b} - 1) \tag{A.4.34}$$

Therefore.

If $i \leq n\text{-}n_{Asph}$:

$$\frac{\partial(\frac{nG^E}{RT})}{\partial n_i} = [\ln \Phi_m + \Phi_a(1-\frac{1}{\overline{\overline{M_N}}}) + \chi\Phi_a{}^2] +$$

$$\sum_{i=1}^{n-n_{Asph}} x_i \left\langle \begin{array}{l} \{\frac{1}{\Phi_m} - (1-\frac{1}{\overline{\overline{M_N}}}) - 2\chi\Phi_a\}\Phi_m\Phi_a - \Phi_a \frac{1}{(1-x_m)\overline{\overline{M_N}}}(1-\frac{M_i}{\overline{\overline{M_N}}}) + \\ \Phi_a{}^2\{\frac{1}{x_m{}^2}(\Phi_i - \Phi_m)\chi + \frac{1}{x_i}\frac{2v_m}{RT}\{\delta_m + (l-1)\delta_a\}\frac{\Phi_i}{\Phi_m}(\delta_i - \delta_m)\} \end{array} \right\rangle \qquad \text{(A.4.35)}$$

$$-[\ln x_i + \sum_{i=1}^{n}(1-x_i)]$$

If $i > n\text{-}n_{Asph}$:

$$\frac{\partial(\frac{nG^E}{RT})}{\partial n_i} = [\ln\Phi_i + \Phi_a(1-\frac{M_i}{\overline{\overline{M_N}}}) - M_i\Phi_m + \chi M_i\Phi_m{}^2] +$$

$$\sum_{i=n_{Asph}}^{n} x_i \left\langle \begin{array}{l} (1-\Phi_i) - \frac{\Phi_a M_i}{(1-x_m)\overline{\overline{M_N}}}(1-\frac{M_i}{\overline{\overline{M_N}}}) - (1-\frac{M_i}{\overline{\overline{M_N}}} + M_i - 2\chi M_i\Phi_m)\times\Phi_m\Phi_a \\ + M_i\Phi_m{}^2\{\frac{1}{x_m{}^2}(\Phi_i - \Phi_m)\chi + \frac{1}{x_i}\frac{2v_m}{RT}\{\delta_m + (l-1)\delta_a\}\frac{\Phi_i}{\Phi_m}(\delta_i - \delta_m)\} \end{array} \right\rangle \qquad \text{(A.4.36)}$$

$$-[\ln x_i + \sum_{i=1}^{n}(1-x_i)]$$

Therefore, If $i \leq n\text{-}n_{Asph}$:

$$\left[\frac{\partial(n^2a)}{\partial n_i}\right]_{T,V,n_{j\neq i}} = nb_iRT[\sum_{i=1}^{n} x_i \frac{a_i}{b_iRT} +$$

$$\frac{1}{A_1}\left\langle \begin{array}{l} \{\sum_{i=1}^{n-n_{Asph}} x_i[\ln\Phi_m + \Phi_a(1-\frac{1}{M_N}) + \chi\Phi_a^2] + \\ \sum_{i=n_{Asph}}^{n} x_i[\ln\Phi_i + \Phi_a(1-\frac{M_i}{M_N}) - M_i\Phi_m + \chi M_i\Phi_m^2] - \sum_{i=1}^{n}(x_i\ln x_i)\} + \sum_{i=1}^{n} x_i \ln\frac{b}{b_i} \end{array} \right\rangle] + nbRT[\frac{a_i}{b_iRT} +$$

$$\frac{1}{A_1}\left\langle \begin{array}{l} \{[\ln\Phi_m + \Phi_a(1-\frac{1}{M_N}) + \chi\Phi_a{}^2] + \\ \sum_{i=1}^{n-n_{Asph}} x_i \left\langle \begin{array}{l} \{\frac{1}{\Phi_m} - (1-\frac{1}{M_N}) - 2\chi\Phi_a\}\Phi_m\Phi_a - \Phi_a\frac{1}{(1-x_m)M_N}(1-\frac{M_i}{M_N}) + \\ \Phi_a{}^2\{\frac{1}{x_m{}^2}(\Phi_i-\Phi_m)\chi + \frac{1}{x_i}\frac{2v_m}{RT}\{\delta_m+(l-1)\delta_a\}\frac{\Phi_i}{\Phi_m}(\delta_i-\delta_m)\} \end{array} \right\rangle\} \\ -[\ln x_i + \sum_{i=1}^{n}(1-x_i)] \end{array} \right\rangle$$

$$+\frac{1}{A_1}\left\langle \ln\frac{b}{b_i} + \sum_{i=1}^{n} x_i(\frac{b_i}{b}-1)\right\rangle]$$

If $i > n\text{-}n_{Asph}$:

$$\left[\frac{\partial(n^2a)}{\partial n_i}\right]_{T,V,n_{j\neq i}} = nb_iRT[\sum_{i=1}^{n} x_i\frac{a_i}{b_iRT} +$$

$$\frac{1}{A_1}\left\langle \begin{array}{l} \{\sum_{i=1}^{n-n_{Asph}} x_i[\ln\Phi_m + \Phi_a(1-\frac{1}{\overline{\overline{M_N}}}) + \chi\Phi_a^2] + \\ \sum_{i=n_{Asph}}^{n} x_i[\ln\Phi_i + \Phi_a(1-\frac{M_i}{\overline{\overline{M_N}}}) - M_i\Phi_m + \chi M_i\Phi_m^2] - \sum_{i=1}^{n}(x_i\ln x_i)\} + \sum_{i=1}^{n} x_i\ln\frac{b}{b_i} \end{array}\right\rangle] + nbRT[\frac{a_i}{b_iRT} +$$

$$\frac{1}{A_1}\left\langle \begin{array}{l} \{[\ln\Phi_i + \Phi_a(1-\frac{M_i}{\overline{\overline{M_N}}}) - M_i\Phi_m + \chi M_i{\Phi_m}^2] + \\ \sum_{i=n_{Asph}}^{n} x_i\left\langle \begin{array}{l} (1-\Phi_i) - \frac{\Phi_a M_i}{(1-x_m)\overline{\overline{M_N}}}(1-\frac{M_i}{\overline{\overline{M_N}}}) - (1-\frac{M_i}{\overline{\overline{M_N}}} + M_i - 2\chi M_i\Phi_m)\times\Phi_m\Phi_a \\ + M_i{\Phi_m}^2\{\frac{1}{{x_m}^2}(\Phi_i-\Phi_m)\chi + \frac{1}{x_i}\frac{2v_m}{RT}\{\delta_m + (l-1)\delta_a\}\frac{\Phi_i}{\Phi_m}(\delta_i-\delta_m)\} \end{array}\right\rangle\} \\ -[\ln x_i + \sum_{i=1}^{n}(1-x_i)] \end{array}\right\rangle$$

$$+\frac{1}{A_1}\left\langle \ln\frac{b}{b_i} + \sum_{i=1}^{n} x_i(\frac{b_i}{b}-1)\right\rangle]$$

Using the *PR-EoS* (11) and an arbitrary set of mixing rules for a and b,

$$P = \frac{RT}{(v-b)} - \frac{a}{v^2+2bv-b^2} \qquad \text{(A.4.39)}$$

the fugacity coefficient of a species i becomes:

$$\ln\phi_i = -\ln\left(\frac{P(v-b)}{RT}\right) + \frac{1}{b}(\frac{\partial nb}{\partial n_i})(\frac{Pv}{RT}-1) + \frac{1}{2\sqrt{2}}(\frac{a}{bRT})\times\ln\left(\frac{v+b(1-\sqrt{2})}{v+b(1+\sqrt{2})}\right)\times\left(\frac{1}{a}(\frac{1}{n}\frac{\partial n^2a}{\partial n_i}) - \frac{1}{b}(\frac{\partial nb}{\partial n_i})\right) \text{or}$$

$$\ln\phi_i = -\ln\left(\frac{P(v-b)}{RT}\right) + \frac{b_i}{b}(\frac{Pv}{RT}-1) + \frac{1}{2\sqrt{2}}(\frac{a}{bRT})\times\ln\left(\frac{v+b(1-\sqrt{2})}{v+b(1+\sqrt{2})}\right)\times\left(\frac{1}{a}(\frac{1}{n}\frac{\partial n^2a}{\partial n_i}) - \frac{b_i}{b}\right)$$

Therefore,

If $i \leq n\text{-}n_{Asph}$:

$$\ln \phi_i = -\ln\left(\frac{P(v-b)}{RT}\right) + \frac{b_i}{b}\left(\frac{Pv}{RT} - 1\right) + \frac{1}{2\sqrt{2}}\left(\frac{a}{bRT}\right) \times \ln\left(\frac{v + b(1-\sqrt{2})}{v + b(1+\sqrt{2})}\right) \times$$

$$\left(\frac{1}{a}\left(b_i RT\left[\sum_{i=1}^{n} x_i \frac{a_i}{b_i RT} + \right.\right.\right.$$

$$\frac{1}{A_1}\left\langle \begin{array}{l} \{ \sum_{i=1}^{n-n_{Asph}} x_i [\ln \Phi_m + \Phi_a (1 - \frac{1}{\overline{\overline{M_N}}}) + \chi \Phi_a^2] + \\ \sum_{i=n_{Asph}}^{n} x_i [\ln \Phi_i + \Phi_a (1 - \frac{M_i}{\overline{\overline{M_N}}}) - M_i \Phi_m + \chi M_i \Phi_m^2] - \sum_{i=1}^{n} (x_i \ln x_i) \} + \sum_{i=1}^{n} x_i \ln \frac{b}{b_i} \end{array} \right\rangle] + bRT[\frac{a_i}{b_i RT} +$$

$$\frac{1}{A_1}\left\langle \begin{array}{l} \{[\ln \Phi_m + \Phi_a (1 - \frac{1}{\overline{\overline{M_N}}}) + \chi {\Phi_a}^2] + \\ \sum_{i=1}^{n-n_{Asph}} x_i \left\langle \begin{array}{l} \{\frac{1}{\Phi_m} - (1 - \frac{1}{\overline{\overline{M_N}}}) - 2\chi \Phi_a\} \Phi_m \Phi_a - \Phi_a \frac{1}{(1-x_m)\overline{\overline{M_N}}} (1 - \frac{M_i}{\overline{\overline{M_N}}}) + \\ {\Phi_a}^2 \{\frac{1}{{x_m}^2} (\Phi_i - \Phi_m)\chi + \frac{1}{x_i} \frac{2v_m}{RT} \{\delta_m + (l-1)\delta_a\} \frac{\Phi_i}{\Phi_m} (\delta_i - \delta_m)\} \end{array} \right\rangle \} \\ - [\ln x_i + \sum_{i=1}^{n} (1 - x_i)] \end{array} \right\rangle$$

$$\left. \left. + \frac{1}{A_1}\left\langle \ln \frac{b}{b_i} + \sum_{i=1}^{n} x_i \left(\frac{b_i}{b} - 1\right) \right\rangle] \right) - \frac{b_i}{b} \right)$$

If $i > n\text{-}n_{Asph}$:

$$\ln\phi_i = -\ln\left(\frac{P(v-b)}{RT}\right)+\frac{b_i}{b}\left(\frac{Pv}{RT}-1\right)+\frac{1}{2\sqrt{2}}\left(\frac{a}{bRT}\right)\times\ln\left(\frac{v+b(1-\sqrt{2})}{v+b(1+\sqrt{2})}\right)\times$$

$$\left(\frac{1}{a}\left(b_i RT\left[\sum_{i=1}^{n}x_i\frac{a_i}{b_i RT}+\right.\right.\right.$$

$$\frac{1}{A_1}\left\langle\begin{array}{l}\{\sum_{i=1}^{n-n_{Asph}}x_i[\ln\Phi_m+\Phi_a(1-\frac{1}{\overline{\overline{M_N}}})+\chi\Phi_a^2]+\\ \sum_{i=n_{Asph}}^{n}x_i[\ln\Phi_i+\Phi_a(1-\frac{M_i}{\overline{\overline{M_N}}})-M_i\Phi_m+\chi M_i\Phi_m^2]-\sum_{i=1}^{n}(x_i\ln x_i)\}+\sum_{i=1}^{n}x_i\ln\frac{b}{b_i}\end{array}\right\rangle\Big]+bRT\Big[\frac{a_i}{b_i RT}+$$

$$\frac{1}{A_1}\left\langle\begin{array}{l}\{[\ln\Phi_i+\Phi_a(1-\frac{M_i}{\overline{\overline{M_N}}})-M_i\Phi_m+\chi M_i{\Phi_m}^2]+\\ \sum_{i=n_{Asph}}^{n}x_i\left\langle\begin{array}{l}(1-\Phi_i)-\frac{\Phi_a M_i}{(1-x_m)\overline{\overline{M_N}}}(1-\frac{M_i}{\overline{\overline{M_N}}})-(1-\frac{M_i}{\overline{\overline{M_N}}}+M_i-2\chi M_i\Phi_m)\times\Phi_m\Phi_a\\ +M_i{\Phi_m}^2\{\frac{1}{{x_m}^2}(\Phi_i-\Phi_m)\chi+\frac{1}{x_i}\frac{2v_m}{RT}\{\delta_m+(l-1)\delta_a\}\frac{\Phi_i}{\Phi_m}(\delta_i-\delta_m)\}\end{array}\right\rangle\}\\ -[\ln x_i+\sum_{i=1}^{n}(1-x_i)]\end{array}\right\rangle\Bigg)$$

$$\left.\left.+\frac{1}{A_1}\left\langle\ln\frac{b}{b_i}+\sum_{i=1}^{n}x_i(\frac{b_i}{b}-1)\right\rangle\right]\right)-\frac{b_i}{b}$$

REFERENCES

1. Danesh, A. PVT and Phase Behaviour of Petroleum Reservoir Fluids, Elsevier Science B.V., Amsterdam, The Netherlands, 1998.

2. Avlonitis, D.; Danesh, A.; Todd, A. C. Prediction of VL and VLL Equilibria of Mixtures Containing Petroleum Reservoir Fluids and Methanol with a Cubic EoS. *Fluid Phase Equilibria* 1994, *94*, 181-216 (Also: Østergaard, K. K. Gas hydrate stability in the petroleum industry and its application in gas-liquid separation, PhD Thesis, Heriot-Watt University, Edinburgh, UK, February 2000).

3. Valderrama, J. O. A generalized Patel-Teja equation of state for polar and non-polar fluids and their mixtures. *J. Chem. Eng. Japan* 1990, *23*, 87-91.

4. Buthod, A. P.; Castillo, G.; Thompson, R. E. How To Use Computers To Calculate Heat, Pressure in Buried Pipelines. *Oil & Gas J.* 1971, *69(10)*, 57-59.

5. Kumar, S. Gas Production Engineering, Gulf Professional Publishing, Houston, TX, 1987.

6. Cimino, R.; Correra, S.; Sacomani, P. A.; Carniani, C. Thermodynamic Modelling for Prediction of Asphaltene Deposition in Live Oils. SPE 28993, *Presented at the SPE International Symposium on Oilfield Chemistry held in San Antonio, TX, USA* 14-17 February 1995.

7. Flory, P. J. Principles of polymer chemistry. Cornell University Press, New York, 1953.

8. Scott, R. L.; Magat, M. The Thermodynamics of High-Polymer Solutions: The Free Energy of Mixing of Solvents and Polymers of Heterogeneous Distribution. *The Journal of Chemical Physics* 1945. *13/5*. 172-177.

9. Hirschberg, A.; DeJong, L. N. J.; Schipper. B. A.; Meijer, J. G. Influence of Temperature and Pressure on Asphaltene Flocculation. *SPE J.* June 1984, *24*, 283-293.

10. Soave, G. Equilibrium Constants from a Modified Redlich-Kwong Equation of State. *Chem. Eng. Sci.* 1972, *27*, 1197-1203.

11. Peng, D.-Y.; Robinson. D.B. A New Two-Constant Equation of State. *Ind. Eng. Chem. Fundam.* 1976, *15(1)*, 59-64.

12. Louli, V.; Dimitrios Tassios, D. Vapor–liquid equilibrium in polymer–solvent systems with a cubic equation of state. *Fluid Phase Equilibria* 2000, *168*, 165–182.

SOME SELECTED PUBLICATIONS & REPORTS:

1. Tohidi B., Danesh A., Todd A.C., Burgass R.W., Ren S.R., Anderson R., Yang J.H., Arjmandi M., Reid A., Ji H.., Masoudi R., Biderkab A.B. and ***Mohammadi A.H.***, "Gas hydrates in offshore production and drilling", *Proceeding of DTI Improved Oil Recovery (IOR) Research Dissemination Seminar*, 25th June 2002, Aberdeen, UK, **2002.**

2. Tohidi B., ***Mohammadi A.H.*** and Ren S., CFD & Gas Hydrates, 2002 CFD workshop, Scandic Hotel 19-21 Nov 2002, Stavanger Norway, **2002.**

3. ***Mohammadi A.H.***, Tohidi B. and Burgass R.W., Equilibrium data and thermodynamic modeling of nitrogen, oxygen and air clathrate hydrates, ***J. Chem. Eng. Data*** **2003,** *48*, 612-616.

4. Tohidi B. and ***Mohammadi A.H.***, Detailed Evaluation of the Risk of Hydrate Formation at the Selected PRS and HPCMS Stations in the Gauteng network, South Africa, Consultancy Report to Sasol Gas (Pty) Ltd duly represented by Sasol Technology (Pty) Ltd., South Africa, ***Final Technical Report***, April **2003.**

5. ***Mohammadi A.H.***, Chapoy A., Richon D. and Tohidi B. Experimental Measurement and Thermodynamic Modeling of Water Content in Methane and Ethane Systems, ***Ind. Eng. Chem. Res.*** **2004,** *43*, 7148-7162.

6. ***Mohammadi A.H.***, Chapoy A., Tohidi B. and Richon D., A Semi-Empirical Approach for Estimating Water Content of Natural Gases, ***Ind. Eng. Chem. Res.*** **2004,** *43*, 7137-7147.

7. ***Mohammadi A.H.***, Chapoy A., Tohidi B. and Richon D., Measurements and Thermodynamic Modeling of Vapor-Liquid Equilibria in Ethane –Water Systems from 274.26 to 343.08 K, ***Ind. Eng. Chem. Res.*** **2004,** *43*, 5418-5424.

8. Chapoy A., ***Mohammadi A.H.***, Richon D. and Tohidi B., Gas Solubility Measurement and Modeling for Methane – Water and Methane–Ethane–*n*-Butane-Water Systems at Low temperature Conditions, ***Fluid Phase Equilibria*** **2004,** *220*, 111-119.

9. Chapoy A., ***Mohammadi A.H.***, Tohidi B. and Richon D., Measurement and Modeling of Gas Solubility and Literature Review of the Properties for the Carbon Dioxide - Water System, ***Ind. Eng. Chem. Res.*, 2004,** *43*, 1794-1802

10. Chapoy A., ***Mohammadi A.H.***, Tohidi B. and Richon D., Gas Solubility Measurement and Modeling for Nitrogen – Water System from 274.18 K up to 363.02 K, ***J. Chem. Eng. Data*, 2004,** *49*, 1110 - 1115.

11. Chapoy A., Mokraoui S., Valtz A., Richon D., ***Mohammadi A.H.*** and Tohidi B., Vapor-Liquid Equilibria for Propane-Water System from 277.62 K up to 338.15 K. ***Fluid Phase Equilibria*, 2004,** *226*, 213-220.

12. Danesh A., Tohidi B., Todd A.C., Gozalpour F., Al-Saleh I., ***Mohammadi A.H.***, Reid A., Bell K. and Malcolm K., PHASE BEHAVIOUR AND PROPERTIES OF RESERVOIR FLUIDS. DTI Maximising Hydrocarbon Recovery from the UKCS Seminar, 22-23 June **2004**, Aberdeen Exhibition and Conference Centre, Bridge of Don, Aberdeen, AB23 8BL.

13. Tohidi B., Danesh A., Todd A.C., Anderson R., Burgass R., Arjmandi M., Masoudi R., Ji H., ***Mohammadi A.***, Yang J., Ren S., Zain Z., Mali G., and Jadhawar P., "GAS HYDRATE AND FLOW ASSURANCE STUDIES", DTI Maximising Hydrocarbon Recovery from the UKCS Seminar, 22-23 June **2004**, Aberdeen Exhibition and Conference Centre, Bridge of Don, Aberdeen, AB23 8BL.

14. Tohidi B., Danesh A., Todd A.C., Anderson R., Burgass R., Arjmandi M., Masoudi R., Ji H., ***Mohammadi A.H.***, Yang J., Ren S., Zain Z., Mali G. and Jadhawar P., Gas Hydrates: Friend or Foe? Presented at the DTI IOR Research Dissemination Seminar, Aberdeen, UK, 24 June, **2004**.

15. ***Mohammadi A.H.***, Chapoy A., Tohidi B. and Richon D., Water Content Measurement and Modeling in the Nitrogen + Water System, ***J. Chem. Eng. Data,*** *50*, 541 – 545, **2005.**

16. Chapoy A., ***Mohammadi A.H.***, Tohidi B. and Richon D., Estimation of Water Content for Methane + Water and Methane + Ethane + *n*-Butane + Water Systems Using a New Sampling Device, ***J. Chem. Eng. Data*** , *50*, 1157 – 1161, **2005.**

17. ***Mohammadi A.H.***, Samieyan V. and Tohidi B., Estimation of Water Content in Sour Gases, *SPE 94133, Proceedings of the SPE Europec/EAGE Annual Conference, Madrid Spain,* **13-16 June 2005.**

18. ***Mohammadi A.H.***, Andersen R. and Tohidi B., Carbon Monoxide Clathrate Hydrates: Equilibrium Data and Thermodynamic Modeling, ***AIChE J.,*** *51*, 2825-2833, **October 2005.**

19. ***Mohammadi A.H.*** and Tohidi B. Prediction of Hydrate Phase Equilibria in Aqueous Solutions of Salt and Organic Inhibitor Using a Combined Equation of State and Activity Coefficient based Model, ***Can. J. Chem. Eng.***, *83*, 865-871, **October 2005.**

20. Chapoy A., ***Mohammadi A.H.***, Tohidi B., Valtz A., Richon D., Experimental Measurement and Phase Behavior Modeling and Literature Review of the

Properties for the Hydrogen Sulfide - Water Binary System, ***Ind. Eng. Chem. Res.***, *44*, 7567-7574, **2005** (Also: ***Ind. Eng. Chem. Res.***, *44*, 10021, **2005**).

21. ***Mohammadi A.H.*** and Tohidi B. A Novel Predictive Technique for Estimating Hydrate Inhibition Effects of Single and Mixed Thermodynamic Inhibitors, ***Can. J. Chem. Eng.***, *83*, , 951-961, **December 2005.**

22. ***Mohammadi A.H.***, Asphaltene and Asphalt: Foe or Friend?, Student paper, The 6th Canadian International Petroleum Conference (56th Annual Technical Meeting), **Calgary, Alberta, Canada, June 7 – 9, 2005**.

23. ***Mohammadi A.H.***, Asphaltene Precipitation Problem During Oil Production and Transportation, Prize Winner of the Institute of Materials, Minerals & Mining (IOMMM, the Scottish section) Young Person's Lecture Competition, **February 2005**.

24. Tohidi B., Danesh A., Todd A.C., Burgass R., Arjmandi M., Anderson R., Yang J., Chapoy A., Zain Z., ***Mohammadi A.H.***, Ji H. Y., Masoudi R., Mali G., Ren S., Jadhawar P. and Zolelmein A., ,Gas hydrates and flow assurance studies, DEVEX 2005: The Production & Development Conference & Exhibition; Featuring Subsurface Techniques to Enhance Recovery, Aberdeen Exhibition & Conference Centre, Aberdeen, UK, **18 May 2005**.

25. Gozalpour F., Danesh A., Tohidi B., Todd A.C., Al-Saleh I., ***Mohammadi A.H.***, Reid A., Bell K. and Malcolm K., Phase behaviour and properties of reservoir fluids- reservoir fluid sampling and properties of HPHT fluids, DEVEX 2005: The Production & Development Conference & Exhibition; Featuring Subsurface Techniques to Enhance Recovery, Aberdeen Exhibition & Conference Centre, Aberdeen, UK, **19 May 2005**.

26. Tohidi, B. and ***Mohammadi A.H.***, Evaluation of the Risk of Hydrate Formation in the York Pipeline, UK, Consultancy Report to ENAA Technical Services, Amerada Hess Limited, London, UK, ***Final Technical Report***, May **2005**.

27. Research Report, Reservoir Fluid Studies, Institute of Petroleum Engineering, Heriot-Watt University, Edinburgh, UK, **2002-2005**.

28. Research Report, Flow Assurance: Gas Hydrates & Wax, Institute of Petroleum Engineering, Heriot-Watt University, Edinburgh, UK, **2002-2005**.

29. ***Mohammadi A.H.***, Chapoy A., Tohidi B. and Richon D., Gas Solubility: A Key to Estimate Water Content of Natural Gases, ***Submitted to Ind. Eng. Chem. Res.***, **2005**.

30. Najibi H., ***Mohammadi A.H.*** and Tohidi B. Estimating the hydrate safety margin in the presence of salt and/or organic inhibitor using freezing point depression data of aqueous solutions, ***Accepted for publication in Ind. Eng. Chem. Res.*, 2006.**

31. ***Mohammadi A.H.***, Chapoy A., Richon D. and Tohidi B., Advances in Estimating Water Content of Natural Gases, Proceedings of 85th Annual GPA Convention, Grape Vine, Texas, USA, 5-8 **March 2006**.

32. Jadhawar P., ***Mohammadi A.H.***, Yang J. and Tohidi B., Subsurface Carbon Dioxide Storage Through Clathrate Hydrate Formation, Pages 111-126. In: Advances in the Geological Storage of Carbon Dioxide, Edited by: Lombardi S., Altunina L.K and Beaubien S.E., NATO Science Series, IV. Earth and Environmental Sciences, Vol. 65, Springer, The Netherlands **2006**.

33. Chapoy A., ***Mohammadi A.H.*** and Tohidi B., An artificial neural network based model for predicting hydrate dissociation conditions of natural gases, ***Submitted to AIChE J.*, 2005**.

34. ***Mohammadi A.H.***, Ji H., Burgass R.W., Bashir A., Tohidi B., Gas Hydrates in Oil Systems, *SPE 99437, Proceedings of the SPE Europec/EAGE Annual Conference,* **Vienna, Austria, 12–15 June 2006.**

35. ***Mohammadi A.H.*** and Tohidi B. Gas Hydrates and Deepwater Operation: Predicting the Hydrate Free Zone, *SPE 99427, Proceedings of the SPE Europec/EAGE Annual Conference,* **Vienna, Austria, 12–15 June 2006.**

36. Chapoy A., ***Mohammadi A.H.*** and Tohidi B., Development of a Henry's constant correlation and solubility measurements of n-pentane, i-pentane, cyclopentane, n-hexane and toluene in water, ***In preparation*, 2006**.

37. ***Mohammadi A.H.***, Najibi H. and Tohidi B. Experimental study of the hydrate safety margin estimation in the presence of salt and/or organic inhibitor using freezing point depression data of aqueous solutions, ***In preparation*, 2006.**

38. ***Mohammadi A.H.*** and Tohidi B. Very High-Pressure Hydrate Phase Equilibria, ***In preparation*, 2006.**

39. ***Mohammadi A.H.***, Burgass R.W. and Tohidi B. High-Pressure Equilibrium Data for Ethane, Propane, Nitrogen and Carbon Dioxide Clathrate Hydrates, ***In preparation*, 2006.**

40. ***Mohammadi A.H.***, Burgass R.W. and Tohidi B. Hydrate Phase Equilibria in Oil systems, ***In preparation*, 2006.**

41. Solubility Measurement and Thermodynamic Modeling in Methanol, Ethylene Glycol and Water Containing Systems, ***In preparation*, 2006**.

42. Hydrogen Storage in Clathrate Hydrate in Presence of a Water Soluble Guest, **In preparation 2006.**

43. Hydrate Phase Equilibria of Systems Containing Water Soluble and Partial Water Soluble Heavy Hydrate Formers, ***In preparation*, 2006.**

44. ***Mohammadi A.H.*** et al., An Activity Coefficient Based Model for Predicting Asphaltene Precipitation, ***In preparation*, 2006.**

45. ***Mohammadi A.H.*** et al., An *EoS* + G^E Based Model for Predicting Asphaltene Precipitation, ***In preparation*, 2006.**